TRANSCUTANEOUS DELIVERY OF T CELL-INDUCING VIRAL VECTOR MALARIA VACCINES BY MICRONEEDLE PATCHES

FRANCES E. PEARSON

MANSFIELD COLLEGE

Faculty of Clinical Medicine, University of Oxford

Thesis submitted for the degree of Doctor of Philosophy

Trinity term 2011

TRANSCUTANEOUS DELIVERY OF T CELL-INDUCING VIRAL VECTOR MALARIA VACCINES BY MICRONEEDLE PATCHES

FRANCES PEARSON, MANSFIELD COLLEGE

Faculty of Clinical Medicine, University of Oxford

Thesis submitted for the degree of Doctor of Philosophy, Trinity term 2011

ABSTRACT

There is an urgent need for improvements to existing vaccine delivery technologies to run parallel with the development of new-generation vaccines. The burdens of needle-based immunisation strategies are exacerbated by poor resource provision in such areas as sub-Saharan Africa, where annual malaria mortality stands at 860,000. Needle-free delivery of vaccine to the skin holds promise for improved immunogenicity with lower doses of vaccine, in addition to significant logistical advantages. Various methods have been described for the transcutaneous delivery of vaccines, including the use of microneedles to overcome the outer *stratum corneum* of the skin for efficient delivery of liquid or solid, microneedle-coated vaccines into underlying strata rich in antigen-presenting cells. This thesis aims to evaluate two transcutaneous silicon microneedle and microprojection patch technologies for the delivery of live recombinant Adenovirus and Modified Vaccinia Ankara-vectored vaccines encoding pre-erythrocytic malaria antigens in mice. Cellular immunogenicity directed against a well-documented epitope of the *Plasmodium berghei* circumsporozoite protein is evaluated, as is protection against lethal *P. berghei* sporozoite challenge. Immunological and logistical benefits of each technology are assessed, as well as mechanisms underlying differences in the generation of a patch-induced immune response to vaccination. These data inform the future development of transcutaneous microneedle patches for the delivery of live vaccine.

ACKNOWLEDGMENTS

I thank Professor Adrian Hill for his constant enthusiasm and support throughout this project, and for the opportunities it has presented me. Thank you to Dr. Arturo Reyes-Sandoval who was a great lab supervisor and is atruly dedicated scientist. The names of countless members of the Jenner Institute (past and present) should also be listed here, but unfortunately can't be. I thank everyone who helped me in designing and carrying out experiments and providing feedback on data. Dr. Alex Spencer deserves special mention for the exceptional amount of support and time she freely gave. Without her a good deal of these experiments would not have been undertaken. Thanks also to Dr. Tess Lambe, who was always happy to help, and Dr. Matt Cottingham and Mr. Matt Dicks selflessly gave of their time to answer my many questions on all things virus and DNA. I also thank Dr. Simon Draper, Dr. Matt Cottingham, Miss. Simone DeCassan and Dr. Sumi Biswas for reading chapters of my thesis, and their continual advice and support. Thanks to Mr. Drew Worth of the Jenner Flow facility, the hard-working staff of the Vector Core, Ms. Julie Furze for excellent lab management and to Ms. Carol Williams and Ms. Viv Smith and their team in the FGF.

At University College, Cork - thanks to Dr. John Carey, Dr. Conor O'Mahony, Dr. Anto Vrdoljak, Miss. Marie McGrath and of course Dr. Anne Moore. Anne was a most dedicated, knowledgeable, supportive supervisor and has seemingly boundless enthusiasm. Anne taught me a great deal about science and immunology and to "eat the elephant one bite at a time". In Brisbane, I was fortunate to spend 8 months working at the Drugs and Genes Delivery Group at the University of Queensland. Prof. Mark Kendall taught me the importance of cross-disciplinary teamwork, and I thank him for being an incredibly supportive and enthusiastic supervisor throughout the project, maintaining close contact despite the long distance. Dr. Celia McNeilly was a fantastic co-worker and friend, and significant contributor to 'the malaria project'. Thanks also to Dr. Xianfeng Chen, Dr. Germain Fernando, Dr. Simon Corrie, Mr. Anthony Raphael, Dr. Chris Flaim, Dr. Rob Falconer (particularly for feedback on Chapter 5) and especially to Miss. Marion Brunck, Miss. Sally Yukiko and Mrs. Clare Primiero - three fantastic RAs. Thanks also to Miss. Holly Corbett and Mr. Michael Crichton, my fellow PhD students, who were thankfully never too tired for an early morning/late night Skype chat. I also thank the staff of the AIBN animal facility, the Queensland Brain Institute for flow cytometry assistance, and Prof. Ian Frazer's group across the river for helpful feedback and use of equipment.

Prof. Charles Lacey employed me as a research assistant in York as a fresh-faced graduate and gave me an introduction to vaccinology and full encouragement to pursue this D.Phil. I also thank my cousins Dr. Andrew Wragg and Dr. Nuria Martinez-Alier for introducing me to the world of malaria research. Mansfield College, Oxford helped me to attend the First International Conference on Microneedles in Atlanta and I was funded by an MRC Capacity Building Studentship Award and supported by a Wellcome Trust Programme Grant (Hill lab) and a Gates Foundation Grand Challenges Explorations Grant (Kendall lab).

My family and friends - Leeds, London, Oxford, Brisbane and everywhere in between - have been a truly amazing support throughout. Helen, Sumi, James Laurence, Alice, Kat, Simone, Leanne, Matt D, Emily, Gez (especially in the later stages), Alex, and Lucy deserve special mention. To my wonderful extended family, especially to James, Jen and Marsh, and of course my parents Catherine and Eric, who have wholeheartedly and lovingly supported every crazy adventure I've decided to undertake.

And remembering Geraldine, whose generous gift enabled me to write this thesis.

PUBLICATIONS AND PATENTS ARISING FROM THIS WORK

Publications

Carey JB, **Pearson FE**, Vrdoljak A, Crean AM, Walsh PR, O'Mahony C, Hill AVS, Moore AC. (2011) Microneedle Array Design Determines the Induction of Protective Memory CD8+ T Cell Responses Induced by a Recombinant Live Malaria Vaccine in Mice. PLoS ONE 6(7): e22442. (1)

Pearson FE, McNeilly C, Crichton ML, Yukiko SR, Primiero CA, Chen X, Gilbert SC, Hill AV, Kendall MAF. Cutaneous Delivery of a Live, Recombinant Viral Vector Vaccine against *Plasmodium berghei* malaria using a microprojection patch. *In Preparation.*

Reyes-Sandoval A, **Pearson FE**, Todryk S, Ewer K. Potency Assays for Novel T-Cell inducing Vaccines against Malaria. Curr. Opin. Mol. Ther. 2009, Feb. 11(1): 72-80.

Patent pending

Moore AC,Carey JB, **Pearson FE**, McGrath M, Crean A, Hill AVS and O'Mahony C. Microneedle Kits for T-Cell-inducing Vaccine Delivery. UK & US Patent Application filed 29th April 2010.

LIST OF CONTENTS

CHAPTER 1 Introduction 15
1.1 Vaccines 16
1.1.1 A brief history of vaccination 16
1.1.2 Types of vaccines 18
1.2 Immunological Basis of Vaccination 20
1.2.1 The initiation of an innate immune response 20
1.2.2 Components of the adaptive immune system 21
1.2.3 Immunological memory 23
1.2.4 Central and effector memory 23
1.3 Vaccine Delivery into the Skin 26
1.3.1 Routes of vaccine delivery to humans 26
1.3.2 Intradermal immunisation and dose-sparing 27
1.3.3 Cutaneous immunological mechanisms 27
1.3.4 Cutaneous dendritic cells 29
1.4 Needle-free Immunisation 30
1.4.1 The urgent need for alternatives to needle injection 30
1.4.2 Needle-free cutaneous immunisation 31
1.5 Microneedles 37
1.5.1 Single microneedle devices 37
1.5.2 Microneedle patches 38
1.5.3 Considerations for implementation 46
1.6 Malaria vaccines 48
1.6.1 The need for a vaccine 48
1.6.2 Malarial disease 49
1.6.3 Developing a vaccine against malaria 50
1.6.4 CSP and ME-TRAP 53
1.6.5 Prime-boost viral vector malaria vaccine regimes 54
1.7 A Microneedle Vaccine Patch for Malaria 55
1.7.1 ImmuPatch 55
1.7.2 Nanopatch 56
1.7.3 Thesis aims 57

CHAPTER 2 Methods and Materials 58
2.1 Solutions 59
2.2 Patch Manufacture 63
2.2.1 ImmuPatch 63
2.2.2 Nanopatch 63
2.3 Vaccines 63
2.3.1 Transgene antigens 63
2.3.2 Generation and propagation of recombinant MVA and Adenovirus-vectored vaccines 64
2.3.3 Ad and MVA titration (J082, J111, J106, J104) 65
2.3.4 Vaccine schedules 65
2.3.5 Preparation of vaccines for needle-based and liquid patch immunisations 65
2.3.6 Dry-coating formulation 66
2.3.7 Dry-coating method 66
2.3.8 Assessment of virus viability 66
2.3.9 Stability studies 67
2.4 Animals 67
2.4.1 Mice and regulated procedures 67
2.4.2 Anaesthesia 67

2.4.3 Blood sampling 67
2.5 Immunisations 68
2.5.1 Conventional needle-based immunisations 68
2.5.2 Liquid patch immunisations 68
2.5.3 Vaccine-coated Nanopatch applicator-assisted immunisation 68
2.6 Assessment of Immunogenicity 68
2.6.1 Preparation of single cell lymphocyte suspensions 68
2.6.2 Peptide re-stimulation 69
2.6.3 *Ex vivo* IFN-γ ELISPOT 69
2.6.4 Intracellular cytokine staining and T cell phenotyping 69
2.7 Plasmodium berghei sporozoite challenge 71
2.7.1 Isolation of *P.berghei* sporozoites 71
2.7.2 Intravenous inoculation of sporozoite preparations and post-challenge monitoring 71
2.8 Assays for Estimating Delivery Efficiency by Patch 71
2.8.1 Quantitative PCR for Adenoviral genomes 71
2.8.2 *Ex vivo* luciferase assay to quantify transgene expression 73
2.8.3 ^{14}Carbon scintillation assay 74
2.9 RT-PCR for Cytokine and Chemokine Expression 74
2.10 Phenotyping Skin and LN Innate Cell Populations 74
2.10.1 Isolation of skin and draining LN cells 74
2.10.2 Staining protocols and panels 75
2.11 Flow Cytometry and Analysis 75
2.12 Microscopy 76
2.12.1 Scanning Electron Microscopy (SEM) 76
2.12.2 Cryo-SEM for analysis of SC penetration 76
2.12.3 Analysis of microprojection penetration by Confocal Microscopy 76
2.12.4 Confocal imaging of delivered Adenovirus 76
2.13 Data Analysis 77
2.13.1 Representation of data 77
2.13.2 Linear regression of parasite growth rates 77

CHAPTER 3 CD8+ T Cell Immunogenicity and Protective Efficacy of Prime-Boost Vaccine Regimes using Silicon ImmuPatch Arrays 79
3.1 Introduction 80
3.2 Statement of Hypotheses 82
3.3 Results 82
3.3.1 MVA/MVA prime-boost immunisation 82
3.3.2 Adenovirus/MVA immunisation 99
3.3.3 Quantification of delivered virus present in skin and draining LN post-immunisation 104
3.4 Discussion 117
3.4.1 The methodology of patch application 117
3.4.2 Design parameters of the ImmuPatch array 118
3.4.3 The dose applied to the ear prior to patch application 120
3.4.4 The number and order of vaccines delivered by ImmuPatch in a prime-boost schedule 120
3.4.5 Other potential factors influencing the ImmuPatch-induced response 122
3.5 Concluding Statement 123

CHAPTER 4 Characterising CD8+ T Cell and Early Innate Responses to ImmuPatch Immunisation 124
4.1 Introduction 125
4.2 Statement of Hypotheses 126

4.3 Results 127
4.3.1 ImmuPatch primes a Pb9-specfic response with an irregular kinetic whilst retaining ability to expand upon boost 127
4.3.2 Antigen-specific CD8+ T cell memory phenotype in MVA/MVA immunisation 129
4.3.3 Cytokine and chemokine expression at the immunisation site and the dLN following ID and ImmuPatch delivery of MVA 132
4.3.4 Summary of sections 4.3.1-4.3.3 134
4.3.5 Trafficking of innate cells from the immunisation site to the dLN following ImmuPatch delivery of MVA 135
4.4 Discussion 150
4.4.1 The method of antigen delivery into the skin influences characteristics of innate and adaptive responses 150
4.4.2 Characteristics of the ImmuPatch-induced T cell response 151
4.5 Concluding Statement 155

CHAPTER 5 Delivery of Viral Vector Malaria Vaccines by Nanopatch including Liquid and Dry-Coated Formulations 156
5.1 Introduction 157
5.2 Statement of Hypotheses 159
5.3 Results 160
5.3.1 Nanopatch application methods, microprojection morphologies used within this chapter 160
5.3.2 Quasi-static application of Nanopatches to the skin for liquid vaccine delivery 163
5.3.3 Formulation and dry-coating of viral vector vaccines onto NP110 microprojections 176
5.3.4 Immunogenicity and protective efficacy of velocity-applied dry-coated Nanopatch 197
5.4 Discussion 202
5.4.1 Overall summary 202
5.4.2 Penetration and delivery characteristics of Nanopatch in murine skin .203
5.4.3 Quasi-static delivered Nanopatch-induced immunogenicity and protection against *P. berghei* sporozoite challenge 204
5.4.4 Formulation of live viral vector vaccines for dry-coating 205
5.4.5 Adenoviral protection during drying and during storage at elevated temperatures afforded by stabilising disaccharides 206
5.4.6 Inherent differences in physical stability between Adenoviral and Poxviral vectors 208
5.4.7 Assessment of immunogenicity and protection against challenge following delivery of dry-coated viral vector vaccine regimes 209
5.5 Concluding Statement 209

CHAPTER 6 Concluding Chapter 211
6.1 Overall Summary 212
6.2 Summary of Main Conclusions 213
6.2.1 ImmuPatch 213
6.2.2 Nanopatch 214
6.3 Future Outlook 216

LIST OF FIGURES

FIGURE 1-1: Models of memory CD8+ T cell differentiation. 25
FIGURE 1-2: The scarification method of smallpox immunisation. 26
FIGURE 1-3: The anatomy of mammalian skin. 28
FIGURE 1-4: Proposed methods for the transcutaneous delivery of vaccines by overcoming the *stratum corneum*. 32
FIGURE 1-5: Modalities of microneedle vaccine delivery to the skin. 38
FIGURE 1-6: Examples of microneedle systems in development. 45
FIGURE 1-7: The estimated global incidence and distribution of malaria. 49
FIGURE 1-8: The life cycle of *Plasmodium*. 50
FIGURE 1-9: ImmuPatch – Innovative solutions to vaccine delivery barriers. 56
FIGURE 3-1: Cellular immunogenicity following MVA/MVA prime-boost immunisation with ImmuPatch. 84
FIGURE 3-2: ImmuPatch is more efficient at priming than boosting responses in MVA.PbCSP homologous prime-boost immunisation. 86
FIGURE 3-3:Methodology of ImmuPatch immunisation impacts upon the magnitude of the resulting response. 88
FIGURE 3-4: Effect of altering priming dose upon the post-prime and post-ID boost response in MVA/MVA immunisation. 89
FIGURE 3-5: Cellular responses following ImmuPatch immunisation are dependent upon patch design. 91
FIGURE 3-6: Microneedles create microchannels upon application the skin. 92
FIGURE 3-7: ImmuPatch primed responses are correlated with Total Array Volume (TAV). 93
FIGURE 3-8: Immunogenicity of ImmuPatch/ID and ImmuPatch/ImmuPatch delivery in MVA/MVA prime-boost immunisation. 95
FIGURE 3-9: Responses following homologous ImmuPatch/ImmuPatch immunisation are correlated with TAV. 97
FIGURE 3-10: The effects of dose reduction in MVA.PbCSP prime-boost immunisation as delivered ID. 98
FIGURE 3-11: Immunogenicity of ImmuPatch priming in AdCh63.ME-TRAP / MVA.ME-TRAP immunisation. 102
FIGURE 3-12: Responses after ImmuPatch immunisation in AdCh63.ME-TRAP/MVA.ME-TRAP immunisation are associated with TAV. 103
FIGURE 3-13: Luciferase activities following ImmuPatch delivery of AdCh63.pLuc are dependent upon specific patch used. 106
FIGURE 3-14: Relative quantification of Adenovirus genomes following ImmuPatch delivery of AdHu5.*hcmv*are dependent upon specific patch used. 109
FIGURE 3-15: Correlations between ear skin and dLN luciferase activity and relative genome copy number with TAV. 110
FIGURE 3-16: ImmuPatch/ID demonstrates high levels of protective efficacy in AdCh63.ME-TRAP/MVA.ME-TRAP immunisation. 114
FIGURE 3-17: ImmuPatch/ID (patches C and H), but not ImmuPatch/ImmuPatch AdCh63/MVA immunisation is partially protective against *P. berghei*challenge.116
FIGURE 4-1: Irregular kinetics of the Pb9-specific CD8+ T cell response following ImmuPatch immunuisation with MVA- or AdCh63-vectored vaccine. 128
FIGURE 4-2: Memory phenotype of Pb9-specific CD8+ T cells at timepoints following immunisation with MVA.PbCSP, delivered ID or by ImmuPatch. 130
FIGURE 4-4: Levels of mRNA encoding inflammatory cytokines and chemokines in the skin and dLN following ID and ImmuPatch F delivery of MVA.PbCSP. 134
FIGURE 4-5: Magnitude of the Pb9-response following immunisation with ImmuPatch G and F… 135

FIGURE 4-6: Design-dependent differences in the cellular infiltration into dLN and migration of cells from the immunisation site 48 and 120 hours after recombinant MVA.137
FIGURE 4-7: Gating strategies used in subsequent analyses. 140
FIGURE 4-8: Kinetics of CD11c+ and CD11b+ infiltration in the dLN following ImmuPatch and ID delivery of recombinant MVA. 140
FIGURE 4-9: Kinetics of CD11c+ and CD11b+ migration away from the immunisation site following ImmuPatch G and ID delivery of recombinant MVA. 141
FIGURE 4-10: Early influx of CD11c+ B220+ plasmacytoid DC into the skin and subsequent influx into the dLN after ID and ImmuPatch G, but not ImmuPatch F immunisation. 143
FIGURE 4-11: Influx of CD11b+ CD11c- polymorphonucelar cells and inflammatory monocytes of greater magnitude after ID than ImmuPatch immunisation. 144
FIGURE 4-12: Influx of CD11b+ CD11c+ myeloid DC into the dLN following immunisation. 146
FIGURE 4-13: Differences in the activation state of infiltrating CD11c+ CD11b+ myeloid DC in the dLN post-immunisation. 149
FIGURE 5-1: The Nanopatch concept. 158
FIGURE 5-2: Nanopatch application methods and microprojection morphologies used within this chapter. 163
FIGURE5-3: NP40microprojections pierce the *stratum corneum*, and create microchannels into underlying tissue to enable delivery of liquid payload into the epidermis. .164
FIGURE 5-4: NP40delivery of MVA.PbCSP induces Pb9-specific CD8+ T cells that are expanded upon boost, and can partially protect against parasite challenge. .168
FIGURE 5-5: Priming dose, and microprojection design specific differences in immunogenicity following quasi-static application. 170
FIGURE 5-6: Delivery efficiency of liquid vaccine delivery by NP40 and NP110 (quasi-static application). 173
FIGURE 5-7: Nanopatchdelivery of human and AdCh63-based vaccines in heterologous prime-boost schedules. 175
FIGURE 5-8: NP110 microprojections delivered at velocity pierce the *stratum corneum* and deliver dry-coated payloads into the viable epidermis and the dermis. 178
FIGURE 5-9: MVA formulations can be dry-coated onto NP110 microprojections and coated material is reduced following insertion in the skin. 181
FIGURE 5-10: Ad-vectored vaccine can be dry-coated onto NP110 microprojections in formulation with 1% $^{w}/_{v}$ MC at both higher and lower doses. 182
FIGURE 5-11: The surfactant Polysorbate 20 improves microprojection coating when formulated with MVA vaccine. 183
FIGURE 5-12: Confocal imaging of coated Ad-vectored vaccine delivery to murine skin. 185
FIGURE 5-13: Delivery efficiency of vaccine-coated NP110 delivered at velocity by spring-loaded applicator is vaccine and dose-dependent. 189
FIGURE 5-14: MVA can be coated onto and recovered from Nanopatch microprojections without loss of viability. 190
FIGURE 5-15: The disaccharides trehalose and sucrose mediate a protective effect upon dry-coating of Ad-vectored vaccine onto NP110 microprojections. 192
FIGURE 5-16: Formulation with the disaccharides trehalose and sucrose mediates long-term thermostability of microprojection coated simian Ad-vectored vaccine. .196
FIGURE 5-17: Nanopatch delivery of dry-coated vaccines in MVA/MVA immunisation, delivered at velocity. 198
FIGURE 5-18: Nanopatch delivery of stabilised dry-coated AdCh63/MVA heterologous prime-boost immunisation, delivered at velocity. 201

LIST OF TABLES

TABLE 1-1: The effectiveness of vaccination as a public health intervention. 16
TABLE 1-2: Attributes and phenotypes of CD8+ T cell subsets arising following expansion of an immune response.....24
TABLE 1-3: An evaluation of methods for delivery vaccines through the skin. 36
TABLE 1-4: Commercial development of microneedles. 44
TABLE 1-5: Summary of *P.falciparum* malaria vaccine developments. 53
TABLE 2-1: List of reagents and kits used in these experiments.....61
TABLE 2-2: List of monoclonal antibodies used in these experiments.....62
TABLE 2-3:Surface staining panel for T cell immunogenicity and phenotyping experiments. 70
TABLE 2-4: Intracellular staining panel for T cell immunogenicity and phenotyping experiments.....70
TABLE 2-5: Panel 1 - for phenotyping of DC subsets in the skin and draining LN. ..75
TABLE 2-6: Panel 2 - for phenotyping of non-DC subsets in the skin and draining LN.75
TABLE 2-7: Table of information about all patches used in this thesis. 78
TABLE 3-1: Details of statistically significant differences from the analysis performed in Figure 3-8.....96
TABLE 3-2: ImmuPatch immunisation regimes induce partial protective efficacy against *P.berghei* sporozoite challenge. .....
TABLE 5-1: Table showing the average delivery efficiencies after quasi-static delivery of liquid vaccine by Nanopatch.....173

ABBREVIATIONS

αα	amino acid
α-	anti-
β-gal	Beta-galactosidase
(m)Ab	(monoclonal) Antibody
Ad	Adenovirus
ADP	Adosine Diphosphate
Ag	Antigen
(p)APC	(professional) Antigen-Presenting Cell
APC	Allophycocyanin
BCG	Bacillus Calmette-Guérin
BCR	B Cell Receptor
BD	Becton, Dickenson and Co.
BMI	Body Mass Index
BSA	Bovine Serum Albumin
-C	- Century
CCR-/CCL-	CC chemokine Receptor/Ligand
CEF	Chick Embryo Fibroblasts
CLA	Cutnaeous Lymphocyte Antigen
(h)CMV	(human) Cytomegalovirus
CSP	Circumsporozoite Protein
CT	Cholera Toxin
Ct	Crossing threshold
CTL	Cytotoxic T lymphocyte
D^2G^2	Drugs and Genes Delivery Group (U. Queensland)
DC	Dendritic cell
dDC	dermal Dendritic Cell
dH_20	de-ionised H_20
DMEM	Dulbecco's Modified Eagle Medium
DMSO	Dimethyl Sulfoxide
(p)DNA	(plasmid) Deoxyribonucleic Acid
dNTP	Deoxyribonucleotide
DRIE	Deep Reactive Ion Etching
EDTA	Ethylenediaminetetraacetic Acid
ELISA	Enzyme-linked Immunosorbant Assay
ELISPOT	Enzyme-linked Immunospot
EpCAM	Epidermal Cell Adhesion Molecule
FACS	Fluorescence-Activated Cell Sorting
FCS	Foetal Calf Serum
FDA	(US) Food and Drugs Administration
FITC	Fluorescein Isothiocyanate
FoxP3	Forkhead box P3
-G	gauge
(m)GAPDH	(murine) Glyceraldehyde 3-Phosphate Dehydrogenase
G/RFP	Green/Red Fluorescent Protein
GDP	Gross Domestic Product
GSK	Glaxo SmithKline Plc.
HA	Haemagglutinin

HBV/HBS	Hepatitis B Virus / HBV S antigen
HCV	Hepatitis C Virus
HEK-293A	Human Embryonic Kidney-293A cells
HGP	Hairless Guinea Pig
HI	Haemagglutinin Inhibition
HIV	Human Immunodeficiency Virus
HMGB-1	High-Mobility Group Box protein-1
HPV	Human Papilloma Virus
HRP	Horseradish Peroxidase
HSV	Herpes Simplex Virus
ICAM-1	Intercellular Adhesion Molecule-1
ICS	Intracellular Cytokine Staining
ID	Intradermal
IFN(-γ)	Interferon (-gamma)
Ig-	Immunoglobulin-
IL-	Interleukin-
IM	Intramuscular
ISCOM	Immunostimulatory complex
IU	Infectious Unit
IV	Intravenous
L+dDC	Langerin+ dermal Dendritic Cell
LC	Langerhans Cell
LFA-1	Lymphocyte Function Antigen-1
(d)LN	(draining) LN
mDC	myeloid Dendritic Cell
ME-TRAP	Multiple Epitope fused to *P. falciparum* Thrombospondin-Related Adhesive Protein
MHC	Major Histocompatability Complex
mono-DC	monocyte Dendritic Cell
MVA	Modified Vaccinia Ankara
NFκB	Nuclear Factor kappa-light-chain-enhancer of activated B cells
NK	Natural Killer (cell)
ns	not significant
OVA	Ovalbumin
P/TBS	Phosphate/Tris Buffered Saline
PAMP	Pathogen Associated Molecular Pattern
PBMC	Peripheral Blood Mononuclear Cells
(Q-)PCR	(Qualitative-) Polymerase Chain Reaction
pDC	plasmacytoid Dendritic Cell
PE	Phychoerythrin
pers. comm.	personal communication
PFU	Plaque Forming Units
PI	Particle : Infectious unit (ratio)
PMN	Polymorphonuclear cells (neutrophils)
PRR	Pathogen Recognition Receptor
PS20	Polysorbate 20
RAGE	Receptor for Advanced Glycation End products
RAS	Radiation Attenuated Sporozoites

RBC	Red Blood Cell
RLU	Relative Light Units
Rpm	revolutions per minute
RT	Room Temperature
S1PR	Sphingosine 1 Phosphate Receptor
SC	*stratum corneum*
SCu	Subcutaneous
SD	Standard Deviation (from the mean)
SEM	Scanning Electron Microsopy
SEM	Standard Error of the Mean
SFC	Spot Forming Cells
TAP(I)	Transporter of Antigen Peptide (Inhibitor)
TAV	Total Array Volume (mm^3)
TB	Tuberculosis
TCI	Transcutaneous Immunisation
T_{CM}	central memory T cell
TCR	T Cell Receptor
T_E	effector T cell
T_{EM}	effector memory T cell
TGF-β	Transforming Growth Factor-beta
Th-	T helper
TLR	Toll-Like Receptor
TNF-α	Tumour Necrosis Factor-alpha
T_{reg}	Regulatory T cell
UCC	University College, Cork
USD	United States Dollar
VCAM-1	Vascular Cell Adhesion Molecule-1
VE	Viable Epidermis
VLP	Virus Like Particle
VP	Viral Particles
WHO	World Health Organization

CHAPTER 1 INTRODUCTION

1.1 VACCINES

1.1.1 A brief history of vaccination

Vaccination is a success story of modern medicine. The method of eliciting protective immunity against infectious agents and the eventual elimination of host-to-host transmission can be described as one of the most effective interventions to have ever impacted upon global public health (2, 3). This is evidenced by the reduction of vaccine-preventable disease incidence since their uptake in the United States (Table 1-1).

Disease	Max. no. cases (year)	Cases in 2001	Reduction in disease incidence (peak-2001)
Smallpox	48,164 (1901)	0	100%
Diptheria	206,939 (1921)	2	99.99%
Pertussis	265, 269 (1934)	4788	98.20%
Tetanus	1560 (1923)	26	98.34%
Polio	21,269 (1952)	0	100%
Measles	894,134 (1941)	96	99.99%
Rubella	57,686 (1969)	19	99.97%
Mumps	152, 209 (1968)	216	99.86%
Hemophilus influenzae	20,000 (1992)	51	99.75%

TABLE 1-1: The effectiveness of vaccination as a public health intervention.

This table is adapted from (3). It demonstrates the impact of vaccination upon infectious disease burden in the United States as assessed in 2001.

The notion of administering vaccines via the skin is thought to date back to ancient India and China (8-10thCentury A.D.), when dried smallpox scabs were inhaled or scratched into the skin of a healthy person to protect against severe disease by administering a small amount in a controlled manner. This method (later termed 'variolation' after the causative organism of smallpox - viruses of the genus *Variola*) was brought to England from Constantinople in 1718 by the wife of the British Ambassador to the Ottoman Empire, and was widely practiced throughout the 18thC despite high risks of death and disfiguration from uncontrollable infection.

A significant breakthrough in the development of vaccines was made when Edward Jenner inoculated cowpox virus into the forearm skin of the boy James Phipps in 1796, to provide evidence that this less virulent but related virus could confer immunity against infection with the often-fatal Variolae, without itself causing significant pathology. As a direct result of this demonstration, the first vaccine-mediated global eradication of a disease was finally achieved in 1980 following a mass smallpox immunisation campaign orchestrated by the World Health Organization (WHO) using the same viral vaccine (4).

In the early days, vaccinology was met with much public distrust as demonstrated by popular cartoons of the time, depicting vaccinated men and women developing

bovine features after receiving the cowpox vaccine ("vaccine" is derived from "*vacca*" meaning 'cow' in Latin). However, by the beginning of the 19thC, the field of vaccinology was growing from strength to strength. In 1881, Louis Pasteur's notion that infectious disease was caused by individual living microbes, which could be inactivated whilst retaining the ability to confer protection against natural infection was to underscore contemporary understanding of human disease and its prevention by vaccination (2). The new science of immunology, pioneered by Paul Ehlich and Ilya Metchnikoff, aimed to describe the underlying mechanisms behind the early observations of vaccinologists(5). The field would have to wait until the latter half of the 20thC for the major components of the immune system to be described (section 1.2.2), equipping it with the tools to manipulate the immune system for optimal acquisition of highly-specific, long-lasting immunological memory – the 'holy grail' of vaccination.

Alongside efforts to describe the theory behind immunisation, technology enabling the safe and reliable mass production of vaccines had been improving since Pasteur's early attenuation techniques, with the advent of cell culture and passage. By selecting against genes unnecessary for *in vitro* replication (e.g. those involved in host range and immune evasion), mutants are less equipped to survive in the living host, whilst retaining their antigenicity. By the 1960s, live-attenuated vaccines for polio, measles, mumps and rubella had been developed. In the latter half of the 20thC the new sciences of genomics, proteomics, genetic engineering and recombinant protein expression contributed to a boom in the number of new vaccines being licensed by providing tools for rational attenuation or subunit antigen choice. Advances in the use of adjuvants improved the effectiveness of protein-based vaccines in particular. The discovery that DNA plasmids incorporating foreign genes express the gene product upon injection into muscle or skin opened the door to recombinant plasmid DNA vaccine development (and later, viral vectors, 1.1.2.4.)

Testament to the true success of vaccination is the complete eradication of smallpox and the near global elimination of polio today. Despite this, vaccination services are globally under-utilised, either through choice or inadequate provision(6). In 2002, the WHO estimated that the number of vaccine-preventable deaths in children was 1.4 million, representing 14% of global total mortality in children under five(7). The development of effective vaccines against diseases such as malaria and HIV has thus far eluded vaccinologists due to the difficulty of defining and emulating protective immunity. The future outlook for vaccines sees expansion beyond communicable diseases to cancers, autoimmune disease and allergy. Some of these new-generation vaccines are likely to be expensive to manufacture due to an increased complexity, and will only be affordable and accessible to those for whom the disease burden is greatest by way of huge international investment and cooperation. Simultaneous assessment of new vaccines in parallel with new proposed delivery systems, such as methods for needle-free cutaneous delivery here described, will reduce both costs incurred and time taken to achieve licensure.

1.1.2 Types of vaccines

1.1.2.1 Whole organism

Killed organism vaccines (examples being cholera, typhoid, polio, rabies and influenza) are inactivated completely by chemicals or heat, rendering them incapable of microbial replication. Live-attenuated vaccines are mainly viral and bacterial vaccines, which remain at least partially capable of replication within the host, but are rendered avirulent. Examples are measles, mumps, rubella, varicella zoster (chickenpox), yellow fever and Bacillus Calmette-Guérin (BCG) of *Mycobacterium bovis*, the only currently licensed vaccine against tuberculosis. Whilst highly immunogenic and a close mimic of natural infection, a major concern with the deployment of inactivated or killed vaccines is the risk of incomplete inactivation or attenuation, or a reversion to virulence (8). Additionally, extreme caution must be used when administering to the immuno-compromised such as HIV+ individuals or those on immunosuppressive therapies, whose ability to control viral replication is limited.

1.1.2.2 Subunit vaccines

In addition to the risk of virulence, the production of whole organism vaccines in cell culture is resource-costly, and some organisms have proved difficult to propagate *in vitro*. The development of recombinant protein expression techniques has enabled the identification and propagation of target antigens within organisms, selected because of their prominent role in the pathogen's sustained existence within the host, or known antigenicity. Guided by advances in genomics, the identification of B and T cell epitopes within antigens has allowed further selective targeting of immunodominant and protective components of an organism's proteome.

A challenge for protein-based subunit vaccines is in the precise mimicking of the tertiary structure of the native protein to ensure recognition of antigen by B cells and induction of high-affinity antibodies. Most protein antigens are poorly immunogenic without adjuvants, and owing to the fact that classical theory states that exogenous antigens are taken up by dendritic cells (DC) into the exogenous processing pathway and presented to CD4+ T cells within the context of MHC class II, MHC I-mediated CD8+ T cell immunity is rarely elicited[1]. Cellular immune induction can be improved by formulation as a particle (such as HPV and HBV VLP, virosomes and the experimental malaria vaccine RTS,S/AS01E).

VLP vaccines, such as the self-assembling Hepatitis B Virus (HBV) surface antigen (Engerix®, GSK) and the L1 major capsid protein of HPV (Gardasil®, Merck/Cervarix®, GSK) maximise the immunostimulatory nature of particulate viruses without the associated virulence risks. Since no viral DNA is contained within

[1] However, exogenous antigens may also be cross-presented within the context of class I MHC to activate CD8+ T cells in a phenomenon termed 'cross presentation', to be discussed in 1.2.1.

VLP, they do not replicate. However, VLP vaccines still require an adjuvant for optimal immunogenicity.

1.1.2.3 Plasmid DNA vaccines

In the early 1990s it was demonstrated that immunisation with a bacterial plasmid expressing a foreign antigen under an appropriate promoter results in host cell-facilitated antigen expression and protective antigen-specific cytotoxic T lymphocytes (CTL) (9). Plasmid vectors have high physical stability, though efficient uptake or transfection of cells is essential for the expression of the antigen and presentation with Major Histocompatability Complexes (MHC). To facilitate this, accurate targeting of sites replete in professional antigen-presenting cells (pAPC), such as the skin, is beneficial. DNA-based vaccines have proved poorly immunogenic in larger animals and humans, despite using over 1000-fold doses of DNA that had proved to be effective in rodent models (10). Efforts to improve their potency and APC transfection by high velocity delivery by gene gun have also met with limited success in pre-clinical models though in prime-boost combination with viral vectors they have yielded greater efficacy (section 1.6.5).

1.1.2.4 Recombinant viral vector vaccines

As potent stimulators of both humoral and cellular immunity, viruses have received considerable attention for development of vaccines (11). Viruses have evolved to take advantage of host protein synthesis machinery for viral protein expression and self-assembly of new particles. Their ability to directly infect professional and non-professional APC mediates the induction of both CD8+ and CD4+ cellular responses, without the requirement for adjuvants. The efficient uptake of antigen by APC is a crucial step in the initiation of a strong immune response. Size plays an important role in this process, with macrophages primarily taking up particles of size >1μm and DC are more efficient within the size range 20–100nm, the size range of most viruses. (12). VLP vaccines, immunostimulatory complexes (ISCOMs) and synthetic nanoparticle vaccines are also of similar particle size. Several studies have pinpointed the optimal size for DC uptake to be 40-50nm (the diameter of an Adenoviral capsid) for induction of antibody and CD8+ T cells in mice following immunisation with a range of Ag-conjugated nanobeads (13-15). Viral components (including those from Adenovirus and MVA) initiate intracellular signalling via surface and cytosolic Pathogen Recognition Receptors (PRR) including Toll-Like Receptors (commonly known as TLR), NOD-like receptors and RIG-1-like receptors to enhance activation and recruitment of APC to orchestrate the immune response(12).

Advances in cell culture and genetic engineering have allowed appropriate attenuation and insertion of exogenous transgenes into the viral genome of vectors including Adenoviruses and Poxviruses (section 1.6.5), resulting in host cell expression of protein antigens from malaria, TB, HIV and influenza amongst others and have entered clinical assessment (11, 16). The first licensed viral vector vaccinefor human use, IMOJEV® (Sanofi Pasteur)- a flavivirus-vectored vaccine against Japanese encephalitis - entered the market in 2010 (17).

1.2 IMMUNOLOGICAL BASIS OF VACCINATION

A vaccine of any design will only be successful if able to elicit responses at least equivalent to those induced by natural infection and if those responses are sufficient to inhibit the pathogen's persistence in the host. The objective of vaccination on an individual level is the accumulation of pathogen-specific immunological memory with which to fight future infection, thus conferring population-wide protective effects in decreasing the in-host presence in a community. This concept, known as 'herd immunity', underlies the public health rationale for vaccination and is dependent on a significant proportion of individuals in a population (~80%) generating adequate immunological memory to ensure a measure of protection for individuals insufficiently protected, or unimmunised by reducing the force of infection (18).

1.2.1 The initiation of an innate immune response

The classical 'self/non-self discrimination' theory of the immune system, held since the 1950s was brought under question during the 1980s due to the observation that lymphocytes themselves were not sufficient to initiate the immune response to an antigen, but that the APC was required as an intermediary. Additionally, APC themselves are critically dependent upon mobilisation by other mechanisms of the innate immune system. In 1989, Janeway proposed that evolutionarily conserved molecular patterns (PAMPs) present on microorganisms, and their subsequent recognition by and signalling through cell surface and cytosolic PRRs, determined whether a response was mounted, or not (19). In 1994, Matzinger proposed a more dynamic 'danger model', whereby host cell-derived endogenous mediators released upon non-programmed cell death (though not during programmed apoptosis) or the effects of physical stress or trauma (20). These cellular products, more recently termed 'alarmins' include defensins, cathelicidin, heat shock proteins, uric acid, IL-33, High-Mobility Group Box protein-1 (HMGB-1)(21, 22). This classic alarmin signals through PRRs such as TLR-2, TLR4 and the Receptor for Advanced Glycation End products (RAGE) resulting in downstream DC maturation and pro-inflammatory cytokine release (21, 23). Whilst these models have caveats (for example, the danger model is yet to explain why the immune system responds to different tissues in different ways), the role of the innate immune system in orchestrating the response to infection is now well accepted as a cornerstone of immunology.

Immediately after a microorganism breaches the epithelial barrier and gains entry to the body (or an antigen is intentionally introduced as a vaccine), a non-specific innate response is mounted at the site of infection. This acts to limit the response during the time required for the expansion of more potent antigen-specific immunity and to activate the immune system via danger signals (described above) and PAMP motifs, including viral nucleic acids, with PRR such as those of the TLR superfamily. These receptors are expressed on the surface of a range of cells of the immune system including DC, tissue-resident macrophages, endothelial cells or fibroblasts. Ligand engagement of PRRs result in signaling mechanisms and downstream transcription of genes coding for inflammatory cytokines such as IL-1, IL-6, type I

IFNs and TNF-α, which act both directly against the invading pathogen and also to conduct the early innate response. Importantly, this early inflammatory response facilitates two essential processes for the expansion of a full response: (1) the up-regulation of maturation factors on DC (and those mediating their migration to the draining lymph node, LN); and (2) attraction of additional populations of APC into the inflamed site from the circulation to bolster the tissue-resident populations.

APC can be directly infected by a live organism such as a virus, which results in endogenous antigen processing by the MHC class I molecule route allowing priming of CD8+ T cells in the LN (by pAPC) or in prolonged or secondary infection for the identification of antigen-bearing MHC I+ cells for direct killing by CTL. Antigens present within the binding-groove of an MHC I molecule are ~8-10αα in length, the products of cytosolic ubiquitin-directed proteosomal degradation. This process is termed 'direct presentation', and results in direct priming of CD8+ T cells. Priming of CD4+ T cells by pAPC only occurs by phagocytosis of exogenous antigen (e.g. bacterial products) and internalisation within lysosomes for complexing with MHC class II and subsequent export to the cell surface for later interaction with CD4+ T cells in secondary lymphoid organs. A second mechanism for priming of CD8+ T cells has been documented, whereby exogenous antigen (released in the form of apoptotic bodies following expiration of infected cells) is taken up by DC and enters the exogenous pathway, before escaping the lysosome and proceeding through the endogenous TAP-dependent pathway to result in presentation within the context of MHC I (24). This phenomenon, termed 'cross presentation', is the subject of much recent research attention due to the ability to retain strong antigen-presenting function without compromising cellular viability through cytopathic effects of direct infection. Accordingly, cross priming is a significant mechanism of immunity against viruses that either cannot infect APC, or have cytopathic or immunomodulatory effects upon DC post-infection, such as poxviruses(25-27).

Migration of tissue-resident DC is associated with down-regulation of anchoring molecules such as LFA-1/ICAM-1 and up-regulation of chemotactic molecules such as CCR7 to allow migration to secondary lymphoid organs and access to the paracortex and T cell zones. For successful interaction with naïve T cells in the LN, DC must undergo a process of maturation characterised by cell-surface expression of co-stimulatory molecules such as CD80/86 concurrently with the export of peptide-MHC to the cell surface for TCR interaction, stabilised by CD3 and CD4/CD8 on the T cell surface. After cell-cell engagement, confirmatory signals are delivered via CD28-CD80/86 interaction for the T cell to undergo clonal expansion, directed by the growth factor IL-2.

1.2.2 Components of the adaptive immune system

1.2.2.1 CD8+ T cells / Cytotoxic T lymphocytes (CTL)

Following clonal expansion initiated by TCR recognition of cognate antigen within the context of class I MHC, antigen-specific effector CD8+ T cells exit the LN by down-regulating LN chemotactic factors such as CCR7, and CD62L and S1PR (in the mouse). These activated CD8+ CTL enter the periphery and home to inflamed

tissues to undertake killing of infected cells exhibiting cognate antigen-MHC I complexes by way of direct cytotoxicity (secretion of perforins/grazymes or Fas-ligand directed apoptosis) or through the production of molecular mediators that undertake direct killing of infected cells, such as IFN-γ and TNF-α.

1.2.2.2 CD4+ T cell / Th

Antigen-specific CD4+ ('T helper') cells are a heterogeneous subset of T cells that may be sub-divided due to their cytokine production and role in assisting the induction of B and CD8+ T cell responses. CD4+ T cells recognise antigen within the context of MHC II. Th1 cells characteristically secrete IFN-γ and IL-2, which mediates T cell proliferation and maintenance (via further activation of DC) of CD8+ T cell responses. Th1 also assist with the activation of B cells that have antigen-complexed BCRs (through CD40/40L interaction) and in the process of antibody isotype switching. Th2 responses are significant in the response against intestinal helminths and in allergy, through secretion of IL-4, IL-5, IL-6, IL-10 and IL-13. A third subtype, Th17 - so called because the main effector molecule that characterises this response is IL-17 may be important in the response against intracellular infections such as *M. tuberculosis*(28).

An alternative differentiation pathway for TGF-□induced $CD4^+$ T cells is the regulatory pathway. T_{reg} cells are defined by the expression of CD4+ and high constitutive expression of CD25 and FoxP3.They characteristically secrete the regulatory cytokines IL-10 and TGF-β, and thus exert an immunosuppressive effect upon immune responses to regulate immunopathology caused by an excess of effector function. T_{reg} also play an integral role in the maintenance of peripheral self-tolerance. However, due to their broad-scale regulation of Th1 and CD8+ T cell responses, in the case of persistent infection they may act to facilitate pathogen survival by curtailing potentially protective responses and so are undesirable within the context of vaccination.

1.2.2.3 B cells

B cells bind linear or conformational antigens specific for their surface immunoglobulin/BCR in the circulation before presentation on MHC class II to CD4+ T cells for help. B cell activation occurs in the germinal centres of the LN, where CD4+ T cells facilitate BCR clustering and ligation of CD40 by CD40L present on the activated CD4+ T cell. Clonal expansion of B cells initiates secretion of specific IgM, before Th-facilitated isotype switching to IgG, IgE or IgA. Antibody-secreting cells or plasma cells, migrate to the periphery to perform their function, whilst a subset of activated B cells remain in the germinal centre to undergo affinity maturation to further refine response specificity. These cells become long-lived high-affinity antibody-secreting plasma cells or memory B cells, which remain in lymphoid tissues primed for rapid proliferation upon antigen re-exposure.

1.2.3 Immunological memory

Following the clonal expansion and dissemination of an antigen-specific effector T cells, 90-95% die by apoptosis in a programmed contraction phase beginning about 7-10 days following response initiation (29). The proportion remaining after this contraction of the response have the ability to survive for prolonged periods in the absence of antigen, being maintained by homeostatic cytokines including IL-7 and IL-15. They re-activate upon subsequent exposure, to mediate a protective response against the pathogen. Factors influencing the magnitude and specific composition of the stable memory T cell pool are present at the priming, expansion and contraction phases, and survival is associated with the acquisition of a phenotype characteristic of memory cells (Table 1-2).

1.2.4 Central and effector memory

Qualitative, as well as quantitative aspects of the surviving T cell memory pool are important to consider in achieving optimal immunological memory by vaccination. Sallusto *et al* were the first to consider that the human CD8+ T cell memory compartment is heterogeneous, and proposed two subsets based on the expression of CCR7, or lack thereof, with differing effector functions and LN homing potential. These subsets were defined as central memory (T_{CM}) and effector memory (T_{EM}) (30). The main features of T_{CM} and $T_{EM,}$ and T_E (activated effector T cells) compared to naïve T cells are given in Table 1-2.

T_{EM} arise shortly after the contraction phase and are characterised by retention of effector function such as IFN-γ and perforin secretion, but are poorly responsive to antigen re-exposure. T_{CM} are established later during the course of infection and have good proliferative capacity, but poor effector function. Due to the expression of CCR7 and CD62L T_{CM} may gain access to the lymphoid organs where they reside following resolution of infection for many years, acting as a reservoir of T cell memory. T_{EM} instead gain access to the circulation and home to peripheral tissues where they are ideally situated for rapid re-activation upon antigenic re-encounter. This division of labour within the memory response is thought to have evolved since it is neither resource-effective nor safe to maintain circulating populations of highly alert, functional T cells for prolonged periods of time. T_{EM} constitute a first line of defence in peripheral tissues whilst allowing T_{CM} time to vigourously proliferate in response to antigen and subsequently exit the LN to replenish T_{EM} in inflamed tissues (31, 32).

CD8+ T cell subset	T_{CM}	T_{EM}	T_E	Naïve T cell
Appearance during response	Late	Early	Immediate	N/A
Proliferative capacity on re-stimulation	High	Low	N/A	N/A

Effector function	Low	High	High	None
Homing potential	Lymphoid	Peripheral	Circulatory + inflamed tissues	Circulatory + Lymphoid
Phenotype:				
CD62L	+	-	-	+
CCR7	+	-	-	+
CD127	+	+	-	-
CD43	-	-	+	-
CD27	+	+	-	-
CD44	+	+	-	-
IFN-γ	-	+/-	lo	-
IL-2	+	lo	+	-

TABLE 1-2: Attributes and phenotypes of CD8+ T cell subsets arising following expansion of an immune response.

Memory cells arise following antigen exposure and clonal expansion and persist following clearance of antigen. They have the ability to re-activate upon secondary antigen-exposure or in response to *in vitro* re-stimulation. T_{CM} have a greater proliferative capacity and have a phenotype enabling them to reside in secondary lymphoid organs (CD62L+ CCR7+). T_{EM} retain high effector function but have limited ability to proliferate. They are present in the circulation and seed peripheral tissues. Memory cells have up-regulated factors promoting survival, such as CD127, CD44 and CD27, whereas T_E are characterised by CD43. Effector cells circulate and home to inflamed tissues immediately following antigen experience before dying by apoptosis during the contraction phase.

1.2.4.1 Models of CD8+ memory differentiation

Based on the observation that T_{CM} arise some time after T_{EM} during a response, one line of thought for the generation of memory T cell subsets proposes T_{EM} convert into T_{CM} following several cell divisions, dependent on the clearance of antigen (33). This 'linear hypothesis' is contested by the 'parallel hypothesis' whereby the fate of a precursor memory cell is decided upon priming (or after some time as an uncommitted intermediate (32)) influenced by the strength of antigen stimulus (Figure 1-1)(34, 35). A stronger or more persistent stimulus is proposed to favour T_{EM} and a weaker stimulus with rapid antigen clearance favours T_{CM}, with either extreme resulting in loss of function and eventual deletion. Recently, it has been proposed that the inflammatory microenvironment at the time of priming has marked effects upon both the generation of memory T cells (36-38), further described in Chapter 4.

A

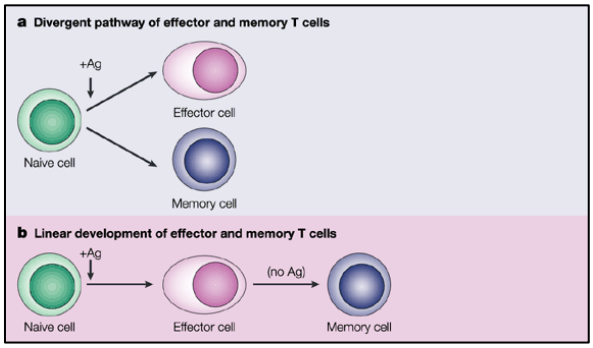

B

Kaech *et al* (2002) Nat. Rev. Immunol. 2:251-262

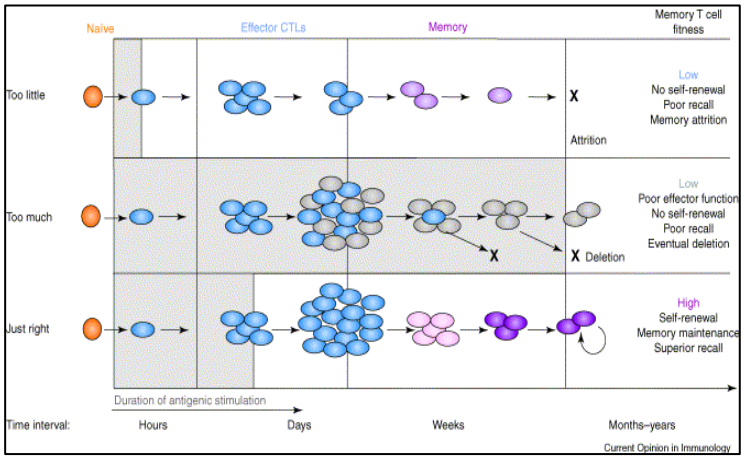

Masopaust *et al* (2004) Immunol. Res. 29(1-3):151-

FIGURE 1-1: Models of memory CD8+ T cell differentiation.

A = adapted from (39). B = from (40). The 'linear hypothesis' proposes that memory cells arise from T_E during the progression of an immune response and following clearance of antigen from the system. The 'parallel hypothesis' proposes that the fate of a memory cell is programmed at the time of priming by various factors including strength or duration of antigenic stimulus (the 'Goldilocks model' – B), the nature of the APC or the inflammatory microenvironment at the time of priming.

1.3 VACCINE DELIVERY INTO THE SKIN

1.3.1 Routes of vaccine delivery to humans

Most existing vaccinations are given into the muscle (IM) or subcutaneous (SCu) tissue using a needle and syringe for ease of technique and flexibility to deliver large volumes. There is considerable research interest in mucosal vaccines as they are simple to administer without the use of needles, and hold promise for enhanced local responses against pathogens utilising this route of entry (41). However, bioavailability is poor due to the altered pH of mucosal tracts and presence of proteolytic enzymes. Experimental cancer vaccines have been given intravenously but this route has serious safety issues and is impractical on a large scale. Only two currently licensed vaccines – cell-cultured rabies vaccine and BCG are given intradermally (ID) using the Mantoux technique (inserting a standard gauge needle at a very shallow angle with the bevel up, creating a raised bleb upon fluid infusion). Edward Jenner's scarification method would be later adapted for mass immunisation during the smallpox eradication campaign, where replication-competent Vaccinia and latterly MVA were delivered using a small-bifurcated needle device to breach the outer *stratum corneum* (SC) delivering a small amount of liquid vaccine into the skin (42)(Figure 1-2). Whilst this transcutaneous method was rapid and efficacious, it offered little control over dose delivery or deposition depth. Reactogenicity was also common at the site of Vaccinia immunisation due to the pathology caused by a combination of epidermal injury and viral replication (43, 44).

Image removed for copyright reasons.

Can be accessed from WHO website:

http://www.who.int/mediacentre/factsheets/smallpox/en/

FIGURE 1-2: The scarification method of smallpox immunisation.

This method was used throughout the smallpox eradication campaign of the 1960-70s due to its simplicity and high throughput. The two-pronged device (developed by Benjamin A. Rubin) was dipped into inoculum to allow a droplet of vaccine to be drawn into the space between the two prongs by capillary action (approx. 2μL). The needle is held at 90° to the deltoid of the arm and scratched into the skin until a droplet of blood is observed. This method was effective at inducing immunity against smallpox, though local reactogenicity was severe. Image from (45).

Since the replication-attenuated viral vector MVA is derived from Vaccinia, in recent clinical trials of MVA-vectored vaccines against malaria, TB, and influenza, vaccines have been given intradermally by needle (46-49). Clinical studies comparing ID, IM and SCu routes of delivery of MVA demonstrated equivalent levels of neutralising antibody and protection against Vaccinia challenge after ID immunisation with only $1/10^{th}$ of the dose delivered by other routes, suggesting a beneficial effect of the ID route for improved immunogenicity with lower doses of vaccine (50, 51).

1.3.2 Intradermal immunisation and dose-sparing

Conventional immunisation routes often bypass immunologically sensitive sites such as the viable epidermis (VE) and dermis of the skin, which offer attractive prospects for efficient induction of immunity with a lower dose of vaccine. This is due to the extensive network of resident APC, of which there is a relative paucity in muscle or subcutaneous tissue (52, 53). A number of studies comparing ID immunisation of existing vaccines with other routes have proposed a 'dose-sparing' effect of delivering antigen into the skin, i.e. a significantly reduced dose of vaccine is required for equivalent immunogenicity as compared to other routes. These observations have implications for preparedness in the face of a pandemic such as influenza, where manufacturing capacity is stretched to meet demand for vaccine. Dose-sparing translates to a lower cost per vaccination, which is a significant consideration for the distribution of a malaria vaccine to target populations in low-income countries or in bringing to market expensive new-generation vaccines. In a review of 90 clinical trials of existing vaccines, seasonal influenza vaccines demonstrated the greatest dose-sparing effect when delivered ID, with levels of immunogenicity comparable to IM immunisation with as little as 23% of the vaccine dose (54). However, the Mantoux method is technically difficult, and as such successful ID immunisation is highly dependent upon vaccinator expertise. Full exploitation of the immunogenic potential of the skin for vaccination is therefore dependent upon the development of a simpler intradermal delivery method.

1.3.3 Cutaneous immunological mechanisms

Positioned at the host-environment interface, the skin has a vital role in immune surveillance and has evolved a plethora of tightly-regulated defence mechanisms to protect against opportunistic microorganisms. The importance of the strict maintenance of an intact immunological barrier in the skin is most evident in its dysregulation in immunocompromised states such as those caused by acquired or genetic immunodeficiencies resulting in cutaneous malignancies (55). The skin's immune repertoire comprises not only a response to an infectious pathogen, but also in regulation of innocuous and self-antigen, which is acquired and processed by cutaneous DC and presented to naïve T cells in the skin-draining LN in the absence of co-stimulation, resulting in T cell anergy and tolerance. Where this fine balance is upset and inappropriate responses are launched in response to antigens that pose no threat, clinical consequences such as atopic dermatitis and psoriasis occur.

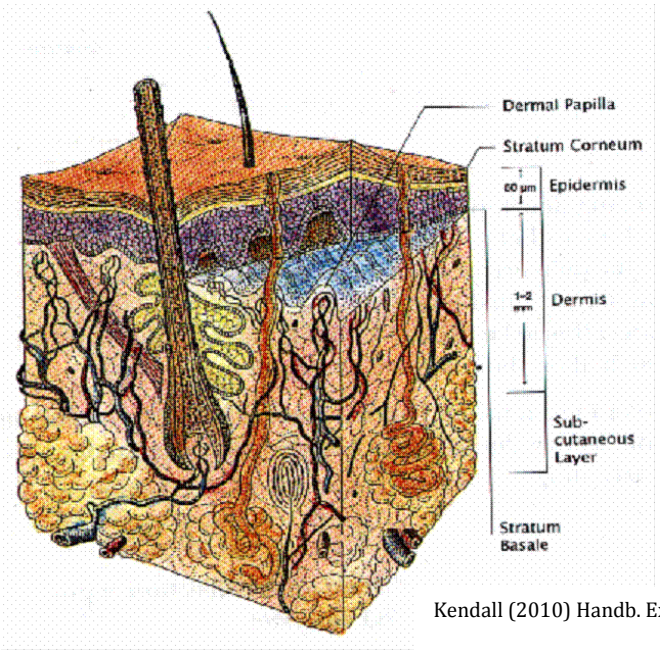

Kendall (2010) Handb. Exp. Pharmacol. 197:193-219

FIGURE 1-3: The anatomy of mammalian skin.

The outermost *stratum corneum* (SC) is a keratinised layer of dead and dying anuclear cells nearing the end of the sloughing pathway, and is continually replenished from cells of the underlying strata roughly every 2 weeks. The thickness of the SC varies significantly between, and within species, and even between different anatomical sites (in a human ranging from 40µm on the heel to 10µm on the eyelid). As the SC does not contain metabolically active cells, it does not play a role in the immunological response. The strata of the underlying viable epidermis or VE (namely the *stratum granulosum, spinosum and basale*) contain keratinocytes (95%), melanocytes, Merkel's cells (involved in touch sensation) and Langerhans cells (2% of cells, 20% of surface area) and dendritic epidermal γδ T cells. The dermis is composed of collagen fibres and bundles and is divided into the papillary dermis (involved in the metabolic and thermal regulation of the epidermis, since it does not have its own blood supply) and the underlying reticular dermis. The dermis contains intraepithelial lymphocytes, mast cells, dermal DCs, Langarin+ dermal DCs, macrophages, fibroblasts (most abundant), and also dermal capillaries and lymphatic vessels. Image from (56).

The response to cutaneous infection is mediated by several cell types in the VE and dermis (Figure 1-3) including a heterogeneous dendritic cell population (section 1.3.4). Following the introduction of an immunological insult via breaching of the SC, innate defense mechanisms are immediately engaged in the underlying layers. In response to various stimuli including physical trauma, epidermal keratinocytes and Langerhans Cells (LC), together with DC, mast cells and macrophages of the dermis, release stored anti-microbial peptides (55, 57). As a result of TLR signaling by epidermal and dermal cells, many products involved in the inflammatory response are synthesised, including IL-1α and TNF-α by keratinocytes. These cytokines have a number of important effects, and can augment each other in the promotion of local innate activation. Keratinocytes, often termed 'bystander' cells due to their position in orchestrating the early skin immune response without a direct role, have highly

significant immune function. Their products induce Th and B cell activation and clonal expansion, enhance Natural Killer (NK) cell activity, activate immature DC and are chemotactic for a number of infiltrating cell types including neutrophils and macrophages(55, 58). Interestingly, they can be induced to express MHC II molecules by IFN-γ *in vitro*, raising the question of whether have the ability to act as APC under inflammatory conditions (59, 60). Keratinocytes also act as 'suicide antigen reservoirs' following viral infection, providing intracellular antigen via apoptotic bodies for cross priming by DC. Keratinocytes also regulate immune function in the steady state, secreting the anti-inflammatory mediators TGF-β and IL-10. Activated dermal mast cells secrete a range of pro-inflammatory cytokines, which have both local and distal effects, in attracting in the second line of defence from the circulation. Neutrophils, NK cells, granulocytes and antigen-specific memory T cells exit post-capillary venules and enter epithelial tissue by rolling, adhesion and diapodesis processes mediated by the cellular adhesion molecules E-selectin, P-selectin, ICAM-1 and VCAM-1(55).

Under direct regulation of this innate response, resident LC of the VE and DC of the dermis mature and endocytose antigen, whilst up-regulating expression of MHC II and co-stimulatory molecules. LC retract their dendrites, detaching themselves from neighboring keratinocytes, for migration to the proximal LN to present antigen within the context of class I or class II MHC to cells with cognate TCRs, initiating expansion of an antigen-specific response. DC entering the cutaneous environment as part of the inflammatory infiltrate, such as plasmacytoid DC and monocyte-derived ('mono'-) DC will encounter a highly inductive cytokine milieu, encouraging their subsequent antigenic uptake, and migration to proximal LNs to augment antigen presentation by skin-migratory DC(55).

An interesting feature of the skin immune response is the 'cross-talk' between cutaneous and mucosal tissue, resulting from homology in the evolution of skin-associated and mucosa-associated compartmentalised immune systems. This is evidenced by sharing of homing molecules such as CD103 (integrin αE) between skin-homing and mucosal homing T cells, and the detection of antigen-specific immune responses in mucosal tissues following transcutaneous immunisation (61-64). Antigen-bearing CD11c+ DC were detected in Peyer's patches following transcutaneous immunisation with HIV peptide, able to activate TCR-specific T cells *in vitro*, suggesting that cutaneous-mucosal communication not only occurs with respect to primed T cells and humoral responses, but also DC. These DC were associated with protection against mucosal HIV challenge, perhaps suggesting a mechanism for the ability of transcutaneous and microneedle immunisation to protect against mucosal pathogens such as influenza (section 1.5.2) (65, 66).

1.3.4 Cutaneous dendritic cells

DC are instrumental mediators of adaptive responses and as such are a critical consideration for the rational design and delivery of vaccines (67). The epidermal Langerhans cell, LC (CD11b+ CD207+) was the first DC to be identified by Paul Langerhans in 1868, though they were initially mistaken for neurons due to their extended dendrites(68). One hundred and seventeen years later, LC were

recognised as cells of the immune system with potent immunostimulatory function *in vitro* by Schluer and Steinmann, who compared them to splenic DC, first described only 12 years earlier (69-71).The 'Langerhans cell paradigm' was proposed to describe three key attributes of LC (at the time, used as a model for all DC): (1) Immature LC reside in the periphery in the steady state and are highly-specialised for antigen uptake; (2) LC transport to skin-draining LN is essential for cognate TCR interaction, characterised by a switch from E-cadherin adhesion to CCR7 chemotaxis and is mediated by pathogen and inflammatory products; (3) During migration, LC undergomaturation during which time theyprocess acquired antigen and present it as complexed with MHC class I/II, and up-regulate co-stimulatory factors and cytokines required for T cell instruction (72, 73). This paradigm was extended to include a tolerogenic role for LC in the steady state (in the absence of activating stimuli or acquisition of co-stimulation) to present epidermal self-antigens to auto-reactive T cells for their subsequent elimination, renewing from local precursors(74).

However, observations using the HSV model of skin-adaptive immunity suggest that the LC paradigm may need to be re-addressed. After cutaneous HSV infection, LC were found not to be responsible for priming of CTL but rather 'shuttled' antigen to the LN, where they transferred antigenic cargo to CD8α+ lymphoid-derived DC for presentation to CTL (75, 76). However, as HSV infection is lytic and known to induce DC apoptosis, LC may not have acted as functional APC within this context as apoptotic bodies may travel as free antigen through the lymphatics - using a non-lytic viral model, antigen was presented by skin-derived, and not CD8α+ DC (77). Elsewhere, LCs were found to be dispensable for presentation of antigens to T cells in *L. major* infection and were associated with the induction of T_{reg}, whereas dermal interstitial (dDC; CD11b+ CD207-) DC were important (78). Langerin+ dermal DC, (L+dDC; $CD11b^{lo}$ CD207+ CD103+, which are distinct from LC (79-81)) have been implicated in cross presentation of viral antigen to CTL (82). LC have also been implicated in the cross presentation of antigen from neighbouring keratinocytes, and are proposed to preferentially induce cellular, over humoral, immune responses (83, 84). Whilst specific roles are unclear, the skin and skin-draining LN possess a plethora of DC subtypes ideally placed for trancutaneously-delivered vaccine uptake.

1.4 NEEDLE-FREE IMMUNISATION

1.4.1 The urgent need for alternatives to needle injection

Standard hypodermic syringes are simple and inexpensive to manufacture on a large scale by plastic injection-moulding, costing as little as $0.02 USD per unit. Most injections can be given quickly and simply with high throughput, and with high accuracy if performed correctly. However, the disadvantages of needle injection are numerous as detailed below.

1.4.1.1 Blood-borne disease transmission

Needles carry an associated risk of transmission of blood-borne infections such as HBV, HCV and HIV from inappropriate disposal and re-use. Globally, an estimated

21 million HBV, 2 million HCV and 230,000 HIV infectionsand 1.3 million deaths per year result from unsafe injections following intentional recycling of syringes by healthcare professionals in poorly resourced settings or by untrained practicioners, particularly in low-income countries (85-87). The WHO estimate that unsafe injection practices account for 28% of liver cancer, 24% of cirrhosis and 5% of all HIV infections worldwide (88). Needle-stick injury and re-use by illicit drug users are also causes of needle-associated disease transmission (89, 90). So great is the burden that in their announcement of their $200 million USD research initiative, the Bill and Melinda Gates Foundation prioritised the '*development of needle-free delivery systems for vaccines*' as one of their 14 Grand Challenges in Global Health (91).

1.4.1.2 Associated costs

In addition to the costs of adequate disposal of needles to avoid inappropriate re-use, costs to healthcare systems include proper training of vaccine administrators (particularly for technically difficult routes) and refrigerated storage of temperature-labile vaccines(92). For ease of distribution, existing vaccines are lyophilised for reconstitution immediately before injection. However, lyophilised vaccines must still be stored between 4-8°C and lose potency rapidly upon reconstitution(93). A network of tightly controlled refrigeration facilities (or a 'cold chain') must be guaranteed for optimal vaccine safety and potency from manufacture to immunisation(94). Maintenance of an uninterrupted cold chain is estimated to account for 14% of an immunisation campaign's total expenditure, and its complete eradication is estimated to make an annual global saving of $200 million USD (92, 94). Costs to the individual also include travel to immunisation clinics, identified as a significant influence upon vaccination uptake and compliance in developing countries with poor transport infrastructure (95).

1.4.1.3 Poor acceptability

Needle injections are associated with pain and fear, particularly in children. Distress caused by needles was proposed as one of the main contributors to reduced parental compliance and incomplete coverage in a paediatric vaccine programme in the US (96). Fear of needles, or belonophobia, also affects 3.5-10% of adult populations, manifesting as extreme anxiety, nausea and possible fainting (97, 98). Twenty percent of UK adults not having received 3 routinely given vaccines cited needle aversion as the reason (99). Thus, poor acceptability of needle-based immunisation has significant detrimental effects upon maintenance of herd immunity.

1.4.2 Needle-free cutaneous immunisation

In response to the drawbacks of conventional needle delivery of vaccines, research effort has been focused upon development of simple, needle-free methods. The skin has been a major target for needle-free vaccine delivery due to its ease of access and potential for inducing potent systemic immune responses with lower doses of vaccine (section 1.3.2). The major barrier to cutaneous vaccine delivery to the APC-rich epidermis and dermis is the highly cornified tough physical barrier of the SC, which limits passive diffusion to molecules <500Da(100). Hence, cutaneous immunisation with large molecules has only been made possible by numerous methods such as kinetic energy (liquid jet injection and biolistic 'gene gun' methods)

(Figure 1-6, A+C) or less-invasive methods to overcome this barrier and increase its permeability. A summary of approaches is given in Figure 1-4 and evaluated in Table 1-3.

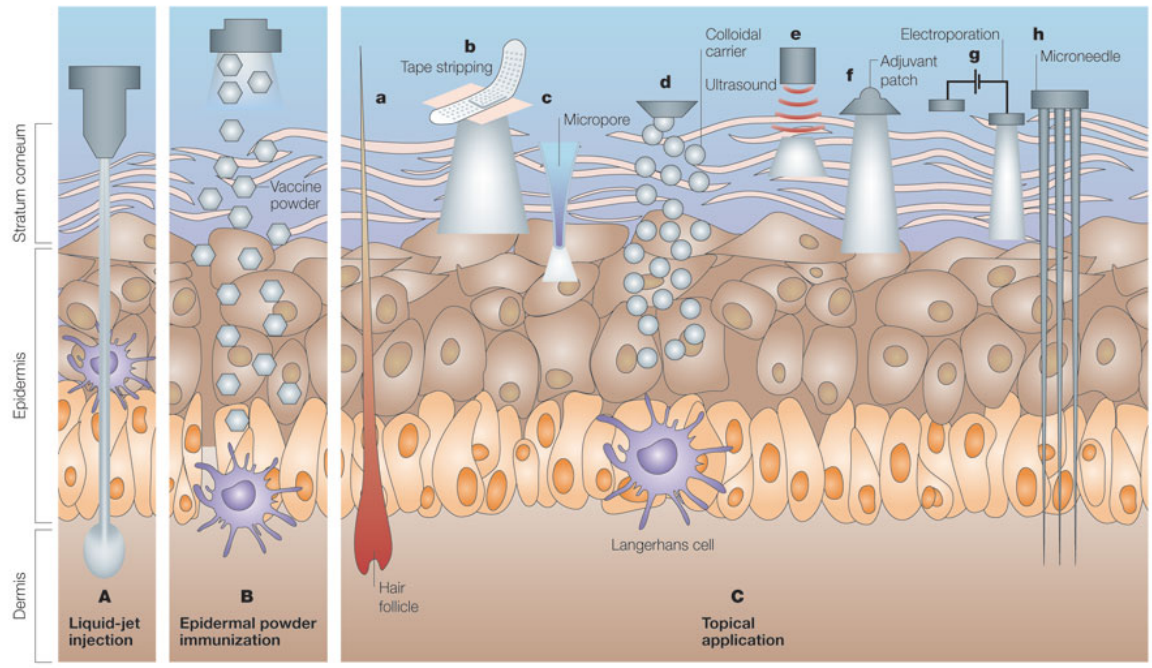

Mitragotri (2005) Nat. Rev. Immunol. 5(12):905-916

FIGURE 1-4: Proposed methods for the transcutaneous delivery of vaccines by overcoming the *stratum corneum*.

From Mitragotri (101). (A) Liquid jet injection uses kinetic energy to propel liquid through the SC and into the cutaneous tissue. (B) Epidermal Powdered Immunisation (EPI) is performed by gene gun, where powdered vaccine particles are accelerated towards the skin at high velocities using a helium propellant. (C) Topical application of vaccine to the skin can be performed in many ways: (a) through hair follicles (usually following tape-stripping) (b) tape-stripping to remove corneocytes (c) microporation using thermal energy (d) as complexed within a colloidal carrier (e) using 'cavitation' methods to create channels through the SC by ultrasound (f) as a topically applied patch + adjuvant (g) electroporation and, (h) by creation of microchannels by microneedles.

In its simplest and least invasive form, trancutaneous immunisation (TCI – Figure 1-4C) involves the application of liquid vaccine onto the skin and application of an occulsive patch or a vaccine-imbibed patch, for passive diffusion of vaccine. The first group to describe successful TCI made use of small molecule bacterial ADP-ribosylating exotoxins including cholera toxin; CT, and *E.coli* heat-labile enterotoxin; LT. These molecules convey potent adjuvanticity but also stimulate the production of anti-CT and anti-LT antibody after TCI - the former being protective against intranasal CT challenge. (63, 102) This demonstration preceded the co-administration of these molecules with other antigens including those from influenza and rotavirus, demonstrating antigen-specific humoral immunity (103, 104). CT co-administed with recombinant OVA induced a CTL response, concurrent with a migration of CD11c+ $CD40^{hi}$ DC that had taken up a topically applied fluorescent dye, into the skin-draining lymph node (105). Administering an LT adjuvant patch

alongside influenza vaccination in states of immunosenesence was found to boost vaccine-induced responses in aged mice and humans (106, 107). This group (IOMAI, now Intercell) was the first to progress a trancutaneous patch to clinical trials with phase II/III trials of an LT enterotoxin vaccine patch against traveller's diarrhoea in South America, though these trials were discontinued due to failure to meet endpoints.

Several methods to enhance the permeability of the skin have been described, all of which have been found to decrease SC barrier function and/or improve responses following TCI as compared to intact skin:

1. *Abrasion/tape-stripping*. Temporary removal of the SC before application of vaccine a technique most often used alongside TCI but is likely to cause undesirable effects (irritation, inflammation e.g. TNF-α release from keratinocytes)(105, 108, 109).
2. *SC hydration/colloidal carriers*. Keratin has a high affinity for water and swelling of corneocytes after hydration mediates changes in lipid ultrastructure, increasing SC permeability (110). Antigen-encapsulated liposomes and transfersomes have been used for facilitated diffusion (111).
3. *Microporation/thermal ablation/laser ablation*. The focussing of thermal/laser energy through an electrically-heated element or laser beam creates a pores in the SC. Application of an Adenoviral vector to thermally-microporated skin resulted in 10-100 fold greater cellular and humoral responses (against a β-gal transgene) than intact skin (112).
4. *Iontophoresis/electroporation*. The application of an electric potential either continuously or in pulses to create pores in the SC through which charged particles (peptides, oligonucleotides) are actively drawn irrespective of concentration gradient (113, 114).
5. *Ultrasound/sonication*. Ultrasonic energy causes cavitation, or the formation of minute bubbles in the skin, which merge to form channels that remain open for up to 12 hours post-treatment, and also activates LC for reasons unclear (115, 116).
6. *Chemical disruption*. Penetration enhancers such as solvents and surfactants have been used to disrupt the hydrophobic lipid matrix within the SC, increasing permeability (117, 118).
7. *Microneedles* (section 1.5)

One of the proposed mechanisms for access through the SC after TCI is diffusion via hair follicles, with immediate access to perifollicular populations of LC. Following tape-stripping, follicular transport of a range of nanoparticles and their transport to draining LN was demonstrated, including 40nm and 200nm synthetic particles (the approximate size of Adenovirus and MVA respectively), protein, pDNA and MVA. Though only modest cellular responses were induced against MVA, these were shown to be partially protective against subsequent Vaccinia challenge (119). The method was demonstrated to be safe and immunogenic in delivery of inactivated influenza vaccine to humans, and preferentially induced multifunctional CD8+ effector T cells when compared to IM immunisation, lending support to the proposal that epidermal LC are inducers of cellular immunity (120).

Needle-free method	Advantages	Disadvantages	Examples	Stage of evaluation	Refs.
Liquid jet injection	• Rapid and high throughput • Excellent bioavailability • Minimal equipment other than multi-use injector (+single-use nozzles) • No special training req'd • No vaccine reformulation • 100% needle-free	• Pain • Reactogenicity • Cross-contamination (HBV) from 'splash-back' blood/tissue fluid when using multi-use devices - 'not recommended' by WHO due to risks of disease transmission • Compressed gas propellant req'd • Intimidating for children	Licensed vaccines incl. Hepatitis B	In clinic since 1950s used by US military and in mass vaccination campaigns. Available for routine vaccine delivery in US at physician's discretion.	Reviewed in (121)
Biolistics / gene gun (biocompatible metal particles /Epidermal Powdered Immunisation)	• Successful transfection of cells with naked plasmid vaccines • Completely needle-free • First technology to target the VE and LC specifically • Minimal training req'd	• Pain • Reactogenicity • Cellular damage and death (extremely high impact velocities) • Th2-type response bias • Intimidating for children • Gas propellant req'd • Formulation req'd (adsorbing onto particles/powdered particles) • High relative cost (equipment, reformulation etc.)	Powderject® (acquired by Chiron Corp., 2003. Acquired by Novartis, 2006) PowderMed® / acq. GSK, 2006	Pre-clinical	Reviewed in (122)
Transcutaneous Immunisation (TCI)	• Simple, easily distributable • Very low cost • No reformulation • Pain free • 100% needle-free • Boosting of existing immunity in the immunocompromised • Self-application feasible	• Limited to molecules under 500 Da unless pre-treatment used to overcome SC • Adjuvant is required (CT, LT) • Low efficiency unless combined with enhancement – increases complexity and cost (exception – tape-stripping+ MVA can be delivered via hair follicles, though modest immune responses - (119)) • Little control over dosing	IOMAI (acq.by Intercell 2008) Altea Therapeutics (GA, USA)– electroporation via metallic filaments on a patch	Clinical	(63, 102, 106, 107, 123-126)

Needle-free method		Advantages	Disadvantages	Examples	Stage of evaluation	Refs.
MICRONEEDLES	Single microneedle	• Epidermal/ dermal access controlled by length • No reformulation of vaccine • Efficient dose delivery • Potentially painless • Faster PK in delivering therapeautics	• Delivery by professional • Not entirely needle-free, sharps disposal req'd • Increased cold chain volume • Increased cost of device • Liquid vaccine – decreased stability	BD Soluvia™– INTANZA/IDflu®, influenza (split virion, pDNA, whole inactivated) and flavivirus vectored JE and anthrax vaccines	Complete (BD Soluvia™) Others - clinical	(127-130)
	Solid microneedle patch (liquid vaccine)	• Simple method • No reformulation of vaccine • Painless, non-intimidating • Small unit size • Needle-free	• Lower delivery efficiency than some methods • 2 step process – inc. risk of user error • Applicator may be required – inc. cost • No thermostability • Increased cold storage volume – patch + vial	Given in more detail in TABLE 1-4		
	Solid microneedle Patch (coated vaccine)	• Thermostbaility • Small unit size, easily distributable • Short wearing time • Painless, non-intimidating • Self-administration • Needle-free	• Reformulation – potential regulatory reassessment, cost • Lower delivery efficiency than some methods (though being improved) • Applicator may be necessary – inc. cost and distribution			
	Dissolvable biopolymer vaccine patch	• No clinical waste • Inexpensive to manufacture • Needle-free, painless • Short wearing time • Potential for composite vaccines and controlled/episodic release	• Polymer - lower compressivestrength than e.g. silicon, potential penetration inefficiency • Requirement to manufacture/heat-sterilise without using high temperatures (which compromise polymer integrity)			

	Hollow microneedle for liquid infusion	• Efficient dose delivery • Good for drug delivery – faster PK than needle method • No reformulation req'd	• Minimal wastage, high delivery efficiency • High mol. wt. or viscous substances can be delivered • Potential for lower patient compliance • Method difficult – professional required • Increased storage volume – patch + syringe + vial	

TABLE 1-3: An evaluation of methods for delivery vaccines through the skin.

A table summarising needle-free delivery methods designed to deliver drugs and vaccines through the skin, positive and negative attributes of each method, and examples of groups/companies undertaking pre-clinical/clinical evaluation. Further details about microneedle patch technologies are given in TABLE 1-4 below. JE = Japanese Encephalitis. PK= Pharmokinetics.

1.5 MICRONEEDLES

Microneedles physically penetrate the SC and create temporary conduits for the delivery of drugs and vaccines into the underlying epidermis and/or dermis. This non-invasive, user-friendly method is painless by virtue of the micron-scale needle length, such that they do not penetrate to depths sufficient to stimulate dermal nociceptors. The first microneedle systems were described in 1976 (131). Advances in microfabrication processes during the 1990s brought about the feasibility of microneedle mass-production from inexpensive materials such as silicon and stainless steel, chosen for their ease of manipulation, physical strength and biocompatibility. Now, many microneedle modalities are described, fabricated from such techniques as dry- and wet-etching of silicon, laser-cutting of steel and 2-photon polymerisation, casting, injection-moulding of polymer materials (reviewed in (132)). Microneedle patches are simple to apply without the need for training with the potential for self-application for optimal vaccine coverage. Microneedle-based strategies to date fall into two categories - those employing a single microneedle, and arrays of microneedles arranged on a patch, which are further subdivided into four modalities described in 1.5.2. Microneedle approaches are evaluated below and in Table 1-3.

1.5.1 Single microneedle devices

Single microneedle devices that have been developed for micro-injection include the BD Soluvia™, which is a prefilled 1.5mm long 30G intradermal needle designed to deliver 100-200μL fluid and is now commercially available for the delivery of trivalent influenza vaccine (INTANZA®/IDflu®, Sanofi-Pasteur). The injection system, which includes a plastic spacer to limit needle penetration to the epidermal or dermal layer, was determined easy to use and safe in clinical trials, and demonstrated accurate and reproducible antigen deposition in porcine skin (128, 133). Using a range of microneedle lengths, neutralising antibodies were raised against rabies vaccine after dermal (but not epidermal) micro-injection, reaching seroconversion with only 25% of the dose required IM (128). Whole inactivated, pDNA and split virion trivalent influenza vaccine delivery by BD Soluvia™ demonstrated 100-fold dose-sparing with H1N1 strain trivalent vaccine and 5-fold dose-sparing of pDNA vaccine, (though only after multiple administrations) when comparing serum anti-HA responses against those resulting from IM immunisation (127).

ChimeriVax™-JE, a recombinant attenuated yellow fever virus-vectored vaccine against Japanese encephalitis was delivered to macaques using a single microneedle device (17, 130). Successful delivery induces low-level viremia resulting from viral uptake by APCs, which was of higher frequency and longer duration following microneedle dermal delivery than SCu. Seven-fold greater neutralising antibody titres were induced against the vector by microneedle compared to the needle-based method. These studies reinforce earlier ID dose-sparing observations proposing a simpler delivery method than the Mantoux technique. However, all devices retain a needle component, and whilst pain experienced by volunteers was reported to be minimal, these technologies still present a risk of needle injury and

require sharps disposal. Single microneedles have also been successful in the delivery of therapeutics, particularly when a short T_{max} is preferable[2], such as with insulin delivery, and for increased bio-availability and reduced invasiveness, such as in the delivery of therapeutics to the suprachoroidal space treat macular degeneration of the eye (134-136).

1.5.2 Microneedle patches

Microneedle patch delivery strategies include: (1) solid microneedles for topical application of liquid vaccine; (2) vaccine-coated solid microneedles for *in situ* vaccine diffusion; (3) biodegradable vaccine-encapsulated microneedles; and, (4) hollow microneedles for liquid infusion through an attached syringe. These four methods are presented in Figure 1-5 and Table 1-3. A summary of the commercial development of microneedles is given in Table 1-4 and images of systems in development are shown in Figure 1-6.

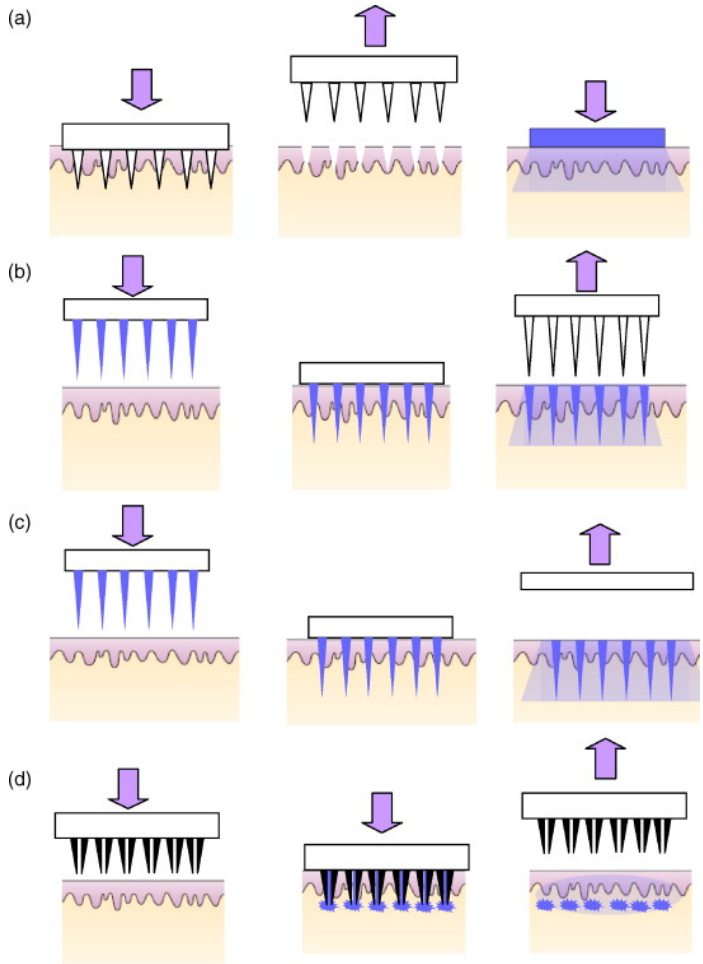

Arora *et al* (2008) Int. J. Pharm. 364:227-236

FIGURE 1-5: Modalities of microneedle vaccine delivery to the skin.

[2] T_{max} is the time taken for maximum plasma concentration of an administered drug to be reached.

Taken from (137) (A) Solid microneedles are applied to the skin to increase permeability to liquid vaccine, either by pre-treatment or application through a topically applied vaccine or vaccine patch. (B) Vaccine-coated solid microneedles are applied to the skin. Vaccine diffuses off the microneedle and into the skin within minutes. (C) Vaccine-encapsulating microneedles made from biodegradable polymers are applied to skin and completely dissolve leaving no clinical waste. (D) Hollow microneedles are applied to skin and liquid vaccine is infused into the skin via an attached syringe or reservoir.

1.5.2.1 Solid microneedles for liquid vaccine delivery

The simplest application of microneedle technology to the delivery of vaccines is to apply liquid to the surface of the skin either before after application of microneedles (either by pressing or scraping), perforating the SC for vaccine diffusion. Penetration of microneedles has resulted in a 4-order increase in permeability of the skin (as measured using an *in vitro* diffusion model) to the model drug calcein after penetration with 150μm microneedles (138). Other studies have since corroborated an increased permeability and delivery of a range of molecules *in vitro* and *in vivo,* and the efficient expression of a reporter gene in the skin was demonstrated following delivery of pDNA (139-142).

Vaccine studies have included HBV pDNA delivery to mice and recombinant Protective Antigen from *Bacillus anthracis*in rabbits, demonstrating dose-sparing effects in reaching seroconversion and conferring protection against disease as compared to IM immunisation. Cellular responses were comparable to IM after delivery of pCMV-HBS (129, 139). However, the methodology was more akin to abrasion than piercing of the SC, as the frustum-tipped structures were swiped across the skin to create furrows through which vaccine diffuses. The only currently published study of microneedle delivery of a live, viral vector -ChimeriVax^{TM}-JE, also uses this device. Interestingly, the level of transient viremia associated with cellular uptake of this virus was variable according to the method – only 1/3 macaques were viremic when vaccine was pre-applied before microneedle treatment, whereas 3/3 were viremic when the skin was abraded through the droplet (130). Another study showed that microneedle length had no significant effect upon anti-OVA antibodies following delivery of recombinant ovalbumin (143). The response did increase with increasing dose (1-80μg) for all routes but was more pronounced after SCu and IM, though all routes demonstrated an equivalent response at the highest dose. This suggests whilst improved responses are evident at lower doses, microneedle delivery does not further increase antibody responses at higher doses, consistent with the 'plateau' of a dose-response curve (144).

1.5.2.2 Vaccine-coated solid microneedles

Using several methodologies, vaccines have been coated onto microneedles for direct deposition into the skin, where they dissolve upon hydration by the extracellular fluid within minutes (144-146). Coating methods usually do not require expensive equipment or denaturing extremes of temperature or pH, making the

procedure applicable to a wide range of vaccines and therapeutics, and generally use FDA-approved aqueous solvents with high safety profiles. However, with necessary reformulation of vaccine, it is likely that coated vaccine patches will be viewed as 'new products' from a regulatory standpoint, requiring additional approvals. The first coating methodology to be described consisted of dipping long microneedles into a solution of recombinant OVA and air-drying for 1h before delivery to hairless guinea pigs (HGP). Delivered dose was controllable by altering coating concentration and patch wear time, though delivery efficiency by mass balance was found to be low (12%, 13% and 4% for coated doses of 1%, 2% and 20%$^{w}/_{v}$ OVA respectively), with the majority of vaccine remaining on the patch (144). The selective dip-coating of steel microneedle tips and shafts without base contamination was achieved by Gill *et al* who tested a range of formulations for optimal coating of number of hydrophilic and hydrophobic compounds, with the optimal formulation containing the viscosity enhancer Carboxymethyl-Cellulose (CMC, 1% $^{w}/_{v}$) and the surfactant Lutrol F-68F (0.5% $^{w}/_{v}$), which improved wetting and distribution of the material along the microneedle shaft(146). Dose was controllable by concentration of riboflavin added to the formulation and number of dips of the microneedle, 1-12 dips were optimal with 24 dips resulting in 'over-loading' and an irregular microneedle shape (146). Using this formulation YOYO-1-conjugated calcein, BSA, pDNA, 1-20μm particles and MVA were successfully coated and imaged by confocal microscopy(145). A high delivery efficiency of 80% of the coated dose of inactivated influenza virus within 5 minutes was demonstrated (147, 148). Antibody responses following coated 330μm microneedle delivery of recominant OVA were equivalent to ID immunisation, 1 order higher than SCu and 2 orders higher than IM, in the HGP(143). Microneedle delivery of HBV pDNA to mice induced equivalent levels of CTL as the more invasive gene gun method (149) and live, replicating BCG-specific induction of highly proliferative cytokine-secreting CD4+ and CD8+ T cells was equivalent between 700μm microneedle and ID delivery, also in HGP (150).

The majority of published work using coated microneedle patches has made use of influenza vaccines. In a series of studies with 700μm microneedles, inactivated virus (147, 151-153) H1N1 and H5N1 VLP (148, 154-156), and recombinant HA (157) influenza vaccines have been coated and delivered to animal models *in vivo*, demonstrating equivalent IgG titres and Haemagglutinin Inhibition (HI), CD4+ and CD8+ T cell responses in the spleen and draining LN and a high frequency of antigen-secreting cells in the lung and virus-specific memory B cells compared to IM. Microneedle delivery was associated with 100% protection against live virus challenge, a reduction in post-challenge weight loss and complete viral clearance from the lungs (151, 152). Post-challenge recall responses were stronger after microneedle than IM delivery, suggesting improved responses and protective efficacy could be attributed to an improved induction of immunological memory (147, 151, 158). Antigen-specific cellular responses resulting from transcutaneous immunisation by microneedle were detected in mucosal tissue of the respiratory tract in addition to the circulation and secondary lymphoid organs (157, 158).

Dose-sparing was demonstrated by delivery of VLP, in that microneedle delivery was more immunogenic than low and high doses of IM delivered vaccine, and lower

doses conferred complete protection against challenge(158). Microneedle-induced responses were found to be long-lasting, with a higher level of memory T and B cells 8 months following H5N1 VLP immunisation and inactivated virus as compared to IM, and complete protection against challenge up to 16 weeks post-immunisation (156, 159). Whereas viral challenge 6 months following SCu immunisation of inactivated influenza resulted in 60% protection and excessive inflammation in the lung, microneedle-immunised mice were completely protected, with no lung inflammation, and a high number of bone marrow plasma cells and splenic antibody-secreting cells (153). Stimulatory effects of microneedle-delivered VLP on Langerin (CD207)+ cells of the skin were demonstrated in a human skin explant model, where LCs were found to retract their dendrites in response to microneedle immunisation and migrate from epidermal sheets, proposing a mechanism for improved responses in the increased motility of LC in response to immunisation (156, 160).

The HI activity of formulated inactivated influenza vaccine was found to decrease following the dip-coating and drying stages, but could be completely restored with the addition of the disaccharide trehalose into the coating formulation (161). Both after microneedle-delivered coated, and IM-delivered microneedle-coated-then-reconstituted vaccine, increases in HI (2% to 48-82% HI), serum IgG, protection against lethal live virus challenge (40%-100% survival) and post-challenge recall responses were observed upon stabilisation with trehalose(162). Results were replicated when coating influenza VLP and recombinant HA vaccines (154, 157). The proposed mechanism was in the retention of functional antigenicity of the HA protein, specifically by preventing aggregation of particles since an increase in trehalose concentration correlated with a decrease in particle size as measured by light scattering. Aggregation was mediated by an increased viscosity, and associated with percentage of CMC used in the coating formulation (162). Trehalose was also found to confer longer-term benefits, as activity loss in stabilised formulations was independent of temperature over a range of 4-37°C for 24 hours (162). In assessment of the stability kinetics, destabilisation was found to occur over two timescales – in the minutes following dip-coating and gradually in storage. The absence of trehalose was associated with a reduction of HI activity to below 10% 1 hour after dip-coating and to almost zero after 1 month, but stabilisation permitted 60% retention of HI after 1 hour, and over 20% after 1 month in storage (163). Interestingly, all studies investigating trehalose stabilisation of influenza vaccines noted a shift in IgG isotypes following immunisation of mice. Unstabilised microneedle-delivered vaccine induced an IgG response dominated by IgG1 (Th2), whereas IM delivery was primarily composed of the IgG2a (Th1) isotype. IgG2a titres in microneedle-immunised mice were 1 order of magnitude higher with trehalose inclusion than without (152, 155).

1.5.2.3 Vaccine-encapsulated dissolving microneedles

Biodegradable polymer excipients (e.g. FDA-approved CMC) have been used to encapsulate vaccine, taking the form of sharp-tipped microneedles, which entirely dissolve upon application to the skin within a few minutes, leaving no clinical waste. In comparison to solid liquid and coated methods, dissolving microneedles demonstrate impressive delivery efficiencies – with up to 90% of vaccine dose

dissolving in the skin, and little remaining on the surface (143, 145). There is also the potential for multi-componant layered microneedles for where antigen release should be sustained or episodic (such as in prime-boost immunisation schedules). This concept has been demonstrated for delivery of model compounds, insulin, erythropoietin, sumatriptan, human growth hormone, recombinant OVA, and inactivated influenza vaccine within polymeric carbohydrate or sugar-based formulations (164-170). When compared to coated microneedle immunisation, dissolving microneedle delivery of inactivated influenza vaccine demonstrated improved cellular responses, most notably IL-4 and IFN-γ secretion from LN cells following virus re-stimulation. Dissolving microneedle-induced antibody and cellular responses were found to be protective against influenza challenge (169). The main challenge for this approach is to develop a fabrication method without use of high temperatures necessary to mould polymers to avoid protein degradation and reduced mechanical integrity (171). Dissolvable microneedles have a reduced compressive strength as compared to silicon, and may require an applicator to overcome the elastic resistance of the skin (104).

1.5.2.4 Hollow microneedles for liquid vaccine infusion

Hollow microneedles systems, based on a patch attached to a standard syringe barrel, a reservoir or a pump offer the advantage of improved control over dose delivery, with no need for reformulation. This is set against an increased cost (incorporating a syringe or liquid reservoir) and likely needforbetter trained vaccinators due to an increased risk of user error and inconsistency. Large volumes can be delivered – up to 1.5mL in porcine models (172). Flow rate must be tightly controlled to prevent leakage and clogging of tips can be avoided by using a beveled tip and slight retraction following insertion, though this has been associated with increased pain (173-175). This method has been particularly successful in delivering drugs via dermal capillaries for a more rapid pharmokinetic than SCu administration (136, 176).

Company	Technology platform	Main product	Applications	Stage of evaluation
Dermaroller S.A.R.L, Germany	Circular rolling drum with rows of steel microneedles 150-1500 μm length, 192 in total	Dermaroller™	Biocosmetics; Collagen Induction Therapy (scars, acne, hyper-pigmentation), melanoma vaccine	In clinical use Clinical assessment (for vaccine application)
TheraJect Inc., CA, USA	Dissolvable 90 μm microneedles	TheraMAT™ DrugMAT™ Applicator in development	Protein drugs; acne Rx; small molecule analgesics; trivalent influenza vaccine Part of the Patterson HIV Vaccine Development Consortium	Pre-clinical
Apogee Technology, MA, USA Inc.	Solid silicon pyramidal microneedles / dissolvable polymer	PyraDerm™	Microneedle-incorporated adjuvants	Pre-clinical
NanoPass Technologies, Israel	Hollow silicon microneedle (micropyramid) array affixed to syringe	MicronJet™	Collaboration with IDRI – development of HIV, tuberculosis, malaria, leishmaniasis and leprosy	Pre-clinical
Corium International Inc. CA, USA	Hollow microstructures (cylindrical or pyramidal) incorporated onto a polymer patch containing dissolvable drug/vaccine	MicroCor™ (microneedle product) Corplex™ (polymer product)	Not stated	Not stated
Zosano Pharma (acq. by Alza Corp.)	Arrowheaded solid silicon projections, coated with vaccine/therapeutic	ZP-PTH (previously Macroflux™)	PTH for osteoporosis 18 large molecule Rx (12 pre-clinical) Vaccines – influenza, tetanus, diptheria lyme disease, Hep B plasmid, Muc1 plasmid (all pre-clinical)	Clinical trials of 5 Rx and mAb complete. ZP-PTH now in Phase II. Phase I clinical trial of vaccine complete (ZP-flu)

3M, Global	Solid, coated and hollow injection-moulded polymer 18-1300 per patch, 500-900 μm	hMTS™(hollow) and sMTS™ (solid)	Working on methods to scale up manufacture and application technologies, patient acceptability.	Pre-clinical
AdminMed (nanoBioSciences, LLC)	Solid steel angled (45°) arrow-shaped projections, 600 - 1500 μm	AdminPatch™ AdminPen™ (patch + syringe)	None stated	Not stated
Debiotech, Switzerland	Hollow solid microneedles ('side-holes' to prevent coring effect)	Nanoject™	Developing for use alongside other drug delivery platforms including an insulin pump	Pre-clinical
Cyto pulse Sciences, MA, USA	Electroporation device with 2000 μm dermal needles	Agile Pulse™ + EasyVax™	pDNA – smallpox, dengue virus, HPV	Pre-clinical
BD, Global	Flat-topped silicon microneedles, abrasion of SC by 'swiping'	Onvax™	Recombinant anthrax vaccine	Pre-clinical
Transderm Inc. CA, USA	Dissolvable microneeles , 100-200 μm, polymer-drawn manufacture.	Soluble Protrusion Array Device (PAD)	pDNA vaccines, siRNAs Collaboration with Juvaris Biotherapeutics on malaria CSP pDNA vaccine delivery	Pre-clinical

TABLE 1-4: Commercial development of microneedles.

A table summarising the research activity of commercial organisations developing microneedle patch technologies as of May 2011, their primary products and stage of evaluation. Due to space limitations, this list is not exhaustive. IDRI = Infectious Disease Research Institute (Seattle, USA). Rx = treatment. PTH = parathyroid hormone. CDC = Centers for Disease Control. siRNA = smallinterfering ribonucleic acids. CSP = circumsporozoite protein.

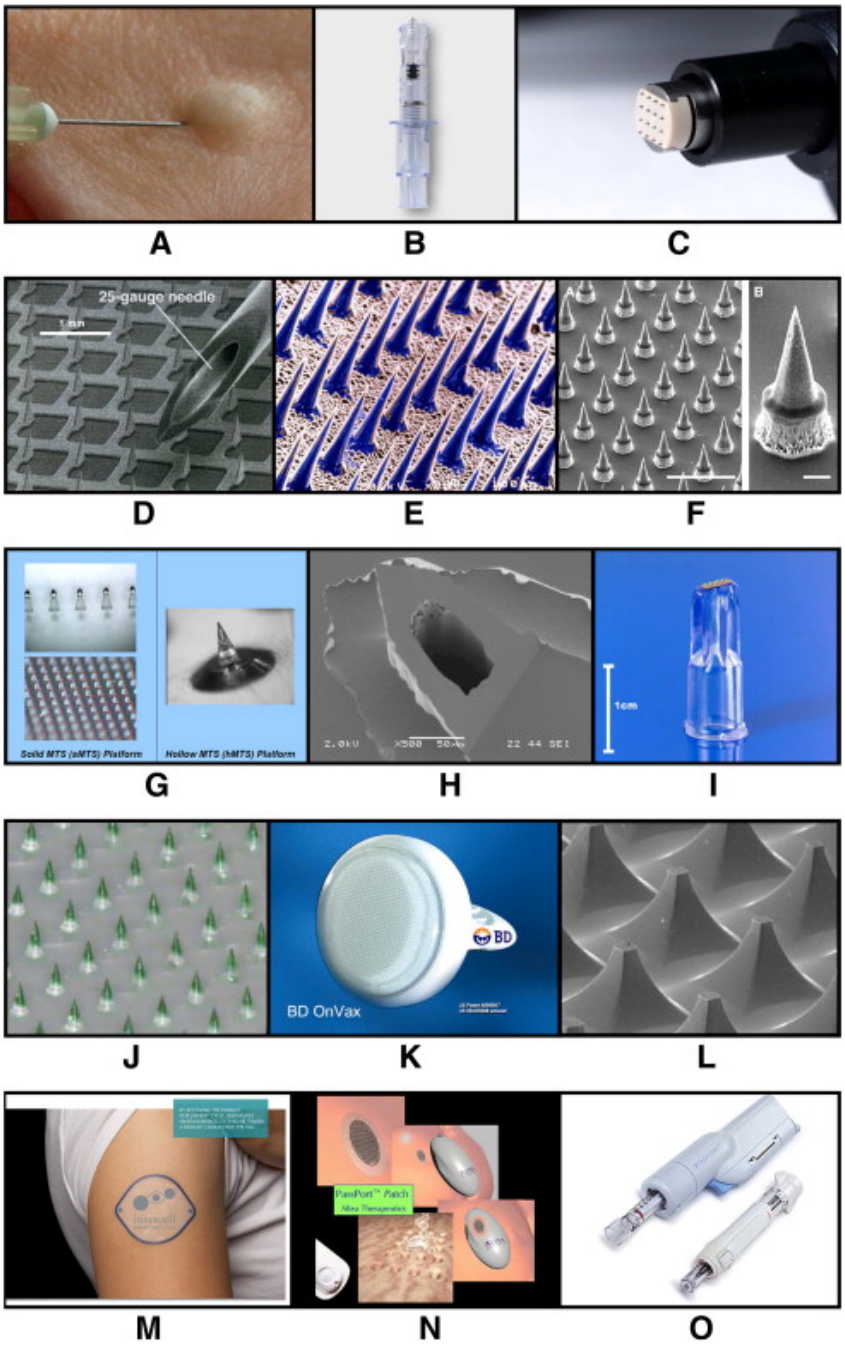

FIGURE 1-6: Examples of microneedle systems in development.

Taken from (104). (A) The Mantoux method of intradermal delivery (showing raised bleb). (B) BD Soluvia™(C) Solid microneedle array (U.Leiden). (D) Zosano Macroflux®. (E) silicon microneedles (Georgia. Inst. Tech.) (F) Nanopatch™ silicon microprojections. (G) coated and hollow 3M MTS™. (H) Hollow microneedle, U. Leiden. (I) Micronjet®, Nanopass. (J) Dissolvable microneedles, BioSerenTach. (K +L) BD abraisive flat-topped microneedles, OnVax® (M) Intercell TCI patch (N) PassPort™ patch (+ electroporation device), Altea Therapeutics. (O) Powderject systems (EPI), Pfizer.

1.5.3 Considerations for implementation

1.5.3.1 Limitations of animal models

Although the majority of microneedle studies to date have been in murine models, there are significant differences between mouse and human skin. Human skin is much thicker (the human VE width is 150μm whereas that of the mouse is ~15μm), which is likely to impact penetration depths and therefore targeting of epidermal/dermal APC. Mouse skin contains more hair follicles, which could potentially impede microneedle penetration, or increase in follicular diffusion (119). The ratio of LC to keratinocyte in the mouse VE was estimated to be 1:15, whereas that of human breast skin was 1:50(177). Accordingly, the contribution of cross presentation of antigen may be more significant in human than mouse studies. Some studies have utilised HGP and porcine models, which have comparatively more homologyin terms of follicle number and lipid content but assessment of vaccine immunogenicity is limited. The patch wearing time, which is restricted due to general anaesthesia in models, can be easily increased in humans, though the area of skin will not be immobilised as in animal experiments. Finally, the elasticity of human skin, with layers of supporting subcutaneous fat, is significantly different to the thin mouse ear, perhaps with differing characteristics under compression.

1.5.3.2 Variations in human skin properties

In addition to interspecies differences in skin, there is significant intraspecies variation within human populations. Skin thickness and viscoelastic properties vary with age, sex, BMI and ethnicity and between different sites on the body (56, 133, 178). For example, it has been suggested that the SC of Afro-Carribean skin contains more layers with increased intracellular adhesion, since a higher number of tape strips were required to expose the VE than in Caucasian skin (179). Aged skin has a decreased collagen component, resulting in dermal atrophy and reduced elasticity(180). Atmospheric humidity is negatively correlated with SC breaking stress in porcine skin (181). Hydration of the skin (affecting permeability and elasticity) varies significantly with age and ethnicity and sun exposure (182). Ultra-violet light has a variety of effects upon keratinocytes, LC, in the induction of T_{reg} and of skin-homing T cells responses after transcutnaeous immunisation (183-185).

1.5.3.3 Design

Whilst long microneedles may hold promise for greater dose delivery and wider vaccine distribution, microneedle length is strongly correlated with discomfort felt upon application (186). Indeed, a 3-fold increase in length (500-1500μm) brought about a 7-fold increase in pain score, whereas a 10-fold increase in the number of needles only translated to 2.5-fold increase in pain score in a clinical study (187). Regardless, microneedle pain scores were only 1/20th of those following IM injection

(188). Any microneedle penetrating deeper than approximately 100μm is likely to access the innervated (and vasculated) dermal compartment, and though theoretically a minimum length of 20μm should be sufficient to breach the SC, due to natural undulation of the skin surface and heterogeneity between individuals, microneedle lengths greater than this will be required (104).

The use of an applicator to deliver patches to the skin at a defined velocity may reduce the required microneedle length by more efficiently overcoming initial deflection, which may act to prevent or reduce penetration of short microneedles when applied by hand (189, 190). Whilst the use of applicators increases unit cost and distribution volume, it permits a standardisation of application method, important in the self-immunisation model of implementation. Ultimately, selection of the best microneedle design, patch type and application method will depend upon a balance of trade-offs e.g. reformulation requirement vs. increased stability (coated microneedles), high delivery efficiency vs. increased complexity and volume (hollow microneedles), complete lack of waste vs. decreased microneedle strength (biodegradable polymer microneedles).

1.5.3.4 Safety

Safety concerns associated with the implementation of microneedles include:
1. Microbial opportunism. Any breach of the skin's barrier, however transient, is a theoretical opportunity for microbial infection. If microneedle systems are single-use, sterile and do not induce bleeding, there is a negligible risk of iatrogenic infection. However, environmental *S. aureus* and *S. pyogenes* can be found on the skin surface and hair follicles (191). The number of individual breaches of the SC can be in the thousands using microneedle patches, as opposed to only one by standard needle. However, infection is likely to be dependent upon conduit depth, and superficial abrasions are caused every day without clinical consequence. The number of microorganisms crossing the SC was significantly reduced following application of microneedles as compared to a 21G needle using an *ex vivo* porcine skin model (192). In over 1000 microneedle applications to 100 human subjects by one group, no skin infection was reported, though skin was pre-cleansed with alcohol wipes to reduce microflora, which may become a safety requirement for implementation (66). Sterilisation of polymer microneedles in particular will be difficult due to a high sensitivity to changes in temperature; potentially affecting microneedle integrity and vaccine loading in clean room facilities will be expensive. Alternatives are being developed, such as a method for coating an antimicrobial layer of silver onto solid microneedles (193).
2. Irritation. No significant skin irritation been noted in animal studies, though localised, transient red spots consistent with mild erythema have been noted in human studies (66). Redness scores were found to increase with microneedle length with a significantly between 200-400μm, but not between different microneedle designs in human skin (186).
3. Bleeding. Since the VE is devoid of vasculature, short microneedles (<100μm penetration) should not breach capillaries. Even longer microneedles (700μm, 1500μm) did not demonstrate bleeding on application to hairless rats (194), though bleeding was observed after application of 600μm to HGP (143).

4. *Skin residuals.* The environmental and safety implications of vaccine remaining on the used patch, or the surface of the skin are dependent upon the type of vaccine, with higher concerns for live, replicating organisms than subunit vaccines. Appropriate engineering and optimisation of high delivery efficiency will minimise this concern, since different designs have shown vaccine remaining on the skin after coated patch application can range from 11.5% to as little as 2% by mass balance (143, 145). Application of an occlusive patch may minimise shedding of residual vaccine from the skin whilst extending microchannel lifetime for potentially improved vaccine diffusion (195). Another consideration for solid microneedles is in the deposition of minute amounts of silicon or steel in the skin, though most microneedles have demonstrated minimal breakage upon application. Materials used to manufacture microneedles are inert and any embedding particles are likely to be expelled during normal skin sloughing processes.

1.5.3.5 Sociological attitudes

There is evidence to suggest that microneedles will be well accepted in clinical practice. A sociological study carried out on focus groups of patients and healthcare professionals in the UK identified perceived benefits including reduced pain, tissue damage and disease transmission and self-administration, though there was concern about confirmation of accurate self-delivery, suggesting the inclusion of a biocompatible dye may improve user confidence. Overall, 100% of public, and 74% of professional participants had positive attitudes to microneedles, with a strong stipulation that efficiency should be equivalent to that of a needle-delivered vaccine (196). When considering implementation in other settings, a re-evaluation will be required, since a study of practices in 19 developing countries highlighted that needle-delivered medicines can carry a higher perceived 'effectiveness' than alternatives (197).

1.6 MALARIA VACCINES

1.6.1 The need for a vaccine

Malaria, caused by parasite species of the genus *Plasmodium,* kills an estimated 860,000 individuals per year, and approximately 250 million clinical episodes are experienced. The disease burden is disproportionate, as only 50% of the world's population is at risk from malarial infection including 50 of 53 African countries where approximately 801,000 of the global malaria related deaths occur, 85% of which are in children under 5 years old (198)(Figure 1-7). Malaria places an economic burden of $12 billion USD/year in lost GDP in Africa alone (199). Costs to the individual include medical treatment and loss of earnings from absenteeism or unemployment due to illness. In addition to reduced school attendance, complications of malaria infection can result in cognitive impairment in children, limiting future employment opportunities (200). There can be no doubt that malaria presents one of the most significant factors potentiating the debilitating cycle of poverty and disease in the disadvantaged world and is proving difficult to control with insecticides and chemotherapeutics (201, 202). A vaccine that interrupts the life cycle of the malaria parasite in the human or mosquito host (or both) would undoubtedly prove the most cost-effective control measure in the battle against malaria.

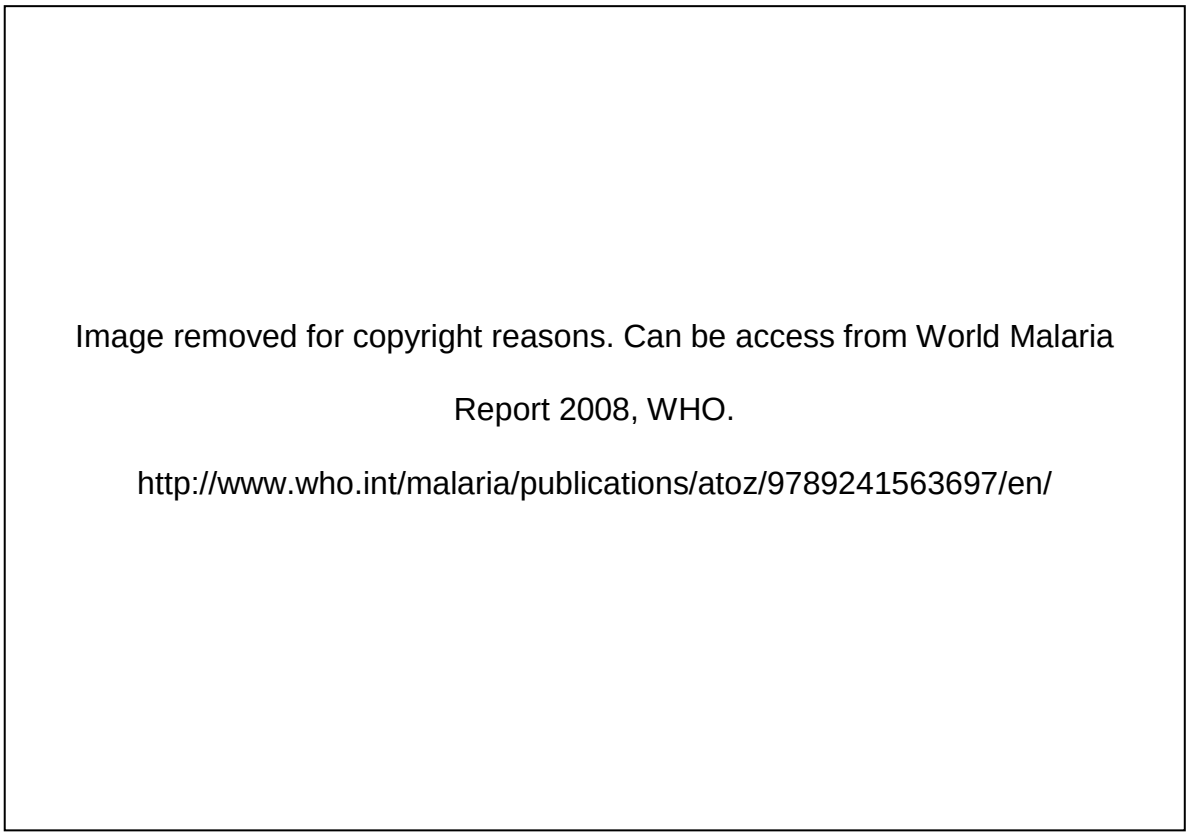

FIGURE 1-7: The estimated global incidence and distribution of malaria.

The incidence is worst in sub-Saharan countries of the African continent, where >200 cases/1000 people occurred in 2006. Of the four human-infecting species of malaria, *Plasmodium falciparum* is the species most closely associated with severe forms and complications of disease. In Africa 75-100% of malarial disease in caused by this parasite species and 0.5-5 deaths/1000 people. Globally, there were 247 million clinical cases in 2008, 91% due to *P.falciparum* infection. Taken from (198).

1.6.2 Malarial disease

Malaria parasites were first described in 1880, in the blood of infected patients(203). Four species of human-infecting Plasmodium protozoa – *P. falciparum*, *P. vivax*, *P. malariae* and *P. ovale*, were subsequently characterised. Shortly afterwards, Ronald Ross demonstrated that malaria parasites are transmitted via the bite of the infected mosquito, and in doing so closed the gap in the highly complex life cycle of the malaria parasite, the intricacies of which continue to fuel malariavaccine research (204) (Figure 1-8). The pathogenesis of malaria occurs during the blood (erythrocytic) stage of infection, where the cyclical patterns of fever-like symptoms coincide with the emergence of merozoites from ruptured erythrocytic schizonts. In complicated and severe malarias caused by *P. falciparum*, parasites can cross the blood-brain barrier and lodge in cerebral capillaries, and falciparum-infected erythrocytes aggregate and sequester causing tissue hypoxia (205).

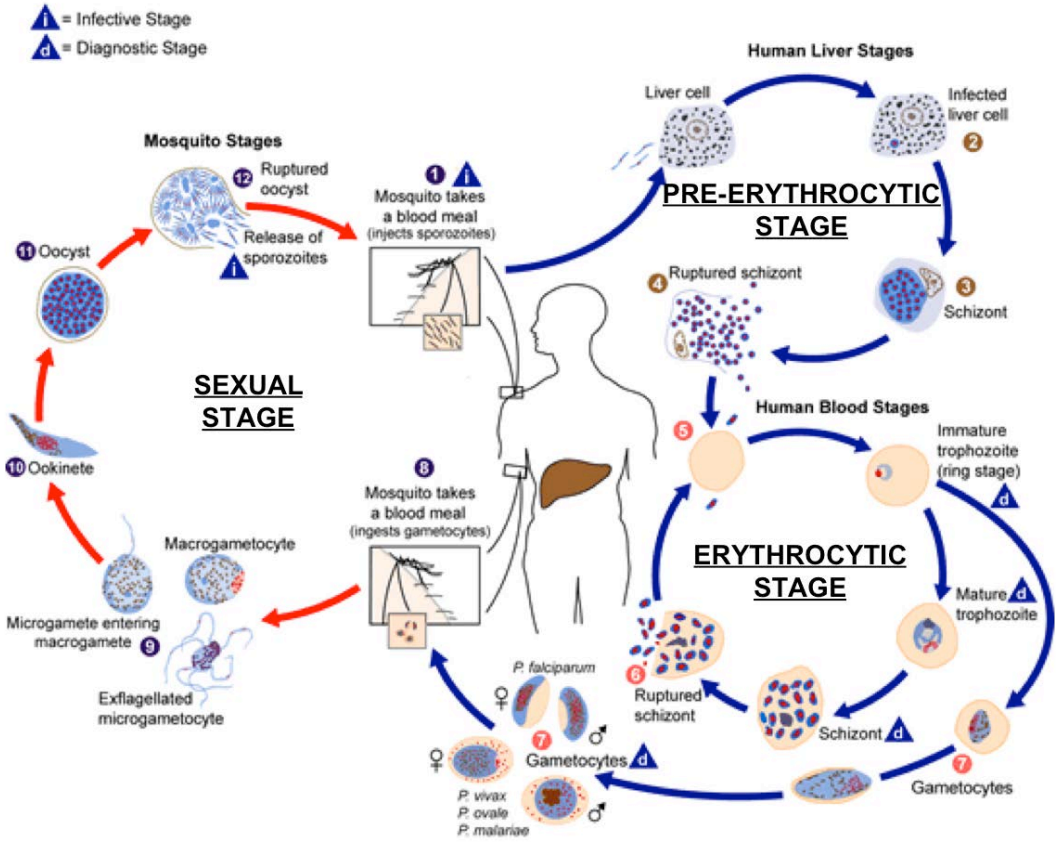

Adapted from the original from CDC Image Library.
http://www.dpd.cdc.gov/dpdx

FIGURE 1-8: The life cycle of *Plasmodium*.

The parasite infects humans via the bite of infected female Anopheles mosquito. Parasites of the sporozoite stage are inoculated either into the dermis or into the bloodstream during a blood meal [1]. During the pre-erythrocytic stage of infection (2-4), malaria sporozoites travel in the circulation to the liver and invade hepatocytes (within 30 minutes), where they replicate and mature into trophozoites then schizonts during a period of 5-7 days. *P.vivax* and *P.ovale parasites* can persist in the liver as hypnozoites for long periods. Schizonts rupture and merozoites emerge (20,000/cell) and enter the bloodstream where they undergo a secondary period of asexual schizogony within RBC in the erytocytic/blood stage of infection, during which cyclical symptoms are experienced (6-7). A subset of merozoites differentiate into male and female gametocytes, which are ingested during a second mosquito blood meal, and the sexual stage of the life cycle proceeds in the midgut of the mosquito (9-12). Finally, sporozoites are released from oocysts and are stored in the mosquito salivary glands for infection of a new human host during mosquito feeding. Adapted from (206)**.**

1.6.3 Developing a vaccine against malaria

The observation that individuals in malaria endemic areas can acquire 'semi-immunity' which accumulates over time through natural boosting supports the theory that vaccination against the disease is feasible (207). Whilst semi-immunity does not prevent infection, it ameliorates the severity of symptoms associated with the blood stage and has been shown to reduce parasite density in the blood. However,

immunity is short-lived, strain-specific and incomplete, indicating that vaccine-induced responses will need to exceed those induced by natural infection. Metabolically-active, radiation-attenuated sporozoites (RAS) were found to confer complete and long-lasting protection against experimental infection first in mice immunised IV (208), and then in humans challenged by over 1000 *P. falciparum*-infected mosquito bites(209-213). Whilst this remains the most effective experimental malaria vaccine, this approach was clinically impractical (209). In a recent return to the whole organism approach, Sanaria (Maryland, USA) has sought to develop a mass-producible, cryo-preserved, attenuated sporozoite vaccine delivered by a more clinically acceptable route (214).

The development of subunit malaria vaccines has met difficulties in identifying appropriate antigens, since the malaria parasite displays a vast array of poorly immunogenic antigens with little homology between life cycle stages. For this reason, it is envisaged that a successful malaria vaccine will need to combine several antigens from different stages for optimal parasite inhibition. Table 1-5 summarises the main malaria vaccine developments to date. The malaria vaccine closest to licensure, RTS,S/AS01E (GSK, Mosquirix®) is thought to mediate protection by eliciting high titres of antibody and CD4+ and CD8+ T cell responses directed against CSP (1.6.4) (215) and has demonstrated 30-55% efficacy at preventing clinical disease in trials in several African countries. It is currently entering evaluation in combination with an Adenoviral (AdHu35) CSP vaccine (47, 216).

Vaccine type	Goal	Target mechanisms	Example vaccines	Stage of development	Related refs
Pre-erythrocytic	Inhibition of sporozoites travelling to or sequestered within hepatocytes. Complete arrest of the parasite to prevent blood stage infection	Anti-sporozoite Ab CD8+ and CD4+ T cell killing of hepatocytes (via IFN-γ secretion)	RTS,S/ASO1E (Mosquirix^{TM}) Recombinant PfCSP /PfLSA -in-adj. VLP – CSP epitopes DNA – CSP, TRAP, LSA, Exp-1 Viral vectors: AdCh63/FP9/MVA. ME-TRAP Ad35.CSP	Phase III (Africa) Phase I/IIa (various) Phase I/IIa (UK) Phase I recruiting (US) Phase I/IIa+b (UK, Africa) Phase I (US, Africa)	(47), (217) (218) (rev'd) (219) (46, 49) (220)O'Hara, *in press* Ewer, O'Hara, *in press*
Blood stage	Prevent merozoite invasion/target iRBC - lessen symptoms, decrease parasite burden	Anti-merozoite Ab CD4+ T cells	Recombinant PfMSP-1/3/PfAMA/ EBA-175/SERA5 -in- adj. Synthetic peptide GLURP -in- adj. Viral vectors/vectors +protein-in-adj.: AdCh63, MVA – AMA-1/MSP-1	Phase I-IIb (various) Phase I (Germany, Africa) Phase I (UK)	(218)(rev'd) (221) (222-225)
Transmission blocking	Prevent host-to-host transmission (no direct benefit to individual)	Anti-gametocyte Ab	Recombinant Pfs25, Pfs48/45	Phase I (US)	(226, 227)
Whole organism strategies	Pre-erthrocytic inhibition	Anti-sporozoite Ab CD8+ T cell killing of hepatocytes (IFN-γ)	PfSPZ - attenuated sporozoite PfGAP – genetically-attenuated parasite	Phase I/IIa (US) Phase I/IIa (US)	(214) (209)

TABLE 1-5: Summary of *P. falciparum* malaria vaccine developments.

Because of the strain-specificity of immunity to malaria and the exceptionally high levels of parasite-specific immunity required it is likely that a combination of subunit vaccines will be more effective. Multistage combination vaccines, combining two or more vaccine types e.g. influenza virosomes (Pevion) + viral vectors are already being trialled. CSP = Circumsporozoite Protein; LSA = Liver Stage Antigen; VLP = Viral -like Particles; TRAP = Thrombospondin-Related-Adhesive-Protein; Exp-1 = Exported Protein-1; ME-TRAP = Multiple Epitope-TRAP; iRPC = infected Red Blood Cell; MSP = Merozoite Surface Protein; AMA = Apical Membrane Antigen; EBA = Erythrocyte Binding Antigen; SERA = SERine Repeat Antigen. Adj = adjuvant. List not exhaustive.

1.6.4 CSP and ME-TRAP

Both RAS and RTS,S/AS01E mediate their protective effects at the pre-erythrocytic stage of infection. The objective of a pre-erythocytic vaccine/pre-erythrocytic component in a multi-stage vaccine is to prevent or minimise parasite progression into the highly pathogenic blood stage. Whilst evidence from murine models, RAS and studies with RTS,S/AS01E suggest that antibody-mediated sporozoite neutralisation is possible and contributes to protective immunity, the short window of opportunity and extremely high titres of antibody necessary suggests T cells directed against the infected hepatocyte are important (228). Pre-clinical studies with RAS combined with *in vivo* depletion and adoptive transfer in mice highlighted protective roles for antigen-specific CD8+ CTL, CD4+ (and their IFN-γ secretion) (229). The association of IFN-γ secreted by both T cell subsets in response to pre-erythrocytic antigens was confirmed in natural infection, with IFN-γ secretion by CD4+ T cells in response to PfCSP correlating with reduced malaria incidence (230, 231). Subsequent *in vitro* studies demonstrated inhibition of intrahepatocytic parasites via IFN-γ, proposed to act *in vivo* following antigen-MHC I engagement of CD8+ T cells (232, 233). IFN-γ is a valuable correlate of protection against malaria, particularly in animal models, but also has been proposed to have direct and indirect effector mechanisms involved in killing the infected hepatocyte. *In vitro*, IFN-γ, even at particularly low concentrations, was found to inhibit schizogony in primary human hepatocytes infected with *P. falciparum*(234). *In vivo*, mice lacking the IFN-γ receptor did not develop protective immunity following administrsation of *P. yoelii* RAS (235). Indirect autocrine effects include the upregulation of MHC I upon hepatocytes, targeting them for CTL cytotoxicity via degranulation of perforin and granzymes (236). IFN-γ acts directly via gene products of the Jak-Stat pathway, which include inducible nitric oxide synthase (iNOS), which catalyses the production of cytotoxic nitric oxide from L-arginine and NADPH. IFN-γ-dependent generation of nitric oxide and nitric oxide radicals have been proposed as a mechanism for killing of *Plasmodium* infected hepatocytes in mice immunised with RAS (237) (238, 239). Elsewhere, depletion of CD8+ (but not CD4+) blocked expression of iNOS mRNA in the liver and ablated protection against *P. berghei* challenge (240).Protection in the murine *P. berghei* model has also been associated with translocation of antigen-specific $T_{EM}$to the liver, indicating that IFN-γ secretion by re-activated memory cells convey their effects locally(241-243).

PfCSP (40-60kDa) is the major component of the sporozoite surface expressed from the oocycst stage in the mosquito up to merozoite differentiation within the infected hepatocyte, during which time it is both shed into the extracellular environment and presented in epitope form by hepatocyte-MHC I. It has a role in gaining access to and gliding through hepatocytes before the initiation of schizogony (244, 245). The $NANP_{38-40}$ B cell epitope of CSP is flanked by N- and C-terminal regions. Mapping of the C-terminus has identified both CD4+ and CD8+ epitopes. In the *P. berghei* murine model, responses against a 9-$\alpha\alpha$ CD8+ epitope within the C-terminus provides almost complete protection against sporozoite challenge (Pb9)(246, 247). This system permits the evaluation of pre-erythrocytic vaccine platforms and regimes in the *P. berghei* model by enumerating CD8+ CTL secreting IFN-γ in response to Pb9 re-stimulation, by methods including IFN-γ ELISPOT and Intracellular Cytokine Staining (ICS) (248). Pb9 is also contained within the pre-erythrocytic clinical construct ME-TRAP, consisting of the Thrombospondin Related Adhesion Protein (PfTRAP – with a similar role in pre-erythrocytic malaria infection to PfCSP) fused to a string of multiple epitopes (249, 250). Pb9 is included to allow the pre-clinical evaluation of vaccines containing the ME-TRAP construct.

1.6.5 Prime-boost viral vector malaria vaccine regimes

Multiple vaccinations are required to generate levels of immunogenicity sufficient to confer protection against diseases using most vaccine strategies including protein subunit and pDNA vaccines. In mice, only recombinant Adenoviruses have been shown to induce protective humoral and cellular responses after a single immunisation, whilst humans require at least two immunisations to achieve the required level of immunogenicity for protection (251, 252) (O'Hara, Ewer, *in preparation*). Optimal immunogenicity and protection is achieved by administering two different viral vectors sequentially encoding the same transgene (heterologous prime-boost), particularly when Ad is used to prime responses and MVA to boost them (253). Efficacy of priming and boosting with the same vector is compromised by the expansion of anti-vector immunity in parallel to that directed against the inserted antigen, limiting the full expansion of a secondary response upon boosting (253). Additionally, MVA is more efficient at boosting than priming responses, whereas Adenovirus can prime or boost responses primed by a different vector. The length of time between prime and boost is crucial, and corresponds to the differential kinetics of expansion and contraction following immunisation with Ad or MVA and must allow for optimal accumilation of T cell memory prior to boost (243). T cell responses peak 1-2 weeks following MVA and 2-3 weeks following Ad immunisation (251, 254). In addition to differences in the rate of antigen clearance (254), recombinant ME-TRAP encoding Ad and MVA induce responses of differing memory phenotype, with MVA primarily inducing CD62L+ CD127+ T_{CM}, and Ad vectors inducing CD62L- CD127+ T_{EM} following Pb9 stimulation (251).

1.6.5.1 Poxviruses

Poxviruses such as MVA have the ability to incorporate up to 25Kb of exogenous DNA without significant effect on viral growth (255). Poxviruses are large (200nm x 400nm), double-stranded DNA viruses with a lipid envelope, and replicate entirely in the host cell cytoplasm. MVA is a highly-attenuated derivative of Vaccinia virus resulting from its multiple passage in Chick Embryo Fibroblasts (CEF) causing the

loss of 31Kb of DNA including host range genes and those essential in late-stage viral assembly (256). Consequently, MVA is replication-deficient in mammalian cells, and has exhibited a high safety profile in human clinical trials with experimental malaria, TB, HIV and influenza vaccines (220, 257-259). MVA also replaced Vaccinia latterly in the smallpox eradication campaign and was delivered to approximately 120,000 vaccinees with no sign of the adverse events experienced by 1/800 Vaccinia recipients (43).

1.6.5.2 Adenoviruses

Adenoviruses e.g. AdHu5, AdCh63, are non-enveloped, isocahedral particles with a protein capsid, causing upper respiratory disease in natural infection (260). Smaller than Poxviruses, Adenoviruses have a particle diameter of 40nm and genome size of 34-43Kb. Selective deletion of the E1 region essential for viral replication has rendered these viruses replication-incompetant whilst allowing space for insertion of transgene, further increased by deletion of the non-essential E3 region (261). Adenoviruses are easy to manipulate and grow *in vitro* (with E1 complementation) and induce both high levels of both cellular and humoral immunogenicity in mice and macaques (252, 262). One limitation is in the high prevalence of pre-existing neutralising antibodies directed to the outer hexon protein in the human population, which diminishes vaccine-induced immunity to human serotypes (263, 264). Simian vectors such as AdCh63 of chimpanzee origincan be used in their place, since anti-vector immunity in humans is low and vectors have similar ability to induce immunogenicity and protection as AdHu5(251, 263). Simian vectors have been shown to be safe and immunogenic in recent clinical trials in malaria-naïve individuals (O'Hara, *in preparation*).

1.7 A MICRONEEDLE VACCINE PATCH FOR MALARIA

This thesis aims to evaluate the use of two solid silicon microneedle patches for the delivery of viral vector malaria vaccines in homologous and heterologous prime-boost regimens in mice.

1.7.1 ImmuPatch

ImmuPatch microneedle technology has been specifically designed to transcutaneously deliver macromolecules such as live, recombinant T cell-inducing viral vector vaccines. Carey *et al* demonstrated the induction of protective memory CD8+ T cell responses in mice following ImmuPatch immunisation with MVA.PbCSP, (265). Initial work has focused on delivery of liquid vaccine deposited onto the surface of the skin followed by application of a microneedle patch by hand (Chapter 3). More recently, 'vaccine-coated ImmuPatch' (using a novel spray-coating method - (266)) and 'dissolvable ImmuPatch' have also been developed, which incorporate multiple layers for sustained or episodic release (267). Silicon microneedle patches are developed at the Tyndall National Institute, Cork, by wet-etch methodology2.2.1(268). The pyramidal microneedles (Figure 1-9) glide smoothly in and out of tissue following application by hand and deliver topically applied liquid into the viable epidermisand dermis (as determined using *ex vivo* porcine and human *in vivo* imaging models)(265, 269). As compared to others

described, ImmuPatch microneedles are short in length, ranging from 100-300μm, and pain and discomfort scores following insertion of similar 280μm and 190μm microneedles into human skin were significantly lower than by 25G hypodermic syringe (187).

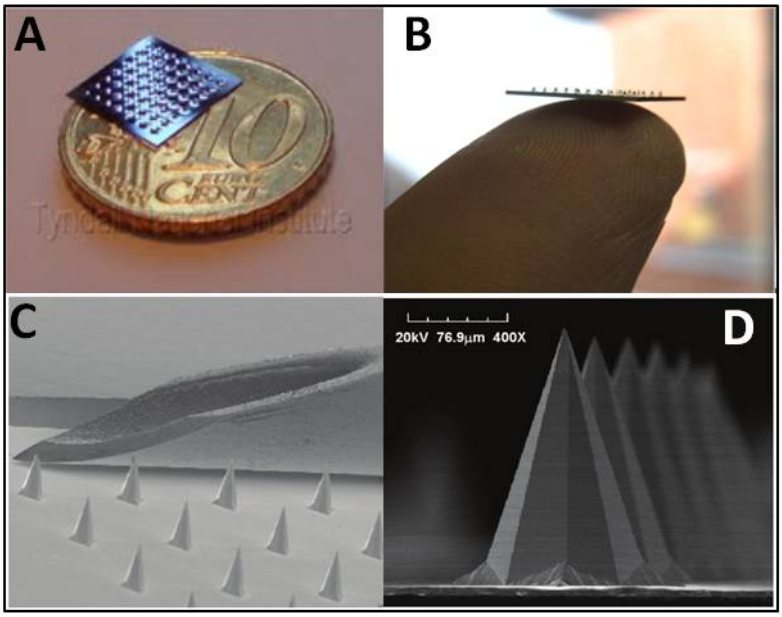

Images courtesy of Tyndall National Institute, Cork
A+B - www.immupatch.com, C+D - Carey *et al* (2011) PLoS ONE 6(7):e22442 (reference (1))

FIGURE 1-9: ImmuPatch – Innovative solutions to vaccine delivery barriers.

Microneedles are manufactured from silicon wafers using 'wet-etch' technology, whereby a photolithic mask is applied to a silicon substrate prior to immersing in a bath of hot potassium hydroxide for a tightly-defined period of time (268). The design of the mask determines the height of the resulting smooth-faced pyramidal microneedles (with aspect ratio 1:3), formed due to anisotropic etching of the directional planes of a silicon crystal. High accuracy in the determination of etch time is important for optimal tip sharpness. (A+B) The dimensions of an ImmuPatch array in relation to (A) a coin and (B) a human forefinger (C+D) SEM images of ImmuPatch microneedles in relation to a 26G needle bevel (C) and of an individual microneedle (D). Scale bar = 100μm.

1.7.2 Nanopatch

Nanopatch microprojections are fabricated using Deep Reactive Ion Etching (DRIE), further described in 2.2.2. Microprojections are either conical in shape (40μm length), or cylindrical with a conical tip (110μm) and are densely packed (21,025cm^{-2}, 4mm^2 patch). They are spaced by 70μm in each direction to allow skin to deflect and compress around each individual projection for optimal penetration when delivered by a custom-designed mechanical applicator at a velocity of ~1.96ms^{-1}(189). A simple, novel method was developed for dry-coating of vaccine material onto microprojections. Coatings remain in place during insertion and diffuse into skin tissue within 3-5 minutes *in situ* (270). Coated Nanopatches have been used to deliver a range of vaccines and demonstrated levels of immunogenicity at least comparable to IM immunisation, and significant dose-sparing of trivalent inactivated influenza with equivalent HI titres to IM immunisation with only 1/30th of the dose

(271-274). Dissolvable Nanopatches have been developed from biocompatible excipients cast from moulds of similar microprojection morphology to solid silicon Nanopatches and can be composed of several composite layers for controlled release (168). Dissolving Nanopatches were shown to induce IgG titres against recombinant OVA protein and to aninactivated influenza vaccine (168).

1.7.3 Thesis aims

- To investigate the cellular immunogenicity of prime-boost regimes featuring delivery of vaccines by solid silicon microneedle patch technologies using the *Plasmodium berghei* mouse model of malaria. Immunogenicity will be assessed using a well-described CD8+ T cell epitope common to *P.berghei* CSP and the fusion antigen ME-TRAP, expressed by replication-deficient simian (AdCh63) Adenoviruses and MVA (246), compared to needle-based immunisation (**Chapter 3+5**).

- To assess levels of protective efficacy of immunisation regimes featuring patch delivery of vaccine in *P. berghei* sporozoite challenge studies (**Chapter 3+5**).

- To evaluate the effect of microneedle design parameters upon resulting immunogenicity and protective efficacy (**Chapter 3**).

- To investigate qualitative aspects of the resulting T cell immune responses and events in the induction of immune responses following patch delivery of vaccine (**Chapter 4).**

- To develop viral vector dry-coated Nanopatches and evalutate viral viability, thermostability, delivery efficiency and immunogenicity and protection of prime-boost immunisation regimes using these dry-coated patches (**Chapter 5**).

CHAPTER 2 METHODS AND MATERIALS

2.1 SOLUTIONS

Phosphate Buffered Saline (PBS)
Five PBS tablets were dissolved into 1L de-ionised H_20 before autoclaving.

Tris Buffer Solution (TBS)
A 10X solution was made up with 1.37M NaCl, 0.02M KCl, 0.25M Tris and adjusted to pH 7.4. This was diluted to 1X with dH_20 to 1L and autoclaved.

ACK lysis buffer
8.29g of NH_4Cl (0.15M), 1g of $KHCO_3$ (1mM), 37.2mg of Na_2EDTA were added to 800mL dH_20. The pH was adjusted to 7.2-7.4 before making up to 1L with dH_20 and autoclaving.

Complete Minimal Essential Medium (C-MEM)
500mL MEM α–modification was supplemented with 50mL batch-tested heat inactivated Foetal Calf Serum (10% $^{v}/_{v}$ FCS), 5mL 2mM L-Glutamine, 100U Penicillin/100µg Streptomycin and 500µl 50µM 2-Mercaptoethanol.

Coating buffer (ELISPOT)
Five 15mM sodium carbonate and 35mM sodium bicarbonate-containing capsules were added to 1L of dH_20 before autoclaving.

2% and 10% Dulbecco's Modified Eagle's Medium (DMEM)
500mL of DMEM was supplemented with 10mL batch-tested heat inactivated FCS (2% or 10% $^{v}/_{v}$ FCS), 5mL 2mM L-Glutamine, 100U Penicillin/100µg Streptomycin and 500µl 50µM 2-Mercaptoethanol.

1% ($^{v}/_{v}$) PBS Formalin
15mL of 4% $^{w}/_{v}$Formaldehyde was added to 45mL PBS.

FACS buffer
2.5g (0.5%$^{w}/_{v}$) Bovine SerumAlbumin (BSA)and 0.25g (0.05%$^{w}/_{v}$) Sodium Azide was added to 500mL PBS.

PBS-BSA1% ($^{w}/_{v}$)
5g (1%$^{w}/_{v}$) BSAwas added to 500uL sterile PBS.

REAGENT LIST

Reagent	Supplier	Catalogue number
Phosphate Buffered Saline (PBS) tablets	Sigma-Aldrich, UK	P4417
Dulbecco's PBS (endotoxin-free)	Sigma-Aldrich	D8537
Sterile water(endotoxin-free)	Sigma-Aldrich	W3500
Ammonium chloride	Sigma-Aldrich	A4514
Potassium bicarbonate	Sigma-Aldrich	P9144
Tris (dihydrate)	Sigma-Aldrich	T-1503
Na_2EDTA	Sigma-Aldrich	ED2SS
EDTA	Sigma-Aldrich	E7889
DMSO	Sigma-Aldrich	D2650
Hydrochloric acid	Sigma-Aldrich	H7020
Minimal Essential Medium (α-modification)	Sigma-Aldrich	M-4526
Dulbecco's Modified Eagle Medium	Sigma-Aldrich	D6546
RMPI-1640	Sigma-Aldrich	R0883
Methanol	Fisher Scientific, UK	M/30900/17
Ethanol (Absolute)	Sigma-Aldrich	E7023
Methocel™ / Methyl cellulose 60HC	Sigma-Aldrich	64670
Sucrose (Dihydrate)	Sigma-Aldrich	S0389
Trehalose (Dihydrate)	Sigma-Aldrich	D6663
Foetal Calf Serum (FCS)	Sigma-Aldrich	F-2442
Polysorbate (TWEEN®) 20	Sigma-Aldrich	P2287
L-Glutamine	Gibco, UK	31350-010
Penecillin-Streptomycin	Sigma Aldrich	P-0781
2-Mercaptoethanol	Gibco	13150-010
Sodium azide	Sigma-Aldrich	S2002
Immersion Oil	Sigma-Aldrich	10890
Neutral buffered formalin	Sigma-Aldrich	HT501128
Bovine Serum Albumin (BSA)	Sigma-Aldrich	A2153
Sodium Azide	Sigma-Aldrich	S2002
Ketaset™(ketamine hydrochloride)	BD Biosciences, UK	OUVS[3]
Domitor™(medetomidine hydrochloride)	Fort Dodge Animal Health, UK	OUVS
Antisedan® (atipamezole hydrochloride)	Pfizer Animal Health, UK	OUVS
Isofluorane	Abbot Animal Health, UK	OUVS
Trypan Blue	Sigma-Aldrich	T8154
Giemsa	Sigma-Aldrich	GS1L
Ovalbumin [methyl-C14]	American Radiochemicals, USA	ARC0431-5
Soluene-350	Perkin Elmer, UK	6003038

[3] Sourced through the Oxford University Veterinary Services.

Reagent	Supplier	Catalogue number
Polysorbate (Tween)-20	Sigma-Aldrich	P7949
High viscosity CMC	BDH VWR, UK	80502-036
Low Melting Point agarose	Sigma-Aldrich	A-4018
Type IV Collagenase	Invitrogen, UK	17104-019
Collagenase-Dispase	Sigma-Aldrich	C1380
DNAse I	Sigma-Aldrich	D5319
BRIGHTGLO™ in vitroluciferase assay kit	Promega, UK	E2610
DNAeasy DNA extraction kit – blood and animal tissues	Qiagen, UK	69506
Lightcycler® FastStart SYBRGreenI Master mix	Roche, UK	03-515-869-001
Cytometer Set-up and tracking (CST) beads	BD Bioscience	340486
Cytofix / Cytoperm™ kit (+Golgi Plug™)	BD Bioscience	554714
QuickTiter™ Hexon Immunostaining kit	Cell Biolabs, USA	VPK-109
Mouse IFN-γ ELISPOT kit (ALP)	MabTech, Sweden	3321-2A
AP conjugate substrate kit	Bio-Rad	170-6432
LIVE/DEAD® Aqua	Invitrogen	L34957
293A cell line	Invitrogen, UK	R705-07
Chick Embryo Fibroblast cell line	Institute for Animal Health, Compton	-
TAPI-2	Merck Chemicals	579052
Triton-X	Fluka, Aus.	93420
Vybrant® DiD™	Molecular Probes, USA.	V-22887
Hoechst 33342	Invitrogen	H1399
Multiscreen ELISPOT nitrocellulose plates	Millipore, UK	MAIP-S4510
70µm cell strainer	BD Falcon™, UK	352350

TABLE 2-1: List of reagents and kits used in these experiments.

Where reagents were sourced both from the UK and Australia, suppliers of UK-sourced reagents only are listed. All other equipment / common reagent suppliers are listed in parentheses in this chapter or in Jenner protocols in Appendix I.

MONOCLONAL ANTIBODY LIST

Specificity (anti-mouse unless specified)	Conjugation	Supplier	Clone	Cat. No.
CD16/32 (Fc block)	None	eBioscience	93	14-0161-82
CD103	Biotin	eBioscience	2E7	13-1031
CD4	APC H7	BD Pharmingen™	GK1.5	560181
CD8	PercP-Cy5.5	eBioscience	53-6.7	45-0081-82
CD62L	Pacific Blue/eFluor 450	eBioscience	MEL/14	57-0621-82/48-0621-82
CD127	PE-Cy7	eBioscience	A.7R34	25-1271-82
IFN-γ	APC	eBioscience	XMG1.2	17-7311-82
IFN-γ	PE	eBioscience	XMG1.2	12-7311-82
TNF-α	FITC	eBioscience	N418	12-0114-83
IL-2	PE	eBioscience	JES6-JH4	12-7021-82
CD11c	PE	eBioscience	N418	12-0114-82
CD11b	APC-AlexaFluor 700	eBioscience	M1/70	56-0112-80
CD207	Alexa Fluor 647	Dendritics, Fr.	205C1	DDX6370A647
B220	PECy7	eBioscience	RA3-6B2	25-042-81
MHC II	APC-Alexa Fluor 780	eBioscience	M5/114.15.2	47-5321-82
CD80	FITC	eBioscience	16-1C0A1	11-0801-82
Isotype cotnrol (Rat IgG2a)	PECy7	eBioscience	eBR2a	57-4321-80
Isotype control (Rat IgG2a)	Pacific Blue	eBioscience	eBR2a	25-4321-81
Ly6G	PECy5	eBiosicnece	RB6-8C5	15-5931-81
Ly6C	APC	eBioscience	HK1.4	17-5932-80
anti-rabbit IgG (polyclonal, $F(ab')_2$ fragment)	Alexa Fluor 633	Molecular Probes, Aus	-	A-21072
Streptavidin	Alexa Fluor 450	eBioscience	-	48-4317-82
MHC II	FITC	Biolegend, Aus.	HIS-19	11-0920-82

TABLE 2-2: List of monoclonal antibodies used in these experiments.

All monoclonal antibodies used in Australia were purchased from Biolegend, Australia.

2.2 PATCH MANUFACTURE

Full details of all ImmuPatch and Nanopatch arrays used in these experiments are given in Table 2-7.

2.2.1 ImmuPatch

ImmuPatch arrays were fabricated from silicon wafers using 'wet-etch' technology at the Tyndall National Institute, Cork. Briefly, silicon wafers were square-patterned using mask photolithography such that 8-sided pyramidal microneedles of a defined length and density could be etched (268). Wafers were immersed in a hot bath of potassium hydroxide solution (80°C) for a pre-defined etch time resulting in the formation of sharp-tipped pyramidal microneedles on a silicon base. Wafers underwent quality control by Scanning Electron Microscopy (SEM).

2.2.2 Nanopatch

Silicon Nanopatches were fabricated by Deep Reactive Ion Etching (DRIE) at the Rutherford Appleton Laboratory, UK. Methodology is described in patent WO-2005/072630 (275). Briefly, after photolithographic application of a mask, wafers are placed inside a chamber with a gaseous mixture, which is subsequently ionised. Plasma ions are drawn towards the silicon substrate and selectively remove material when a potential difference is applied. Sharp-tipped microprojections (tip radius 200-500nm) are formed at a density of 21,025cm^{-2}. Two specifications of Nanopatch were manufactured – NP40, comprising 40µm conical microprojections, and NP110 – comprising a 70µm cylindrical shaft and a 40µm conical tip. Microprojections were sputter-coated with gold for optimal surface smoothness. Sample Nanopatches from each manufactured wafer were assessed for uniformity of microprojections by SEM.

2.3 VACCINES

All viral vector vaccines were made, propagated and titrated by past or existing members of the Jenner Institute and its Vector Core Facility. Brief details are given here, with reference to published methods or Jenner Protocols compiled in Appendix I.

2.3.1 Transgene antigens

2.3.1.1 PbCSP

PbCSP is the native circumsporozoite protein from the ANKA strain of *Plasmodium berghei* (accession number: PBANKA_040320; www.plasmodb.org). The full αα sequence is:

MKKCTILVVASLLLVNSLLPGYGQNKSIQAQRNLNELCYNEGNDNKLYHVLNSKNG
KIYNRNTVNRLLADAPEGKKNEKKNEKIERNNKLKQPPPPPNPNDPPPPNPNDPPP
PNPNDPPPPNPNDPPPPNANDPPPPNANDPAPPNANDPAPPNANDPAPPNANDP

APPNANDPPPPNPNDPAPPNANDPPPPNPNDPAPPQGNNNPQPQPRPQPQPQP
QPQPQPQPQPQPQPRPQPQPQPGGNNNNKNNNNDD**SYIPSAEKI**LEFVKQIRDSITE
EWSQCNVTCGSGIRVRKRKGSNKKAEDLTLEDIDTEICKMDKCSSIFNIVSNSLGFVI
LLVLVFFN - 340αα

The immunodominant CD8+ (H2-K^d) restricted epitope Pb9 (αα 253-261 of the C terminal region) is highlighted.

2.3.1.2 ME-TRAP

ME-TRAP is a composite antigen fusing the full length *P.falciparum* strain T9/96 TRAP (Thrombospondin-Related-Adhesion-Protein) with a Multiple-Epitope (ME) string consisting of 14 CD8+ epitopes, one CD4+ epitope and two B cell epitopes from six pre-erythrocytic antigens and two non-malarial T cell epitopes (P11 and P15 of Ag85A of *Mycobacterium bovis*)(250). It also contains the CD8+ H2-K^drestricted epitope Pb9 of *P.berghei*CSP (SYIPSAEKI).

2.3.1.3 Reporter transgenes

GFP is the enhanced Green Fluorescent Protein (derived from *Aequorea victoria*) and RFP is the Red Fluorescent Protein derived from *Discosoma* spp. pLuc is the luciferase enzyme derived from the firefly *Photinus pyrillis*.

2.3.2 Generation and propagation of recombinant MVA and Adenovirus-vectored vaccines

2.3.2.1 MVA (Jenner Protocols J013, 16-19, 79)

The construction of MVA.PbCSP has been described (276, 277). Transgenes are driven by the P7.5 promoter and flanked by non-essential Thymidine Kinase sequences. Homologous recombination between an MVA.RFP with an MVA shuttle vector (encoding the gene of interest plus a selection marker gene *lacz* or *gfp* – coding for β-galactosidase and GFP, respectively) occurs, displacing the RFP to allow positive selection of recombinants. The markerless clinical construct MVA.ME-TRAP was selected by the transient dominant method as has been described (278). Recombinant MVA was grown up in CEF and purified by ultra-centrifugation through a 36% $^w/_v$ sucrose cushion following sonification. Master stocks were stored as aliquots in 10mM TBS (pH 9) at -80°C. MVAs were assessed for correct ID and purity by PCR.

2.3.2.2 Adenoviruses (Jenner Protocols J005, 07-09)

Recombinant AdHu5 and AdCh63 constructs were generated using the ViraPower Adenoviral expression system (Invitrogen). Adenoviral vectors with E1 and E3 regions deleted can accommodate up to 7.5Kbp of inserted DNA whilst retaining genetic stability (279). Deletion of E1 also renders Adenoviruses replication-incompetent. The Virapower system uses site-specific recombination using bacteriophage lambda, a phage of *E.coli*. Using this system the transgene is ligated into the E1 site of a pENTR4.hCMV.BGH entry vector containing the human CMV promoter with regulatory element, enhancer and intron A (252). This is then recombined using a bacteriophage lambda LR clonase enzyme and inserted into a pAd-DEST destination vector lacking a promoter and recombination confirmed by restriction digest. This vector is then used to transfect the packaging cell line HEK-

293A, which are permissive for Adenovirus infection and growth since they provide E1 supplementation. Following virus infection and amplification, cells are lysed and fresh HEK-293A cells are re-infected with lysate for further amplification before purification.

Recombinant Adenoviruses were purified using an isopycnic caesium chloride ($CsCl_2$) density gradient method. The virus band observed by eye was collected and dialysed into storage buffer (10mM TBS containing 7.5% $^{w}/_{v}$ sucrose, pH 7.8). Both MVA and Adenovirus vaccines were tested for sterility (i.e. absence of aerobic bacteria and fungi).

2.3.3 Ad and MVA titration (J082, J111, J106, J104)

MVA viruses were titratedby standard plaque assay (J082) or immunostaining (markerless MVA, J111). Plaques were visualised by expression of an inserted reporter transgene -fluorescence of GFP or by β-gal activity. MVA titres/doses are expressed as Plaque Forming Units (PFU). Ad were titrated by photospectrosopy (number of viral particles - VP, J106) and also by immunostaining of the common hexon protein (number of infectious particle units – IU, J104). Viral particle: infectious unit (PI) ratios were used to account for differences in infectious titre between Ad preparations when calculating dosage. Ad doses are expressed in VP and titres (Chapter 5) in IU.

2.3.4 Vaccine schedules

Two prime-boost immunisation schedules were used throughout these experiments:
MVA/MVA homologous prime-boost: A recombinant MVA prime was given. 2 weeks before a recombinant MVA boost (encoding the same transgene). Post-prime immune responses were assessed 1 or 2 weeks post-prime and post-boost responses were assessed 2 weeks following the boost. Where mice were challenged, this was performed 2 weeks following a boost immunisation.

Ad/MVA heterologous prime-boost: A recombinant Ad prime was given and 8 weeks later a recombinant MVA boost (encoding the same transgene) was given. Post prime responses were assessed at various timepoints post-prime (usually given after 2 or 3 weeks), and post boost responses 2 weeks after the boost.

2.3.5 Preparation of vaccines for needle-based and liquid patch immunisations

Vaccine aliquots were removed from -80°C storage and allowed to thaw before diluting in endotoxin-free sterile PBS to the required dose. Single doses were delivered in a total volume of 50uL (intradermal and intramuscular immunisation) or in 10uL (liquid patch immunisation) divided bilaterally between ears/caudal thigh muscles.

2.3.6 Dry-coating formulation

Vaccine aliquots were thawed and mixed with Methyl Cellulose (MC) and the surfactant Polysorbate 20 (PS20) at concentrations of 1% $^{w}/_{v}$ and 0.1% $^{v}/_{v}$ respectively. For Ad formulations, solutions of the stabilising sugars trehalose + sucrose (10% $^{w}/_{v}$ each) were added. In one experiment trehalose only was included (Figure 5-15). The total volume applied per Nanopatchwas 6-8uL. Vaccine either added to this mixture undiluted or after first being diluted to a desired dose with endotoxin-free sterile PBS.

2.3.7 Dry-coating method

Nanopatch microprojections were coated with vaccine formulations using a nitrogen jet method optimised at the D^2G^2, described in (270).A volume of coating solution was pipeted onto microprojection tips. Using curved forceps, Nanopatches were held at a 45° angle to a rubber tube supplying nitrogen gas at a constant rate (see Figure 5-1B). The tube was moved in a circular motion to spread the solution down towards the base whilst simultaneously coating microprojection tips and shafts. All coating procedures were carried out at the D^2G^2, U. Queensland.

2.3.8 Assessment of virus viability

2.3.8.1 MVA viability by plaque assay

After seeding CEF at a density of $1x10^6$ cells per well in 6-well plates (Corning) and incubating at 37°C + 5% CO_2 until 70% confluent, MVA.GFP coating formulations/patch eluates were prepared and were serially diluted from 10^0 to 10^{-8} (thoroughly vortexing between dilutions) and used to infect CEF in duplicate. 100µL dilution was added to 1mL 10% DMEM in each well. One hour following infection of seeded cells with dilutions 10^{-6} to 10^{-8}, Carboxymethyl Cellulose (CMC) diluted 1:3 in 2% DMEM was overlaid. After a further incubation for 2 days, fluorescent green plaques were visualised and counted by fluorescent microscope (Leica).

2.3.8.2 Adenovirus viability by hexon immunostaining

HEK 293A cells were seeded in poly-L-lysine pre-treated 96-well plates at a density of $4.4x10^4$ cells/well in a 96-well plate and incubated overnight at 37°C, 5% CO_2. AdCh63.ME-TRAP coating formulations and patch eluates were prepared and serially diluted from 10^0 to 10^{-10}. 50µL of dilutions 10^{-7}–10^{-10} were added in triplicate and incubated overnight at 37°C, 5% CO_2. The following day, 50µL 10% DMEM was added to each well to supplement cells, and plates were incubated overnight. Forty-eight hours after virus infection, media was aspirated from each well and cells were fixed with 100µL chilled methanol, and plates were incubated at -20°C for 20 minutes. Cells were immunostained using a kit from Cell Biolabs (D^2G^2) or using individually purchased mAbs (Oxford). Wells were washed 3 times with PBS before blocking for 1h at RT with 100uL PBS-BSA1%. After further washing, 50µL/well primary anti-hexon antibody (1:1000 in PBS-BSA1%) was added and incubated for 1h at RT. Plates were washed as before and 50µL/well secondary anti-HRP antibody (1:1000 in PBS-BSA1%) was added and incubated for 1h at RT. After both assays above viral viability (titre) was ascertained using the following formula:

PFU or IU per mL = Average no. plaques (MVA) or single-stained cells (Ad) x serial dilution x dilution factor

2.3.9 Stability studies

Coated Nanopatches were placed in airtight containers containing a quantity of hygroscopic lithium chloride salts to maintain a constant humidity of 11%(280). Containers were placed at room temperature (~22°C) or at 37°C for varying time periods before elution of coating material into PBS in 1.5mL tubes overnight (Fisher Scientific) after 1 minute of vortexing. To evaluate Adenovirus viability (ability to infect cells) elutions were added to cell monolayers in plaque hexon immunostaining assays. (2.3.8.2)

2.4 ANIMALS

2.4.1 Mice and regulated procedures

Female BALB/c (haplotype H-2^d) mice were purchased from the Biomedical Services Unit (Oxford) or Monash University (Australia) or from the commercial suppliers Harlan or Charles River (UK). C57BL/6 mice were bred in-house (U. Queensland). Ages ranged from 6-12 weeks upon experiment commencement and all mice within one experiment were age-matched within 2-4 weeks. Mice were housed sterilely in individually ventilated cages. All experimental procedures carried out in the UK were according to the terms of the Animals (Scientific Procedures) Act under a Project License (PPL 30/2414) and Personal License (PIL 30/7793) and approved by the University of Oxford Animal Care and Ethical Review Committee. Animal work carried out in Australia was done so according to the regulations of the University of Queensland Animal Ethics Committee.

2.4.2 Anaesthesia

Animals were immobilised prior to immunisation procedures by injectible (UK, Australia) or inhalational anaesthesia (UK only). Injectable anaesthetic – mice were injected with a mixture of 35mg/kg Ketaset™ and 0.5mg/kg Dormitor™ in endotoxin-free water into the peritoneum. Following the procedure, mice were given 100µL Antisedan™ diluted 1:10 with endotoxin-free water and incubated at ~20°C until mobile. Inhalational anesthesia – mice were placed in an airtight container supplied with a mixture of oxygen and isofluorane. During the procedure, anaesthesia was maintained using a nose cone.

2.4.3 Blood sampling

Groups of mice were warmed to 37°C in individual compartments of a heated chamber to induce dilation of the tail vein. Mice were removed individually and placed into a restrainer. A small incision was made in the tail vein and 4-9 drops of blood were taken into a tube containing 200µL 10mM EDTA/PBS. In experiments

performed in D^2G^2, blood was taken from the retro-orbital plexus into heparinised capillary tubes by trained technicians.

2.5 IMMUNISATIONS

2.5.1 Conventional needle-based immunisations

Intradermal vaccine doses were administered bilaterally into the dorsal ear pinnae in a total volume of 50µL using a 29G insulin syringe (BD Micro-Fine^{TM}). Intramuscular immunisations were given bilaterally into the caudal thigh muscle (total volume 50uL) using a 25G needle following removal of hair covering the muscle using hair clippers.

2.5.2 Liquid patch immunisations

Patches were prepared for immunisation: individual ImmuPatch arrays were affixed to the plunger of a 2mL (5mm^2 arrays) or 5mL (7mm^2, 10mm^2) syringe (BD) after removal of the rubber bung. Three Nanopatch arrays were affixed to a steel rod of length 70mm in 'L-shape' arrangement to best fit the mouse ear. Anaesthesised mice were placed atop a polystyrene board covered with tissue paper. 5uL of vaccine was pipeted onto the dorsal surface of each ear pinna in a single drop. Patches were applied for 10 seconds, removed for 10 seconds, and re-applied for 10 seconds. This process was performed on both ears. One patch / patch array was used to immunise both ears of 4-5 mice.

2.5.3 Vaccine-coated Nanopatchapplicator-assisted immunisation

Vaccine-coated Nanopatches were applied to mice within 1 hour (experiments performed in D^2G^2) or maximum 3-4 days (shipping time Brisbane to Oxford). A single patch was placed onto an adhesive carbon tab (Electron Microscopy Services, Aus) onto the exterior of a custom-made spring applicator device (189). To set the device, the inner spring was retracted and held in place by inserting a pin into a hole on the exterior. Anaesthetised mice were positioned on the base of an applicator stand with the ear pinnae resting on a linolium block. The device was suspended ~1cm above the surface of the ventral of the mouse ear. When the pin was removed, the mass was released and struck the carbon tab and delivering the Nanopatch to the ear at a velocity of 1.96ms^{-1}(189). The Nanopatch remained in place for 5 minutes after application to the ear. Two or 3 individual Nanopatches were applied to each mouse sequentially.

2.6 ASSESSMENT OF IMMUNOGENICITY

2.6.1 Preparation of single cell lymphocyte suspensions

PBMC: Blood samples (taken into 10mM EDTA) were treated with 1mL ACK lysis buffer before centrifugation at 4000rpm for 4 minutes. The supernatant was discarded and 1mL ACK added again before centrifugation and removal of

supernatant. Cell pellets were resuspended in volumes of C-MEM: 500uL after single or MVA/MVA immunisation; or 800µL after Ad/MVA immunisation.

Spleens and auricular LNs: Organs were harvested from euthanised mice using ethanol-cleaned instruments and homogenised by hand in PBS before being passed through a 70µm strainer. After centrifugation at 1500 rpm for 5 minutes pellets were re-suspended in 5mL ACK lysis buffer and incubated at RT for 5 min. An excess of PBS was added and cells were centrifuged at 1500 rpm for 5 min. Pellets were re-suspended in 0.5-1mL (LN) / 5mL (spleens). RBC debris was removed from spleen samples by pipette.

2.6.2 Peptide re-stimulation

The peptide Pb9 were synthesised by Invitrogen (Paisley, UK) was reconstituted in DMSO and kept at a stock concentration of 10 mg/mL at -20°C. Working stocks were further diluted to 1mg/mL and kept at -20°C. The H2-K^d restricted CD8+ T cell epitope Pb9 is a 9-amino acid peptide located at the C-terminal region of the *P. berghei* CSP. Pb9 was used to re-stimulate cells following immunisation with PbCSP and ME-TRAP expressing vaccines at a final concentration of 1µg/mL.

2.6.3 *Ex vivo* IFN-γ ELISPOT

Cell suspensions were plated on anti-IFN-γ AN18 mAb pre-coated nitrocellulose membrane plates (Millipore) and incubated for 18 hours at 37°C, 5% CO_2 with the peptide Pb9. Aliquots of cells were taken for counting using a CASY™ cell counter (or by eye after Trypan Blue staining/Invitrogen Countess® counter in U.Queensland). Spleen cells were plated at concentrations of $5x10^6$ cells/mL (following a single immunisation, or MVA prime/MVA boost) or $2x10^6$ cells/mL (after Ad/MVA prime-boost). Naive splenocytes at a cell concentration of $5x10^6$ cells/mL were added to wells containing PBMC to amplify antigen presentation. Unstimulated control wells contained cells but no peptide. Each sample was plated at 10^0 and serial dilutions of 10^{-2}, 10^{-4}, and 10^{-8}. The following day, cells were discarded and plates washed 3 times with PBS. Anti-IFN-γ biotin-conjugated antibody (50µL, 1:1000 in PBS) was added to wells and was incubated for 2 hours at RT. Following further plate washing with PBS, Steptavidin-Alkaline Phosphatase was added to wells (50µL, 1:1000 in PBS) and incubated for 1 hour at RT. To develop the assay, plates were washed as before and colorimetric substrate was added, as made according to the kit manufacturers' specifications (Biorad). Spots were counted using an ELISPOT plate reader and software (AID). The number of Spot Forming Cells (SFC) per million cells was calculated.

2.6.4 Intracellular cytokine staining and T cell phenotyping

Lymphocyte preparations were plated in U-bottom 96-well plates (Corning) and incubated with Pb9 (1µg/mL) and Golgi Plug™ (Brefeldin A, 2µg/mL) in 100µL per well C-MEM. For cells to be stained with CD62L, TAPI-2 was added (1:250). Only Golgi Plug™ and TAPI-2 were added to unstimulated control wells. Cells were incubated for 5 hours at 37°C and 5% CO_2 and kept at 4°C overnight. The following

day cells were transferred to V-bottom wells (Nunc) and centrifuged at 1500 rpm for 5 minutes at 4°C. Pellets were re-suspended in anti-CD16/32 to block Fc binding sites, diluted 1:100 in FACS buffer (total volume per well - 50µL). Cells were incubated for 15 minutes at 4°C. Following washing of cells with FACS buffer, cell pellets were re-suspended in a surface-staining antibody cocktail - Table 2-3 (total volume 50µL/well, diluted in FACS buffer).

Specificity	Fluorochrome	Reciprocal dilution
*CD4	APC H7	100
CD8	PercP Cy5.5	100
CD62L(/IgG2a)	Pacific Blue	100 (800)
CD127(/IgG2a)	PECy7	100 (100)

TABLE 2-3: Surface staining panel for T cell immunogenicity and phenotyping experiments.

***CD4 APC H7 was included to aid differentiation of CD4+ and CD8+ populations but was not included in some early experiments. Gating strategies are detailed in individual figure legends.**

Isotype controls for the memory markers CD62L and CD127 were stained with the irrelevant marker IgG2a (in parentheses in table). Cells were incubated in the dark at 4°C for 30 minutes. Following washing of cells, i.e. adding 150µL/well FACS buffer, centrifugation at 1500rpm for 5 minutes, discard of supernatant and re-suspension of pellets, cells were permeablised using a BD Cytofix/Cytoperm^{TM} kit (BD). Cells were intracellularly stained using the monoclonal antibody panel (Table 2-4) in a total volume of 50µL Cytoperm[4] per well.

Specificity	Fluorochrome	Reciprocal dilution
IFN-γ	APC	500
TNF-α	FITC	100
IL-2	PE	100

TABLE 2-4: Intracellular staining panel for T cell immunogenicity and phenotyping experiments.

In one experiment IFN-γ PE was used instead of IFN-γ APC, as indicated in the corresponding figure legend.

Cells were incubated in the dark at 4°C for 15 minutes. Following centrifugation at 1500 rpm they were washed twice with Cytoperm and twice with FACSbuffer before final suspension in 1% $^{v}/_{v}$ PBS-Formalin for data acquisition by flow cytometry. Data is presented as average CD8+ IFN-γ+ or CD8+ cytokine+ (where a gate is set to include all cells secreting any combination of IFN-γ, TNF-α and IL-2) as described in individual figure legends, with details of gating strategies.

[4] First diluted from 10X in deionised H_20 according to kit instructions.

2.7 PLASMODIUM BERGHEI SPOROZOITE CHALLENGE

2.7.1 Isolation of *P.berghei* sporozoites

Female *Anopheles stephsensi* mosquitoes were propagated and infected with *Plasmodium berghei (*ANKA strain clone 234*)* by ingestion of a blood meal from infected mice by Mark Tunnicliff at Imperial College, London or by Andrew Williams at the Jenner Institute, Oxford. Infected mosquitoes were cooled on ice before removal of salivary glands under dissection microscope. Salivary glands were placed into RPMI 1640 and gently homogenised using a glass pestle and mortar (Fisher Scientific). Sporozoites were counted under a phase contrast microscope (Leica) and the concentration adjusted such that each mouse received 1000 sporozoites per 100µL inoculation.

2.7.2 Intravenous inoculation of sporozoite preparations and post-challenge monitoring

Immunised mice were individually identified by ear notch and placed into a warming chamber. Each mouse received a 100µL inoculation of *P berghei* sporozoites, injected into the tail vein using a 1mL insulin syringe. Mice were monitored days 1-20 post-challenge for signs of malaise and by thin blood smear for the presence of blood-stage parasitaemia day 5-20. Mice testing positive for parasites were euthanised after confirmation of blood stage infection by 3 positive smears. To prepare thin blood smears, one drop of blood from the tail tip was smeared across a glass slide. Slides were air-dried, fixed in methanol for 5 minutes and subsequently stained with Giemsa (5% $^{v}/_{v}$ in dH_20) for 2h at room temperature. After air-drying the slide was examined under a light microscope at 100x magnification and mineral oil immersion. Each slide was scored positive or negative for blood-stage parasiteamia/erythrocyte-associated parasites were counted (see 2.13.2). Protection was defined as the complete absence of parasites in the blood to day 20.

2.8 ASSAYS FOR ESTIMATING DELIVERY EFFICIENCY BY PATCH

2.8.1 Quantitative PCR for Adenoviral genomes

2.8.1.1 DNA extraction from skin and LN tissues

A real-time PCR assay was used to quantify of Adenoviral genomes (the sequence corresponding to the human CMV promoter, *hcmv*, which is inserted into the Adenoviral genome upon recombinant Adenovirus construction) present in skin and auricular LN following immunisation, relative to the housekeeping gene murine GAPDH (*mgapdh*). Ears and LNs from mice immunised with $1x10^{10}$ VP AdCh63ME-TRAP by ImmuPatch or ID were excised 2 hours following the procedure. Tissues from naïve animals were also taken. Two hours was pre-determined as the optimal timepoint post-immunisation for assessment. Ears were separated down the coronal plane using curved forceps and cut into small pieces into Dispomix^{TM} tubes (Thistle

Scientific) and adding 1mL PBS before fixing tightly into a Dispomix^{TM} machine in an inverted position. A 2-step program was applied: 1) a 20 second gradation spin/cut cycle followed by 2) a fibrous tissue specific program with 90 seconds of homogenisation. Tubes were removed, reverted and centrifuged at 1500 rpm to collect all homogenate at the bottom. Homogenates were transferred to microcentrifuge tubes (Starstedt) containing silica beads. A mini-bead beater (Glen Mills Inc.) was used (2 x 1 minute per sample) to yield a homogneous tissue extract. LNs were taken into 1mL PBS, cut into pieces using fine scissors. Smooth tissue extracts were yielded by bead beating only. Extracts were transferred to fresh microcentrifuge tubes (200uL) with 20uL proteinase K + 180uL tissue lysis buffer (part of a Qiagen kit for DNA extraction from animal tissues). After a 4 hour water bath incubation (56°C) 200uL of pre-mixed AL buffer + 100% ethanol was added and vortexed, before transferring to an extraction column (Qiagen). The remainder of the DNA extraction protocol was followed according to Qiagen kit instructions(281), and extracted DNA was stored at -20°C.

2.8.1.2 *hcmv* promoter-specific quantitative PCR

Samples (DNA template extracted from skin and LN) were allowed to thaw to room temperature. Primers specific for *hcmv* and murine *gapdh* were previously designed by Dr. Simon Draper (*mgadph*-(223) / Clinical Biomanufacturing Facility (*hcmv*) and ordered from Eurofin MWG Operon, Germany. Primers were reconstituted to a concentration of 100 pmol/µL using DNAse free water. Sequences were as follows:

hcmv-F : 5'-GTACGGTGGGAGGTCTATATAAGC A-3' (Jenner Oligo. J309)
hcmv-R: 5'-GGTGTCTTCTATGGAGGTCAAAACA-3' (Jenner Oligo. J310)
mgapdh-F:5'-TTCACCACCATGGAGAAGGC-3' (Jenner Oligo. J-43/598)
mgapdh-R: 5'-GGCATGGACTGTGGTCATGA-3' (Jenner Oligo. J-44/598)

Primer mixes were made by diluting 1:10 (100mM to 10mM) in DNAse free water, combining forward and reverse in a total volume of 1µL per primer per reaction. A master mix was made:

Per well:

Combined F+R primer mix (0.5µM per primer)	2µL
SYBRGREEN® master mix (containing Taq polymerase + dNTPs)	10µL
DNAse free water	3µL
Sample DNA template	5uL
∑	20uL reaction volume

Samples were added to a V-well PCR plate (Corning) in duplicate and standards in triplicate. A non-template control was also added as a negative control (water replacing DNA template). An adhesive plate cover was added and the plate was centrifuged (1500 rpm, 5 minutes) to concentrate the reaction mix at the bottom of the well before the reaction was run on a LightCycler 450® PCR machine using the following conditions:

hcmv reaction: Stage 1 – hot start (5 minutes at 95°C). Stage 2 – denaturation and annealing (45 cycles of 10 seconds at 95°C, 10 seconds at 60°C, 15 seconds at 72°C). Data was acquired at the end of each cycle. Stage 3 – melt curve (10 seconds at 95°C, 1 minute at 65°C ramp to 95°C at a rate of 2.2°C/seconds with 5 acquisitions per °C. This was followed by a cooling stage of 10 seconds at 45°C.
mgapdh reaction: Stage 1 – hot start (10 minutes at 95°C). Stage 2 – denaturation and annealing (35 cycles of 15 seconds at 95°C, 1 minute at 60°C) (282). Data was acquired at the end of each cycle. Stage 3 – melt curve (10 seconds at 95°C, 1 minute at 65°C ramp to 95°C at a rate of 2.2°C/seconds with 5 acquisitions per °C. This was followed by a cooling stage of 10 seconds at 45°C.

Since an appropriate plasmid control for *mgapdh* was not available for absolute quantification, a relative ratio of the *hcmv*Ct:*mgapdh* Ct was calculated using the formula: 2^{-dCt}, where dCt is the difference in cycle threshold (i.e. the number of PCR cycles taken forthe fluorescent signal to cross a pre-defined background level) between *hcmv*, and *mgapdh* nucleic acid amplification (283).

2.8.2 *Ex vivo* luciferase assay to quantify transgene expression

Expression of firefly luciferase from recombinant Adenoviral vectors was determined from primary skin cell and draining LN cell supernatants in an *in vitro* luciferase assay. BALB/c mice were immunised with AdCh63.pLuc (expressing firefly luciferase from *Photinus pyrallis*) either ID or by ImmuPatch. Twenty-four hours later immunised and naïve mice were euthanised and ear pinnae and auricular LNs collected into bijou tubes. LNs were collected into 2mL PBS and cut into small pieces using fine scissors. 20uL of 30mg/mL collagenase-dispase was added (0.3mg/mL final concentration) with 4uL DNAse I (final concentration 0.02mg/mL). Dorsal and ventral aspects of the ear pinnae were separated using curved forceps and cut into pieces and returned to the bijou tube. 2mL PBS was added to each tube with 2µL type IV collagenase. LNs were rotated at RT for 30 minutes. Skin samples were incubated at 37°C for 35-40 minutes in a water bath. To inactivate collagenase enzymes 200uL 0.5M EDTA was added to LN tissue lysates, and 200uL FCS was added to skin tissue lysates. Cells were recovered from lysates by passaging through a 70µm strainer (Corning) and centrifuging at 1350 rpm for 5 minutes.

Supernatants were discarded and pellets re-suspended in PBS for counting. One million cells/well in a 96-well plate were re-suspended in 200µL BRIGHTGLO™ cell lysis buffer and underwent one freeze-thaw cycle at -80°C before centrifugation at 1350 rpm to remove cell debris. Supernatants were transferred to a black 96-well plate (Corning) and BRIGHTGLO™ beetle luciferin reagent added (1 part to 1 part supernatant). PBS was added to control wells. After a reaction time of 5 minutes luciferase activity (in Relative Light Units) was assayed by luminometer (Varioskan).

2.8.3 ^{14}Carbon scintillation assay

To quantify Nanopatch payload delivery to skin, ovalbumin labelled with radioactive ^{14}Carbon (^{14}C-OVA) was mixed with varying doses of vaccine in liquid and coating solutions. Each coated Nanopatch/liquid dose for Nanopatch delivery contained ^{14}C-OVA at final concentration of 1µCi/µL. Ear surfaces were swabbed twice with a cotton bud to remove remaining on the skin after immunisation. Cotton buds and used Nanopatches were collected in scintillation vials and 1mL PBS was added and mixed. Ear pinnae were excised and added to 750µL tissue solubiliser solution (Solvable®) in a Reactivial™ (Thermoscientific, USA) and heated to 60°C for 2 hours. β-particle emission from radioactive decay of ^{14}C (half-life 5700 yrs) from used patches, swabs and solubilised ear samples was collected using a scintillation counter.

2.9 RT-PCR FOR CYTOKINE AND CHEMOKINE EXPRESSION

Carried out by A. Vrdoljak at UCC, Ireland. Excised ear pinnae and LNs were snap-frozen in liquid nitrogen immediately after harvesting, 6, 12 or 18 hours post-immunisation. Naïve tissues were also taken. Methods for RNA extraction, cDNA preparation and real time PCR from tissues was as described in (265) The relative expression of the following genes was measured: *tnf-□ il1□, il1-□, il6, il-10, tgf-□1, ccl4, ccl5, il12 □□□*. Cycle numbers at threshold crossing (Ct) values were subtracted from Ct values for a control housekeeping gene, *mgapdh* (dCt) using the calculation described in 2.8.1.2.

2.10 PHENOTYPING SKIN AND LN INNATE CELL POPULATIONS

2.10.1 Isolation of skin and draining LN cells

At timepoints post-immunisation mice were sacrificed and ear pinnae and auricular (skin-draining) LN were excised. LNs were collected into 2mL PBS in bijou tubes and chopped using fine scissors. 20uL of 30mg/mL collagenase-dispase was added at 0.3mg/mL final concentration with 4uL DNAse I at final concentration 0.02mg/mL. Tubes were rotated at room temperature for 30 minutes before enzyme inactivation by adding 200uL 0.5M EDTA. Dorsal and ventral aspects of the ear pinnae were separated using curved forceps and cut into pieces and returned to the bijou tube. 2mL PBS was added to each tube with 2µL type IV collagenase and they were

incubated at 37°C for 35-40 minutes in a water bath, before inactivation with 200uL FCS. Cells were recovered by passing through a 70µm strainer (Corning) and centrifuging at 1350 rpm for 5 minutes. Supernatants were discarded and pellets re-suspended in FACS buffer for staining.

2.10.2 Staining protocols and panels

Following re-suspension in FACS buffer an aliquot of cells was taken for counting using a CASY™ counter and plated out in V-bottom 96 well plates (Nunc) (100uL/well) and centrifuged at 1500 rpm for 5 minutes at 4°C. Pellets were re-suspended in anti-CD16/32 to block Fc binding sites (diluted 1:100 in FACS buffer), anti-CD103-biotin (panel 1 only) (1:50) and LIVE/DEAD® Aqua, which was reconstituted in DMSO according to kit instructions and used at 1:200. Following 15 minutes incubation at 4°C in the dark, 150uL FACS buffer were added/well and plates were centrifuged at 1350 rpm for 5 minutes. Cells were re-suspended in one of the two staining panels (Tables 2-5 and 2-6) and incubated for 30 minutes at 4°C in the dark. Cells were washed with FACS buffer as before twice before re-suspension in 200uL FACS buffer for data acquisition by flow cytometry.

Specificity	Fluorochrome	Reciprocal dilution
CD8	PercP Cy5.5	100
CD11c	PE	50
CD11b	Alexa Fluor 700	100
CD207	Alexa Fluor 647	200
B220	PECy7	200
MHC II	Alexa Fluor 780	400
CD80	FITC	100
Streptavidin	Pacific Blue	100

TABLE 2-5: Panel 1 - for phenotyping of DC subsets in the skin and draining LN.

Specificity	Fluorochrome	Reciprocal dilution
CD11c	PE	50
CD11b	Alexa Fluor 700	100
F4/80	Pacific Blue	100
Ly6G	PECy5	100
Ly6C	APC	100

TABLE 2-6: Panel 2 - for phenotyping of non-DC subsets in the skin and draining LN.

2.11 FLOW CYTOMETRY AND ANALYSIS

Following preparation of surface and/or intracellularly stained cells, data acquisition was performed on a BD LSR II flow cytometer and BD FACSDiva software. Datafiles were subsequently analysed using FlowJo software (version 8.8.7, www.flowjo.com). Anti-mouse Ig κ or anti-mouse/anti-hamster Ig κ mixed BD CompBeads™ were used for compensation. Gates for cytokines were based on unstimulated controls in ICS experiments and these background responses were subtracted from immunised responses. Gates for surface markers were set by eye, with the aid of isotype (anti-

IgG2a) and/or markerless controls (including all fluorochromes except the one of interest). Boolean gates were set for analysis of T cell phenotype before using Pestle and SPICE (v5.2) programs for detailed analysis and graphical representation. SPICE can be downloaded from http://exon.niaid.nih.gov/spiceand is its functions are described in (284).

2.12 MICROSCOPY

2.12.1 Scanning Electron Microscopy (SEM)

Scanning Electron Microscopy was performed on a Phillips XL30 or JEOL JSM 6400 microscope with assistance from members of the D_2G_2 and SEM facility, U. Queensland. Uncoated and vaccine-coated Nanopatcharrays were positioned on an adhesive carbon tab (Electron Microscopy Services, Aus) and placed under vacuum before imaging at a 45° tilt and under 15kV. Image analysis was performed on accompanying software.

2.12.2 Cryo-SEM for analysis of SC penetration

A qualitative overview of the skin surface during Nanopatchapplication was obtained by examination under SEM, using a method previously described (189). Briefly, individual Nanopatches were applied to the ear skin of C57BL/6 mice. Ears were snap-frozen after sacrifice and excision of ears plusNanopatch *in situ* in a slush liquid nitrogen solution. The Nanopatch was then removed in a vacuum and imaged at 5kV on a stage cooled to-180 °C within a Philips XL30 microscope (Philips, Netherlands).

2.12.3 Analysis of microprojectionpenetration by Confocal Microscopy

To measure penetration depths of microchannels created in murine skin, a lipophilic dye was applied as described in (189). Briefly, 2% $^{v}/_{v}$ Vybrant®DiD (Molecular Probes Inc., USA) was delivered as liquid or as mixed with 1%$^{w}/_{v}$ MCand dry-coated onto patches delivered to C57BL/6 ears. Ears were excised, fixed and cryo-preserved as previously described (285). Using a cryostat (Leica), 10µm sections of whole ear were taken from a number of areas across the patched area of ear skin and imaged using a confocal microscope (LSM510, Carl Zeiss, Germany).

2.12.4 Confocal imaging of delivered Adenovirus

Mice were immunised on the ventral of the ear pinnae with AdHu5.ME-TRAP coated Nanopatch microprojections and were euthanised 15 minutes later. Ears were excised and fixed in 2% $^{v}/_{v}$ paraformaldehyde in dH_20 and split along the coronal plane using forceps and the cartilage and dorsal side of the ear removed. After blocking for 1 hour with 5% $^{w}/_{v}$BSA in TBS and permeablising with 0.25%$^{v}/_{v}$ in Triton-X in TBS for 30 minutes, ear sections were stained with the following mAbs: rabbit anti-hexon, (1:1000), anti-MHCII FITC (1:50) and anti-CD207 Alexa Fluor 546 (1:100) all diluted in TBS for 1hour at RT, in the absence of light and under agitation.

After rinsing with TBS, sections were incubated with a secondary stain of anti-rabbit IgG Alexa Fluor 633 (1:100 in TBS) for 1 hour in the dark under agitation. Sections were washed 3 times in TBS before counterstaining with the DNA-binding nuclear stain Hoechst 33342 (1:10,000) for 30 minutes in dark before rinsing with TBS. Before imaging, ear sections were placed patch-site facing up onto a glass slide with cover slip. Fluorescence imaging was performed on a Zeiss LSM510 confocal microscope and analysed using accompanying software.

2.13 DATA ANALYSIS

2.13.1 Representation of data

Normality of distribution was assessed by use of the Kolmogorov-Smirnov test. Normally distributed data were expressed as mean ± Standard Error of the Mean (SEM), and statistically significant differences were defined using the unpaired t test or one-way Analysis of Variance (ANoVA) with Bonferroni's multiple comparison post-test to compare between groups. Data not demonstrating normal distribution was expressed as mean/median ± the Standard Deviation (SD)/range and differences determined using the non-parametric Mann Whitney U test or Kruskall-Wallis test with Dunn's post-comparison between groups. Correlations were performed using the Spearman's rank test. Analysis of data in SPICE was performed using Students t test (284). Graphpad Prism v5 was used for all other analyses (San Diego, www.graphpad.com). Significance was assigned to any P value less than 0.05. Levels of significance were indicated by asterisks - *P<0.05, **P<0.005, ***P<0.001.

2.13.2 Linear regression of parasite growth rates

After challenge of immunised mice, the number of parasitised RBC was ascertained for each mouse by taking an average count from 5 fields per thin blood smear from days 5-8 after the challenge. One confluent field of view was assumed to contain an average of 500 RBC in confluency, and percentage parasitaemia was calculated. Using a linear regression model developed by D. Wyllie (Jenner Inst.), the time in days at which each mouse would reach 0.5% parasitaemia was calculated for those that succumbed. The value 0.5% was chosen as an arbitrary point in the linear portion of the exponential growth curve. Using this data, a Cox's Proportional Hazards Regression model was implemented to test for differences in the chance of each group reaching the 0.5% parasitaemia threshold at any one timepoint, as compared to the control group during the monitoring period. The statistical package STATA was used to perform this analysis (by H. Watt and N. Williams, Centre for Statistics in Medicine, Oxford). Significance in differences between hazard ratios (i.e. the risk of 'the event' of a mouse becoming parasitaemic occurring within the time period as compared to that of naïve animals) was assigned to any P value less than 0.05.

Patch name	Chapter referred to	Patch side length (mm)	Patch surface area (mm^2)	Total number of microneedles	Micro-needle length (μm)	Microneedle density (per mm^2)	Microneedle base diameter (mm)	Total microneedle surface area (mm^2)	Total microneedle array volume (mm^3)	TAV catagory (ImmuPatch only)
A	3	5.4	29.16	16	100	0.55	69	0.18	0.0019	Small
F	3+4	5.4	29.16	100	100	3.43	69	1.14	0.0120	
B	3	5.4	29.16	16	200	0.55	138	0.73	0.0154	Intermediate
D	3	5.4	29.16	25	200	0.86	138	1.14	0.0240	
T190	3	6	36	36	190	1.00	126.6	1.43	0.0285	
E	3	5.4	29.16	36	200	1.23	138	1.64	0.0346	
T280c	3+4	5	25	16	280	0.64	186.6	1.38	0.0406	
C	3	5.4	29.16	16	300	0.55	207	1.64	0.0518	
G	3+4	7.4	54.76	81	200	1.48	138	3.69	0.0778	Large
T125	3	10	100	400	125	4.00	83.6	6.89	0.0902	
T280	3	6	36	36	280	1.00	186.6	3.11	0.0913	
H	3	7.4	54.76	36	300	0.66	207	3.69	0.1166	
T280b	3+4	10	100	81	280	0.81	186.6	7.00	0.2053	Extra Large
NP40	5	4	16	3364	40	210.25	70	19.65	0.1714	**-**
NP110	5	4	16	3364	110	210.25	70	*	*	**-**

TABLE 2-7: Table of information about all patches used in this thesis.

***Not determined as microprojection structure did not resemble a cone (see Figure 3-6).**

CHAPTER 3 CD8+ T CELL IMMUNOGENICITY AND PROTECTIVE EFFICACY OF PRIME-BOOST VACCINE REGIMES USING SILICON IMMUPATCH ARRAYS

3.1 INTRODUCTION

The case for prioritising the development of needle-free methods for delivering vaccines is particularly convincing within the context of diseases such as malaria, which is endemic in areas where healthcare resources are inexorably stretched. One of the most promising platforms for eliciting cellular immunogenicity against malaria antigens is their delivery by recombinant viral vectors such as replication-incompetant human and simianAdenovirus and MVA (286, 287). These vectors have been most extensively studied in the delivery of pre-erythroytic malaria vaccines, with the goal of eliciting high numbers of antigen-specific T cells capable of mediating intrahepatocyte parasite inhibition, completely preventing its progression to the symptomatic blood stage of infection (or lessening the erythrocytic burden in the case of a multi-component vaccine).

Prime-boost immunisation schedules using Adenovirus and MVA-based vaccines are demonstrating significant clinical promise against diseases such as malaria, tuberculosis, influenza, HIV and cancer, as reviewed in (11). Simian Adenovirus and MVA-vectors expressing the malaria-specific transgene ME-TRAP have demonstrated safety and immunogenicity in malaria-naïve recipients in an AdCh63/MVA prime-boost regimen and are now progressing to phase IIb clinical assessment in Africa (Ewer, in preparation). These studies are underpinned by substantial pre-clinical evaluation in mice and non-human primates that have established this regimen as the current leading approach for the induction of high level humoral and cellular responses (223, 262, 288, 289).
In the *P.berghei* model of malaria, priming with pDNA encoding PbCSP and subsequently boosting with MVA.PbCSP (i.e. 'heterologous' prime-boost)was found to be significantly more immunogenic and protective against live parasite challenge than a MVA.PbCSP prime, MVA.PbCSP boost 'homolgous' regimen (276). The reason for this is likely in part to be dueto the expansion of of anti-vector immunity following the primary MVA immunisation, which acts to inhibit secondary expansion upon boosting. This is mediated by virus neutralisation and/or competition between T cell clones specific for vector antigens with a single clone specific for the inserted epitope, specifically for peptide-MHC complexes and growth factors (253). Consequently, the weakly efficacious MVA/MVA regimen presents a useful tool for the assessment of interventions designed to improve upon immunogenicity and protective efficacy of malaria vaccines, such as targeting vaccine to the APC-rich microenvironment of the skin.

In order to access the cutaneous environment, the highly resistant SC must first be breached to allow deposition of immunogen. The SC is largely impermeable to particles of molecular weight greater than 500Da and so, for delivery of large molecules such as viral vectors (of the order of 10^7 Da), this barrier must be overcome (100, 290). This has been successfully achieved for the delivery of viral and non-viral vaccines and therapeutics by transient removal of the SC by abrasion, scarification or by dermal delivery using a single microneedle device to animal models and humans (44, 125, 127, 130, 291)(discussed in 1.4.2). However, abrasion and scarification may result in excessive inflammation and undesirable adverse

effects, and accurate intradermal immunisation is difficult to achieve using a needle and syringe, even when using a single microneedle device (43, 128).

In contrast, ImmuPatch is a simple, non-invasive microneedle technology designed to transcutaneously deliver vaccines via temporary conduits (microchannels) created by the physical breaching of the SC by microneedles, and their penetration into the superficial layers of the skin. Manufactured using 'wet-etch' technology and by virtue of their sharp tips and smooth sidewalls, ImmuPatch microneedles glide smoothly into tissue at very low insertion forces (approximately 15mN per microneedle) and without breaking (266), O'Mahony, *in preparation*. Optical Coherence Tomography imaging of human skin following application of 280µm microneedles demonstrated that microchannels created measured an average depth of 179µm±14µm, penetrating into 61% of the viable epidermis (accounting for epidermal deformation upon application)(269). Epidermal and dermal fluorescent dye delivery was confirmed using an *ex vivo* porcine skin model and an ImmuPatch array consisting of 200µm microneedles, whereas ID immunisation delivered only into the dermis (265).

Elsewhere, Bal *et al* have demonstrated that the specific design of microneedles on a patch influences the shape and depth of conduits formed and the transport of a topically applied dye into human skin (292). Studies investigating the influence of microneedle design upon the magnitude of the induced response are limited to antibody induction, and microneedle length, density (and area of application) were found to be independent factors in the induction of OVA-specific IgG, following delivery of recombinant ovalbumin by microneedles to HGP. However, increasing the antigen dose did increase titres (143). In the experiments presented in this chapter (and those reported by Carey *et al* - (265)) a number of ImmuPatch designs were used in order to investigate the effects of geometric parameters upon the CD8+ T cell response following immunisation. Details of all ImmuPatch arrays used are presented in Table 2-7.

Microneedle studies have thus far concentrated upon the delivery of subunit vaccines. Only three studiesat the time of writing had evaluated the transcutaneous delivery of live organism vaccines. Cytokine-secreting CD4+ T cells were induced following delivery of live, replicating mycobacterial BCG as coated onto 700µm microneedles to HGP(150). Another study reported the induction of neutralising antibodies against a licensed flavivirus-vectored vaccine against Japanese encephalitisfollowing delivery to macaques using a single hollow microneedle and an abrading patch with frustum-shaped microstructures. Titres were up to 7-fold higher than after cutaneous delivery compared tovaccine delivered SCu (130). The third study by Carey *et al*, was the first to report the induction of cellular immunity against a topically-applied, live viral vaccine following delivery bysolid microneedles, where a range of ImmuPatch microneedle arrays were found to induce antigen-specific cytokine-secreting CD8+ T cells following delivery of MVA.PbCSP to BALB/c mice(265).

In this chapter, Adenovirus and MVA viral vectors encoding pre-erythrocytic antigens (PbCSP and ME-TRAP) were delivered to BALB/c mice by ImmuPatch arrays of differing parameters. Immunogenicity was compared to that induced by the currently used needle-based route for the particular vaccine (ID/IM), in an attempt to assess the ability of ImmuPatch to induce comparable/superior responses. Efficacy of

immunisation was assessed using assays designed to evaluate CD8+ T cell responses to vaccine antigens, and protective efficacy evaluated using the *P. berghei* challenge model of malaria.

Specific aims of the work described in this chapter:

- To assess the immunogenicity of live $CD8^+$ T cell-inducing viral vectored regimes featuring ImmuPatch delivery of either the priming, or the priming and boosting immunisations. Both homologous (MVA/MVA) and heterologous (Ad/MVA) regimes are investigated.
- To delineate the effects of altering application methodology, microneedle design and applied dose upon the resulting cellular responses both after ImmuPatch prime and after ID or ImmuPatch boost.
- To quantify the amount of vaccine delivered into the skin and draining to the proximal LN following ImmuPatch immunisation, making comparisons between differing designs and against ID delivery.
- To evaluate the protective efficacy of ImmuPatch/ID and ImmuPatch/ImmuPatch prime-boost vaccination using lethal *P. berghei* sporozoite challenge.

3.2 STATEMENT OF HYPOTHESES

Here, I hypothesise that topically-applied liquid live viral vector vaccines may be successfully delivered by hand application of solid silicon microneedle arrays to murine skin, inducing antigen-specific T cell responses at least comparable to the needle-based method. Responses following malaria vaccination by ImmuPatch will demonstrate protection against *P.berghei* challenge. Specific design attributes of ImmuPatch arrays will influence the magnitude of the induced response, which isproposed due to differences in microchannel size/shape and hence the delivered dose of vaccine.

3.3 RESULTS

3.3.1 MVA/MVA prime-boost immunisation

3.3.1.1 ImmuPatch primes an antigen-specific T cell response that can be boosted to levels comparable to ID priming

To determine the ability of ImmuPatch to prime responses in a homolgous prime-boost regimen, mice were immunised with MVA.PbCSP either by using ImmuPatch T190 or ID. Two weeks following the prime, a boost of MVA.PbCSP was delivered to all mice ID. Numbers of IFN-γ-secreting T cells were enumerated by IFN-γELISPOT following Pb9 peptide stimulation of PBMC 2 weeks post-prime and 2 weeks post-boost (Figure 3-1A) and of splenocytes 2 weeks post-boost (Figure 3-1B). All mice in the T190-vaccinated group responded to the primary immunisation, though the mean level of the T190-primed response was lower than that of the ID-primed response

(1668, as compared to 3246 IFN-γ SFC/million PBMC). This difference was not found to be statistically significant (ns, P=0.220). A control group receiving only PBS by T190 did not induce a detectable response (P=0.019 compared to ID). Following the boost, T190- and ID-primed responses demonstrated equivalent levels of response. Mice receiving PBS by T190 demonstrated an increase in response attributable to a single dose of MVA.PbCSP post-boost, confirming that T190-PBS had not induced a response. Splenic responses 2 weeks following the boost immunisation were slightly higher in T190-primed mice compared to ID-primed mice, though not statistically significant (P=0.060, Figure 3-1B).

This experiment was performed a total of 5 times using T190 (Figure 3-1, C+D). To assess the variability of responses induced by T190 priming, IFN-γ ELISPOT results from 5 direct repeat experiments were pooled and each data point normalised to the mean of the ID-primed response within each experiment. Ratios of mean T190 response/mean ID response are presented as box and whisker plots in Figure 3-1, C+D. Across the 5 experiments there is a decreased average response ratio after T190 priming as compared to ID priming (ratio of IFN-γ SFC: mean ID IFN-γ SFC = 1:0.531) and an increased response ratio following T190/ID immunisation compared to ID/ID (1:2.185) after the boost. The interquartile range was greater following T190/ID boost than after ID/ID or T190 priming only. The splenic response ratio is close to 1 (1:1.175), indicating similar level of response in the spleen following ID/ID and T190/ID across the 5 experiments (Figure 3-1D). Again, the interquartile range was greater following T190/ID immunisation than ID/ID. This analysis suggests whilst post-prime variation in the T190 response is low, some T190-primed mice respond more effectively to an ID boost immunisation than others. More broadly, T190/ID immunisation was found to be at least as immunogenic as ID/ID immunisation, despite a trend to a lower response following the prime immunisation.

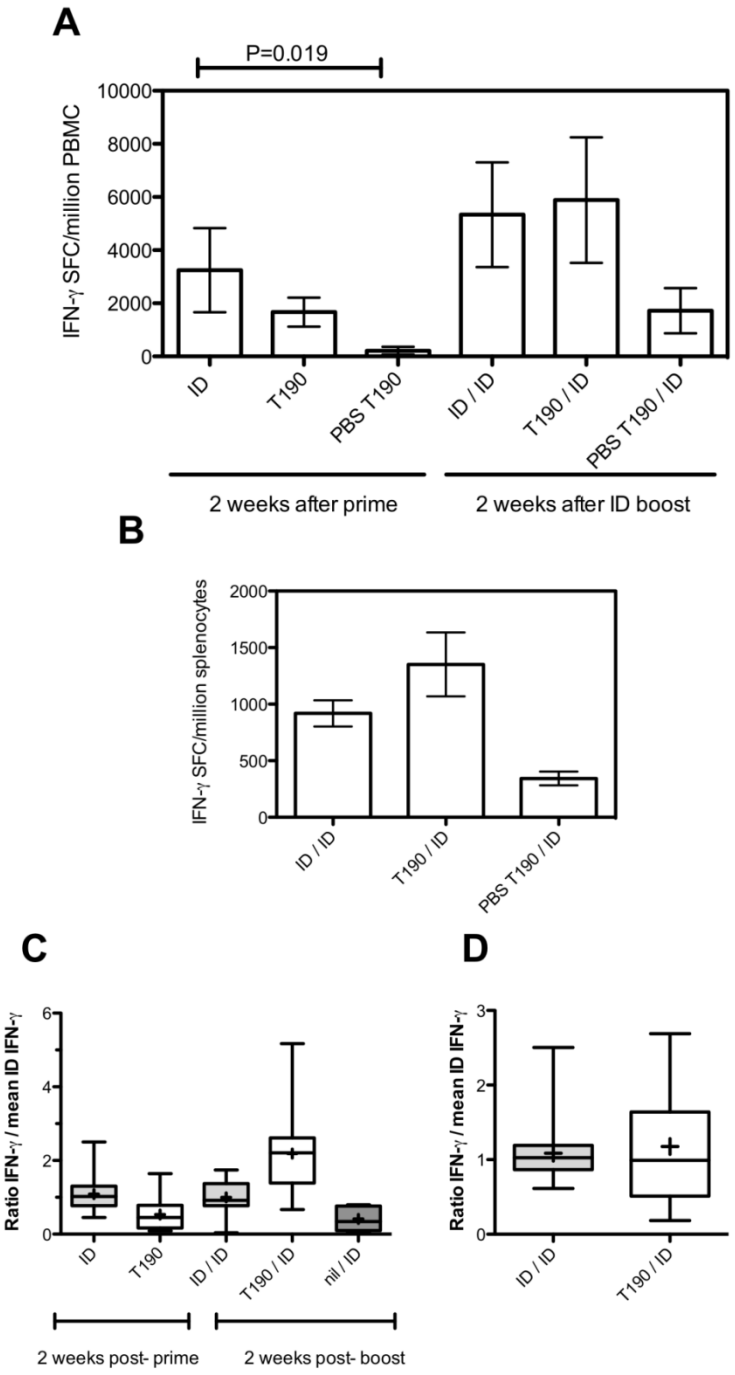

FIGURE 3-1: Cellular immunogenicity following MVA/MVA prime-boost immunisation with ImmuPatch.

ImmuPatch T190 (190μm microneedles – see Table 2-7 for more details).(A+B) Female BALB/c mice (n=4) aged 6 weeks were primed with $1x10^6$ PFU MVA.PbCSP either by ImmuPatch T190 or ID and boosted 2 weeks later with $1x10^6$ PFU MVA.PbCSP ID. A control group received only PBS by T190 at the prime and were boosted as other groups. Blood was taken for isolation of PBMC and incubation with Pb9 peptide (SYIPSAEKI) in an IFN-γ ELISPOT assay 2 weeks after the prime, and 2 weeks after the boost immunisation. Mice were euthanised and spleens were harvested 2 weeks post-boost and IFN-γ ELISPOT performed on splenocytes following incubation with Pb9. Background responses (from unstimulated samples) were subtracted in the analysis. Bars represent mean Spot Forming Cells (SFC) ± SD. P=0.019 by Kruskall Wallis

with Dunn's comparison. (C+D) ELISPOT results (IFN-γSFC/million cells) from 5 experiments identical to the one described above were pooled and each datapoint normalised to the mean of the ID response(2 weeks post-prime) or theID/ID (2 weeks post-boost) in PBMC (Figure 3-1C), or 2 weeks post-boost in the spleen, (Figure 3-1D), presented as a box and whisker plot. Means are represented by '+'. Light grey = ID and ID/ID, Clear = T190 and T190/ID, dark grey = single shot ID given at boost (which was normalised to the mean of the ID/ID response).

3.3.1.2 ImmuPatch prime / ID boost is the optimal route combination for induction of Pb9-specific T cell responses

The ability of ImmuPatch to deliver a boost immunisation was assessed, following delivery of the prime ID or by ImmuPatch T280, using the MVA.PbCSP homologous prime-boost regimen (as described above). Blood was taken from ID- and T280-immunised mice (n=10) 1 week following MVA.PbCSP priming (corresponding to the peak of the post-MVA response (251)). PBMC were re-stimulated with Pb9 before ICS for IFN-γ. Frequencies of CD8+ IFN-γ+ PBMC are presented in Figure 3-2A. These groups were each split into two groups of 5, which were boosted either by ID or by T280. Figure 3-2B presents post-boost responses as assessed in splenocytes. T280 priming induced a post-prime response similar to delivery ID (Figure 3-2A). T280/ID was the most immunogenic of prime-boost combinations including T280, with post-boost responses comparable to ID/ID. T280 was less able to boost responses primed by ID or T280, and mice receiving both prime and boost immunisations by T280 demonstrated a significantly diminished response as compared to ID/ID (P=0.0062, Figure 3-2B).

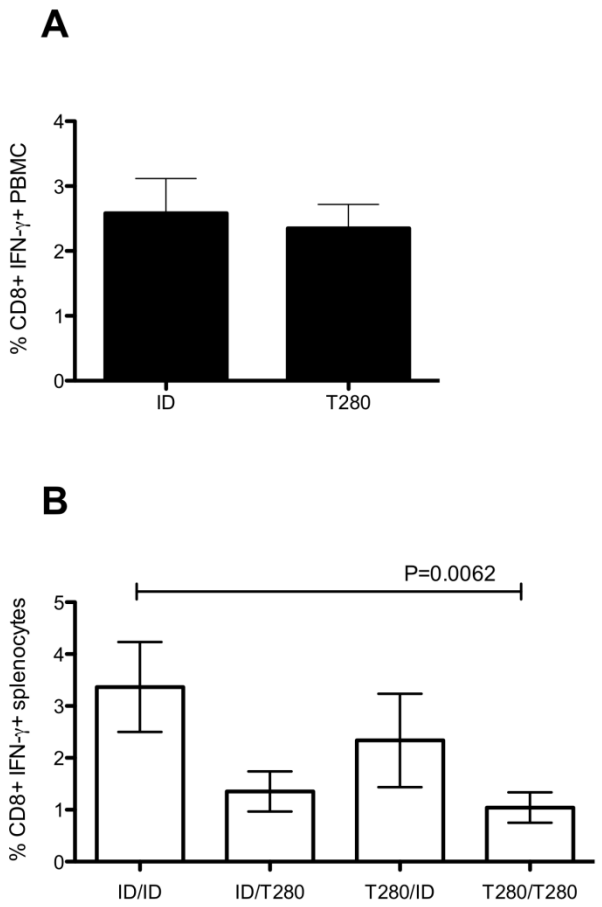

FIGURE 3-2: ImmuPatch is more efficient at priming than boosting responses in MVA.PbCSP homologous prime-boost immunisation.

Female BALB/c mice (n=10) were primed with 1x10^6 PFU MVA.PbCSP either ID or by ImmuPatch T280. Two weeks later groups of ten mice were split into two groups of 5, one of which was boosted ID and one boosted with T280 (1x10^6 PFU MVA.PbCSP). Frequencies of IFN-γ+ CD8+ T cells were assessed by ICS 1 week after the prime in PBMC (Figure 3-2A) or 2 weeks after the boost in the spleen (Figure 3-2B). Mean IFN-γ+ CD8+ T cells are presented as bars ± SEM (A) or SD (B). Gating was as follows singlets>lymphocyte size gate>CD8+>IFN-γ+. Background responses (from unstimulated samples) were subtracted before further analysis. P=0.0062 by Kruskall Wallis with Dunn's post-comparison.

3.3.1.3 Methodology of ImmuPatch immunisation impacts upon response outcome

The precise order in which liquid vaccine and microneedle patch are applied to mouse skin has been proposed to affect the proportion of liquid delivered (130, 292). Histological examination of explanted porcine skin confirmed the creation of microchannels following ImmuPatch insertion and removal (265). It was considered

feasible that the microchannel may immediately contract following microneedle removal, due to recoil of the highly elastic skin following deformation. It was hypothesised that applying the ImmuPatch before applying the vaccine may result in reduced immune responses compared to applying the patch 'through' the vaccine droplet due to a decreased volume available for diffusion. Mice were immunised with MVA.PbCSP either ID or by T190, where skin was pre-treated with microneedles prior to vaccine application (T190-MVA) or through the vaccine droplet (MVA-T190). IFN-γ ELISPOT was performed on PBMC, spleens and auricular (skin-draining) LNs 2 weeks later (Figure 3-3). When vaccine was placed on the ear prior to application of the T190 patch responses were improved as compared to when the ear was 'pre-treated' with the patch prior to vaccine application. Though no statistically significant differences were detected between the two methods directly, T190-MVA responses were significantly lower than ID responses in PBMC ($P=0.0198$, Figure 3-3A) and splenocytes ($P=0.0073$, Figure 3-3B) whereas MVA-T190 and ID responses were not significantly different from each other. This result was also observed in draining LN cells (Figure 3-3C), though as cells were pooled from 4 animals/group statistical comparisons could not be made. These data suggest that application of the patch through a droplet of vaccine placed on the ear results in better immunogenicity than by pre-treating the ear with microneedles.

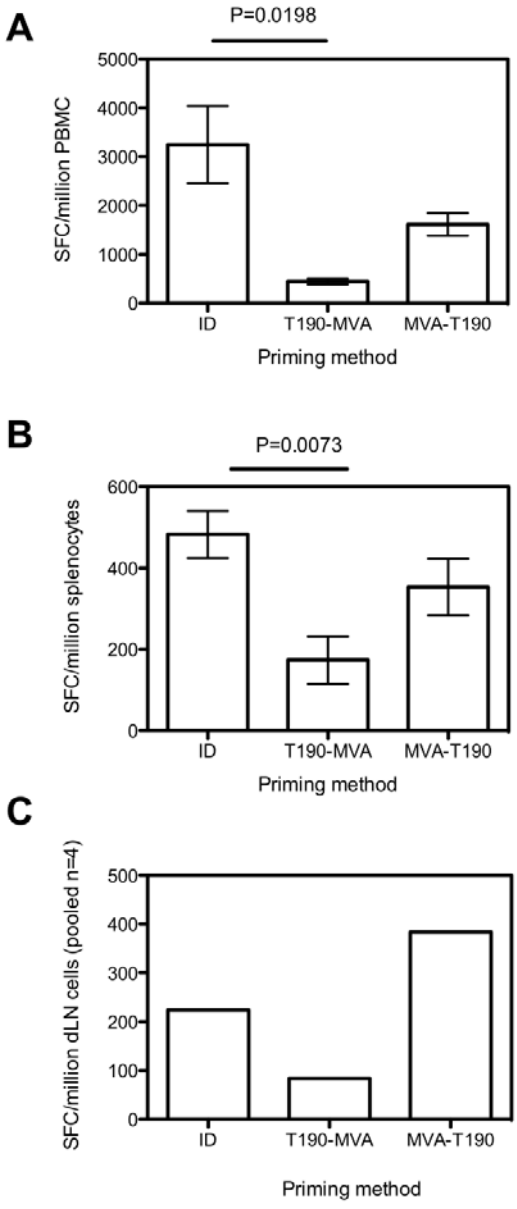

FIGURE 3-3: Methodology of ImmuPatch immunisation impacts upon the magnitude of the resulting response.

Female 6-week old BALB/c mice (n=4) were immunised with 1x10^6 PFU MVA.PbCSP by ID, or by ImmuPatch T190. ImmuPatch immunisations were either given by pre-treating the skin with T190 microneedles (T190-MVA), and then applying vaccine onto the ear surface, or by applying microneedles through the vaccine droplet (MVA-T190). Two weeks following immunisation mice were sacrificed and blood, spleens and auricular (draining) LNs were harvested for for Pb9 re-stimlulation and IFN-γ ELISPOT. LN cells from animals in one group were pooled before stimulation (C). Background responses (unstimulated samples) were subtracted from stimulated responses. Bars represent mean SFC/million cells ± SD. Significant differences were defined using Kruskall Wallis with Dunn's post-comparison.

3.3.1.4 Effect of the dose of MVA.PbCSP in ImmuPatch immunisation

Upon application of the ImmuPatch through the vaccine droplet, some liquid was observed to be lost from the sides of the patch, or remained on the patch following its removal thus an incomplete dose was delivered. It was hypothesised that responses could be thus improved by increasing the concentration of viral particles in the priming dose. This was assessed in homologous prime-boost immunisation whereImmuPatch F was used to deliver the priming immunisation. Mice were primed with MVA.PbCSP at doses of $1x10^7$ PFU, $1x10^6$ PFU or $1x10^4$ PFU, either ID or using another ImmuPatch F. All mice were given a ID boost of $1x10^6$ PFU 2 weeks later. In both ID primed, and patch F-primed mice, post-prime responses followed a trend whereby responses increased with increasing dose, though all ID-primed responses were higher than patch F primed responses (P=0.0041, Figure 3-4). Despite this, all ID and ImmuPatchF primed responses could be boosted to an equivalent level with no differences between post-boost responses, when the priming dose was reduced to $1x10^4$ PFU. In summary, altering the dose applied to the skin influenced the post-prime response, but did not alter the response following an ID boost, over the range of doses tested and using ImmuPatch F. This result was confirmed using another ImmuPatch array of a different design and using MVA.PbCSP doses of $1x10^6$ PFU and $1x10^7$ PFU (not here shown).

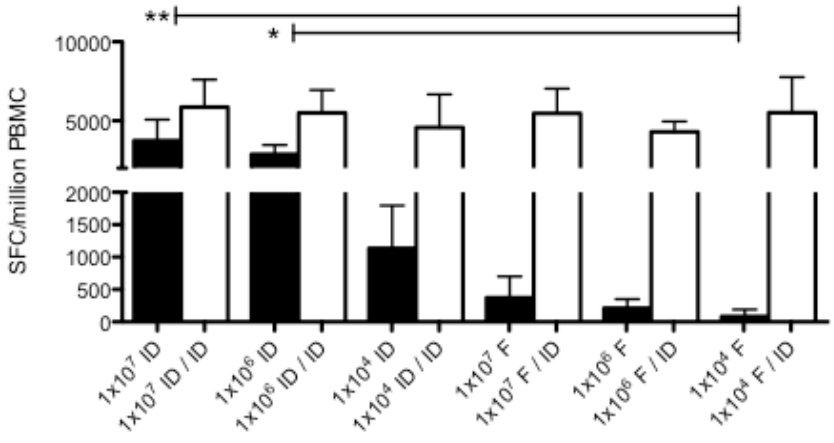

FIGURE 3-4: Effect of altering priming dose upon the post-prime and post-ID boost response in MVA/MVA immunisation.

Female BALB/c mice (n=4, 8 weeks) were primed with $1x10^7$ PFU, $1x10^6$ PFU, $1x10^4$ PFU either ID, or by ImmuPatch F. Mice were boosted 2 weeks later with $1x10^6$ PFU MVA.PbCSP ID. Blood was taken for Pb9 restimulation of PBMC in an IFN-γ ELISPOT 1 week post-prime (filled bars) and 2 weeks post-boost (open bars). Bars aremean SFC/million PBMC ± SEM. P=0.0041 by Kruskall Wallis with Dunn's comparison.

3.3.1.5 T cell responses following ImmuPatch priming are influenced by array design

It was hypothesised that design may influence the induction of T cell responses following ImmuPatch immunisation. A number of ImmuPatch arrays were specifically designed to enable evaluation of the influence of the parameters of microneedle length, density and volume (relating to thedimensions of microchannels created). These arrays, named A-H, have microneedle lengths ranging from 100-300µm, densities ranging from 0.54-1.47 microneedles/mm^2 and patch surface areas of either 29.16 or 54.76 mm^2 (Table 2-7). Mice were immunised with MVA.PbCSP in a homologous prime-boost regimen as previously described. Figure 3-5 presents post-prime (A) and post-boost, given ID (B) IFN-γ ELISPOT responses following Pb9 re-stimulation. Two identical replicate experiments (n=5) yielded similar results and so datapoints were pooled in this analysis.

ImmuPatch design was found to influence responses both after a prime and after prime-boost immunisation. Differences were more pronounced post-prime ($P<0.0001$, Figure 3-5A), compared with those following an ID boost ($P=0.0010$, Figure 3-5B). Priming with patches A, B and F demonstrated significatly lower responses compared to patches C, D and E, and as compared to ID ($P<0.0001$, Figure 3-5A). Responses induced by patch B were significantly lower than those induced by patch D. Following an ID boost, F/ID immunisation exhibited a significantly higher response than G/ID and H/ID ($P=0.0010$, Figure 3-5B). These data demonstrate that ImmuPatch arrays of differing design (i.e. microneedle length and density) induce responses of differing magnitude. The extent to which ImmuPatch responses are boosted ID is related to the design of the ImmuPatch used to prime. These observations are supported by separate experiments performed using this regimen with patches A-H presented in Carey *et al* (265).

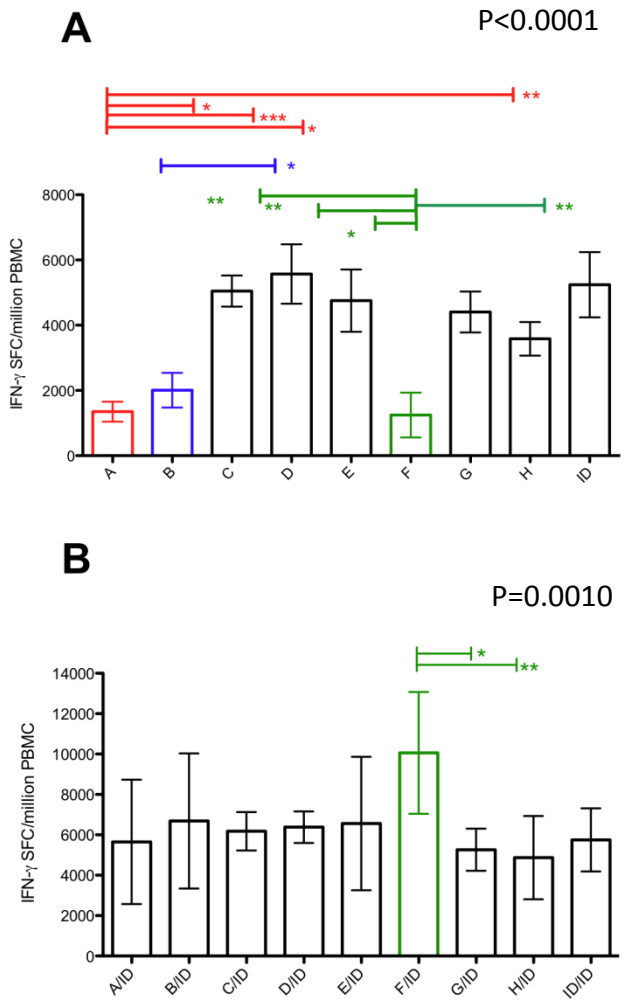

FIGURE 3-5: Cellular responses following ImmuPatch immunisation are dependent upon patch design.

Female BALB/c mice (6 weeks) were primed with 1x10^6 PFU MVA.PbCSP either ID or by ImmuPatch array A-H, with a range of microneedle heights and densities (Table 2-7). Blood was taken for IFN-γ ELISPOT on PBMC 7 1 week post-prime (A) or 2 weeks post-boost (B). Two identical experiments yielded similar results and so datapoints were pooled (total n=10). Mean SFC/million PBMC are presented as bars ± SEM (A) or SD (B). Statistical analysis was performed by one-way ANoVa with Bonferroni's multiple comparison post-test (A) or Kruskall Wallis with Dunn's comparison (B).

3.3.1.6 ImmuPatch-primed responses correlate with total microneedle array volume (TAV)

To explore the specific factors associated with in the induction of responses of varying magnitudes when priming with ImmuPatch arrays of different parameters, IFN-γ ELISPOT results (Figure 3-5) were plotted against microneedle length and microneedle density. Responses were also plotted against 'total microneedle surface

area' and 'total microneedle array volume' (henceforth abbreviated to TAV) which are defined as the surface area or volume of a cone-shaped microneedle with height (microneedle length), l and radius (microneedle base radius), r multiplied by the number of needles on the patch, n as represented in Figure 3-6. These parameters are descriptive of the surface area and volume of all microchannels created on application to the skin[5]. The relationships between microneedle parameters and the resulting response post-prime and following an ID boost are given in Figure 3-7.

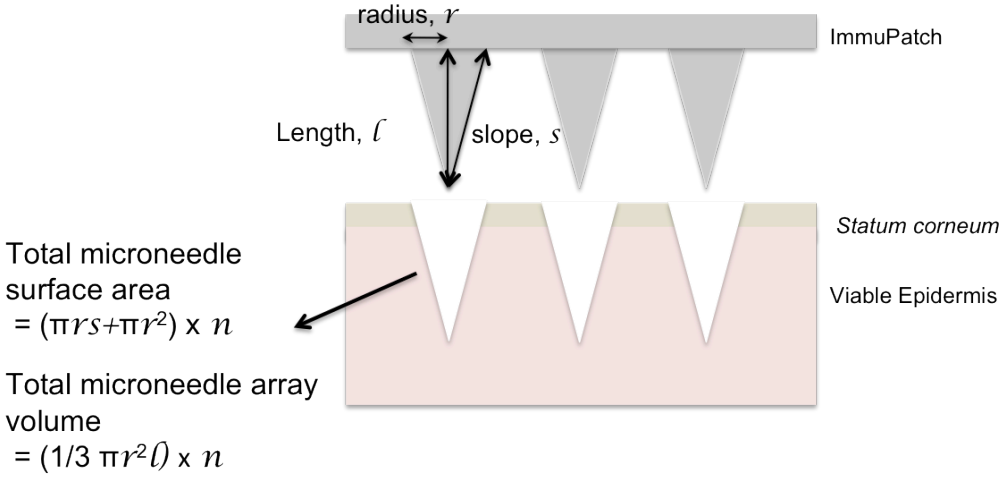

FIGURE 3-6: Microneedles create microchannels upon application the skin.

Microchannel surface area and volume are related to the parameters of a single microneedle. The summed total surface area and volume of all microneedles on a patch are termed 'total array surface area' and 'total array volume' abbreviated to 'TAV'. Not to scale.

After a prime immunisation, there was a strong positive correlation between microneedle length and IFN-γsecreting T cells circulating in the blood (Spearmann's rho=0.56, P<0.0001, Figure 3-7, Ai) and weak negative correlation between needle density and IFN-γ secreting cells (rho= -0.204, P=0.046, Figure 3-7 Bi). No correlation between these parameters and post-boost response was found (Figure 3-7, A+B ii). Whilst there is no relationship between the total array surface area and response either post-prime or post-boost (Figure 3-7C), theTAV of the ImmuPatch was strongly positively correlated with post-prime responses (rho=0.5721, P<0.0001, Figure 3-7, Di), and negatively correlated with response following an IDboost (rho= -0.2363, P=0.034, Figure 3-7, Dii).

[5] NB: These parameters are related to, but are not directly descriptive of total microchannel surface area and volume i.e. 280µm microneedles were found to create microchannels penetrating to 64% of their total length (this is due to the deformation of this skin, which is highly visco-elastic). Enfield J, O'Connell ML, Lawlor K, Jonathan E, O'Mahony C, Leahy M. In-vivo dynamic characterization of microneedle skin penetration using optical coherence tomography. J Biomed Opt. 2010;15(4):046001.

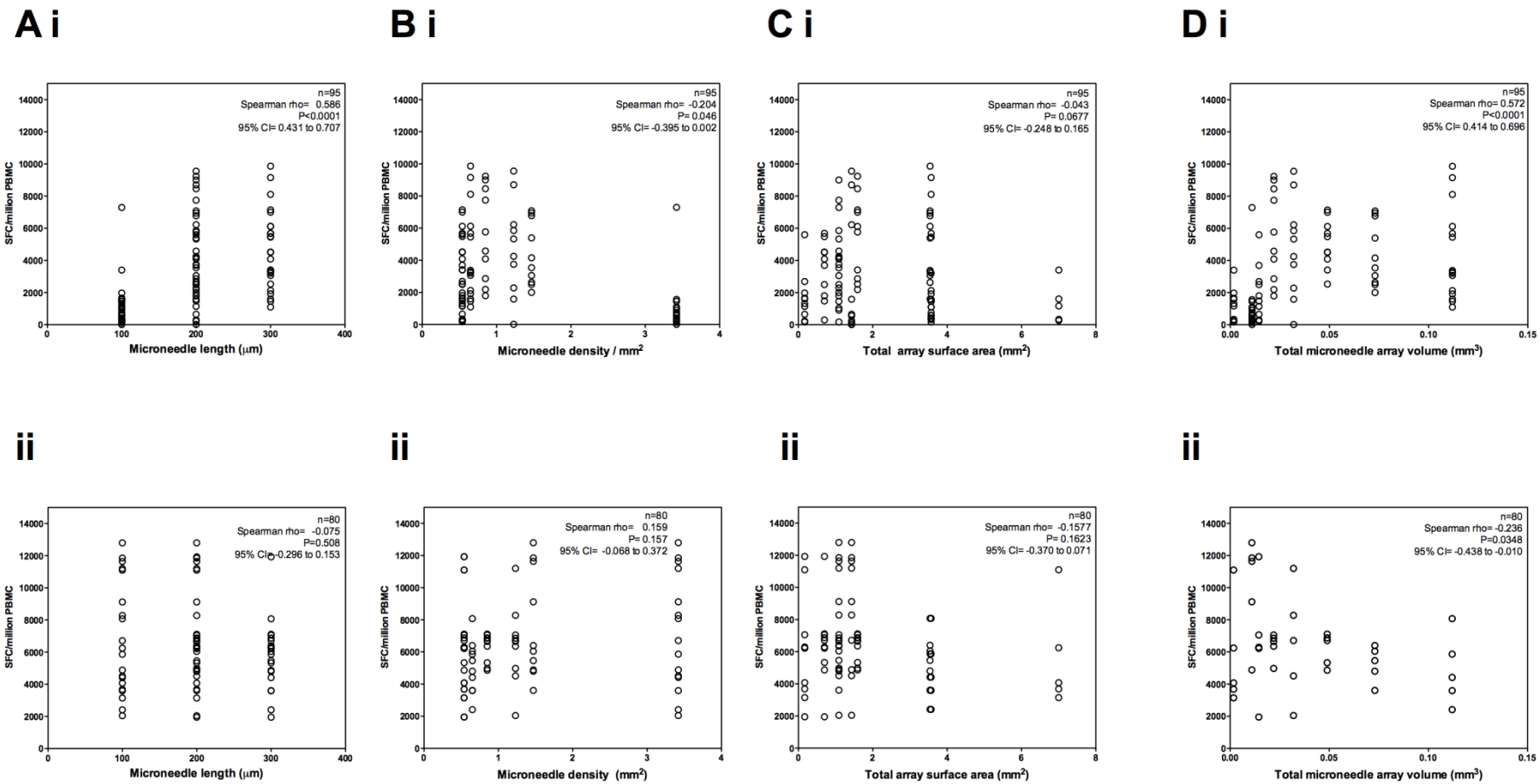

FIGURE 3-7: ImmuPatch primed responses are correlated with Total Array Volume (TAV).

Female BALB/c mice were immunised with ImmuPatch arrays A-H as per the schedule detailed in the legend for Figure 3-5. Pooled (n=10) SFC/million PBMC 1 week post-prime (A-D, i) and 2 weeks post-ID boost (A-D, ii) for all ImmuPatch arrays were plotted against microneedle length, microneedle density, or by total microneedle surface area and total array volume, TAV (calculated as the surface area/volume of a cone of equivalent proportions as those of the microneedle, multiplied by the total number of needles/patch - Figure 3-6). Relationships were assessed using Spearmann's rank correlation as detailed beneath individual plots.

The list of patch information given in Table 2-7 is ordered according to increasing TAV. ImmuPatch arrays were classified as ‘small’ (A+F), ‘intermediate’, (B, D, E, C) ‘large’ (G, H) in terms of TAV. In Figure 3-7, patch F (‘small’ TAV) primed a response that was significantly lower than ‘intermediate’ TAV patches C, D and E and ‘large’ TAV patch H. Despite this, when F-primed responses were boosted ID, the post-boost response was significantly higher than responses primed by large TAV patches G and H. Taken together, Figures 3-5 and3-7 suggest that microneedle design has a significant effect upon response magnitude, with patches of small TAV priming responses that are optimally boosted, despite demonstrating lower responses post-prime.

3.3.1.7 ImmuPatch boosting of responses is less effective than ImmuPatch priming, but can be improved by selection of optimal array

ImmuPatch priming with ID boost, and priming+boosting was further explored using patches A-H in homologous prime-boost immunisation with MVA.PbCSP as previously described. Irrelevant antigen (Red Fluorescent Protein, RFP) and ‘flat patch’ (silicon base with no microneedles) negative controls were included. Two replicate experiments were performed yielding similar results so are pooled in this analysis (Figure 3-8). In agreement with the results presented in Figure 3-5, 1 week post-prime patch F (small TAV) primed a lower response than ID or patch G (large TAV, ns, P=0.09, Figure 3-8A). Mice immunised with MVA.RFP did not respond to Pb9 stimulation (either after priming, or after homologous boosting) confirming that the responses observed were Pb9-specific, and mice immunised with a patch with no microneedles failed to demonstrate priming of a response.

When mice were boosted ID with MVA.PbCSP, F/ID immunised mice demonstrated the highest response, which was significantly higher than flat/ID (P<0.0001, Table 3-1). G/ID, although slightly lower than F/ID, induced a comparable response to ID/ID. No statistically significant differences were detected between patch/ID regimes, andin this experiment post-boost responses showed equivalence to that of ID/ID immunisation. Mice immunised using patch F to prime and G to boost induced higher post-boost responses than homologous patch combinations (F/F and G/G) though no statistically significant difference was detected between patch/patch groups (Figure 3-8B). However, all patch/patch responses were significantly reduced as compared to ID/ID responses (P<0.0001, summarised in Table 3-1). Whilst F/ID responses are enhanced over any patch/patch regime, there was no significant difference between F/Gand G/ID, and that between ID/ID and F/G only weakly statistically significant (*=P<0.05, Table 3-1). In summary, ImmuPatch primed responses at least as efficiently as ID immunisation (in terms of their ability to expand upon boost) but were less able to boost pre-primed responses than ID, as demonstrated before (Figure 3-2). However, a heterologous combination of arrays (F/G) is superior to a homologous combination (F/F, G/G) - an observation also noted by Carey *et al*using a wider range of patch/patch combinations(265).

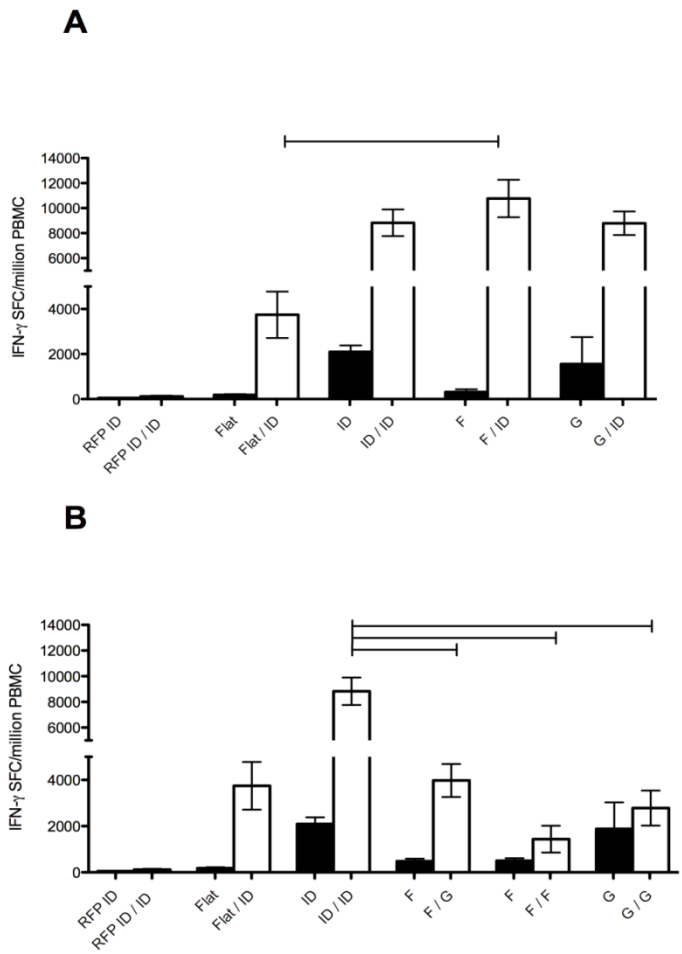

FIGURE 3-8: Immunogenicity of ImmuPatch/ID and ImmuPatch/ImmuPatch delivery in MVA/MVA prime-boost immunisation.

In two replicate experiments female BALB/c mice (n=12 total, pooled) were primed with $1x10^6$ PFU MVA.PbCSP delivered ID, or by ImmuPatch F or G or by 'flat' patch (no microneedles). An irrelevant transgene control group received $1x10^6$ PFU MVA.RFP ID ('RFP ID'). Two weeks later, boost immunisations (MVA.PbCSP $1x10^6$ PFU) were delivered ID, ImmuPatch F or ImmuPatch G. 'RFP ID' was boosted with $1x10^6$ PFU MVA.RFP ID. Blood was taken for assessment of IFN-γ SFC/million PBMC by ELISPOT 1 week post-prime (closed bars) and 2 weeks post-boost (open bars). ImmuPatch/ID groups are presented in Figure 3-8A, and ImmuPatch/ImmuPatch groups in Figure 3-8B.Bars represent the mean response ± SEM. Background responses (unstimulated samples) were subtracted. Statistically significant differences were calculated using a one-way ANoVA with Dunn's comparison (P<0.0001) the results from which are detailed in Table 3-1.

Bonferroni's Comparison	Mean Difference	Significance score	95% CI of difference
ID/ID vs F/G	4816	*	30.65 to 9679
ID/ID vs F/F	7352	***	2567 to 12215
ID/ID vs G/G	6010	**	1224 to 10872
F/ID vs F/G	6794	***	1969 to 11618
F/ID vs F/F	9330	***	4505 to 14154
F/ID vs G/G	7987	***	3163 to 12811
G/ID vs F/G	4816	ns	-7.805 to 9641
G/ID vs F/F	7352	***	2528 to12177
G/ID vs G/G	6010	**	1185 to 10834

TABLE 3-1: Details of statistically significant differences from the analysis performed in Figure 3-8.

Statistically significant differences detected by one-way ANoVA in Figure 3-8. Bonferroni's comparison performed on the post-boost dataset.*=P<0.05, **=P<0.005, ***=P<0.0001. ns= not significant.

3.3.1.8 Immunogenicity of patch/patch combinations correlate with TAV

Following the suggestion that post-boost responses may be influenced by array design in patch/patch immunisation, IFN-γ ELISPOT responses from following prime immunisation with ImmuPatch F or G (left Y axis closed circles, Figure 3-9), and following prime-boost with the same patch (right Y axis open circles, Figure 3-9) taken from Figure 3-8 were plotted against ImmuPatch TAV. Only homologous patch/patch combinations were included due to the low number of F/G datapoints available for analysis. After an ImmuPatch prime, there was a strongly significant positive correlation between Pb9-specific response (Spearmann's rho=0.543, P=0.0008, Figure 3-9, closed symbols), as had been observed with patch/ID(Figure 3-7). However, in contrast to boosting ID, there was a positive correlation between TAV and post-boost response when the same ImmuPatch was used to boost responses as that used to prime (Spearmann's rho=0.494, P=0.014, Figure 3-9,open symbols). Whilst more data points would allow a more confirmatory analysis, this switch in association may suggest a greater reliance on a larger TAV for ImmuPatch boosting, whereas a smaller TAV was optimal for priming of a response. This is supported by the improved response of F/G as compared to F/F and G/G in Figure 3-8 (though this was not a statistically significant difference).

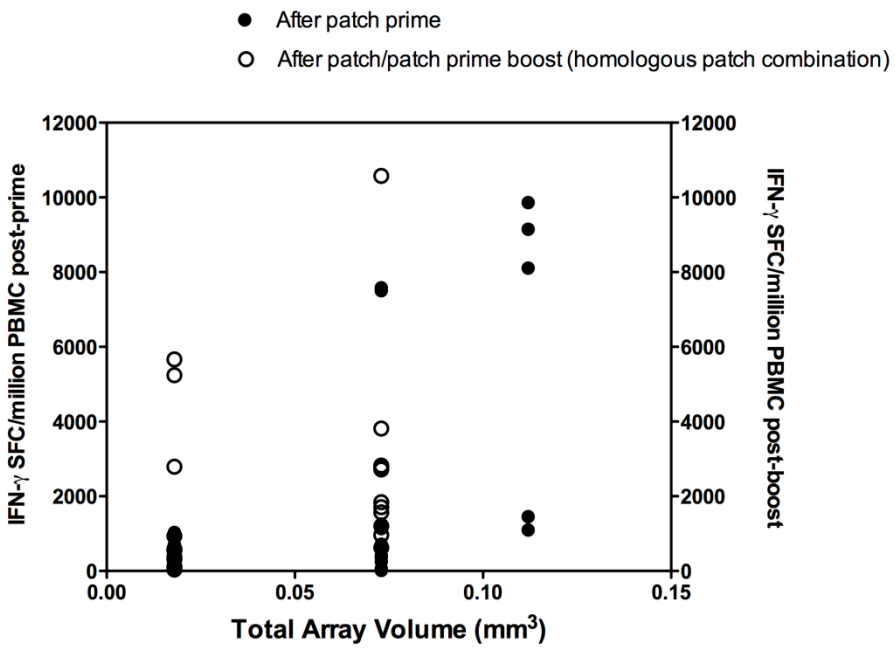

	Post prime	Post homologous patch boost
Number of XY Pairs	35	24
Spearman r	0.5429	0.4936
95% confidence interval	0.2462 to 0.7465	0.1000 to 0.7536
P value (two-tailed)	0.0008	0.0142
P value summary	***	*

FIGURE 3-9: Responses following homologous ImmuPatch/ImmuPatch immunisation are correlated with TAV.

BALB/c mice were immunised with homologous ImmuPatch regimes (F/F or G/G) as described in the legend for Figure 3-8. SFC/million PBMC post patch prime (left Y axis, black circles), and post-patch boost (right Y axis, open circles) were plotted against TAV. Spearmann's rank correlation was performed and results are detailed in the table within the figure.

3.3.1.9 The effect of decreasing boosting dose in intradermally delivered prime-boost immunisation with MVA.PbCSP

A possible explanation for the observation that ImmuPatch boosts a previously ID- or ImmuPatch-primed response less efficiently than ID boosting may be that there is a likely reduced delivered doseas compared to ID immunisation due tovaccine spillage on patch application. Carey *et al* demonstrate that approximately 3% of the total number of fluorescent nanoparticles applied to the ear are recovered from the skin after application of the ImmuPatch (F - 3.17%, C-2.58% and H-2.87%)(265). It was hypothesised that delivery of a defined dose may be a more important factor in boosting a response, than in priming one in MVA.PbCSP/MVA.PbCSP prime-boost immunisation considering that patch priming is more efficient than patch boosting. To test this, an experiment was carried out using varying doses of MVA.PbCSP at prime and boost, delivered ID.

When a universal priming dose of $1x10^6$PFU was delivered, doses below an optimal boosting dose of $1x10^6$ PFU were less effective, and $1x10^2$ PFU did not enhance pre-boost levels of immunogenicity at all (P=0.005, Figure 3-10A vs. $1x10^6$ PFU boosting). In contrast, reducing the dose of the priming immunisation had little effect upon the post-boost outcome following a universal boost of $1x10^6$ PFU (Figure 3-10B). Though a reduction in priming dose was associated with a decreased post-prime response (P=0.042 comparing $1x10^6$ PFU with $1x10^2$ PFU, Figure 3-10B). Post-boost responses were not significantly different. Interestingly, priming doses as low as $1x10^2$ PFU were able to boost the response to levels equivalent to those primed with $1x10^6$ PFU MVA.PbCSP. In summary, a reduction in the priming dose affects the post-prime response but responses primed by each dose tested demonstrated similar responses after boosting with $1x10^6$ PFU. A reduction in the boosting dose given to mice primed with $1x10^6$ PFU had a significant effect, with doses below $1x10^6$ PFU being insufficient to effectively boost responses demonstrating a 'threshold effect' of boosting, but not priming dose.

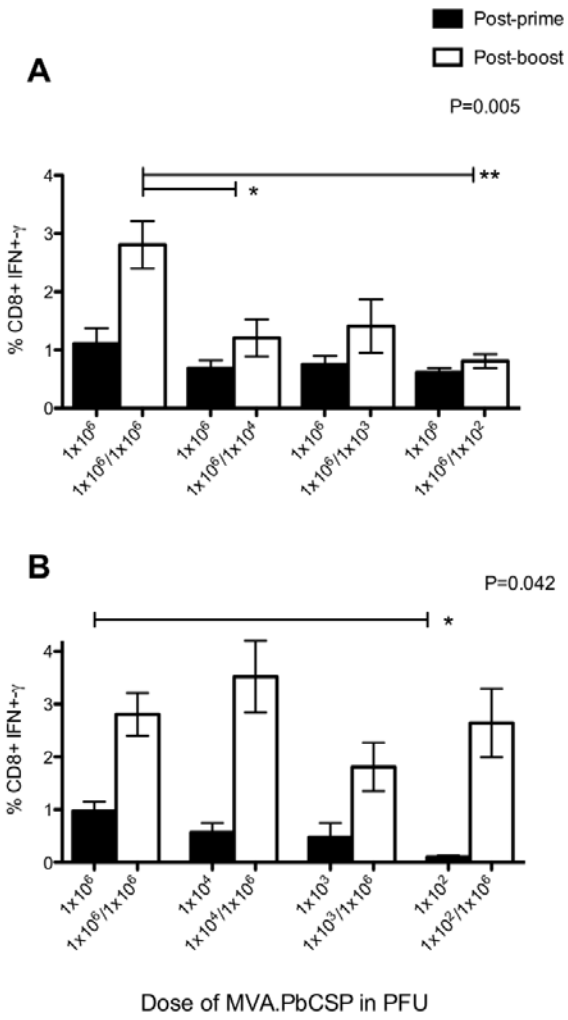

FIGURE 3-10: The effects of dose reduction in MVA.PbCSP prime-boost immunisation as delivered ID.

Female BALB/c mice (6 weeks, n=5) were primed with MVA.PbCSP at doses of $1x10^6$ PFU $1x10^4$ PFU, $1x10^3$ PFU or $1x10^2$ PFU ID and boosted 2 weeks later with $1x10^6$ PFU, $1x10^4$ PFU, $1x10^3$ PFU or $1x10^2$ PFU MVA.PbCSP ID. ICS was performed on PBMC 1 week post-prime (closed bars) and 2 weeks after the boost (open bars). Gating strategy: singlets (FSC-A x FSC-H) > lymphocytes (FSC-A x SSC-A) > CD8+ (CD8 PercP-Cy5.5 x CD4 APC H7) > IFN-γ+ (CD8 PercP-Cy5.5 x APC). Background was subtracted from unstimulated controls. Bars represent mean % cytokine+ CD8+ cells ± SEM. P=0.005 (A) and P=0.042 (B) by one way ANoVA with Bonferroni's comparison.

3.3.1.10 Summary of section 3.3.1 - MVA/MVA immunisation

- ImmuPatch priming induces CD8+ T cell responses that are expanded optimally upon ID boosting, reaching a post-boost level at least comparable to ID/ID immunisation[6].
- Responses are improved when microneedles are applied through the vaccine droplet as opposed to prior to vaccine application.
- Increasing the priming dose applied to the skin increases post-prime response marginally, but does not significantly affect response post ID-boost (using patch F and the dose range tested).
- The parameter of TAV influences both post-prime and post-ID boost responses. Optimal post-ID boost responses are induced by arrays with small TAV.
- ImmuPatch boosting is less efficient than ID boosting (proposed due to a reduced dose delivery by patch, which has a greater effect upon expansion of a secondary response, than a primary response within this regimen). However, choice of a small TAV priming patch and a large TAV boosting patch is improved over homologous combinations.
- A patch of small TAV used to prime responses combined with a one of large TAV for delivery of the boost is the combination most likely to induce optimal responses in patch/patch immunisation.

3.3.2 Adenovirus/MVA immunisation

3.3.2.1 ImmuPatch- and dose-specific Pb9 immunogenicity during AdCh63.ME-TRAP / MVA.ME-TRAP immunisation

Due to its clinical relevance, delivery of the AdCh63.ME-TRAP/MVA.ME-TRAP regimen using ImmuPatch arrays was assessed in mice. Intramuscular delivery of Ad has been shown to elicit similar immunogenicity to ID immunisation with the advantage of greater ease of technique (225), so ID and IM controls were included in this experiment. The ImmuPatch arrays chosen had equivalent microneedle length but differing TAV: T280c (280μm microneedle length, 0.0406mm^3TAV) and T280b (280μm, 0.2053 mm^3 TAV) due to differences in array surface area (Table 2-7). Groups of mice were immunised with two commonly used pre-clinical doses of AdCh63.ME-TRAP ($1x10^9$ VP + $1x10^{10}$ VP) and 8 weeks later boosted with $1x10^6$ PFU MVA.ME-TRAP. The magnitude of the post-prime ImmuPatch response was

[6] Though both post-prime and post ID-boost response magnitude was found to be array design-specific, see point 4.

low as compared to ID and IM-primed responses at both priming doses (P=0.0006, vs. IM, Figure 3-11A), though slightly higher after $1x10^{10}$ VP T280b priming than by T280c (ns, Figure 3-11B). However, all post-prime ImmuPatch responses were greater than zero after background correction. Following an MVA.ME-TRAP ID boost, all groups except T280b/ID ($1x10^{10}$VP) demonstrated secondary expansion. T280c/ID responses were equivalent to those following ID/ID immunisation at both doses. Whereas T280b primed responses were boosted following delivery of a dose of $1x10^{9}$ VP, those induced by T280b priming with $1x10^{10}$ VP were not boosted from the post-prime level (P=0.004 compared to IM and ID, Figure 3-11B).

A second experiment using this regimen aimed to investigate patch/ID and patch/patch immunisation using 3 arrays with TAV ranging from intermediate-extra large. Mice were immunised with $1x10^{10}$ VP AdCh63.ME-TRAP using ImmuPatch C, H or T280b. After T280b and H priming, the response was similar to that delivered ID (Figure 3-11C). ImmuPatch C responses were slightly lower than those following ID immunisation (ns). After an ID boost, C/ID and ID/ID demonstrated equivalent responses, with H/ID also being efficiently boosted. Importantly, boosting of patch C primed responses with patch C was successful, with post-boost responses were similar to that following ID/ID and C/ID immunisation. Similar to the observation in Figure 3-11B, the T280b primed response was not increased following intradermal boosting, or by T280b boosting. In summary, in AdCh63/MVA immunisation, ImmuPatch can successfully prime and boost a response but similar to MVA/MVA immunisation, though careful selection of patch design is required for optimal immunogenicity. In contrast to the homologous regimen, priming dose also was shown to influence post-boost response outcome when considering T280b.

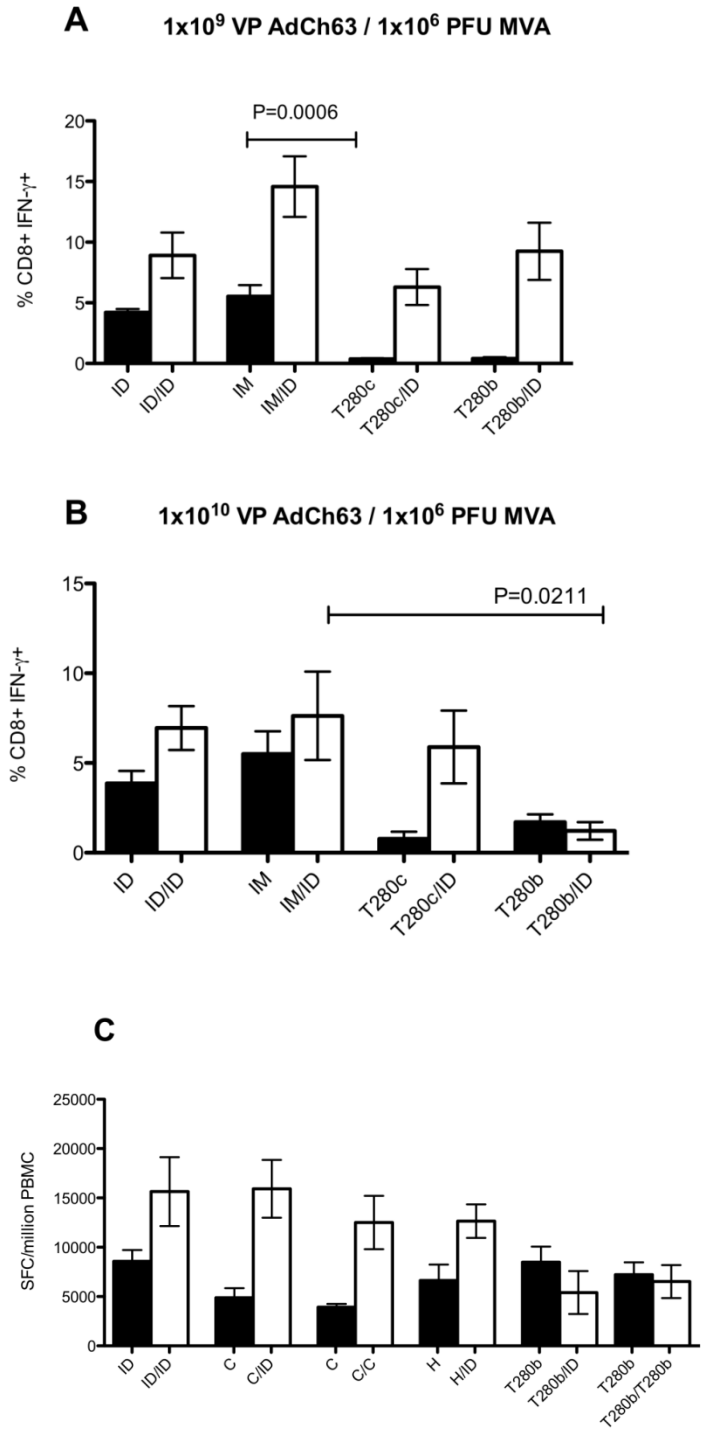
A
1x10^9 VP AdCh63 / 1x10^6 PFU MVA
P=0.0006
% CD8+ IFN-γ+
20
15
10
5
0
ID
ID/ID
IM
IM/ID
T280c
T280c/ID
T280b
T280b/ID
B
1x10^10 VP AdCh63 / 1x10^6 PFU MVA
P=0.0211
% CD8+ IFN-γ+
15
10
5
0
ID
ID/ID
IM
IM/ID
T280c
T280c/ID
T280b
T280b/ID
C
SFC/million PBMC
25000
20000
15000
10000
5000
0
ID
ID/ID
C
C/ID
C
C/C
H
H/ID
T280b
T280b/ID
T280b
T280b/T280b

FIGURE 3-11: Immunogenicity of ImmuPatch priming in AdCh63.ME-TRAP / MVA.ME-TRAP immunisation.

(A+B) Female BALB/c mice (n=5) were primed with $1x10^9$ VP or $1x10^{10}$ VP Ad.C63ME-TRAP given ID, IM or by the ImmuPatch arrays T280c or T280b. Eight weeks later a boost immunisation of $1x10^6$ PFU MVA.ME-TRAP was delivered ID. Blood was taken for re-stimulation of PBMC with Pb9 and ICS 2 weeks post-prime (black bars) and 2 weeks post-boost (open bars). Error bars are SEM. Statistical differences were determined by Kruskall Wallis + Dunn's Comparison. Gating strategy as follows: singlets (FSC-A x FSC-H) > lymphocytes (FSC-A x SSC-A) > CD8+ (CD8 PercP-Cy5.5 x CD4 APC H7) > IFN-γ (CD8 PercP-Cy5.5 x IFN-γ). (C) In a separate experiment female BALB/c mice (n=6) were primed with $1x10^{10}$ VP AdCh63.ME-TRAP given ID, or by ImmuPatch C, H or T280b. Mice were boosted at 8 weeks with $1x10^6$ PFU MVA.ME-TRAP. Blood was taken for PBMC re-stimulation with Pb9 in an IFN-γ ELISPOT 2 weeks post-prime (black bars) and 2 weeks post-boost (open bars, ± SEM). P=0.014 by one-way ANoVA with Bonferroni's comparison.

3.3.2.2 Immunogenicity of AdCh63.ME-TRAP/MVA.ME-TRAP regimes correlate with ImmuPatch TAV

To ascertain whether the magnitude of the response after Ad priming, and after Ad/M prime-boost demonstrated a similar relationship with TAV as had been observed with MVA/MVA immunisation, IFN-γ ELISPOT datapoints from the experiment presented in Figure 3-11C were plotted against TAV on a scatter plot (Figure 3-12). Post-prime responses are presented in Figure 3-12A and post-boost responses are presented in Figure 3-12B. Mirroring the MVA/MVA results, there was a positive correlation between response and TAV after a single immunisation with AdCh63.ME-TRAP (Spearmann's rho = 0.4779, P=0.007, Figure 3-12A) and a negative relationship between post-ID boost and TAV of the priming patch (Spearmann's rho=-0.577, P=0.012, Figure 3-12B). Also similar to MVA/MVA, no relationship was found between post-boost responses with microneedle length or total microneedle surface area (not shown), and is evident from the difference in magnitudes of response induced by T280c and T280b, which possess the same microneedle length but have a different total number of microneedles.

A

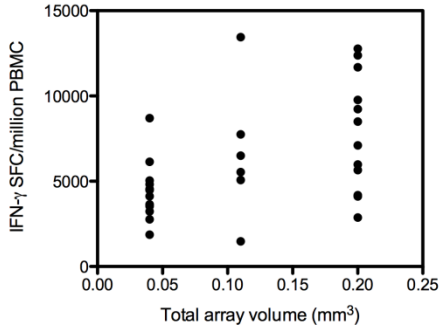

	Post prime
Number of XY Pairs	30
Spearman r	0.4779
95% confidence interval	0.1311 to 0.7205
P value (two-tailed)	0.0076
P value summary	**

B

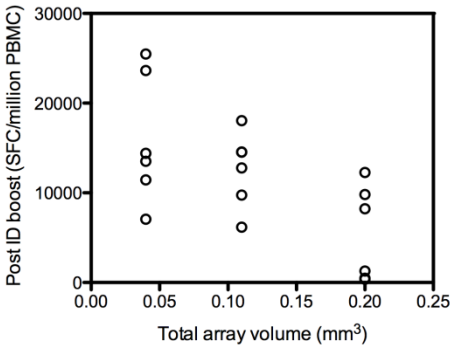

	Post ID boost
Number of XY Pairs	18
Spearman r	-0.5771
95% confidence interval	-0.8272 to -0.1360
P value (two-tailed)	0.0122
P value summary	*

FIGURE 3-12: Responses after ImmuPatch immunisation in AdCh63.ME-TRAP/MVA.ME-TRAP immunisation are associated with TAV.

BALB/c mice (n=6) were immunised with AdCh63.ME-TRAP ($1x10^{10}$ VP) and MVA.ME-TRAP ($1x10^{6}$ PFU) 8 weeks later as described in Figure 3-11C. IFN-γ ELISPOT responses (SFC/million PBMC) ascertained 2 weeks post-prime (Figure 3-12A) or 2 weeks post-ID boost (Figure 3-12B) were plotted against TAV. Associations were evaluated using Spearmann's correlation and results are detailed in the figure tables.

3.3.2.3 Summary of section 3.3.2 - AdCh63/MVA immunisation

- ImmuPatch delivery of AdCh63.METRAP primes a Pb9-specific response, which can be expanded upon ID boosting with MVA.METRAP. Post-boost responses (excluding T280b) were comparable to ID/ID immunisation.
- In contrast to MVA/MVA immunisation, priming dose was a factor in the ability of T280b-primed responses to undergo boosting, responses primed with

$1x10^9$ VP increasing upon boost, but those primed with $1x10^{10}$VP demonstrating no boosting at all (in both experiments performed - Figure 3-11B and 3-11C). T280c-primed responses were boosted following priming with both doses.

- Patch/patch immunisation was successful using patch C, but not patch T280b.
- Similar to MVA/MVA immunisation, post-prime responses correlated positively, and post ID-boost response correlated negatively with TAV.

3.3.3 Quantification of delivered virus present in skin and draining LN post-immunisation

It was hypothesised underlying the relationship between the TAV and the resulting antigen-specific cellular response was that the TAV of a particular array influences the volume of liquid that will diffuse into the microchannels it creates and hence the amount of vaccine delivered to the skin. Two methods were utilised for the estimation of delivered recombinant Adenovirus present in (i) skin of the ear pinnae, and (ii) the auricular LNs draining the immunisation site (dLN) following delivery by patches of differing TAV.

3.3.3.1 *In vitro* luciferase assay measuring transgene expression in skin and dLN following ImmuPatch delivery of AdCh63.pLuc

Mice were immunised with AdCh63.pLuc using a range of ImmuPatch arrays described in Table 2-7: F (small TAV), E (intermediate) G (large), T125 (large), T280b (extra large) or a patch without needles (Flat patch). The peak of luciferase expression following AdHu5.pLuc immunisation is reported by Geiben-Lynn *et al* to occur 24 hours post-immunisation, so this timepoint was chosen for assessment of luciferase activity within extracted dLN and skin cell lysates(254).

The detection of luciferase activity from dLN (Figure 3-13A) and skin (Figure 3-13B) lysed cell supernatants was demonstrated following immunisation, the level of which was ImmuPatch-dependent. Naïve mice did not exhibit activity in either the skin or dLN. Whilst luciferase activity could not be detected in the dLN following immunisation with patch F at this timepoint, high expression was detected for patches E and G ($P<0.001$ compared to naïve and flat patch controls, Figure 3-13A) and intermediate expression following T125 and T280b. Mean luciferase activity in the skin following F delivery was higher than in the dLN, and highest of all the patches tested, though no specific comparisons between arrays were made, means were significantly different ($P=0.016$, Figure 3-13B). Luciferase activity in the skin was decreased for the larger TAV patches E and G as compared to F.

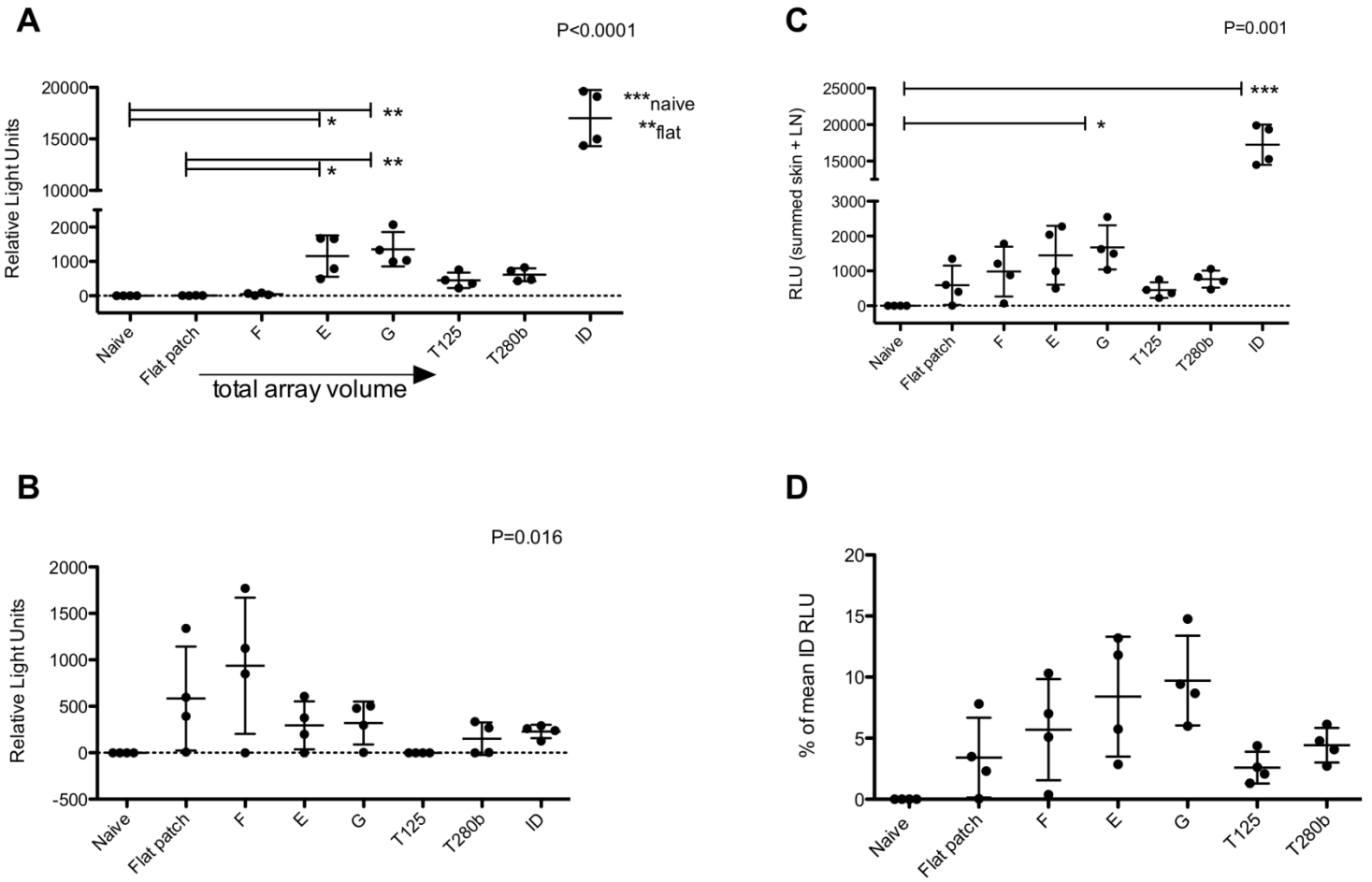
A
P<0.0001
Relative Light Units
20000
15000
10000
2000
1000
0
***naive
**flat
*
**
*
**
Naive
Flat patch
F
E
G
T125
T280b
ID
total array volume
B
P=0.016
Relative Light Units
2000
1500
1000
500
0
-500
Naive
Flat patch
F
E
G
T125
T280b
ID
C
P=0.001
RLU (summed skin + LN)
25000
20000
15000
3000
2000
1000
0
***
*
Naive
Flat patch
F
E
G
T125
T280b
ID
D
% of mean ID RLU
20
15
10
5
0
Naive
Flat patch
F
E
G
T125
T280b

FIGURE 3-13: Luciferase activities following ImmuPatch delivery of AdCh63.pLuc are dependent upon specific patch used.

Female BALB/c mice (n=4) were immunised with 1x10^{10} VP AdCh63.pLuc ID, using a patch without needles ('flat patch') or by ImmuPatch F (0.011 mm^{3}TAV), E (0.033 mm^3), G (0.074 mm^3), T125 (0.090 mm^3), or T280b (0.205 mm^3). Twenty-four hours later mice (+ 4 naïve mice) were sacrificed and ear pinnae and auricular LNs were harvested. After enzymatic tissue digestion and recovery of cells, 1x10^6 cells/sample were lysed using BRIGHTGLO™ cell lysis buffer to release the trangene product firefly (*Photinus*) luciferase. Following removal of cell debris by centrifugation, supernatants were added to BRIGHTGLO™ substrate (1:1 ratio) and luciferase activity (RLU) was recorded by luminometer. Mean luciferase activities of auricular LN supernatants (A) and of skin supernantants (B) are presented ± SD. Significant differences were detected by Kruskall Wallis test with Dunn's comparison. Background activity (PBS + substrate only, average of 4 wells) were subtracted before further analysis. (C) Luciferase activities from skin and LN supernatants were summed for each individual to assess 'total luciferase activity' per mouse. (D) Summed RLU were presented as percentages of the mean summed RLU following ID immunisation.

No activity could be detected in the dLN following T125, but 2 of 4 mice demonstrated low level of activity following T280b. Though T125 and T280b had larger total patch sizes than F, E and G (10mm^2 compared to 5.4mm^2) resulting in a higher TAV, it is unlikely that all 100% of needles on these large patches penetrate the skin due to the small size of the mouse ear pinna. Unexpectedly, luciferase activity was detected in the skin following flat patch administration, at a similar mean level to that of patch F (though both had a wide range), indicating that Ad was delivered to the skin without microneedles. However, activity was not detected in the dLN, perhaps explaining the inability of a patch without microneedles to prime an immune response (Figure 3-8). ID immunisation resulted in approximately 20-fold expression of luciferase in the dLN, though low levels in the skin, suggesting rapid translocation of antigen to the LN following ID immunisation. Given that these results may indicate a different kinetic or distribution between skin and dLN for patches of total different TAV, skin and dLN luciferase activities were summed for each mouse (Figure 3-13C) and plotted as percentages of the mean summed activity following ID immunisation (Figure 3-13D). Luciferase activity increased from F to E to G, with the two large patches T125 and T280b demonstrating an intermediate overall delivery (Figure 3-13C). Average total activities were 2.59% (T125), 4.42% (T280b), 5.70% (F), 8.40% (E), 9.72% (G) of the mean of the ID-immunised group (Figure 3-13D).

3.3.3.2 Human CMV promoter-specific quantitative PCR for Adenoviral genomes

A real-time quantitative PCR assay for the quantification of Adenoviral genomes in skin and dLN was performed. Oligonucleotide primers were designed as specific to the human CMV promoter used to drive the translation of encoded transgenes within human and simian Adenoviruses (252). Amplification and quantification of *hcmv*sequences allows relative quantification of viral particles within the sample, normalised to a tissue-specific control sequence - murine *gapdh* - coding for a ubiquitously expressed enzyme, which controls for differences in DNA loading. Mice were primed with AdHu5 expressing an irrelevant transgene driven by the hCMVpromoter. A preliminary timecourse experiment had determined 2 hours post-immunisation to be the most appropriate timepoint for detection of *hcmv* sequences in skin and dLN (not shown). Ear and dLN tissues were homogenised using a method similar to that described by Minassian *et al* (293) before extraction of total DNA. Q-PCR was performed using *hcmv* and *mgapdh*-specific primers and by

quantification of an intercalating fluorescent molecule (SYBRGREEN®), the signal from which doubles with each amplification. Since an appropriate plasmid control for *mgapdh* was not available for absolute quantification, a relative ratio of *hcmv*copies: *mgapdh* copies was found using the formula 2^{-dCt}, where dCt is the difference in cycle threshold (i.e. the number of cycles taken for the fluorescent signal to cross a pre-defined background level, Ct) between *hmcv* and *mgapdh* sequences (283).

Figure 3-14 shows 2^{-dCt} values from DNA extracted from dLN (Figure 3-14A) and skin cells (Figure 3-14B). As for expression of luciferase transgene, detection of *hcmv*-specific seqeunces differed between patches of differing TAV, though differences were not as distinctive. Patch G and T280b demonstrated higher relative Ad genome detection in the dLN. As observed in the luciferase assay, priming with a flat patch delivered vaccine to the skin, but no *hcmv* sequences were detected in the dLN. Detection was greater in the skin following patch F than for other microneedle patches as before, though no differences were statistically significant. When skin and dLN 2^{-dCt} values were summed, the mean level following patch G was highest of the microneedle patches tested, though ns. Significant differences were found between ID and flat patch and naïve in the LN and skin (P=0.005 and P=0.0009, Figure 14), similar to the previous experiment.

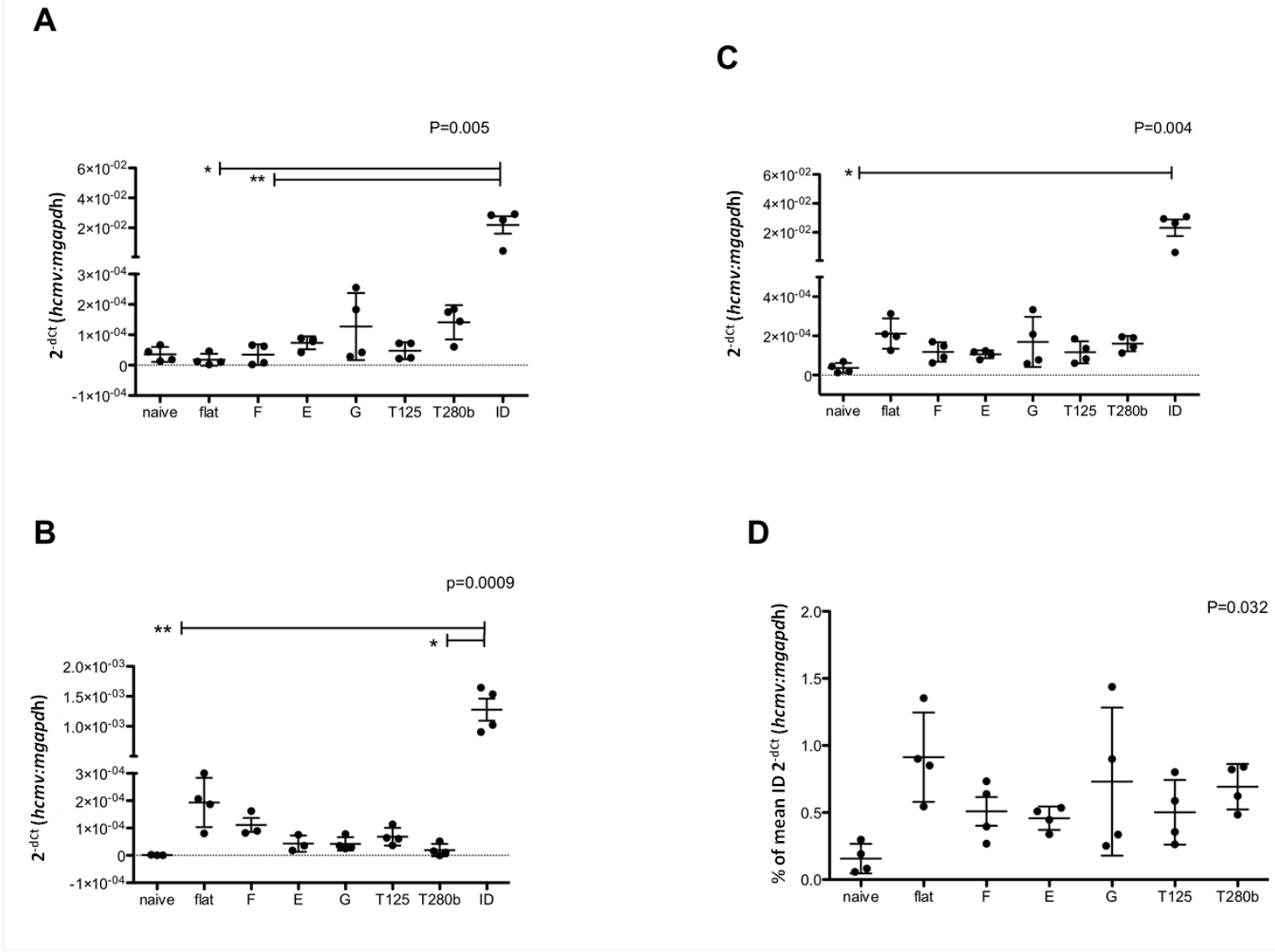
A
P=0.005
*
**
6×10-02
4×10-02
2×10-02
3×10-04
2×10-04
1×10-04
0
-1×10-04
2-dCt (hcmv:mgapdh)
naive
flat
F
E
G
T125
T280b
ID
C
P=0.004
*
6×10-02
4×10-02
2×10-02
4×10-04
2×10-04
0
2-dCt (hcmv:mgapdh)
naive
flat
F
E
G
T125
T280b
ID
B
p=0.0009
**
*
2.0×10-03
1.5×10-03
1.0×10-03
3×10-04
2×10-04
1×10-04
0
-1×10-04
2-dCt (hcmv:mgapdh)
naive
flat
F
E
G
T125
T280b
ID
D
P=0.032
2.0
1.5
1.0
0.5
0.0
% of mean ID 2-dCt (hcmv:mgapdh)
naive
flat
F
E
G
T125
T280b

FIGURE 3-14: Relative quantification of Adenovirus genomes following ImmuPatch delivery of AdHu5.*hcmv*are dependent upon specific patch used.

Female BALB/c mice (n=4) were immunised with 1x10^{10} VP AdHu5.*hcmv* ID, using a patch without needles ('flat patch') or by ImmuPatch F (0.011 mm^{3}TAV), E (0.033 mm^3), G (0.074 mm^3), T125 (0.090 mm^3), or T280b (0.205 mm^3). Four hours later, mice (+ 4 naïve mice) were sacrificed and ear pinnae and auricular LNs were harvested. Tissues were homogenised, treated with proteinase K and underwent DNA extraction using a kit from Qiagen. The quantification of *hcmv* DNA was normalised to that of the tissue loading control *mgapdh*, and was presented as 2^{-dCt}, a value derived from the measurement of the crossing threshold (the number of cycles taken to generate sufficient signal to overcome a pre-defined threshold) for both *hcmv* and *mgapdh*. Mean 2^{-dCt} (CMV:GAPDH) in draining LN samples (A) and skin samples (B) are presented ± SD. Significant differences were detected by Kruskall Wallis with Dunn's comparison. (C) Datapoints from skin and LN samples were summed for an appreciation of the total *hcmv* (relative Ct) per mouse (D) Summed values were presented as percentages of the mean summed value following ID immunisation.

These data should be interpreted with caution since the level of extracted *hcmv*-specific DNA detected was very low. Amplification curves were not significantly shifted to the left as compared to a containing no template DNA (not shown). This could perhaps be explained by inefficiencies in extraction of DNA from skin and LN using columns since trouble-shooting studies indicated that the PCR yielded accurate results when*hcmv* DNA was extracted directly from viruses. In conclusion of these studies, the Q-PCR assay requires further optimisation but has the potential for higher sensitivity. Nevertheless, trends were similar between the luciferase assay and Q-PCR methods.

3.3.3.3 Association between TAV and amount of Adenovirus delivered

Luciferase activities and2^{-dCt} values were plotted against TAV in Figure 3-15. A positive association was found between TAV and amount of vaccine present within the dLN, based on luciferase activity (Spearmann's rho=0.536, P=0.007, Figure 3-15A) and relative genome number (rho=0.546, P=0.0057, 3-15B, Figure 3-15B). Conversely, there was a negative association between TAV and luciferase activity (rho=-0.542, P=0.006) and relative genome number (rho=-0.727, P<0.0001) as assessed in the skin. These data suggest that the observed differences in immunogenicity of MVA/MVA and Ad/MVA regimes as delivered by ImmuPatch arrays of different design may be attributed to an overall difference in vaccine delivery across different TAV. However, since only one timepoint was investigated here, differences in the kinetics of antigen transport to the LN or in the persistence of vaccine in the skin versus its draining to the LN for different patches remain to be investigated.

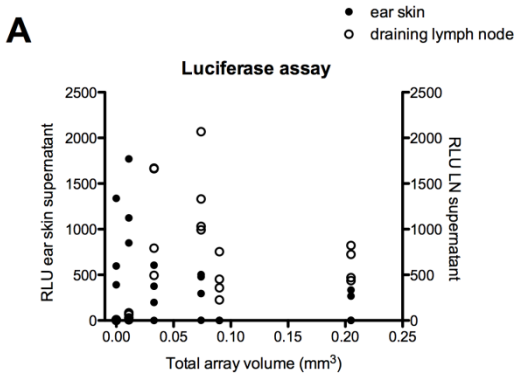

	ear skin	draining lymph node
Number of XY Pairs	24	24
Spearman r	-0.5424	0.5357
95% confidence interval	-0.7810 to -0.1655	0.1564 to 0.7773
P value (two-tailed)	0.0062	0.0070
P value summary	**	**

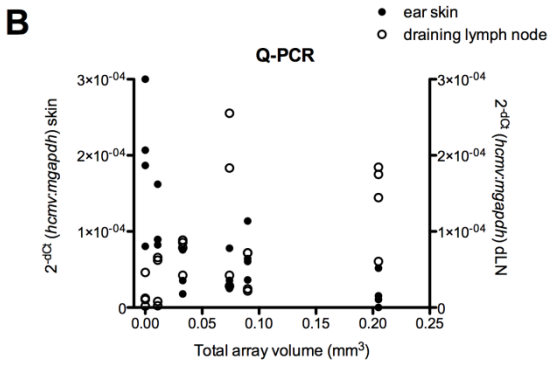

	ear skin	draining lymph node
Number of XY Pairs	23	24
Spearman r	-0.7273	0.5463
95% confidence interval	-0.8797 to -0.4396	0.1709 to 0.7832
P value (two-tailed)	< 0.0001	0.0057
P value summary	***	**

FIGURE 3-15: Correlations between ear skin and dLN luciferase activity and relative genome copy number with TAV.

Ear skin and draining LN luciferase activities in RLU (A) and relative genome copy number 2^{-dCt} (CMV:GAPDH) correlate with TAV. Skin (left Y axes, closed circles) and LN (right Y axes, open circles) datapoints were plotted against TAV following experiments detailed in Figure 3-14 and 3-15. Correlations between TAV and luciferase activity were assessed by Spearmann's rank correlation.

3.3.3.4 Protective efficacy of MVA / MVA ImmuPatch immunisation

The duration of the liver stage in *Plasmodium berghei* infection of BALB/c mice is approximately 48 hours (294). Following a standard challenge of 1000 *P. berghei* sporozoites incoculated into naïve mice, parasites are visible by microscopic

analysis of blood smears from day 5. The absence of parasites in the blood from day 5-20 signifies absolute protective efficacy of a vaccine regimen, and a delay in the acquisition of parasites (compared to naives) represents a partial inhibitory effect.

The protective efficacy of ImmuPatch delivery of vaccines in homologous MVA.PbCSP prime-boost regimes was assessed. Mice were primed with arrays A-H and boosted ID (as Figure 3-6), or by patch/patch combination F/G. Two weeks following the boost immunised and naïve mice were challenged and individually monitored from days 5-20 post-challenge by daily blood smear for blood-stage parasite forms. In mice that succumbed to blood stage infection, % parasitaemia was determined for each day from day 5 to day 8. Using a linear regression model developed by Dr. D. Wyllie, Jenner Institute, the time taken to reach 0.5% parasitaeamia was extrapolated (an endpoint chosen semi-arbitrarily as one corresponding to the linear part of the exponential growth curve) by finding the slope and intercept of a graph of log parasitaemia over time.

Results from 2 identical studies are given in Table 3-2. A Cox's Proportional Hazards Ratio Analysis was performed to compare time to 0.5% parasitaemia between immunised groups; incorporating mice remaining aparasitaemic with those with delayed acquisition of parasites within a group to give an overall likelihood (hazard ratio) of reaching this defined endpoint within the monitoring period. An interaction variable was included in the analysis, which detected no significant differences of individual groups between the two studies, except for the group H/ID (subsequently discounted from evaluation).

The regimes F/ID (P=0.02), F/G (P=0.011) and ID/ID (P=0.02) all had significantly decreased hazard ratios as compared to naïve challenged mice (Table 3-3). The difference between A/ID immunisation and naïve controls was of borderline significance (P=0.05) though the median time to 0.5% parasitaemia was particularly high in this group. The greatest median time to 0.5% parasitaemia was after F/ID immunisation (7.46 days). All other groups demonstrated a similar risk of developing blood stage parasitaemia following sporozoite challengeas naïve mice. There were no significant differences between ID/ID and ImmuPatch regimes, though the F/G regimen resulted in the most reduced risk of becoming parasitamic within the period (hazard ratio = 0.18, Table 3-2). Overall, these challenge studies demonstrate that ImmuPatch priming or priming+boosting is as efficacious as ID/ID immunisation in partial or complete protection against blood stage malaria infection following MVA.PbCSP/MVA.PbCSP.

Study	Immunisation Regimen (Prime/Boost)	Protected/group	Median time to 0.5% parasitaemia[a]	Combined median time to 0.5% parasitaemia	Combined protection (% combined group)	Combined Hazard Ratio[b]	Combined p-value[c]
1	Naïve	0/5	6.67	6.52	0		
2	Naïve	0/5	6.38				
1	A/ID	3/5	-	6.76	30	0.33 (0.11 – 1.00)	0.050
2	A/ID	0/5	6.35				
1	B/ID	3/5	-	6.49	40	0.39 (0.13 – 1.16)	0.09
2	B/ID	1/5	6.42				
1	C/ID	4/5	-	6.55	40	0.61 (0.22 – 1.74)	0.36
2	C/ID	0/5	6.40				
1	D/ID	2/5	6.76	6.66	20	0.44 (0.16 – 1.22)	0.12
2	D/ID	0/5	6.56				
1	E/ID	3/5	-	6.38	30	0.59 (0.22 – 1.59)	0.30
2	E/ID	0/5	6.27				
1	F/ID	3/5	-	7.46	50	0.25 (0.08 – 0.80)	0.02
2	F/ID	2/5	6.61				
1	G/ID	2/5	6.91	6.47	40	0.39 (0.13 – 1.17)	0.09
2	G/ID	2/5	6.29				
1	H/ID	5/5	-	-	60	0.04 (0.005 – 0.32)	0.002[d]
2	H/ID	1/5	6.96				
1	F/G	3/5	-	6.88	50	0.18 (0.05 – 0.68)	0.011
2	F/G	2/5	6.88				
1	ID/ID	3/5	-	6.91	40	0.25 (0.08 – 0.81)	0.02
2	ID/ID	1/5	6.54				

TABLE 3-2: ImmuPatch immunisation regimes induce partial protective efficacy against *P.berghei* sporozoite challenge.

Female BALB/c mice (n=5) were immunised with 1x10^6 PFU MVA.PbCSP, and given a homologous boost 2 weeks later. Immunisations were given either by ImmuPatch A-H or ID as detailed in the table. Two weeks following the boost immunisation, mice were challenged with 1000 *P.berghei* sporozoites, given IV. Mice were monitored from day 5-20 by thin blood smear and microscopic examination for blood stage parasites. The time taken for parasitaemic mice to reach 0.5% parasitaemia was calculated as described in the text. A Cox's Regression Hazard Ratio analysis was performed on data pooled from 2 identical challenge studies (numbered 1 and 2). No group except group H/ID demonstrated a significantly different result between the two studies. Hazard ratios are presented with 95% confidence intervals in parentheses. [a]Excluding mice surviving challenge without blood-stage infection, '–' indicates that less than 50% reached the outcome of interest (i.e. becoming parasitaemic), therefore the median could not be calculated. [b]As compared to naïve, unimmunised mice (95% CI)[c]As compared to naïve, unimmunised mice *p <0.05, ** p <0.01;[d]Study 1 and study 2 results were significantly different for H/ID, and so this group discounted from further evaluation.

3.3.3.5 Protection against sporozoite challenge - AdCh63/ MVA immunisation

The ability of ImmuPatch T280c (intermediate TAV) to induce protective immunity following the clinically-relevantprime-boostregimeAdCh63.ME-TRAP/MVA.ME-TRAP was evaluated in two experiments. Mice were immunised with 1x10^9 VP AdCh63.ME-TRAP ID and boosted with MVA.ME-TRAP, and 2 weeks later challenged alongside unimmunised controls. Pb9-specific immunogenicity by IFN-γ ELISPOT is presented in Figure 3-16, Aii or by ICS (IFN-γ+ CD8+)in Figure 3-16, Bii.In both studies, T280c/ID demonstrated high levels of protective efficacy - 63% T280c/ID (Figure 3-16A) and 90% (Figure 3-16B) as compared to 90% (Ai) and 80% (Bi) following ID/ID immunisation. Whereas 1/8 mice did not sucumb to blood stage malaria in the experiment in Figure 3-16A, all naïve mice presented in Figure 3-16B were positive by day 5. Responses were measured by 2 days before challenge by IFN-γ ELISPOT (Figure 3-16Aii) and by quantifying IFN-γ+ CD8 T cells (Bii) were equivalent between ID/ID and T280c/ID immunised groups.

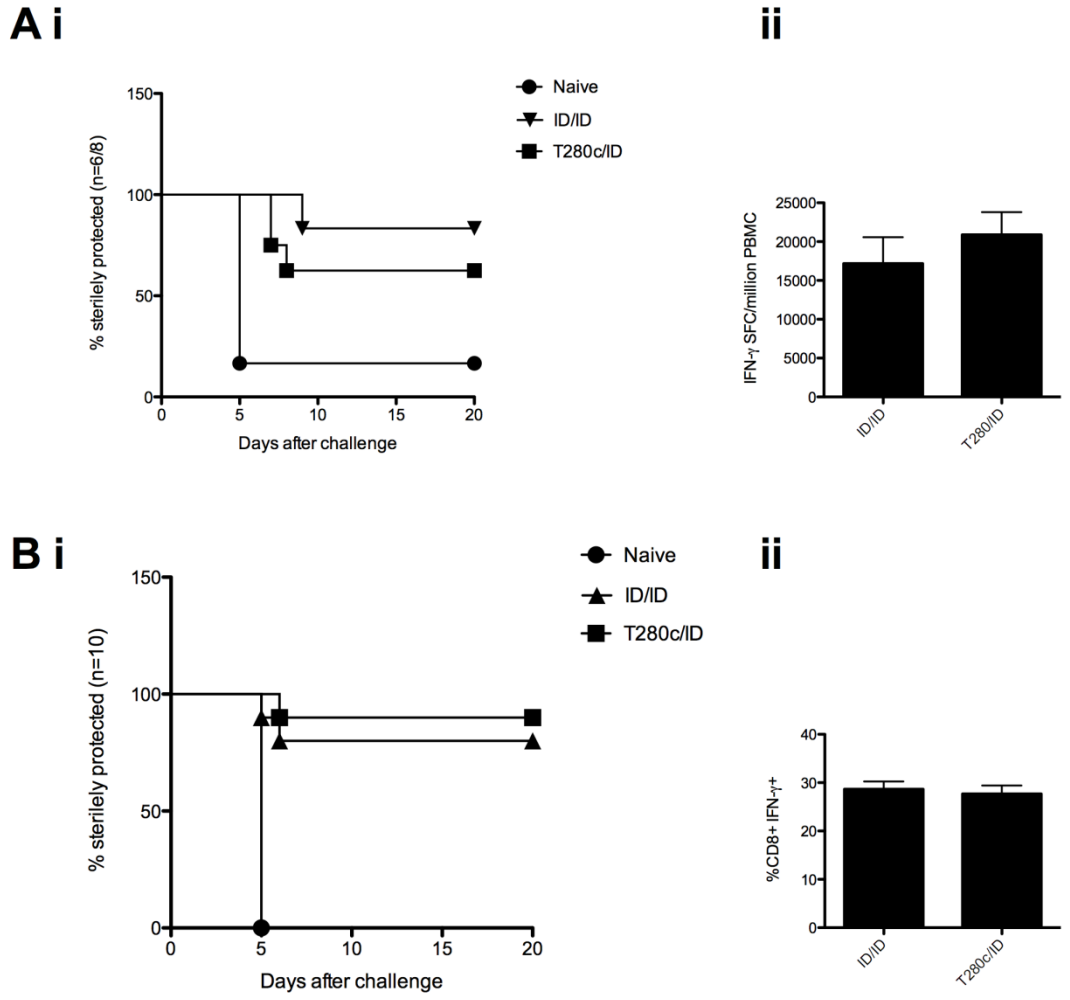

FIGURE 3-16: ImmuPatch/ID demonstrates high levels of protective efficacy in AdCh63.ME-TRAP/MVA.ME-TRAP immunisation.

In two separate experiments, female BALB/c mice (A-n=6/8, B-n=10) were primed with 1x10^9 VP AdCh63.ME-TRAP ID or by ImmuPatch T280c. Eight weeks later all mice were boosted with 1x10^6 PFU MVA.ME-TRAP ID. Two weeks following the boost immunisation mice were challenged with 1000 *P.berghei* sporozoites IV with naïve, unimmunised controls and followed up by thin blood smear and daily scoring for presence/absence of blood-stage parasites for 20 days. Two days prior to challenge, immunised mice were bled for PBMC isolation and IFN-γ ELISPOT or ICS (staining of IFN-γ + CD8+ T cells) following re-stimulation with Pb9 - A+Bi. Percentages of sterilely protected animals/immunisation group are presented on Kaplan Meier plots against time after challenge - A+Bii .

In a final challenge study, mice were primed with AdCh63.ME-TRAP ID, or by ImmuPatch C (intermediate TAV) H (large TAV) or T280b (extra large,TAV). In Figure 3-11, T280c (intermediate TAV, similar to C) exhibited boosting at both priming doses tested whereas T280b (extra large TAV) primed responses that could only be boosted when a priming dose of 1x10^9 VP was used. Thus 1x10^{10} VP was chosen as the priming dose to further investigate whether this dose-specific difference in immunogenicity was translated into differences in protective efficacy (Figure 3-17A). A secondary aim was to assess the protective efficacy of homologouspatch/patch regimes in AdCh63/MVA immunisation (C/C and

T280b/T280b - Figure 3-17B).Pre-challenge immunogenicity was assessed by IFN-γ ELISPOT (Figure 17, A+B ii).

ID/ID immunisation afforded 33% protection, in which is ordinarily a highly protective vaccine regimen (80-100% when delivered ID/ID (262)), -this leads to the speculation that the particular batch of sporozoites had anincreased virulence. Of patch regimes, C/ID (33%) and H/ID (66%) demonstrated good levels of sterile protection. However, as expected T280b/ID did not demonstrate protection and pre-challenge immunogenicity was low as compared to other patch/IDregimes, (Figure 3-17, Aii, ns). Patch/patch regimes did not demonstrate protective efficacy despite the pre-challenge level of response following C/C immunisation being similar to ID/ID, demonstrating the imperfect relationship between immunogenicity and protection. The T280b/T280b pre-challenge response was low and not increased from the post-prime level (Figure 3-17, Bii).

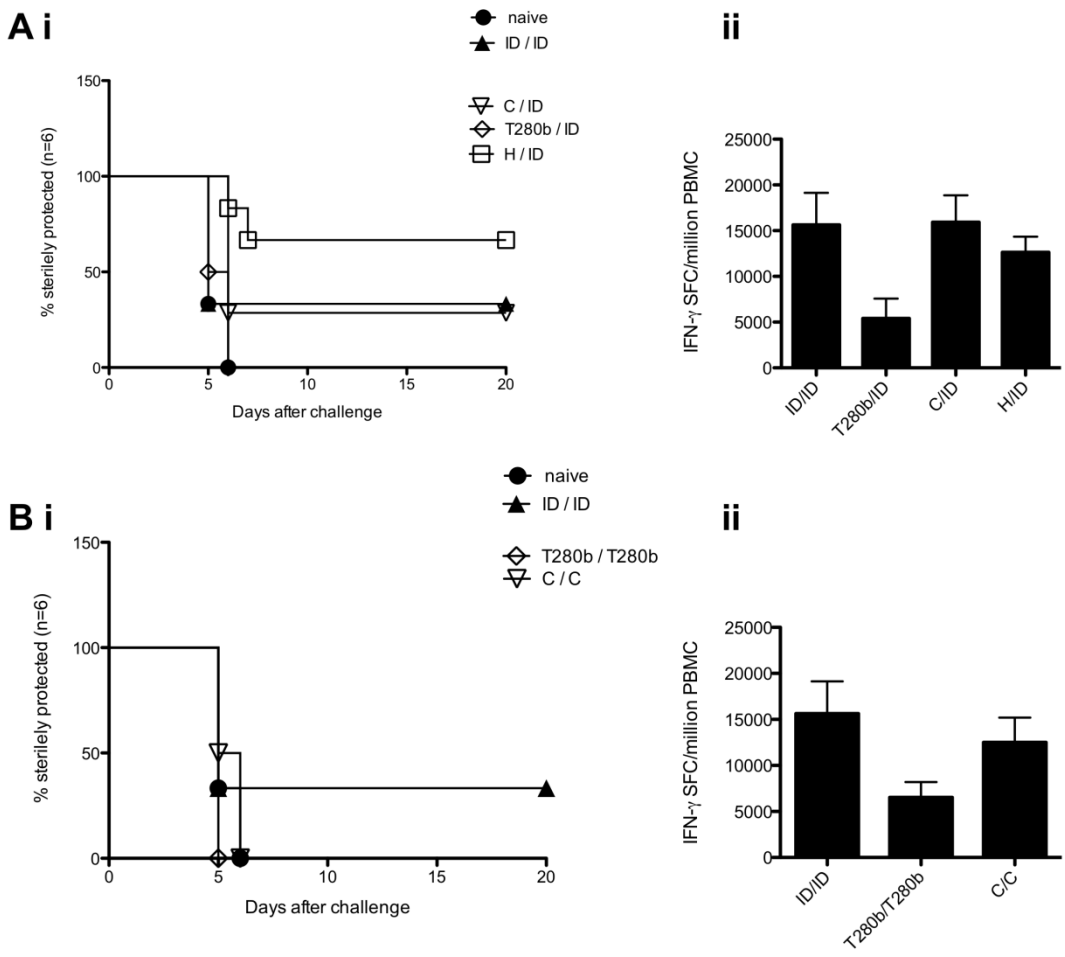

FIGURE 3-17: ImmuPatch/ID (patches C and H), but not ImmuPatch/ImmuPatch AdCh63/MVA immunisation is partially protective against *P. berghei* challenge.

Female BALB/c mice (n=6) were primed with 1x10^{10}VP AdCh63.ME-TRAP ID, or by ImmuPatch C, H or T280b. Eight weeks later primed mice received a boost immunisation of 1x10^{6} PFU ID, or by ImmuPatch C or T280b. Two weeks following the boost mice were challenged with 1000 *P.berghei* sporozoites IV. Six naïve animals were also challenged. Mice were followed up by thin blood smear and daily scoring for presence/absence of blood-stage parasites for 20 days. Percentages of sterilely protected mice are presented against time after challenge on Kaplan Meier plots (Figure 3-20 A+Bi). Blood was taken 2 days prior to challenge for assessment of pre-challenge responses by IFN-γ ELISPOT (Figure 3-20 A+Bii).

These data suggest that of those tested, patches of an intermediate and large TAV induce a higher protective efficacy than extra large (T280b) TAV in patch/ID immunisation. In three separate studies, patches of intermediate and large TAV demonstrated levels of protection ranging from 33% (C) to 90% (T280c). The patch/patch regimes T280b/T280b and C/C were not protective, but this experiment requires repetition to confirm this.

3.3.3.6 Summary of section 3.3.4 - *P. berghei* challenge

- Patch/ID regimes were partially protective against sporozoite challenge (and equivalent to ID/ID) in both AdCh63/MVA and MVA/MVA regimes. F/G was partially protective following MVA/MVA immunisation.
- The small TAV priming patch regimes A/ID, F/ID and F/G demonstrated significantly decreased risk of acquiring blood stage parasites as compared to naives.
- Though results from H/ID were inconclusive, 100% of H/ID immunised mice were protected in study 1 (MVA/MVA, Table 3-2).
- T280c (intermediate TAV)/ID induced high levels of protection following AdCh63.ME-TRAP/MVA.METRAP immunisation in two similar studies (80%, 90%, similar to ID/ID).
- T280b (extra large TAV)/ID and T280b/T280b were not protective.
- The regimes C/ID (33%) and ID/ID (33%) were similarly protective and H/ID (66%) slightly better, in what was considered a particularly virulent sporozoite challenge (due to the fact that ID/ID immunisation using these doses and this regimen usually demonstrates 80-100% protection-(262)).

3.4 DISCUSSION

The studies described in this chapter aimed to evaluate the ImmuPatch platform for delivery of vaccines in live vector homologous and heterologous prime-boost immunisation regimes, whilst attempting to delineate the factors influencing the magnitude of the ImmuPatch-induced T cell response. These factors included:

1. The methodology of patch/vaccine application
2. Design parameters of the patch
3. Dose delivered by the patch
4. The number and order of vaccines delivered by ImmuPatch in a prime-boost schedule

Early experiments using homologous MVA.PbCSP prime-boost demonstrated the potential for ImmuPatch to prime a CD8+ T cell response that could be boosted to equivalent level as compared to delivering both immunisations with a needle and syringe intradermally. Some ImmuPatch designs and route combinations were more immunogenic and efficacious than others and indeed, better than ID/ID immunisation.

3.4.1 The methodology of patch application

The number of antigen-specific IFN-γ-secreting cells was improved by applying the patch to skin already treated with vaccine, as compared to *vice versa.* This may be

due to instantaneous contraction of the skin due to its highly elastic nature upon removal of microneedles, reducing the volume of the microchannel available for vaccine diffusion during the time taken to apply a droplet of vaccine. The hydrophilic surface force attracting the liquid to the silicon microneedle may also allow vaccine to flow down the needle shaft *in situ* and into the microchannel, facilitating its further diffusion once the patch is removed. Using a liquid viral vector vaccine against Japanese encephalitis, frustum-tipped microneedles were swiped across the SC to mediate diffusion into non-human primate skin. Whilst only 1/3 macaques became viremic when the skin was pre-treated with microneedles, 3/3 became viremic when microneedles were applied through vaccine droplet demonstrating efficient delivery (130). Confocal microscopy of conduits in human skin where fluorescent dye was either applied before, or after the application of microneedles indicated greater delivery when skin was pre-treated(292). However, when dye was applied before microneedles in this study, dye remaining on the surface was immediately removed whereas application time following pre-treatment was 1 minute, allowing more dye contact time following pre-treatment. The fact that dye did diffuse when microneedles were applied *through* the dye (and subsequently removed) indicates that some dye is internalised upon microneedle penetration, but dye also is likely to continue to enter the microchannel post-removal since a separate study showed that retracting hollow microneedles following their insertion increased dye flow rates by releasing insertion compaction forces inhibiting local flow conductivity in an *ex vivo* human skin model. (173) A confirmatory analysis of delivered vaccine employing two methods using the same patch (using luciferase expression and/or Q-PCR for viral genomes) could further validate this hypothesis. The microchannel closure time (i.e. healing of the skin rather than closure due to elastic recoil) may also be a factor in delivered amount. Imaging data from Enfield *et al* suggest that microchannels reseal at a relatively slow rate (>85 minutes) in human skin, using arrays similar to T280c (269). Others report a recovered barrier functiononly 2 hours after treating human skin using 750µm microneedles, which can be extended to 48 hours when an occlusive patch is applied to the microneedle-treated site to inhibit the onset of skin repair mechanisms normally triggered by differences in moisture gradient. This study also demonstrated an increased healing time with increased microneedle length, cross-sectional area and density(195).

3.4.2 Design parameters of the ImmuPatcharray

The design of the microneedle patch was found to be strongly and significantly associated with the magnitude of the overall T cell response, with patches with a smaller TAV priming the lowest responses post-prime, but with increased ability to expand following ID boost. This observation was also reported by Carey *et al*, though noted significantly higher post-boost responses for A/ID and F/ID regimes compared to ID/ID immunisation(265). This result was supported by a statistically strong positive correlation between TAV after ImmuPatch prime and negative correlation after these responses were boosted ID (with both vaccine regimes). This was in contrast to reports that the microneedle geometry had no effect upon resulting response when assessed by the generation of antibody following recombinant protein delivery (143).

The design of the microneedle patch was found not just to impact upon the level of the induced response, but in some cases, whether a response could be boosted from the post-prime level at all. When immunising with T280b (of extra large TAV) to prime a low response with $1x10^{10}$ VP AdCh63.ME-TRAP this response did not expand upon ID boosting,and demonstrated no protection against challenge. However, responses primed with T280c (intermediateTAV) were boosted as were T280b responses primed with $1x10^{9}$ VP. These data demonstrate the importance of choice of patch and dose (further discussed later).

A proposed rationale for the observed differences in immunogenicity related to ImmuPatch design was that differences in TAV translate to differences in vaccine delivery, with patches of larger TAV delivering more vaccine into the skin due to the creation of larger conduits into which vaccine can flow. Quantifying transgene expression and inserted DNA sequences from Ad vectors in the skin and the draining LN following immunisation indicated that the biodistribution of vaccine between the skin and the LN 24h after delivery differs between patch designs. Interestingly, this work highlighted a potentially different kinetic in terms of luciferase expression/*hcmv* detection in the skin vs. dLN, with TAV correlating negatively with luciferase activity in the skin, but positively in the dLN. This may indicate a greater proportion of vaccine delivered into the SC*,* following delivery by small TAV patches which is not transported to the LN and remains in the skin (since the SC is not vascularised and does not contain APC) or a longer persistence of vaccine in the skin following immunisation with patches of smaller TAV. In contrast, transport of vaccine delivered by patches of larger TAV may progress to the draining LN more rapidly (i.e. by 24h post-immunisation). This retention of antigen in the skin by patches of smaller TAV may have consequences for response kinetics and/or specific phenotype of primed T cells (further discussed in Chapter 4).

Following delivery of the fluorescent marker FITC ID, or by ImmuPatch F, fewer FITC+ cells were visualised in the draining LN following ImmuPatch than ID, though these cells were capable of antigen presentation (MHC+ CD80+), whilst a similar number of FITC+ cells were present in the skin up to 96 hours post-immunisation(265). This difference in biodistribution of antigen may be directly attributed to the method of delivery. Injection of a bolus of liquid into the dermis has been reported to favour direct lymphatic drainage of antigen due to an increased local interstitial pressure impacting upon lymphatic capillary permeability and increasing flow (108, 295). This improved lymphatic drainage is considered one of the mechanisms underlying the dose-sparing attributes of ID immunisation over other needle routes(41), and has also been demonstrated in drug delivery by single microneedle (176). It may be considered that a minute increase in interstitial pressure such as that caused by delivering vaccine by large TAV ImmuPatch as opposed to one of small TAV may be sufficient to promote increased lymphatic drainage, since dLN transgene expression and TAV were significantly associated. Smaller TAV patches may result in a wider distribution of vaccine, with an increased amount remaining in the skin. Differences in lymphatic drainage following ImmuPatch delivery using patches of different TAV, compared to ID immunisation, remain to be demonstrated. A time-course experiment, perhaps using an *in vivo* model of luciferase expression, would aid in the further examination of the kinetics of vaccine delivery to the LN and in level of antigen persistence in the skin. Using such an *in vivo* system, T cell responses against described T cell epitopes within firefly

luciferase, could determine the magnitude and phenotype of the response, alongside a real-time kinetic analysis of luciferase expression (296).

Surprisingly, a patch with no microneedles allowed accumulation of vaccine in the skin but without progression to the LN. It is possible that virus may have gained entry to the skin via hair follicles, as was shown to occur in application of fluorescent MVA to the skin after tape stripping pre-treatment (119). However, since no luciferase signal was detected in the dLNs of these animals, it could be speculated that virus remains in the SC and does not gain entry to epidermal APC to allow transport to lymphoid tissue.

3.4.3 The dose applied to the ear prior to patch application

Decreasing the dose of MVA.PbCSP applied to the ear decreased post-prime responses following immunisation with patch F, though statistically significant differences were not determined. However, altering the priming dose did not affect the post-boost response following delivery of a standard boosting dose ID. Surprisingly, as little as $1x10^4$ PFU MVA.PbCSP delivered by patch F (corresponding to an actual delivered dose of approximately $5x10^2$ PFU, as determined from luciferase expression) was sufficient to prime a response that could be boosted as efficiently as those induced by higher priming doses. Others have found that the dose-sparing attributes of microneedle delivery are more pronounced at the lower end of the dose-response curve, with no difference in antibody induction following protein vaccine delivery between IM, SCu and microneedle routes at higher doses. Intramuscular delivery of AdHu5 and AdHu35 vectors encoding CSP from *P. yoelli* demonstrated a similar plateau of the dose response curve in for antigen-specific T cell responses (297). It could be suggested this plateau is reached at a lower dose after microneedle delivery than after IM delivery (the dose-response curve is shifted to the left), so priming with a lower dose may have immunological in addition to logistical advantages in microneedle vaccine delivery which remain to be fully elucidated within the context of live viral vaccines.

In contrast to MVA/MVA immunisation, priming with a lower dose of $1x10^9$ VP by T280b was successfully boosted ID, whereas priming with $1x10^{10}$ VP by T280b was not. Whilst reasons for this are not clear, delivery by T280b (by luciferase expression) was lower than expected for an extra large TAV patch, perhaps due to its larger surface area meaning not all microneedles on the patch may come into contact with the mouse ear, overestimating TAV. It is feasible that during this experiment, T280b delivered a lower amount of vaccine by chance when $1x10^{10}$ VP were applied, as compared to $1x10^9$ VP, and the signficance of this result remains to be defined.

3.4.4 The number and order of vaccines delivered by ImmuPatch in a prime-boost schedule

ID primed responses were not boosted efficiently by T280, and significantly lower responses were elicited by T280/T280 immunisation than ID/ID, and T280/ID (though not significant) – a result observed in a number of experiments when comparing patch/ID with patch/patch regimes (two here represented). However, it is clear from

this experiment and others performed by colleagues at UCC, that 'heterologous' patch boosting – i.e. using a different array for priming, to that used for boosting – is more efficacious than using the same array for delivery of both immunisations in MVA.PbCSP prime-boost immunisation. Patch combinations of A/G and F/G were found to induce a higher % CD8+ IFN-γ as compared to other combinations (265). More specifically, regimes where a small TAV was used to prime responses and a large TAV patch was used to boost them were significantly more efficacious than small/small or large/large combinations,supporting the result in Figure 3-8. In homologous patch/patch the TAV used was weakly positively correlated with post-boost response indicating perhaps a larger TAV is required to boost a response by patch. Thus, considering that lower TAVs prime responses that are optimally boosted, a small TAV/large TAV combination appears to be the optimal combination.

These data can be explained by the observation that boosting, but not priming of responses within this regimen is highly sensitive to a reduction in dose. Whilst priming with $1x10^2$ PFU induces a response that is increased to equivalent levels as $1x10^6$ PFU priming (after a standard dose boost), priming of responses with $1x10^6$ PFU and boosting with $1x10^2$ PFU is inefficient, and responses significantly lower. This will be due in part to the expansion of anti-vector in addition to antigen-specific immunity following priming with MVA, requiring a higher 'threshold' boosting dose of MVA to overcome. The data in Figure 3-10 suggest this threshold is approximately $1x10^6$ PFU when delivered ID. Given that the delivered amount is significantly less (of the order of 10^4-10^5 PFU) when this dose is applied by patch, secondary responses are inefficiently mobilised.

In order to access the full potential of microneedle patches in prime-boost immunisation in the clinical situation, a system whereby both immunisations can be given by the same route is preferred, removing the requirement for needles completely. These data suggest that by careful patch design and optimal doses for prime and boost (smaller TAV prime + large TAV boost) responses can be improved, and Carey *et al* suggest that levels acheived can be compared to ID/ID(265). Indeed, immunisation with F/G exhibited significantly improved protection (50% sterile protection and a median delay in the progression to the blood stage of 0.36 days over the naives) following homologous MVA.PbCSP prime-boost despite having a lower immunogenicity than some other non-protective regimes, highlighting the complexity of functional immunity to malaria, and our still incomplete understanding of IFN-γ production as a definitive cellular correlate of protection.

ImmuPatch/ImmuPatch immunisation using heterologous patch combinations were not assessed in AdCh63.ME-TRAP/MVA.ME-TRAP immunisation, but in a challenge with what was considered to be particularly virulent batch of sporozoites (due to the reduced level of protection for ID/ID immunised mice compared to that routinely observed (262)) C/C and H/H immunisation were partially protective (33% and 66% respectively) and of similar immunogenicity compared to ID/ID. However, T280b/T280b immunised mice were not protected, nor were T280b primed responses efficiently boosted by T280b, again highlighting the importance of appropriate choice of patch.

3.4.5 Other potential factors influencing the ImmuPatch-induced response

One factor that remains to be investigated in further detail is the role of microneedle length in the induction of responses. A number of distinct CD11c+ CD11b+ dendritic cell subsets have been proposed to take up and internalise foreign antigen in the cutaneous environment for presentation to T cells in the LN. However, specific roles are unclear – epidermal Langerhans cells mayplay a part in tolerising responses to host and innocuous antigen rather than orchestrating the response to an immunogen (298-300). The TAV was the most appropriate parameter with which to assess the range of patches in these studies, as a controlling parameter linking both microneedle length and needle density with which to assess these arrays. Microneedle length did positively correlate with post-prime response when considering all patches (of varying needle density). However, this could be an indication of its close relationship with TAV, rather than a specific association with depth or APC types targeted, since microneedle length is related to the volume of the microchannel it will create, thus the patches with the longest needles (up to 300µm) are likely to be the ones with the highest TAV. A suggestion that TAV may be a more significant factor than length was proposed when ImmuPatch G with 81 x 200µm microneedles (TAV = 0.077mm^3) was directly compared with T125 comprising 400 x 125µm microneedles (TAV=0.090mm^3) and equivalent resulting responses were observed, which were significantly different to those following immunisation with similar needle length but different TAV (265). It should be noted, however, that the 125µm patch used here demonstrated lower luciferase transgene expression than patches of slightly smaller TAV, perhaps due to a larger surface area, meaning perhaps not all microneedles penetrated the ear skin, and hence TAV may have been reduced.

Microneedle length also has implications for the acceptability of microneedle patch immunisation. Microneedles (within the range of 100-300µm in length) are not expected to stimulate the nociceptors of the dermis. Volunteers attributed less pain and discomfort using patches of the same dimensions as T190 and T280, as compared to injection by hypodermic needle (187). Due to the fact that the skin is an elastic and homogeneous tissue, the properties of which vary with age, sex, ethnicity, hydration (i.e. environment) and anatomical location, a microneedle length of >20µm will be required to ensure piercing of the SC. Physical breaching of the SC using microneedles has been demonstrated here to be essential for vaccine transport from the skin to the draining LN, since vaccine present within the skin following flat patch immunisation did not drain to the LN. It could be speculated that this is because the vaccine enters via hair follicles, but is retained in the SC, which is neither vascularised nor contains migratory APC.

It will be important to balance the immunological and logistical attributes of microneedle patch designs within the specific context of the type of vaccine being delivered. Whilst increasing the needle density may allow a greater spread of application force across the patch reducing breaking stress – this may lead to a ‘bed of nails’ effect, whereby penetration is inhibited due to the low sheering force on each individual microneedle (C. O’Mahony, *pers. comm*.). In addition to its larger surface area, this could explain the similar/slightly lower overall levels of delivery of

the T125 (125µm) as patch F (100µm), despite having four times the total number of needles (Figure 3-13+4).

3.5 CONCLUDING STATEMENT

To summarise, topical application of liquid AdCh63 and MVA vectored malaria vaccines prior to ImmuPatch application induces antigen-specific CD8+ T cells that are optimally expanded upon ID boost when a small TAV patch is used to prime responses. Interestingly, and somewhat surprisingly, patch/patch immunisation can be improved by correct combination of array parameters (e.g. F/G). ImmuPatch priming, ID boosting (and ImmuPatch priming+boosting in the case of F/G) demonstrates partial protection against *P.berghei* challenge following MVA/MVA and high protection in AdCh63/MVA immunisation. Overall, patch/ID immunisation is as effective as ID/ID in terms of immunogenicity and protective efficacy, despite the fact that the amount of vaccine actually delivered by ImmuPatch was estimated to between 2-10% of that delivered ID.

CHAPTER 4 CHARACTERISING CD8+ T CELL AND EARLY INNATE RESPONSES TO IMMUPATCH IMMUNISATION

4.1 INTRODUCTION

In the previous chapter, a direct relationship was demonstrated between the magnitude of the Pb9-specific CD8+ T cell response primed by an ImmuPatch and its geometry, specifically the parameter of TAV, used as an indicator of the total volume of microchannels created upon application to the skin. Differential expression of a luminescent transgene suggested that the design (specifically TAV) influences the volume of vaccine delivered, with patches with higher TAV exhibiting a higher expression of luciferase in the draining LN 24 hours after immunisation. However, since a higher expression was observed in the skin following smaller TAV immunisation, this difference may not simply be quantitative but qualitative, and perhaps indicative of a differential kinetic of antigen drainage from the immunisation site compared to ID/large TAV patches, warranting further investigation. Remarkably, the relationship between TAV and the magnitude of the post-boost CD8+ T cell response was inverse, when the boost was delivered ID, in both homologous and heterologous prime-boost regimes. The experiments described within this chapter aimed to explore these differences further, with respect to the kinetics and memory phenotype of induced T cell responses following ImmuPatch immunisation with Pb9-encoding Ad or MVA in relation to their ability to expand upon boost, and to explore differences in innate events early after MVA immunisation, that may give rise to clones of antigen-specific T cells with a specific phenotype.

Following foreign antigen encounter accompanied by APC-associated MHC I and appropriate co-stimulatory signals, cognate CD8+ T cells rapidly expand and differentiate and reach a peak in magnitude in the weeks following exposure (1 weeks following MVA prime, 2-3 weeks following Adenovirus prime)(251). These cells contribute to pathogen clearance by mediating effector function such as direct killing of infected cells or cytokine production such as IFN-γ and TNF-α. Proposed mechanisms of IFN-γ are described in section 1.6.4. Antigen-specific cells then undergo a contraction phase whereby 90-95% die by apoptosis, triggered by the absence of proliferative and survival factors such as IL-2, IL-7 and IL-15. The remaining memory pool persists in the absence of antigen and by cytokine homeostasis in both peripheral and lymphoid tissues and in the circulation. Boosting responses allows for a secondary peak of greater magnitude and a higher resting level of antigen-specific immunological memory (242). Memory cells have been subdivided into central memory, T_{CM} or effector memory, T_{EM} subtypes based on hallmark attributes such as their ability to expand upon secondary exposure (T_{CM}>T_{EM}) and retention of effector function (T_{EM}>T_{CM}), anatomical location and for purposes of identification - surface marker expression (30-32).

Two hypotheses were proposed to explain the observation that patches of smaller TAV demonstrated a lower post-prime response compared to ID immunisation and yet were boosted to equivalent or superior levels as those resulting from priming ID:

- The kinetic of the ImmuPatch-induced response was different to that following ID priming. As such, the timepoint chosen for sampling of post-prime responses (pre-determined as the peak of the ID response) did not correspond to the peak of response following ImmuPatch immunisation. (If

this is the case, subsequent contraction before boost was sufficient to permit efficient boosting, since small TAV patch-primed responses were well expanded upon boost).

- ImmuPatch priming generates a response comprising a different memory subset composition compared to ID priming. Given that the enhanced ability to rapidly proliferate upon re-exposure is a key feature of T_{CM}, the hypothesis was stated that a greater proportion of Pb9-specific CD8+ T cells induced by ImmuPatch, especially patches of small TAV would demonstrate a central memory phenotype (cytokine+ CD62L+ CD127+) than after ID immunisation.

The second part of this chapter aimed to investigate the early events in the innate response following immunisation with recombinant MVA that may potentially influence the priming of a T cell response. During activation of naïve CD8+ T cells by Ag-MHC I complexes in the lymphoid organs, specific attributes described above such as effector function, memory phenotype and homing potential are programmed (36, 40, 67, 301). Factors reported to influence this process include the specific nature and activation state of the APC, the duration of antigen stimulus and the cytokine milieu of the priming environment (29, 36, 37, 302). Since ImmuPatch (G) has been shown to deliver antigen into microchannels extending into the viable epidermis and dermis whereas ID immunisation deposits antigen as a bolus into the dermis(265), it was speculated that the inflammatory response and trafficking of innate cells from the immunisation site to the LN following ImmuPatch immunisation might be of a different composition and/or magnitude as compared to ID immunisation. Related to this, that the differential distribution of antigen (i.e. VE+dermis vs. dermis, within discrete microchannels vs. deposited as a bolus) may impact upon the level of local inflammatory cytokine induction by innate cells in the skin following immunisation, thus creating a distinct T cell priming environment as compared to ID immunisation, with the potential to impact upon specific programming of a CD8+T cell response.

4.2 STATEMENT OF HYPOTHESES

- ImmuPatch-primed CD8+ T cell responses follow a slower kinetic than those following ID priming, though with contraction complete by the time of boost. Patches of small TAV follow a slower kinetic than large TAV patches (from observations made in Figure 3-15).
- ImmuPatch primes an antigen-specific response with a higher proportion of T_{CM}-phenotyped CD8+ T cells, whereas the ID response will comprise mainly T_{EM} cells.
- The delivery biodistribution differences between ImmuPatch and ID will influence the level of inflammation in the skin and dLN following immunisation.
- The kinetic, magnitude and composition of innate cells in the skin and dLN following ImmuPatch immunisation will differ to ID, and between patch F (small TAV) and patch G (large TAV. To account for a difference in dose delivery, two doses will be delivered ID: 1) equivalent dose to that applied to the ear, 2) a '3%' dose, based on the delivery of nanospheres into the skin as reported by Carey *et al* (265).

4.3 RESULTS

4.3.1 ImmuPatch primes a Pb9-specfic response with an irregular kinetic whilst retaining ability to expand upon boost

The kinetics of CD8+ T cell responses primed by two patches of differing TAV were assessed. Mice were primed with MVA.PbCSP either ID, by ImmuPatch T280c (intermediate TAV) or T280b (extra large TAV). Two weeks after the prime, all mice were boosted with MVA.PbCSP ID. When frequencies of IFN-γ+ CD8+ T cells were assessed two weeks following the boost immunisation after Pb9 re-stimulation, all prime-boost responses were equivalent and approximately 3-fold higher than the response 2 weeks following a single immunisation given ID (Figure 4-1A, P=0.0541 for T280c/ID).

In a separate experiment, mice were immunised with $1x10^6$ PFU MVA.PbCSP either ID, or by T280c or T280b as before (Figure 4-1B). Pb9-specific CD8+ T cell responses were assessed 1, 2 and 4 weeks following immunisation by ICS. As expected the ID-primed response at 1 week post-prime of greater magnitude compared to both patches (though not significant, ns)(251). This response decreased from one to four weeks after immunisation, consistent with the normal course of T cell expansion and contraction. Surprisingly, neither ImmuPatch primed a response with a clear peak, or a significant contraction phase but maintained a similar level low throughout, with little difference in response between the patches. All responses were of a similar magnitude by 4 weeks post-immunisation.

To investigate the response following AdCh63/MVA prime-boost immunisation, mice were primed with AdCh63.METRAP at $1x10^9$ VP (Figure 4-1, Ci) or $1x10^{10}$ VP (Figure 4-1, Cii) delivered ID, IM, or by T280c or T280b. Frequencies of IFN-γ+ CD8+ T cells at various timepoints post-immunisation. A boost immunisation of $1x10^6$ PFU MVA.METRAP was given to all mice ID 8 weeks following the prime, consistent with an AdCh63/MVA heterologous prime-boost immunisation schedule (262). Similar to the observation made following MVA.PbCSP immunisation, neither ImmuPatch demonstrated an expansion or contraction phase, with responses maintaining a similar low level following both doses until the boost was given. Conversely, ID and IM-primed responses peaked 2 weeks following priming with both doses, which contracted down by week 5. However, whilst both ImmuPatch-primed responses were successfully expanded upon the boost after priming with $1x10^9$ VP, only T280c responses were boosted following priming with $1x10^{10}$ VP, whereas T280b $1x10^{10}$VP primed responses were not boosted. Additionally, whilst the T280c-primed response ($1x10^9$ VP) was slightly lower than other groups 2 weeks following the boost (10 weeks), it was slowly increased from 10 to 14 weeks such that it was equivalent to all other immunised groups at the final timepoint.

These data show that despite failing to demonstrate a detectable peak of response and contraction phase, ImmuPatch responses are able to expand upon boost to equivalent levels as for ID/ID immunised mice in MVA/MVA and (with the exception of T280b $1x10^{10}$ VP) AdCh63/MVA immunisation. This data supports the rejection of hypothesis pt.1.

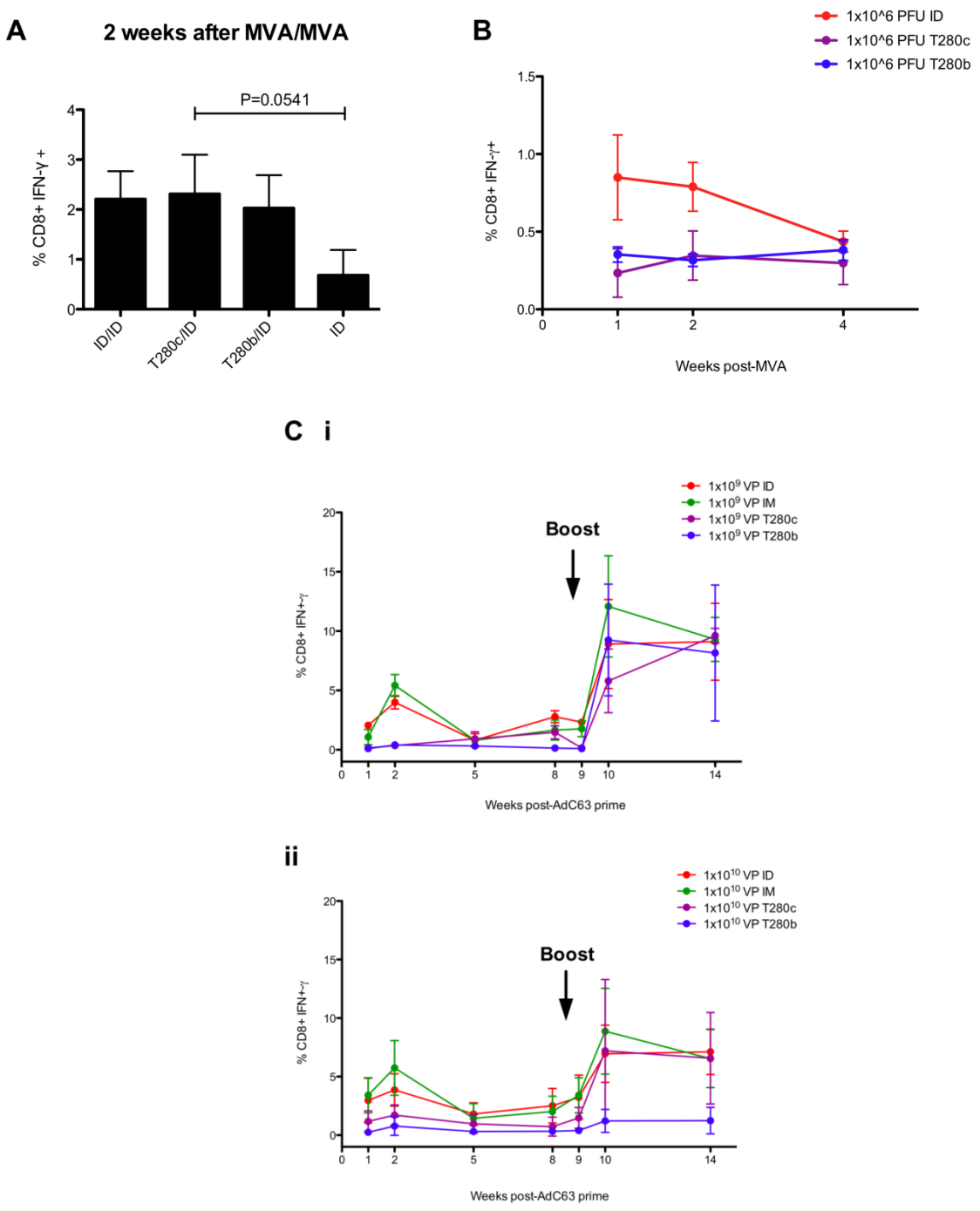

FIGURE 4-1: Irregular kinetics of the Pb9-specific CD8+ T cell response following ImmuPatch immunuisation with MVA- or AdCh63-vectored vaccine.

(A) Female BALB/c mice (n=5) were immunised with MVA.PbCSP and boosted at 2 weeks post-prime with 1x10^6 PFU ID. One group was given a single immunisation ID at the time of the boost. Spleens were harvested 2 weeks post-boost and cells were stimulated with Pb9 and stained with anti-mouse CD8 PercP Cy5.5 and IFN-γ APC. Gating was as follows: singlets > lymphocytes > CD8+ > CD8+ IFN-γ+. Bars show mean %CD8+ IFN-γ+ T cells ± SD, P=0.0541 by Kruskall Wallis + Dunn's comparison. (B) In a separate experiment, female BALB/c mice (n=12)

were immunised with 1x10^6 PFU ID, by ImmuPatch T280c ('intermediate') or T280b ('extra large' TAV). One, 2 or 4 weeks post-immunisation 4 mice per group were sacrificed and spleens harvested for Pb9 stimulation and ICS as above. Datapoints and error bars represent mean frequencies of IFN-γ+ CD8+ T cells ± SD. (C) Female BALB/c mice (n=4) were immunised with 1x10^9 VP or 1x10^{10} VP AdCh63.METRAP ID, IM or by ImmuPatch T280c or T280b. Blood was taken at timepoints post-immunisation for Pb9 stimulation of PBMC and ICS (staining and gating protocol as above). A boost immunisation of 1x10^6 PFU MVA.METRAP was delivered ID 8 weeks following the prime. These data and those presented in Figure 3-11A-B (2 timepoints) are from the same experiment. Datapoints are mean frequencies of IFN-γ+ CD8+ T cells ± SD.

4.3.2 Antigen-specific CD8+ T cell memory phenotype in MVA/MVA immunisation

The memory phenotype of Pb9-specific CD8+ T cells primed by MVA.PbCSP delivered ID, by ImmuPatch T280c or T280b, prior to boost was assessed. Splenocytes isolated 2 and 4 weeks following immunisation were stained with mAbs raised against CD8, IFN-γ, TNF-α, IL-2 and the memory markers CD62L and CD127 to allow phenotyping of antigen-specific T_{CM}, T_{EM} and T_E cytokine+ cells. Figure 4-2 presents absolute frequencies (A+B, i) and relative proportion of the total response (A+B, ii) exhibiting the phenotypes T_{CM}, T_E and T_{EM} as characterised by expression / lack of expression of CD62L with CD127 (32) or an intermediate phenotype - T_{int} (CD62L+ CD127-)(32). Figure 4-2, A+Biii demonstrates this in FACS plots of cytokine+ cells against CD62L and CD127 axes.

A higher proportion of the total response was CD62L+ CD127+ (T_{CM}) following ImmuPatch immunisation as compared to ID immunisation, as were absolute frequencies of CD62L+ CD127+ amongst cytokine-secreting CD8+ T cells ($P<0.05$ when comparing both ImmuPatch arrays with ID, Figure 4-2, Ai). Whilst the dominant phenotype for all groups 2 weeks following a single immunisation of MVA.PbCSP was T_{EM}, there were specific differences in the proportion of T_{EM} between immunised groups, with ID immunisation generating a higher frequency of T_{EM} making up a higher proportion of the total response, as compared to ImmuPatch groups. Two of four T280c-immunsed mice demonstrated a low frequency of T_E, resulting in a lower mean frequency as compared to ID and T280b. Between 2 and 4 weeks, there was a marked increase in both frequencies and relative proportions of T_{CM} in all groups, despite the fact that the magnitude of the response did not appear to decrease significantly in ImmuPatch-primed groups during this time period (Figure 4-1B). Frequencies and proportions of T_E were reduced from the 2 week to the 4 week timepoint in all groups. The frequency of T_{CM} phenotyped cells was higher after ImmuPatch than ID immunisation, but the difference was not significant. The increase in the frequency and proportions of T_{CM} between 2 and 4 weeks after ImmuPatch immunisation is greater than that following ID immunisation, suggesting that ImmuPatch immunisation promotes the early emergence of a central memory phenotype compared to ID immunisation. When mice were primed in the same way as in Figure 4-2 and boosted with 1x10^6 PFU MVA.PbCSP ID 2 weeks after the prime, the phenotype of ID, T280c and T280b primed responses differed compared to post-prime (Figure 4-3). Specifically, T_{EM} was the dominant phenotype with very low representation of T_{CM}, and a higher T_E component as compared to post-prime, for all groups. In summary, ImmuPatch primes a response of an early T_{CM}phenotype

with the ability to expand upon boost, whereupon this phenotype is converted to T_{EM}.In the linear model of memory differentiation (Figure 1-1), T_{int} is associated with weak and short Ag stimulation and is associated with a lack of peripherally measurable clonal expansion (see Figure 4-1) and indicative of abortive T cell expansion, though can be converted to $T_E$with sufficient Ag (32). T_{int} was of similar, low frequency between groups both post-prime and post-boost.

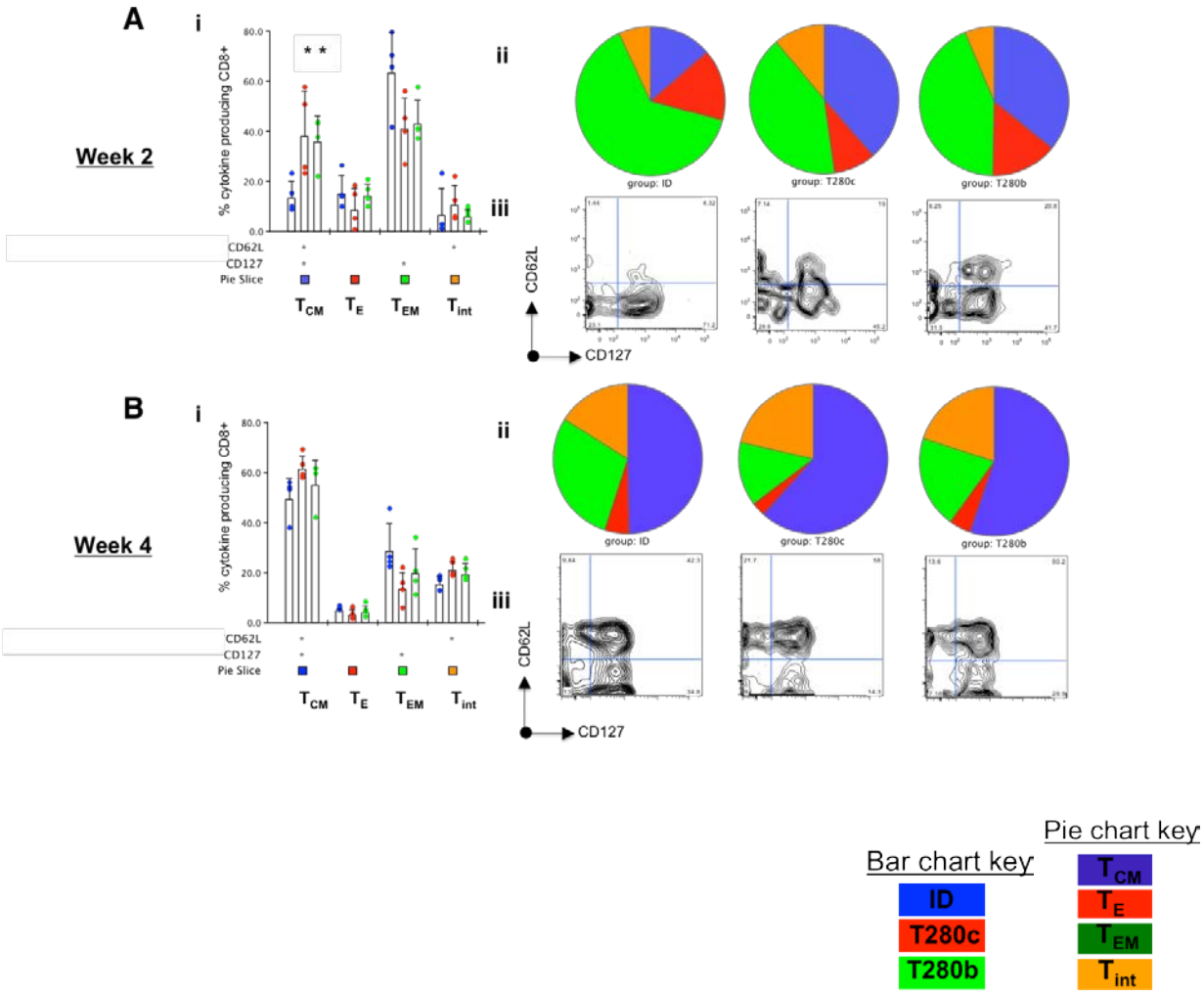

FIGURE 4-2: Memory phenotype of Pb9-specific CD8+ T cells at timepoints following immunisation with MVA.PbCSP, delivered ID or by ImmuPatch.

(A) Female BALB/c mice (n=4) were immunised with 1x10^6 PFU, ID or by ImmuPatch T280c or T280b. This analysis was performed as part of the experiment presented in Figure 4-1B. Two weeks (A), or 4 weeks (B) following the immunisation harvested splenocytes were stimulated with Pb9 and stained with anti-mouse CD8 PercP Cy5.5, IFN-γ APC, TNF-α FITC, IL-2 PE, and the memory markers CD62L Pacific Blue and CD127 PE Cy7. In Flowjo the following gates were set: singlets > lymphocytes > CD8+ > IFN-γ/TNF-α/IL-2. A combined gate including all antigen-specific cells (i.e. all those expressing at least one cytokine – 'cytokine+') was set on the CD8+ population. CD62L+ and CD127+ gates were set from the cytokine+ population and a Boolean analysis yielded all combinations of CD8+ cytokine+ expression of CD62L and CD127. Pestle and SPICE software were used to present absolute levels as % CD8+ cytokine+ (A+B, i)

shown for ID, T280c or T280b and relative proportions of each total response (A+B, ii) exhibiting a central memory (T_{CM} – CD62L+ CD127+, blue pie section), effector memory (T_{EM} – CD62L- CD127+, green pie section), T effector (T_E – CD62L-CD127-, red pie section) or intermediate phenotype (T_{int} – CD62L+ CD127-, orange pie section). *=P<0.05 compared to ID (unpaired student t test, performed as part of the SPICE analysis). (A+B, iii). Representative contour plots of cytokine+ CD8+ expression of CD62L (Y axis) and CD127 (X axis).

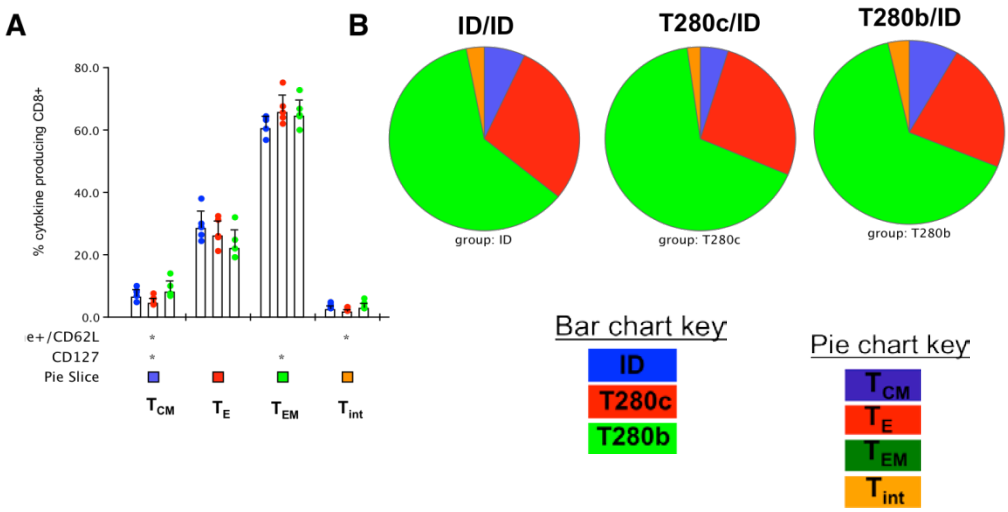

FIGURE 4-3: Memory phenotype of responding CD8+ following MVA/MVA prime-boost immunisation.

(A) Female BALB/c mice (n=5) were immunised with MVA.PbCSP ID/ImmuPatch T280c/ImmuPatch T280b and given a homologous boost 2 weeks later. Spleens were harvested 2 weeks post-boost, stimtulated with Pb9 and stained and analysed as in Figure 4-2. Pestle and SPICE software were used to present absolute levels as % CD8+ cytokine+ (A) and relative proportions of the total response (A) that exhibited a central memory (T_{CM} – CD62L+ CD127+, blue pie section), effector memory (T_{EM} – CD62L- CD127+, green pie section), T effector (T_E – CD62L-CD127-, red pie section) or an intermediate phenotype (T_{int} – CD62L+ CD127-, orange pie section).

In these experiments there were no significant differences in either response magnitude or phenotype between ImmuPatch arraysT280c (intermediate-) and T280b (extra large TAV). However, in a study carried out by Carey *et al* using a range of TAVs ranging from small to large, patch-specific differences in memory phenotype were observed. Significantly higher frequencies of T_{CM} were observed when comparing the three patches with the smallest TAV - A, F and B with ID immunisation. Additionally, frequencies of T_{EM} after A and F priming were significantly lower than ID. When all groups were given an ID boost all groups demonstrated a T_{EM} phenotyped response, with a significantly higher frequency of T_{EM} phenotyped cells after F/ID as compared to ID/ID(265).

4.3.3 Cytokine and chemokine expression at the immunisation site and the dLN following ID and ImmuPatch delivery of MVA

In an attempt to further explore the observations following ImmuPatch immunisation with recombinant MVA with particular attention to the manner in which T cells are primed, it was hypothesised that the inflammatory state of the priming environment may differ as compared to ID immunisation. More specifically, that ImmuPatch induces an innate response of a less inflammatory nature, which has been proposed to favour a rapidly-acquired T_{CM}-phenotyped memory response (37). Mice were immunised with $1x10^6$PFU MVA.PbCSP either ID or by ImmuPatch F (of small TAV) and sacrificed at timepoints 6, 18 and 48h post-immunisation (n=5/timepoint) for quantification of mRNA expression of several cytokines and chemokines associated with the pro- and anti-inflammatory response within ear skin and dLN tissue, by RT-PCR, normalised to the mRNA expression of the housekeeping gene *mgapdh* (A. Vrdoljak, UCC).

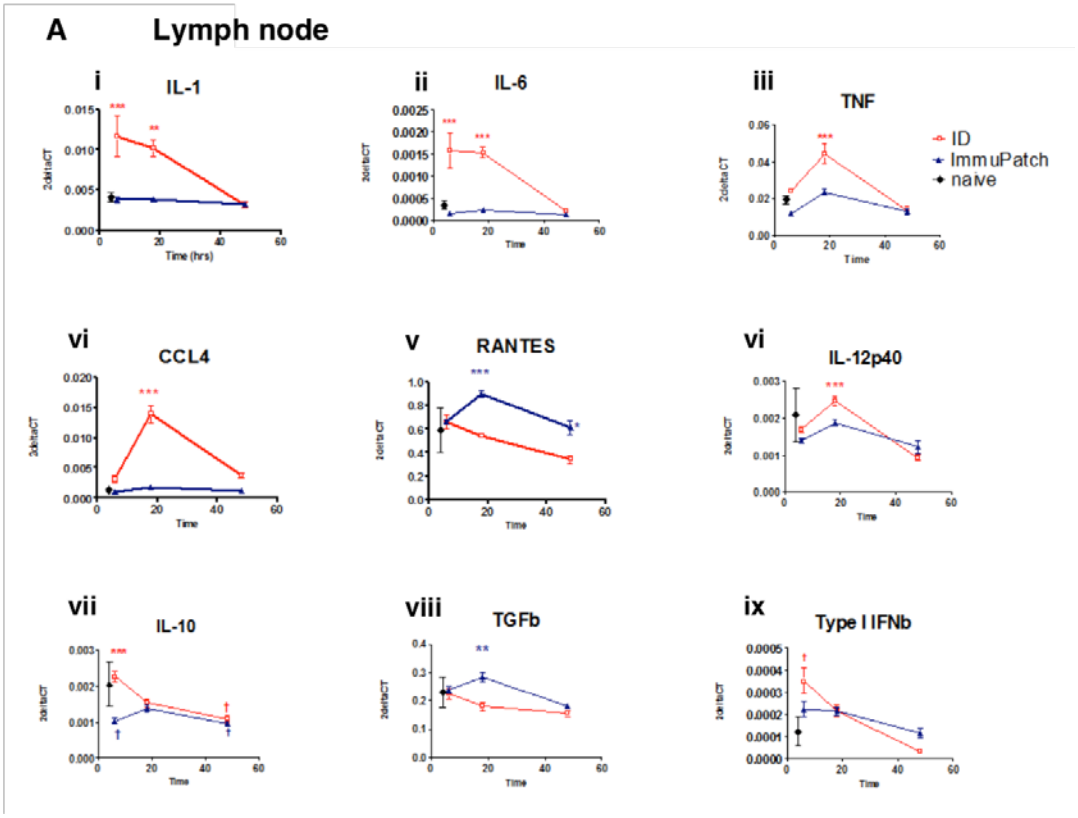
A
Lymph node
i
IL-1
ii
IL-6
iii
TNF
ID
ImmuPatch
naive
vi
CCL4
v
RANTES
vi
IL-12p40
vii
IL-10
viii
TGFb
ix
Type I IFNb
Time (hrs)
Time

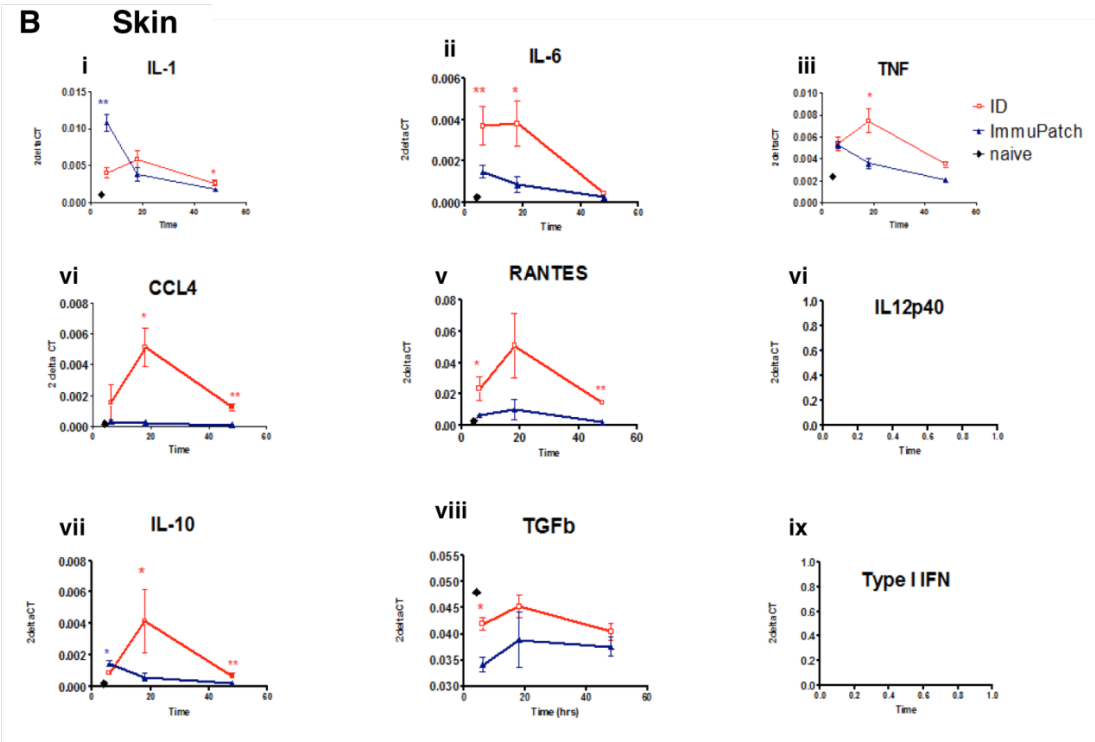
B
Skin
i
IL-1
ii
IL-6
iii
TNF
ID
ImmuPatch
naive
vi
CCL4
v
RANTES
vi
IL12p40
vii
IL-10
viii
TGFb
ix
Type I IFN
Time (hrs)
Time

FIGURE 4-4: Levels of mRNA encoding inflammatory cytokines and chemokines in the skin and dLN following ID and ImmuPatch F delivery of MVA.PbCSP.

Female BALB/c mice were immunised with MVA.PbCSP ($1x10^6$ PFU) ID or by ImmuPatch F. Six, 18 and 48 hours following immunisation, 5 mice/group were euthanised and auricular LN and ear pinnae excised and snap frozen in liquid nitrogen. Background levels of expression were determined from tissues of naïve mice (n=2). Concurrently with RT-PCR using cytokine and chemokine-specific primers, murine GAPDH mRNA expression. GAPDH codes for a glycolytic enzyme and is ubiquitously expressed. mRNA expression (i.e. crossing threshold, Ct) was calculated relative to that of *mgapdh* expression using the formula $2^{-\Delta Ct}$. Individual points on XY plots represent mean ± SEM. Red = ID, Blue = ImmuPatch F, Black = Naïve. * P<0.05, ** P<0.01, ***P<0.001 by unpaired t test of the two immunised groups, †P<0.05 compared to naïve mice. No IL-12p40 or type I IFN mRNA was detected in the skin for either group. Experiment performed by A. Vrdoljak, UCC and is presented in (265).

Six hours after immunisation in the dLN, pro-inflammatory cytokines including IL-6 (P<0.001, Figure 4-4A) and IL-1 (P<0.001) were induced to a significantly higher level in ID-immunised mice as compared to ImmuPatch F, which had similar levels to naïve mice.Type I IFN was higher after ID immunisation as compared to naives (P<0.05). A second wave of mRNA expression in the LN occurred 18h after ID immunisation where expression of TNF-αand IL-12p40 and the chemokine ligand CCL4 were significantly increased over ImmuPatch immunisation, and IL-6 was sustained (all P<0.001). Expression of the regulatory cytokine TGF-β was significantly increased18h after ImmuPatchcompared to ID immunisation (P<0.01), as was RANTES (CCL5, P<0.001). No other pro-inflammatory cytokine following ImmuPatch immunisation was significantly different from naïve. Delayed expression of all cytokines was noted after ImmuPatch (18h) as compared to ID (6h/18h). A similar pattern was observed at the immunisation site (Figure 4-4B), with IL-6 (P<0.05) and TNF-α (P<0.001) peaking 6h and 18h after ID immunisation, repectively, and at a significantly higher level compared to ImmuPatch delivery.

ImmuPatch-immunised skin exhibited a significantly higher level of IL-1 (P<0.05, Figure 4-4B) and an equivalent level of TNF-α transcript at 6h, decreasing thereafter, whereas these cytokines peaked 18h after ID. Also peaking at this timepoint post-ID was RANTES, mirroring the expression of this molecule 18h after ImmuPatch in the dLN. Expression of all cytokines was higher at 6h following ImmuPatch compared to other timepoints, excluding TGF-β (18h).

4.3.4 Summary of sections 4.3.1-4.3.3

- ImmuPatch primes a response with an irregular kinetic, with no observable expansion and contraction phase, but despite this retains the ability to expand upon boost (with the exception of T280b $1x10^{10}$ VP AdCh63.ME-TRAP, discussed in Chapter 3).
- ImmuPatch priming favours a T_{CM} phenotype early in the response, whereas ID immunisation induces primarily T_{EM}. After an ID boost responses have a T_{EM} phenotype. Correlations between TAV and T_{CM} post-prime and T_{EM} post-boost were found by Carey *et al*, suggesting a conversion of T_{CM} to T_{EM} upon ID boost (265).

- Delivery of MVA by ID induced significantly higher and earlier expression of pro-inflammatory cytokines and chemokines than ImmuPatch F, as measured in the skin and dLN. ImmuPatch delivery was associated with up-regulated expression of RANTES (CCL5) in the dLN and TGF-β in the skin and a transient early increased expression of IL-1 in the skin.

4.3.5 Trafficking of innate cells from the immunisation site to the dLN following ImmuPatch delivery of MVA

The following experiments were designed to investigate how observed differences in the inflammatory environment in the dLNmay influence the magnitude and composition of the innate response, which may in turn influence the phenotype of primed T cells. During these experiments ImmuPatch G (large TAV) and ImmuPatch F (small TAV) were used to deliver recombinant MVA, in separate experiments. Twenty-four, 48 and 120 hours post-immunisation vaccinated and naïve mice were euthanised and auricular LNs and ears harvested. These timepoints were chosen based on the differential migration patterns of the cell subtypes studied here, as described in literature (301, 303-305). The magnitude of the Pb9-specific CD8+ response 7 days following immunisation is given in Figure 4-5. ImmuPatch G primes a response equivalent to ID and significantly higher than naïve animals or those immunised with a patch without needles (P=0.0045, Figure 4-5). ImmuPatch F primes a lower response, equivalent to that following ID delivery of only 3% of the dose ($3x10^4$ PFU). These data are consistent with observations made in Chapter 3.

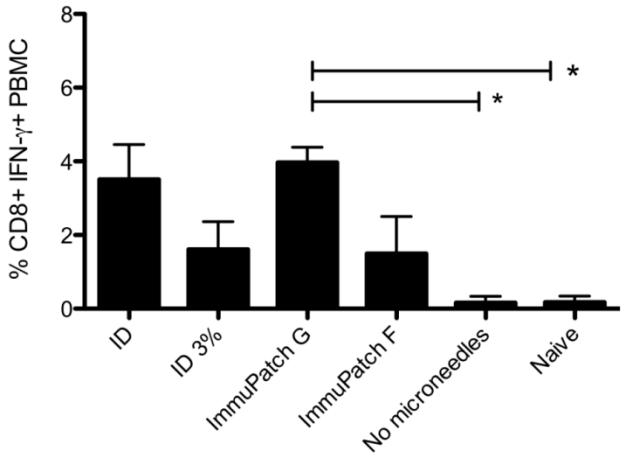

FIGURE 4-5: Magnitude of the Pb9-response following immunisation with ImmuPatch G and F.

In the following experiments the ImmuPatch arrays G and F were used. ImmuPatch G has a 'large' TAV (0.0734 mm^3) and ImmuPatch F a 'small' TAV (0.0113 mm^3). To demonstrate their ability to induce a CD8+ T cell response, female BALB/c mice (n=3) were immunised with $1x10^6$ PFU MVA.PbCSP either ID, ImmuPatch F, ImmuPatch G, using a patch with no microneedles or ID with a dose of $3x10^4$ PFU (estimated delivered dose by ImmuPatch). Blood was taken 1 week post-immunisation for re-stimulation of PBMC with Pb9. Cells were subsequently stained with anti-mouse mAbs CD3, CD8 and IFN-γ. Gating strategy = singlets>lymphocyte size gate>CD3+>CD8+>IFN-γ. P=0.0045 by Kruskall Wallis + Dunn's comparison. *=P=0.0045.

4.3.5.1 ImmuPatch-specific cellular migration into and away from the immunisation site, and infiltration into the dLN

Mice were primed with $1x10^6$ PFU recombinant MVA, either ID or by ImmuPatch G (Figure 4-6A). One group of mice were immunised with a 3% dose delivered ID ($3x10^4$ PFU – 'ID 3%'). In a separate experiment, mice were similarly primed with recombinant MVA ID, ID (3% dose) or by ImmuPatch F (Figure 4-6B). Figure 4-6 presents the magnitude of the cellular infiltrate into the LN draining the immunisation site (Figure 4-6, A+B i) and the total number of cells present at the immunisation site (Figure 4-6, A+B, ii). Data points throughout represent the sum of both dLN/ears per animal.

In both experiments, the cellular infiltrate into the LN peaks 48h post-immunisation with ID or a 3% dose given ID ('ID 3%') and is maintained at a simlar level to 120h. Following ImmuPatch G immunisation, the number of cells follows a similar kinetic to ID immunised groups (Figure 4-6, Ai). Conversely, the total number of cells infiltrating the dLN after ImmuPatch F is similar to naïve animals at 24h and 48h and slightly higher at 120h (though ns). In all groups except F, there is an early infiltrate of cells into the dLN as the number of cells is higher than the naïve level by 24h post-immunisation. An increased number of cells in these groups was maintained to 120h, and is significantly higher after ID compared to naïves (P=0.0234, Figure 4-6 Bi,).Twenty-four hours after immunisation with ID and ID 3% (in both experiments) and ImmuPatch G (Figure 4-6, Aii) but not F (Bii) there was a higher number of cells in the skin as compared to naïve animals, which decreased thereafter. This suggests an early infiltration of cells into the immunisation site, which migrate out from 24-48h post-immunisation. By 120h the number of cellswas similar to naïve mice in all groups (the ID 3% number is increased at 120h due to one high outlier) except ImmuPatch F, which is lower than the naïve level, though the difference is ns.

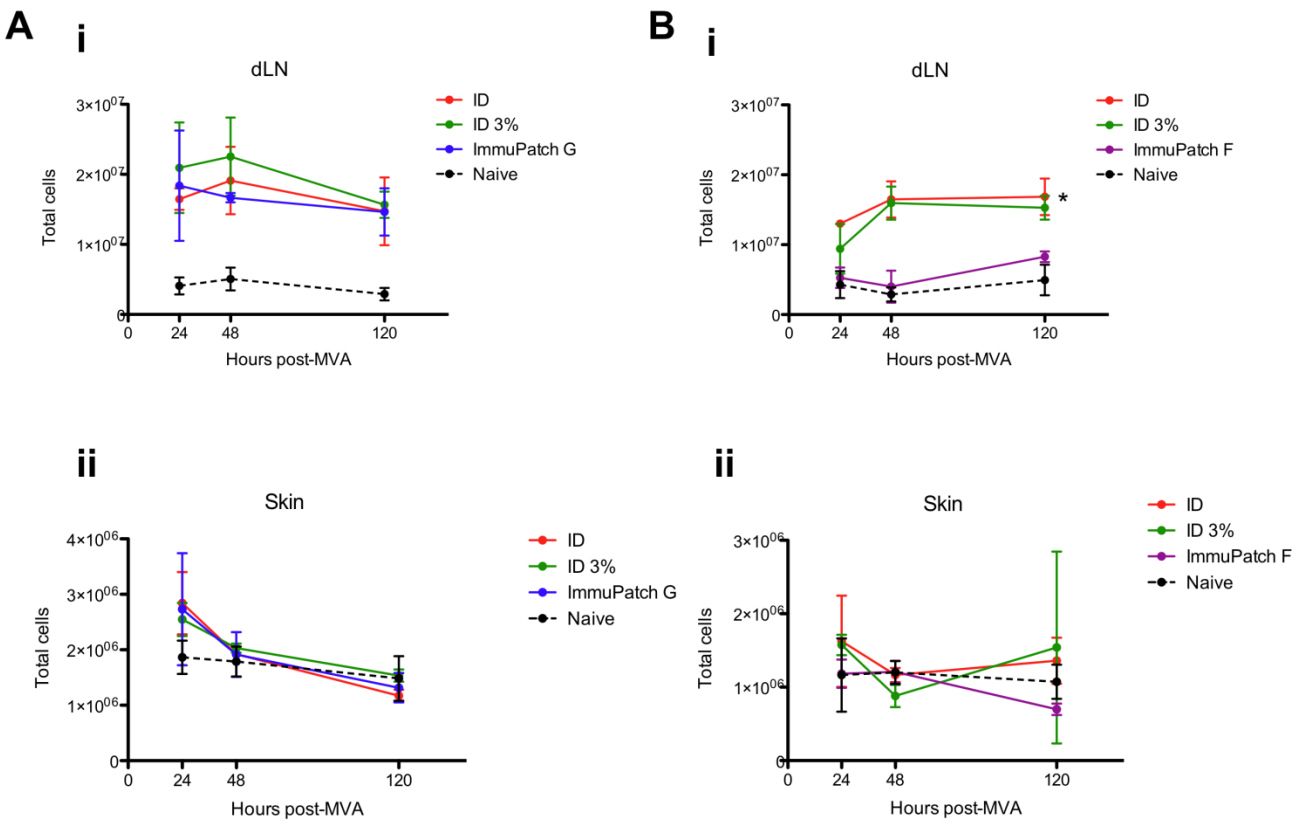

FIGURE 4-6: Design-dependent differences in the cellular infiltration into dLN and migration of cells from the immunisation site 48 and 120 hours after recombinant MVA.

(A) Female BALB/c mice (n=3) were immunised ID with recombinant MVA at 1x10^6 PFU or at a 3% dose (3x10^4 PFU) or by ImmuPatch G. (B) In a separate experiment, mice were immunised with recombinant MVA at 1x10^6 PFU or at a 3% dose (3x10^4 PFU) ID or by ImmuPatch F. Twenty-four, 48 and 120 hours later, immunised and naive mice were euthanised and ear pinnae and auricular LNs (dLN) excised, isolated by enzymatic digestion and counted using a CASY® cell counter. The number of cells extracted from both auricular LNs/ear pinnae was calculated. Data points represent mean number of cells (per 2 LNs/animal - A+B, i, or per 2 ears – A+B, ii) ± SD. *P=0.024 by Kruskall Wallis + Dunn's comparison.

In the following experiments, staining panels described in Figure 4-7 were used to identify CD11c+ DC and subsets ('gating strategy 1') or CD11b+ cells and the CD11b+ CD11c- non-DC subsets ('gating strategy 2') including inflammatory monocytes (CD11b^{hi}CD11c- Ly6C^{hi} Ly6G-) and polymorphonuclear neutrophils (PMN; CD11b+ Ly6C+ Ly6G+)(301, 306). CD11c+ dendritic cells were further characterised by expression of CD8 (lymphoid), B220 (plasmacytoid, pDC) and CD11b+ (myeloid DC, mDC, including skin-resident and monocyte-derived circulatory subtypes which exit the blood to enter inflamed sites). The expression of the markers CD207 (Langerin) and CD103 (Integrin α-E) by skin-migrating mDC have been used to further differentiate between Langerhans cells (LC - CD207+ CD103-), Langerin+ dermal DC (L+dDC – CD207+ CD103+) and classical dermal interstitial DC lacking both these markers (dDC). Another infiltrating myeloid subtype, termed inflammatory 'mono' DC, derived from circulating Ly6C+ monocyte precursors, is present in skin and skin-draining LN only during inflammation and lack

both CD207 and CD103, thus are currently indistinguishable from dermal interstitial DC (307, 308).

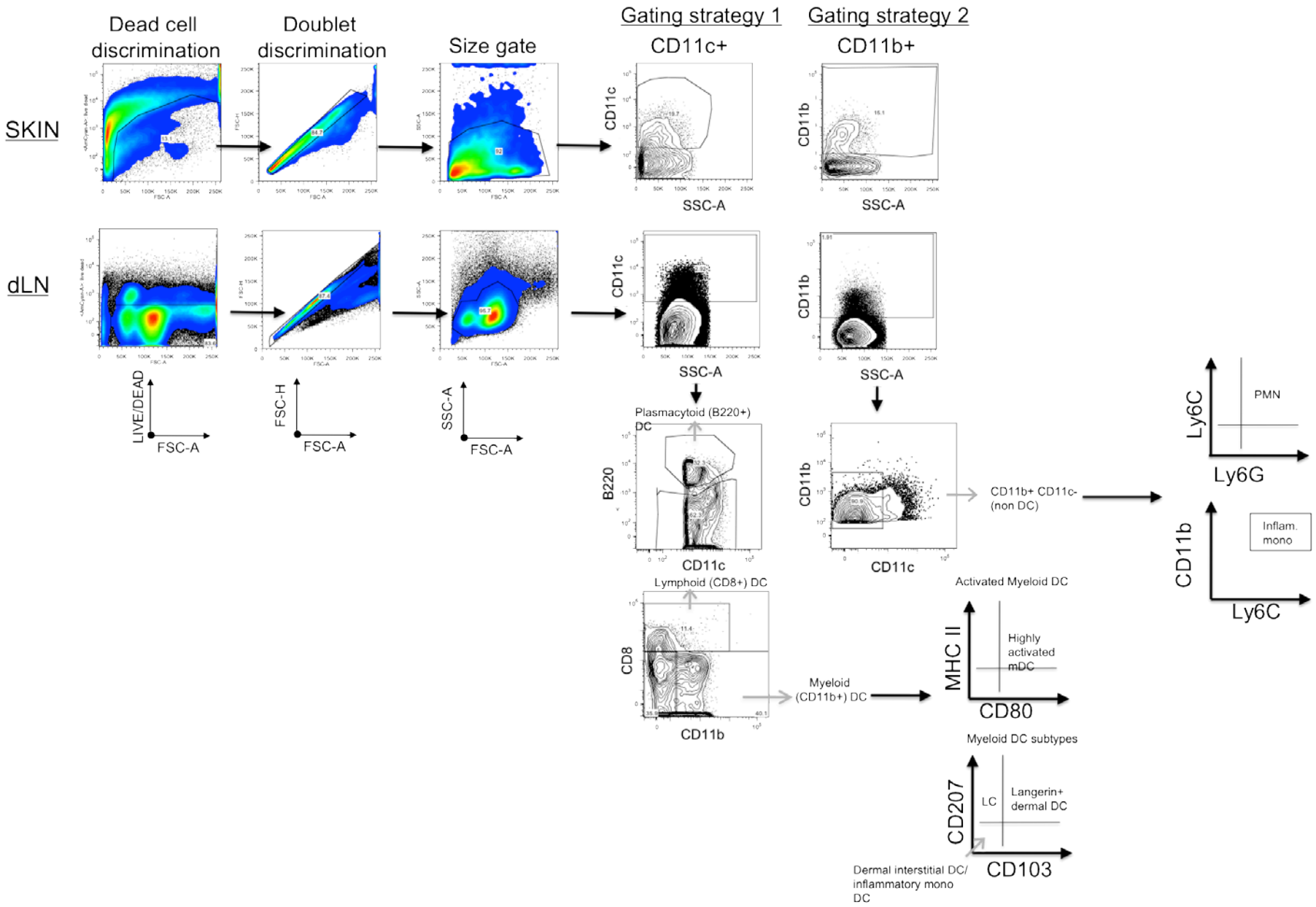
Dead cell discrimination
Doublet discrimination
Size gate
Gating strategy 1
CD11c+
Gating strategy 2
CD11b+
SKIN
dLN
LIVE/DEAD
FSC-A
FSC-H
SSC-A
CD11c
CD11b
Plasmacytoid (B220+) DC
B220
Lymphoid (CD8+) DC
CD8
Myeloid (CD11b+) DC
CD11b+ CD11c- (non DC)
Activated Myeloid DC
MHC II
Highly activated mDC
CD80
Myeloid DC subtypes
CD207
LC
Langerin+ dermal DC
CD103
Dermal interstitial DC/ inflammatory mono DC
Ly6C
Ly6G
PMN
Inflam. mono

FIGURE 4-7: Gating strategies used in subsequent analyses.

At timepoints post-immunisation mice immunised ID or by ImmuPatch were sacrificed and ear pinnae and dLN were excised. Single cell suspensions were prepared by collagenase digestion. Cells were immediately stained with LIVE/DEAD® Aqua viability stain and one of two anti-mouse monoclonal antibody panels. Panel 1 (DC-specific): CD11c+ PE, CD11b-Alexa Fluor 700, B220 PECy7, CD8 PercPCy5.5, MHC II Alexa Fluor 780, CD80 FITC, CD207 (Langerin) Alexa Fluor APC, CD103-biotin-streptavidin Pacific Blue. Panel 2 (non DC): CD11c+ PE, CD11b-Alexa Fluor 700, Ly6C APC, Ly6G PECy5. Gating strategy 1 allowed identification of CD11c+ populations including plasmacytoid DC (CD11c+ B220+), LN resident DC (CD11c+ CD8+ B220-, gated out in analyses), and myeloid DC (CD11c+ CD11b+ CD8- B220-). Gating strategy 2 allowed identification of CD11b+ CD11c- (non DC) – inflammatory monocytes (CD11b^{hi} CD11c- Ly6C^{hi}) and polymorphonuclear neutrophils (CD11c- CD11b+ Ly6C+ Ly6G+).

Total numbers of CD11c+ and CD11b+ cells infiltrating the dLN following immunisation ID, ID 3% dose or by ImmuPatch F are given in Figure 4-8. CD11c+ cells were increased at 24h compared to naive in all groups except ImmuPatch F and remain elevated to 120h. Levels of CD11c+ and CD11b+ cells following patch F were similar to naïve at 24 and 48h increasing at 120h (more so for CD11b+, though neither subtype were significantly higher than naive). In ID groups, immunisation induced an early influx of CD11b+ cells (<24h), decreasing thereafter to 120h, though still increased above the naïve level at this timepoint.

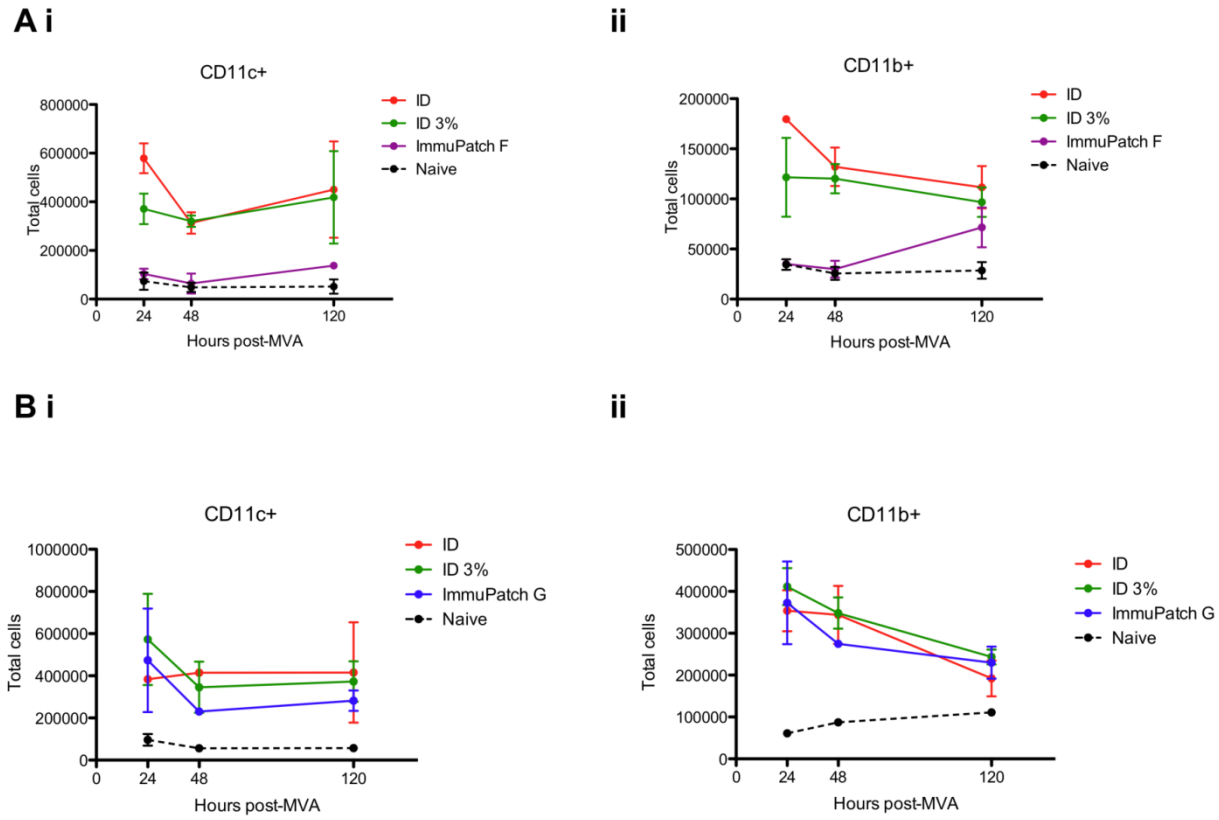

FIGURE 4-8: Kinetics of CD11c+ and CD11b+ infiltration in the dLN following ImmuPatch and ID delivery of recombinant MVA.

Female BALB/c mice (n=3) were primed with 1x10^6 PFU or 3x10^4 PFU (3% dose) ID, or with 1x10^6 PFU recombinant MVA by ImmuPatch F (A) or in a separate experiment ImmuPatch G (B). Auricular LNs were excised from immunised and naïve animals sacrificed at 24, 48 and

120 hours post-immunisation. Cells were isolated, counted and stained with panel 1+2 (see previous figure). Datapoints are mean (± SD) total numbers of CD11c+ (A+B, i) and CD11b+ (A+B, ii) cells extracted from dLN.

Figure 4-9 shows the migration of CD11c+ and CD11b+ cells away from the immunisation site following immunisation with ImmuPatch G. By 24h there was an increased number of CD11c+ and CD11b+ in the skin in all groups compared to naïve, which decreased with time such that levels at 120h were equivalent between immunised and naïve groups. The number of CD11b+ after ID immunisation was higher after 24h decreasing towards 120h, though in other groups CD11b+ remained slightly elevated over naive throughout.

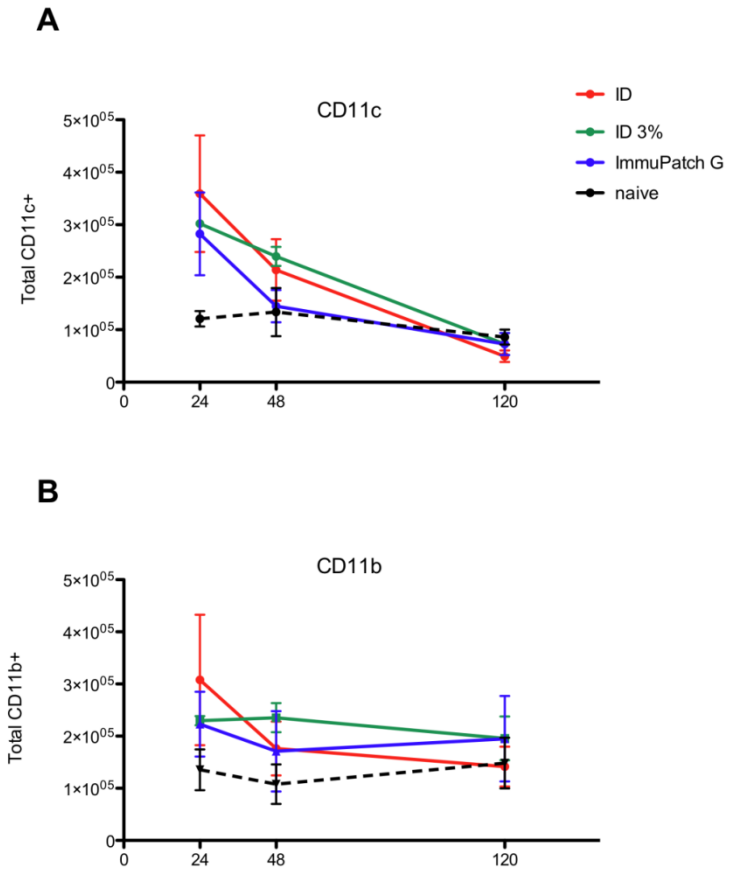

FIGURE 4-9: Kinetics of CD11c+ and CD11b+ migration away from the immunisation site following ImmuPatch G and ID delivery of recombinant MVA.

Female BALB/c mice (n=3) were primed with $1x10^6$ PFU or $3x10^4$ PFU (3% dose) ID, or with $1x10^6$ PFU recombinant MVA. (A) Total CD11c+, or (B) Total CD11b+. Ears were excised from immunised and naïve animals sacrificed at 24, 48 and 120 hours post-immunisation. Cells were isolated, counted and stained with panel 1+2. Datapoints are mean (± SD) total numbers of CD11c+ (A+B, i) and CD11b+ (A+B, ii), cells from 2 ears were pooled.

These data suggest whilst the kinetics of the cellular migration away from the immunisation site and into the draining LN (confirmed to be CD11c+ and CD11b+ innate cells) are similar for ID groups as for ImmuPatch G, they differ for ImmuPatch F, which is slower (with numbers differing at 120h) and of a much lower magnitude compared to other groups.

4.3.5.2 Early influx of CD11c+ B220+ pDC after ID, which is absent/of lower magnitudeafter ImmuPatch immunisation

Plasmacytoid DC are circulatory cells found in extremely low numbers in naive skin, but may enter during inflammation (309). Approximately 15% of CD11c+ cells within the skin and 30% CD11c+ in the dLN following immunisation ID or by ImmuPatch G also expressed B220. Figure 4-10 shows the total number of CD11c+ B220+ pDC at the immunisation site and within the dLN following delivery of ID and ImmuPatch G. Figure 4-10, Bii shows the total number of CD11c+ B220+ pDC at 24h and 48h following ID/ImmuPatch F immunisation. Within the first 24h after ID delivery, there was a marked increase in pDC infiltrating the skin as compared to naïve animals. This is also true following ImmuPatch G immunisation, though to a lesser extent (Figure 4-10A). By 120h post-immunisation, numbersreduced to the naive level, but remain higher than naives in the skin. At 48h (24h later than the peak in the skin) the number of CD11c+ B220+ cells in the dLN peaks for both ID immunised groups and decreases thereafter. In contrast to ImmuPatch G and immunisation of both doses ID, the total number of pDC in the dLN after patch F immunisation was similar to naïve animals at both timepoints (Figure 4-10, Bii).

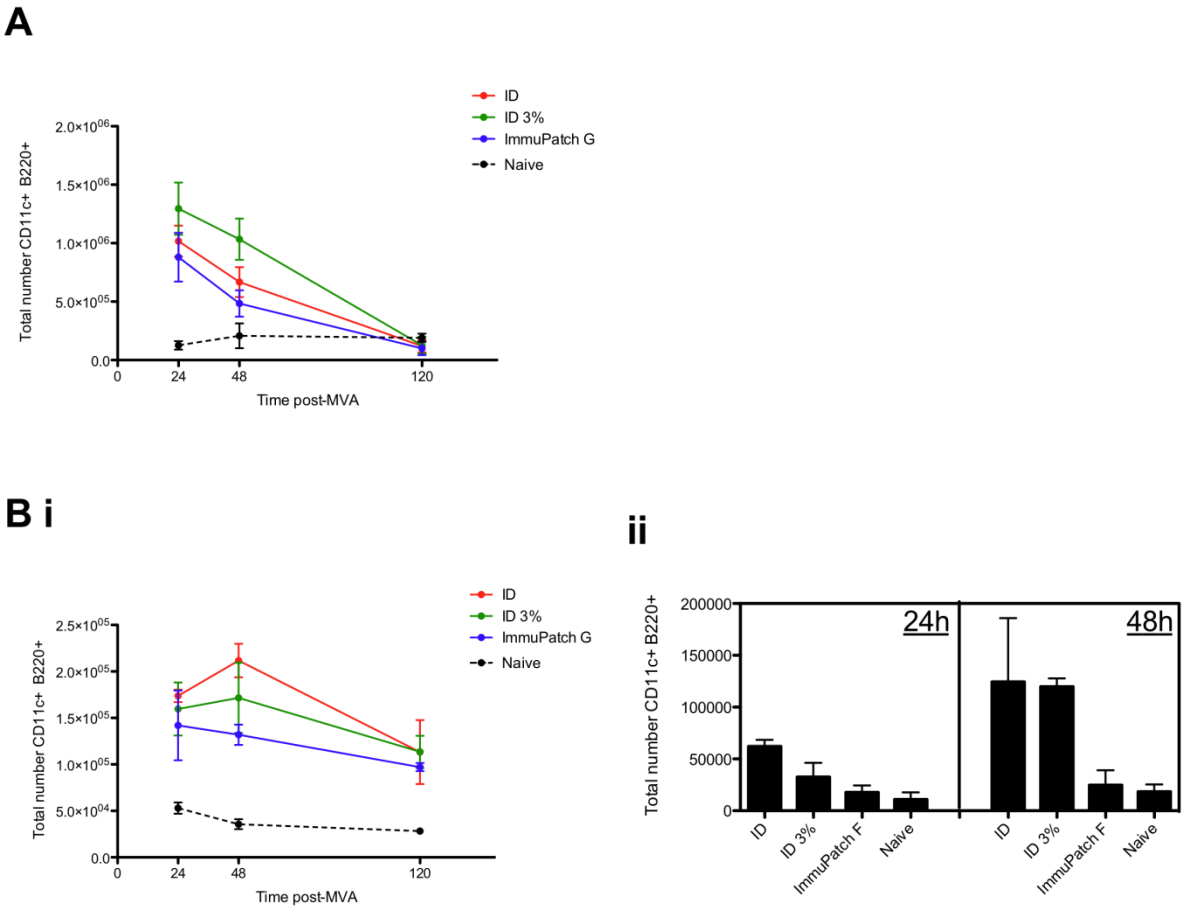

FIGURE 4-10: Early influx of CD11c+ B220+ plasmacytoid DC into the skin and subsequent influx into the dLN after ID and ImmuPatch G, but not ImmuPatch F immunisation.

Female BALB/c mice (n=3) were primed with 1x10^6 PFU or 3x10^4 PFU (3% dose) ID, or with 1x10^6 PFU recombinant MVA by ImmuPatch G (A, Bi) or in a separate experiment, ImmuPatch F (with the same control groups)(Bii). Ears and dLN excised from immunised and naïve animals sacrificed at 24, 48 and 120 hours post-immunisation. Cells were stained with panel 1. Datapoints are mean (± SD) total numbers of CD11c+ B220+ pDC in skin (A) and in dLN (Bi and Bii). Two ears/dLN were pooled per animal.

4.3.5.3 Early influx of PMN and inflammatory monocytes into the dLN after ID, but not ImmuPatch G immunisation

Figure 4-11 demonstrates the early influx of cells with a CD11b+ Ly6C+ Ly6C+ phenotype, characteristic ofpolymorphonuclear neutrophils (PMN) following ID, but not following reduced dose ID or ImmuPatch G immunisation as assessed at 24h (P=0.0421 compared to naives). The total number of PMN was reduced at 48h where the total numbers of PMN were equivalent across all immunised groups. Numbers of PMN in the dLN at 120h following all immunisation routes are equivalent to those of naïve animals (Figure 4-11, Aii). A second infiltrating CD11b+ CD11c- cell type was identified as CD11b^{hi} CD11c- Ly6C^{hi} Ly6G-, consistent with the phenotype

of inflammatory monocytes (306). Figure 4-11, Bii demonstrates an early influx of these cells into the dLN following ID immunisation with both doses, of higher magnitude than that following ImmuPatch G immunisation, which was only slightly increased over naïve animals (P=0.0337, ID compared to naive).

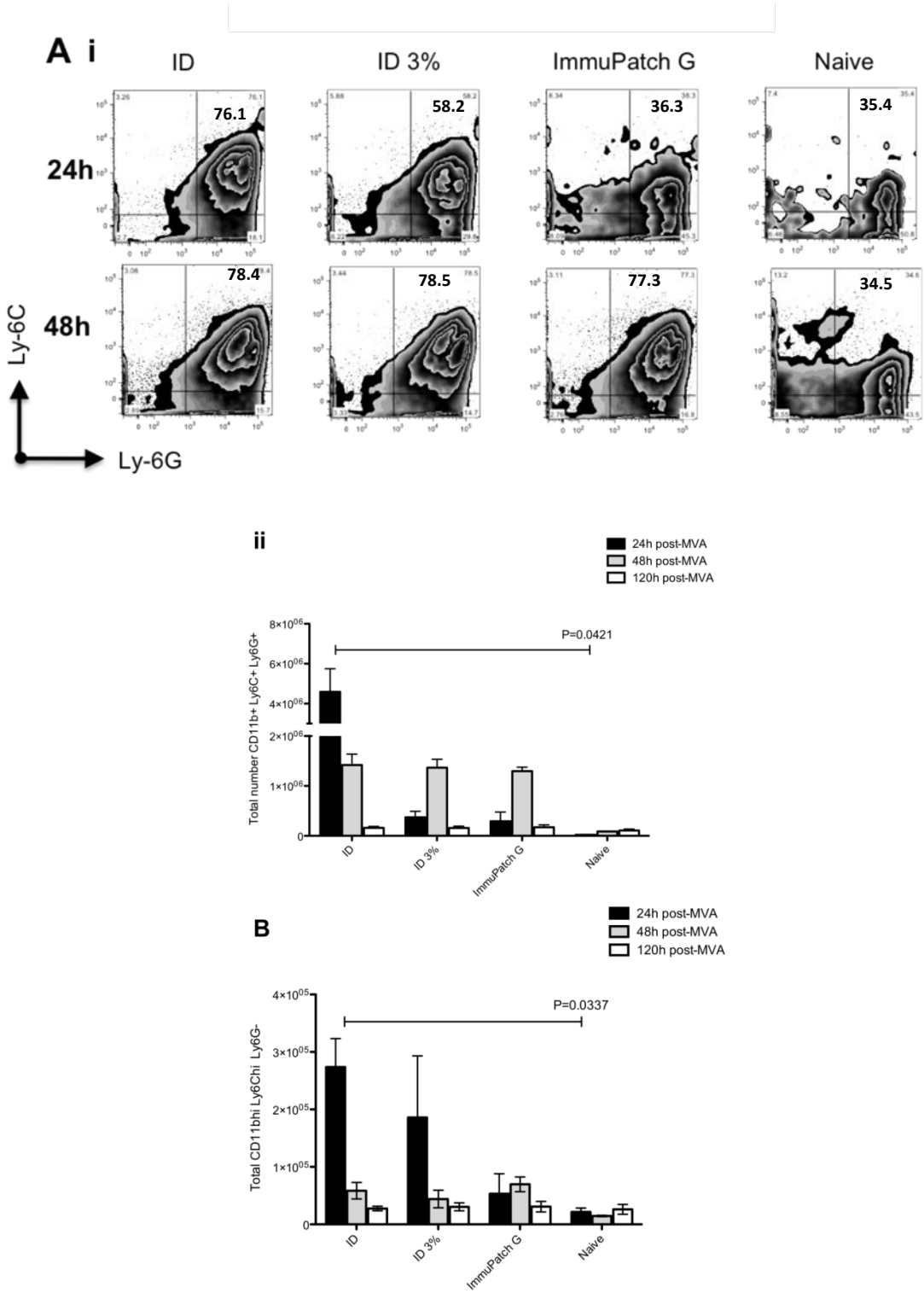

FIGURE 4-11: Influx of CD11b+ CD11c- polymorphonucelar cells and inflammatory monocytes of greater magnitude after ID than ImmuPatch immunisation.

Mice (n=3) were primed with $1x10^6$ PFU or $3x10^4$ PFU (3% dose) ID, or with $1x10^6$ PFU recombinant MVA by ImmuPatch G. Auricular LNs excised from immunised and naïve animals sacrificed at 24, 48 and 120 hours post-immunisation. Cells suspensions were isolated by collagen digestion and stained and gated as in Figure 4-7 gating strategy 2. (Ai) FACS plots of CD11b+ CD11c- events set on Ly6C and Ly6G axes demonstrating their distribution (frequencies in bold). (Aii) Total numbers of CD11b+ CD11c- Ly6C+ Ly6G+ cells per 2 dLN. Data points are mean (± SD). (B) Total numbers of $CD11b^{hi}$ CD11c- $Ly6C^{hi}$ Ly6G- (inflammatory monocytes). Datapoints are mean numbers of cells ± SD. P=0.0421 (Aii) and P=0.0337 (B) by Kruskall Wallis + Dunn's comparison.

These data and those from Figure 4-10 suggest that circulating innate subtypes PMN, monocytes and pDC, usually recruited to a response via inflammatory signals, are strongly associated with ID immunisation. In contrast, pDC were not shown to be recruited to the innate response 24-48h following ImmuPatch F, and after ImmuPatch G fewer PMN are recruited later in the response, and inflammatory monocytes not at all.

4.3.5.4 Subset composition of CD11c+ CD11b+ mDC infiltrating the dLN is dependent upon timepoint and ImmuPatch

The total number of CD11c+ CD11b+ mDC in the dLN peaks at 24h for all groups except naïve, with the number after ID immunisation lower than other immunised groups (ns, Figure 4-12A). By 120h, total numbers are equivalent between immunised groups. Bar graphs in Figure 4-12, B-D represent the total number of CD11c+ CD11b+ mDC in the dLN at 24h (B) 48h (C) and 120h (D). The experiment carried out at 120h also included one group of mice immunised with ImmuPatch F. Bars are subdivided according to mDC subtype – CD207- CD103- (dermal interstitial, dDC or mono-DC); CD207+ CD103+ (Langerin+ dDC) and CD207+ CD103- (LC).

The subset composition of the infiltrate differed with timepoint and between immunised groups. The predominant subtype after all immunisations at 24 and 48h was CD207- CD103- (dDC/mono-DC) with equivalently low numbers of CD207+ CD103- (LC) and CD207+ CD103+ (L+dDC). The proportions of these subsets differ little between groups at 24h and 48h. However, at 120h, there was a greater proportion of other subsets, with increased numbers of Langerin+ dDC and LC. These subsets were similar between ID, ID3% and ImmuPatch G immunised groups, but the number of LC 120h following ImmuPatch F immunisation was significantly higher than naïves (P=0.0171, Figure 4-12C). In summary, infiltrating mDC are primarily CD207- CD103- mDC at 24h and 48h and have a mixed composition at 120h with higher numbers of CD207+ CD103- LC after immunisation with ImmuPatch F.

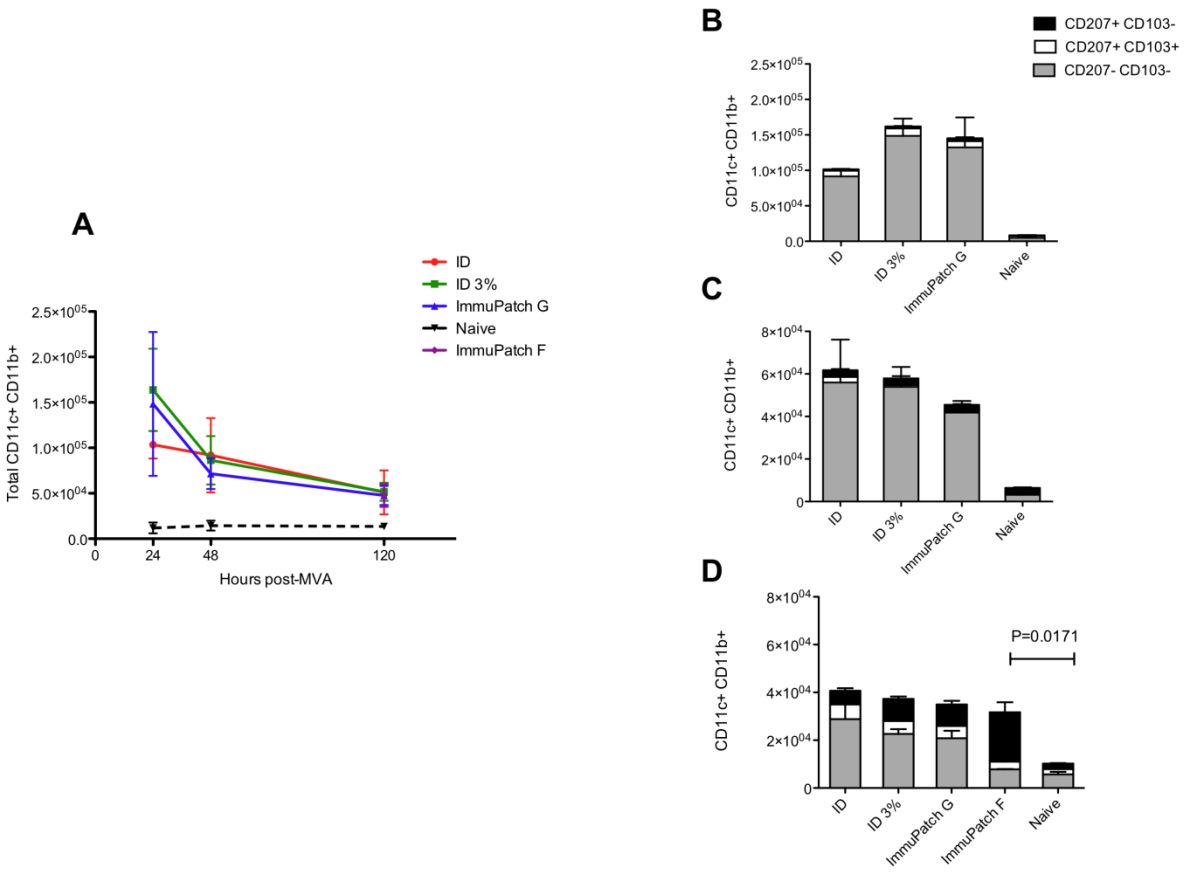

FIGURE 4-12: Influx of CD11b+ CD11c+ myeloid DC into the dLN following immunisation.

BALB/c mice (n=3) were primed with 1x10^6 PFU or 3x10^4 PFU (3% dose) ID, or with 1x10^6 PFU recombinant MVA by ImmuPatch G. dLN were excised from immunised and naïve animals sacrificed at 24, 48 and 120 hours post-immunisation. The harvest at 120h included one group of mice immunised with ImmuPatch F. Cells were isolated and stained and analysed according to staining/gating strategy 1 in Figure 4-8. (A) Total numbers of CD11c+ CD11b+ (CD8- B220-) mDC infiltrating the dLN following immunisation. (B-D) Bars represent mean CD11c+ CD11b+ total numbers, subdivided into total numbers of CD207- CD103- (dermal interstitial/mono-DC) – grey portion; CD207+ CD103+ (langerin+ dermal DC) – clear portion; and CD207+ CD103- (Langerhans cells) – black portion ± SD. B= 24h, C=48h, D=120h post-immunisation. P=0.0171 by Kruskall Wallis + Dunn's comparison (referring CD207+ CD103- subset).

4.3.5.5 ImmuPatch induces a high proportion of mDC with a highly activated phenotype, later than ID immunisation

The up-regulation of MHC II and co-stimulatory factors such as CD80 is a key process in the acquisition of antigen-presenting capability by immature DC (67). The activation of CD11c+ CD11b+ mDC in the dLN was assessed at timepoints after immunisation ID, or by ImmuPatch. Figure 4-13A demonstrates that the frequency of MHC II^{hi} CD80+ mDC following ImmuPatch G immunisation increases from 24-48h, and was maintained at this level to 120h. The frequency 120h after ImmuPatch F immunisation was similar to that of ImmuPatch G. Frequencies of highly activated

mDC after ID immunisation peaked earlier at 24h with a decrease in number to 120h, whereas the level in the ID 3% group remained at a constant level throughout. Figure 4-13B shows frequencies at 120h, where there was the greatest difference in the frequency of activated cells between ID and ImmuPatch (P=0.02299 ImmuPatch F vs. naives). Separate gates were set for naïve samples as total populations were slightly shifted towards the Y axis upon immunisation (Figure 4-13C, where both quadrant gates are shown in red in naïve samples, numbers refer to black gates). MHC II^{hi} CD80+ mDC were further phenotyped at 120h and were found to be predominantly CD207+ CD103- (LC), with a higher proportion following ImmuPatch F than by ID or ImmuPatch G (as shown in plots, Figure 4-13D).

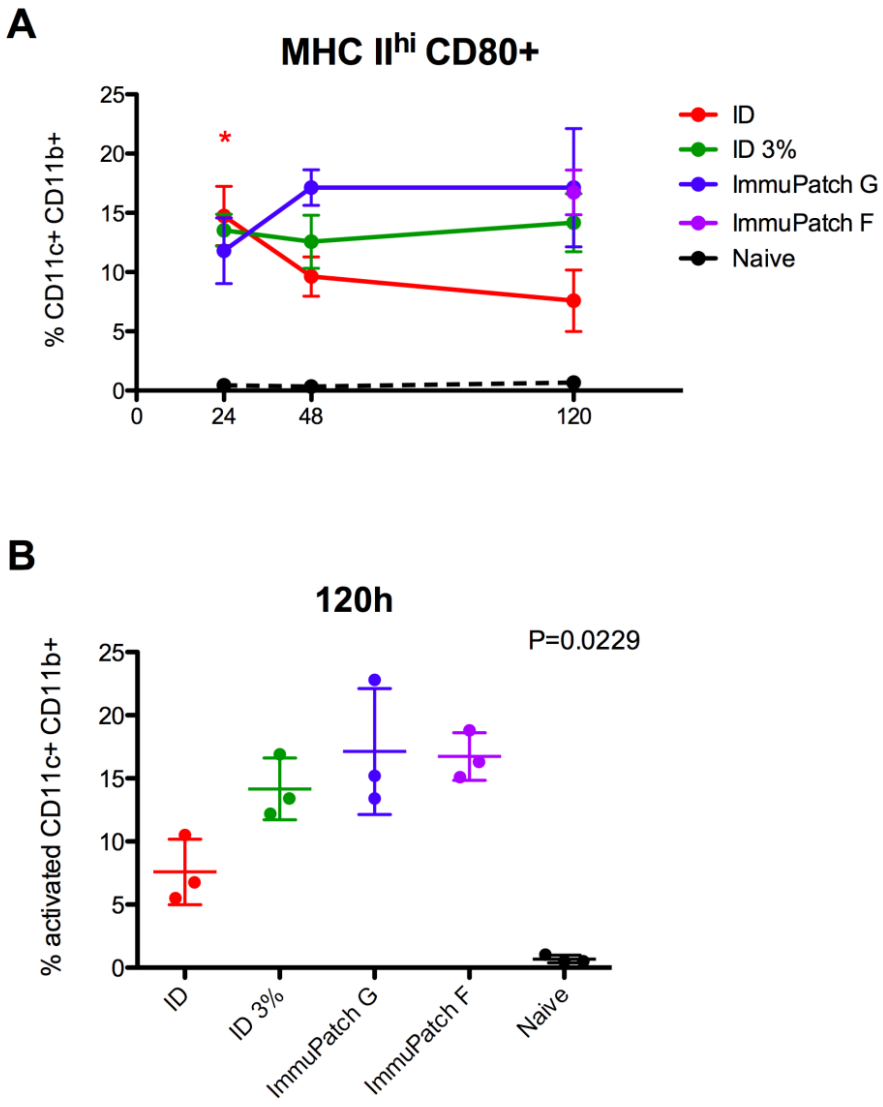

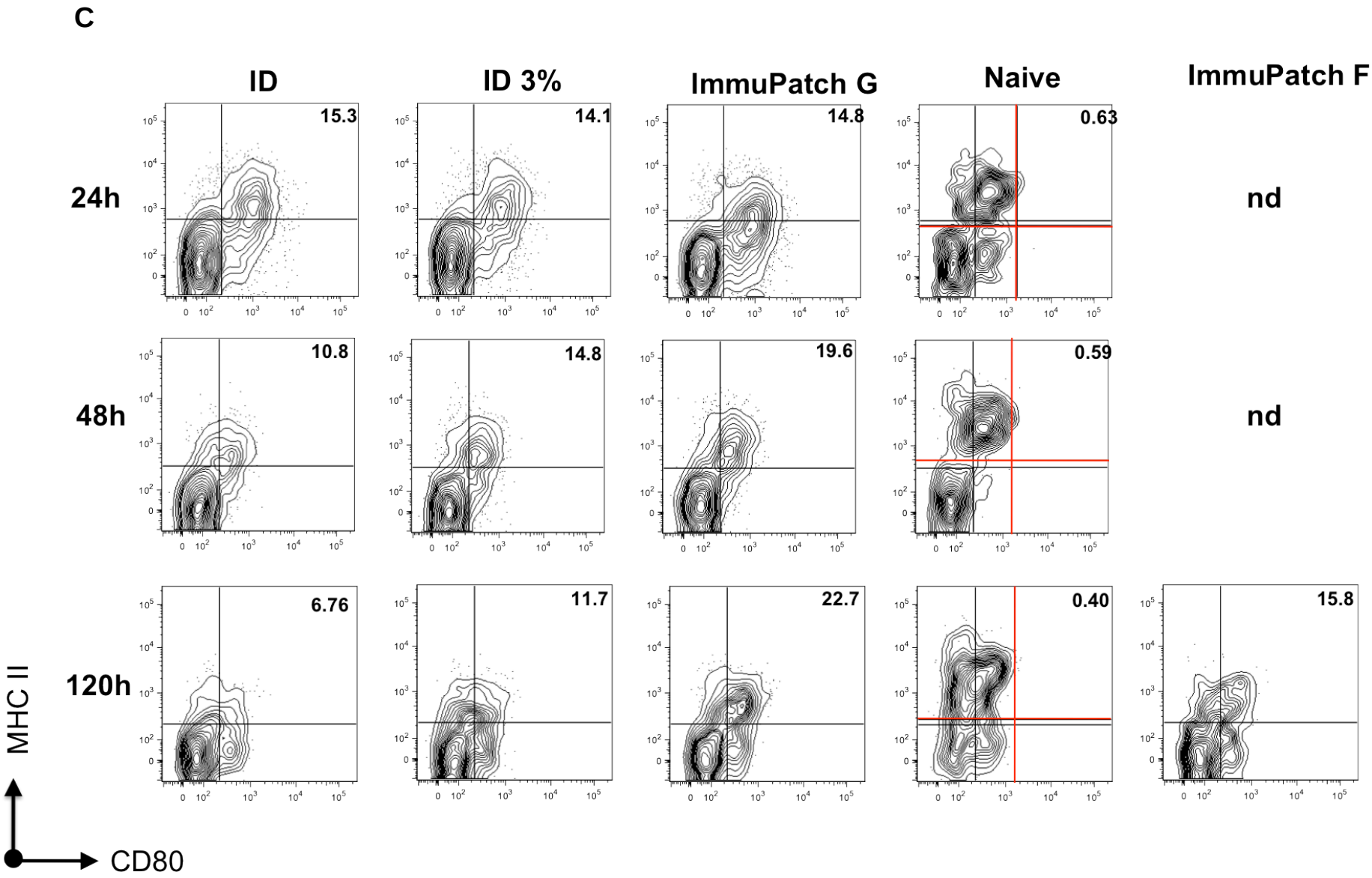
C
ID
ID 3%
ImmuPatch G
Naive
ImmuPatch F
24h
48h
120h
15.3
14.1
14.8
0.63
nd
10.8
14.8
19.6
0.59
nd
6.76
11.7
22.7
0.40
15.8
MHC II
CD80

D

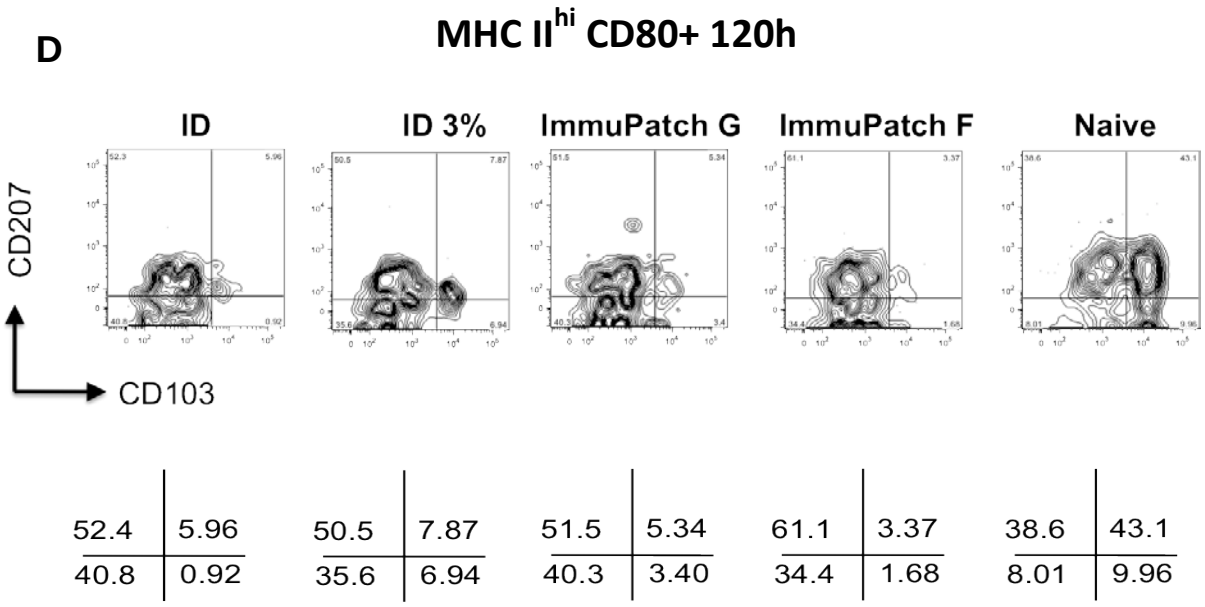

FIGURE 4-13: Differences in the activation state of infiltrating CD11c+ CD11b+ myeloid DC in the dLN post-immunisation.

Female BALB/c mice (n=3) were immunised ID, ID 3%, by ImmuPatch G or ImmuPatch F (120h timepoint only). Animals were sacrificed at 24, 48 or 120h post-immunisation and auricular LN cells isolated and stained according to gating strategy 1 (Figure 4-8). (A) Mean frequencies of CD11c+ CD11b+ cells with a highly activated phenotype MHC II^{hi} CD80+ ± SD. (B) Bar chart showing the mean % MHC II+ CD80+ 120h post-immunisation ± SD, P=0.0229, Kruskall Wallis and Dunn's comparison. (C) Representative FACS plots of CD11b+ CD11c+ events set on MHC II and CD80 axes. Two sets of quadrant gates were set due to a shifted population in naïve samples compared to immunised. Values given in quadrants are for immunised mice. 'Naïve gate' values were used for naive datapoints in A+B. nd= no data. (D) MHC^{hi} CD80+ cells from (C) were further phenotyped according to CD11c+ CD11b+ subtypes by setting against CD207 and CD103 axes.

4.3.5.6 Summary of section 4.3.5

- There is an early infiltration of cells into the dLN and away from the skin after ID, ID3% and ImmuPatch G immunisation, but not ImmuPatch F. These cells were confirmed to be innate cells (CD11c+/CD11b+)
- The kinetic of cellular migration was slower, and of a smaller magnitude following ImmuPatch F as compared to ID groups.
- pDC infiltrate the skin and subsequently the dLN following ID and patch G immunisation, but are not associated with patch F.
- PMN and inflammatory monocytes enter the dLN early following ID immunisation. Infiltration of PMN is delayed (to 48h, similar to ID 3%) and there was no observable infiltration of inflammatory monocytes over the naive statefollowing patch G immunisation.
- The subset composition of mDC entering the dLN differed between immunised groups, with ID and patch G demonstrating similarilities. There was a late influx of CD207+ CD103- LC 120h following patch F immunisation, which was significantly higher than naives.

- The activation state of mDC induced by ImmuPatch immunisation increased from 24-120h, whereas that after ID immunisation decreased from 24h. At 120h, the activation state was significantly higher following ImmuPatch F immunisation compared to naives. Highly activated mDC were predominantly CD207+ CD103- (LC), and there were more 120h after ImmuPatch F than in other groups.
- Differences between ImmuPatch and ID do not appear to be influenced by a difference in delivered dose, as patterns following delivery a 3% dose delivered ID were largely similar to patch G, but distinct from patch F.

4.4 DISCUSSION

4.4.1 The method of antigen delivery into the skin influences characteristics of innate and adaptive responses

Many factors have been proposed to influence the shaping of the T cell response during the sensitive stage of APC-T cell interaction in the dLN such as the nature of the APC, the duration and strength of the antigen stimulus and the inflammatory microenvironment in which the naive T cells are primed (36, 301, 310). These data suggest that the mode of antigen delivery (ID vs. ImmuPatch) into the skin influences the specific characteristics of both the innate response to the antigen and subsequently the resulting T cell response. Moreover, early events in the innate response to immunisation with a small TAV patch differed to those following a large TAV patch. This suggests a difference in the specific priming conditions between patches of differing design, offering an explanation for the heterogeneity in the ability of patch-primed responses to undergo secondary expansion upon ID boost (discussed in 3.4.2).

Epidermal and dermal deposition of fluorescent dye by ImmuPatch G was confirmed by histological assessment of porcine skin, whereas ID immunisation placed the vaccine as a bolus into the dermis (265, 269). In addition to the possibility that epidermal+dermal vs. dermal deposition of vaccine activate different populations of skin-resident mDC, the method of delivery may also impact upon the rate of antigen drainage to the LN due to the difference in biodistribution. ImmuPatch delivers vaccine into discrete microchannels created by individual microneedles, and so biodistribution of vaccine into the skin is substantially different to delivery by standard intradermal injection. Intradermal liquid deposition has been associated with an increase in local interstitial pressure, in turn impacting upon the permeability of dermal lymphatics, increasing direct drainage to the LN, particularly for viral sized particles (311, 312). Improved lymphatic drainage has been proposed as one mechanism for the efficacy of ID delivery of vaccines over IM or SCu routes, where antigen primarily drains into the circulation, and also for improved pharmokinetic profiles for the delivery of drugs by hollow dermal microneedles(176). Nanoparticles injected ID demonstrated the ability to activate LN resident (CD8α+) DC via lymphatic drainage(312), whereas dispersed distribution of antigen to the epidermis and/or upper dermis (i.e. by microneedle patch) is proposed to preferentially target skin-resident DC including epidermal LC, and dermal L+dDC and dDC to take up antigen and migrate to the dLN (148, 156, 159, 265).

4.4.2 Characteristics of the ImmuPatch-inducedT cell response

The method of delivery was found to impact upon both the kinetic and the memory phenotype of the antigen-specific CD8+ T cell immune response. ImmuPatch responses demonstrated no clear peak of response, but maintained a similar low level of response until boosting, when they increased to levels similar to ID/ID, which had followed a regular kinetic before boost(with one exception - T280b $1x10^{10}$ VP AdCh63.METRAP).

The contraction phase ensures space and resources are available for generation of T cell responses against new pathogens, whilst maintaining a heightened sensitivity to the encountered pathogen. Contraction isnormally triggered by clearance of antigen, though some have challenged this theory, since the onset and degree of contraction were found to be independent of the dose and duration of bacterial or viral infection, but rather 'programmed' upon priming by the relative presence or absence of inflammatory cytokines including IFN-γ (29, 37). A diminished CD8+ T cell contraction occurs in IFN-γ-deficient treated mice following infection with attenuated *L.monocytogenes* and Lymphocytic Choriomeningitis Virus (LCMV)(313, 314). However, even in the absence of a contraction, the memory CD8+ response is fully functionaland long-lasting suggesting that inflammatory signals, rather than the magnitude of the expansion direct the extent of the contraction, which is necessary for acquisition of a memory phenotype (36). Furthermore, inhibition of inflammation in ampicillin pre-treated mice was associated with a faster acquisition of an *L.monocytogenes*-specific T_{CM} phenotype than untreated mice, which was better able to respond to secondary immunisation (315). These studies support the observation that despite a diminished expansion and contraction phase, ImmuPatch responses may be efficiently boosted, and suggest that the observed lack of a pro-inflammatory response may be a factor in this kinetic.

ImmuPatch priming was associated with a faster acquisition of a T_{CM} phenotype than ID immunised mice that was greater in both magnitude and proportion of the total response, an observation also found by Carey *et al* using patches A-H (265). It is proposed that the lack of a strong inflammatory response favours the early emergence of increased numbers of T_{CM} following ImmuPatch immunisation, which are more able to rapidly expand upon boost, despite an overall lower number of antigen-specific T cells than ID immunisation. This phenotype was subsequently converted to T_{EM}following ID boost, a phenotype thought to be associated with protection against liver-stage malaria infection (T_{EM} have the ability to reside in peripheral tissues such as the liver, where they are best placed to encounter parasite antigen-MHC I complexes)(242). The relative proportions of T_{EM} were similar between between ID and ImmuPatch primed groups following an ID boost perhaps explaining the overall comparable levels of vaccine-induced protective efficacy observed in challenge experiments (Chapter 3).

These observations support the range of post-boost outcomes demonstrated by priming with patches with varying TAV, in that smaller TAV patch priming preferentially induces T_{CM}(265). It was speculated that this is due to subtle differences in delivered dose by smaller TAV patches, or that as the dose delivered increases with TAV, so this impacts uponlevels of pro-inflammatory cytokine secretion (though differences in the inflammatory microenvironment across a range

of ImmuPatch TAVs remain to be determined). The strength of the antigenic stimulus has been proposed as a factor involved in T_{CM}/T_{EM} differentiation, in that stronger signals give rise to T_{CM} and weaker signals to T_{EM}, with either extreme failing to survive (the 'Goldilocks model', Figure 1-1B)(34, 35). Whilst memory phenotyping of the AdCh63.ME-TRAP primed response was not possible here due to low frequencies of IFN-γ+ CD8+ following ImmuPatch immunisation, it could be speculated that the lack of ability to expand upon boost with 'extra large' TAV patch T280b upon priming with $1x10^{10}$ VP may be associated with a diminished level of T cell memory before the boost, perhaps resulting from too strong an antigenic signal being delivered into the skin, since this patch was able to prime responses capable of boosting with a lower priming dose ($1x10^{9}$ VP).

4.4.2.1 Diminished pro-inflammatory response following delivery of MVA by ImmuPatch

ImmuPatch F delivery was shown not to induce a significant pro-inflammatory response, whilst ID showed up-regulation of several classical pro-inflammatory cytokines in the dLN. In contrast to scarification and abrasion methods for physically removing the SC to allow large molecule diffusion, microneedles are less disruptive and so it is proposed that cells are not induced to secrete large amounts ofinflammatory mediators in response to physical stress/damage. This is significant in minimising local and systemic adverse adverse effects that have been associated with SC ablation methods or the needle-based intradermal delivery of live vaccines (43). ImmuPatch immunisation induced enhanced expression of only two pro-inflammatory cytokines IL-1 and TNF-α in the skin, which are the primary cytokines secreted by epidermal keratinocytes, further supporting the epidermal delivery of vaccines by ImmuPatch (55, 316). The factor with the greatest increase in expression following ImmuPatch F delivery of MVA was RANTES (CCL5). A β-chemokine, RANTES facilitates the recruitment of cells to the dLN and the skin in an innate response, and is constitutively expressed but up-regulated during DC maturation, peaking 24h *in vitro* following stimulation of immature DC with LPS (317). RANTES is also produced in response to epidermal keratinocyte stimulation, and is strongly induced by IL-1 and TNF-α(318). CCL4 (MIP-1β), which was up-regulated in both skin and dLN following ID, but not ImmuPatch immunisation, is chemotactic for inflammatory monocytes and mono-DC Ly6C+ precursors(108).

4.4.2.2 Differences in cellular trafficking influenced by mode of delivery

Since lymphatic drainage of antigen is more rapid than APC uptake, maturation and subsequent migration from the immunisation site to enable T cell stimulation, and that DC are activated via a complex network of pro-inflammatory interactions one might expect there to be differences in both the composition and the kinetic of the cellular infiltrate into the LN draining the site of ImmuPatch or ID immunisation. Interestingly, the magnitude of the cellular migration away from the skin and infiltrate into the dLN also differed between patches of differing TAV. Whereas ImmuPatch G followed a similar kinetic to ID groups, ImmuPatch F demonstrated a slower kinetic of innate cell migration, of low magnitude. The number of CD11c+ and CD11b+ in the dLN following ImmuPatch F immunisation only increased at the 120h timepoint,

suggesting either the later infiltration of a CD11c+ CD11b+ cell type (not present in the ID/patch G infiltrate), or overall slower kinetic of cells draining to the LN.

There were differences in the magnitude of infiltrating PMN and inflammatory monocytes in the dLN following ID and ImmuPatch delivery of MVA, with ID immunisation inducing an early (24h) influx of these cell types of high magnitude decreasing by 48h, which was not demonstrated in ImmuPatch immunisation. This pattern was also observed following ID administration of MVA.GFP by Abadie *et al*, with increased numbers of $CD11^{hi}$ $Ly6C^{hi}$ F4/80+ macrophages in dLN over 48h following immunisation (301). However, macrophages could not be measured here due to a lack of F4/80 staining, and because Ly6C+ monocyte precursors can differentiate into both macrophages and CD11c+ CD11b+ mDC upon entry into tissue, it should be noted that the decrease after ID may be indicative of a shift in phenotype rather than a decrease in absolute monocyte number with time. It could be suggested that the early infiltration of circulating PMN and inflammatory monocytes after ID, but not ImmuPatch immunisation is associated with an increased pro-inflammatory cytokine secretion.

Also related to the heightened inflammatory state following ID immunisation is the early infiltration of pDC into the skin and subsequent migration to the dLN by 48h, entirely absent following ImmuPatch F, and of lower magnitude after ImmuPatch Gimmunisation.(301). Plasmacytoid DC are potent producers of type I IFNs and play a role in the induction and maintenance of inflammation. These bone marrow-derived cells are virtually absent in naïve skin, but are identified in the dermis under inflammatory atopic conditions (309) and after MVA immunisation (ID)(301). Though pDC migrate into the dLN post–immunisation, it is unclear what role these cells having in the induction of adaptive immune responses due to their poor T cell stimulatory capability (72, 319).

The specific role of DC populations in the skin-draining LN for priming of adaptive responses against cutaneous pathogens is the subject of much debate. Epidermal Langerhans Cells were long thought to be the major mediators of skin immune responses but recently have been shown to be dispensable for responses after cutaneous infection with HSV and *Leishmania major* (75, 320, 321). This was supported by the observation that LC are unresponsive to bacterial LPS, and so a more tolerogenic role was proposed, though others have suggested that LC can induce potent cellular (as opposed to than humoral) responses in humans (84, 322, 323). Elsewhere, dermal Langarin+ DC have also been implicated in the induction of responses after epicutaneous immunisation with OVA (324). The authors of the HSV study found that CD8α+ LN resident DC, rather than mDC were responsible for cross-priming of CD8+ T cells, with skin-derived mDC shuttling antigenic cargo from the site of infection to the dLN whereupon they transfer it to CD8α+ lymphoid DC, whereas a role was proposed for CD8α- Langerin- DC (dermal interstitial) DC following *L. major* infection(75, 321). Others have shown that freshly recruited mono-DC are necessary for the cross priming of CTL after skin immunisation (304). Abadie *et al* demonstrate that although a number of cell types infiltrate the dLN following ID immunisation with MVA, only CD11c+ CD11b+ mDC and CD11b+ F4/80+ macrophages (but not CD11c+ CD8α+ lymphoid DC) present MVA antigen to T cells in an *ex vivo* assay, though mDC subtypes were not further investigated

(301). In summary, the roles of resident and infiltrating mDC subtypes in the presentation of skin-derived antigen to T cells are still a matter of debate.

Whilst the number of mDC in the dLN 120h post-immunisation is similar between immunised groups, the majority of mDC following ID, ID3% and ImmuPatch G immunisation were phenotyped as CD207- CD103- dDC, whereas the majority of cells following ImmuPatch F immunisation were CD207+ CD103- LC. This is consistent with the literature on LC migration, in that whilst dDC and Langerin+ dDC migration to the dLN peaks approximately 24h following pathogen encounter, LC migration peaks later after approximately 4 days (303). Epidermal cytokines including IL-1β and TNF-α induce the activation of LC and and down-regulation of anchoring adhesion molecules, enabling retraction of dendrites and migration towards the dLN, later in the innate response (325, 326). However, the significance of the differences in subtype composition of APC remains to be elucidated, by assessment of their antigen-presentating ability, as reported by Abadie *et al* (301).

Carey *et al* demonstrated that despite there being a lower level of inflammatory cytokine expression in the skin and dLN following ImmuPatch F immunisation, and a lower total number of CD11c+ cells in the dLN following delivery of FITC, these CD11c+ FITC+ cellsdemonstrated the phenotype necessary for T cell interaction i.e. MHC II^{hi} CD80+(265). Here, this is supported by the demonstration that despite there being a similar number of CD11c+ CD11b+ mDC in the dLN 48 and 120h following ID and ImmuPatch immunisation, a higher proportion of these mDC display this highly activated phenotype at 120h.

4.4.2.3 ImmuPatch design-specific differences in innate response

These data suggest that the design of an ImmuPatch has implications for the magnitude, kinetic and composition of cellular infiltrate into the dLN. It could be speculated that this is due to differences in the induction of an inflammatory response between patch designs – overall, ImmuPatch G demonstrated similar levels of DC migration and infiltration as ID groups (with diminished infiltration of innate cells such as neutrophils and monocytes). ImmuPatch F induced no pDC infiltration, an altered kinetic of CD11c+ and CD11b+ migration and an mDC infiltrate primarily composed of epidermal LC. Nevertheless, it was shown that ImmuPatch F can prime a response that is optimally boosted due to an increased T_{CM} component. It was noted that there is a greater amount of luciferase expression in the skin following ImmuPatch F delivery of Ad.pLuc than after ImmuPatch G (Chapter 3) and it remains to be determined if this is due to decreased lymphatic drainage as compared to ID/larger TAV patches.Such retension of vaccine in the skin could permit a more sustained interaction with epidermal LC, favouring the slow migration of skin-resident DC over the rapid infiltration of dermal and circulatory APC. Abadie *et al* noted that the length of antigen persistence in the immunised tissue had effects upon the composition of the innate response and the functionality of the resulting T cell response (301).

4.5 CONCLUDING STATEMENT

The hypothesis that ImmuPatch-primed CD8+ T cell responses follow a slower kinetic than those primed ID was rejected, as an irregular response kinetic, lacking a clear contraction phase, was demonstrated. Regardless, all ImmuPatchresponses (with one exception) retained the ability to undergo expansion upon boost. This is proposed to be due to an early accumilation of antigen-specific T_{CM}, particularly following priming with small TAV patches (265). ImmuPatch F was associated with the lack of a significant inflammatory response, proposed to influence both the kinetic and the memory phenotype of the induced response. In addition, the kinetic, magnitude and composition of the innate response to immunisation was different between ID and ImmuPatch, and patches of differing TAV, potentially due to differences in the inflammatory response and/or biodistribution between skin and LN (to be proven).The data presented here provide suggested underlying mechanisms for the observations made in Chapter 3.

CHAPTER 5 DELIVERY OF VIRAL VECTOR MALARIA VACCINES BY NANOPATCH INCLUDING LIQUID AND DRY-COATED FORMULATIONS

5.1 INTRODUCTION

Desirable attributes of a thermostable, needle-free, skin-targeted vaccine patch include: (1) ease of distribution; (2) simple, accurate and reproducible self-administration; (3) needles long and sharp enough to pierce the SC and penetrate into the viable epidermis and/or dermis but short enough not to stimulate dermal nociceptors or pose a disposal problem; (4) a simple coating procedure without the requirement for denaturing temperatures or changes in pH; (5) efficient, reproducible and rapid release of coated material into the skin; and, (6) long-term stability of coated vaccine patches ideally at high ambient temperatures. Additionally and perhaps most importantly, for such an intervention to replace well-established existing needle-based methods in the clinic, immunogenicity and protective efficacy must be at least comparable, and ideally with a reduced amount of vaccine.

The primary challenge in the delivery vaccines into the skin is in overcoming the semi-impermeable outer SC, diffusion through which is restricted to molecules smaller than 500Da (i.e. molecules 300,000 times smaller than an Adenoviral capsid) (100, 290). To address this, the Nanopatch was designed to perforate the SC and directly place microprojection-coated vaccine directly into the underlying strata, into the vicinity of a highly-structured network of epidermal and dermal APC (271) (Figure 5-1A). Vaccine payloads are delivered into microchannels created on Nanopatch application, depositing into the viable epidermis and dermis (270).

Nanopatch microprojections are distinct from standard microneedles reported in the literature which range 100-700µm in length and patches constitute less than 350 needles per cm^2 (described in1.5.2).Current Nanopatch microprojections are 40-110µm only and are of particularly high density – 21,025cm^{-2}. They were designed as such to allow optimal targeting of APC without an impractically large overall patch surface area. Microprojections are densely packed, but retain a structural integrity during application to the skin (270). They are spaced by 70µm in each direction to allow skin to deflect and compress around each individual projection for optimal penetration. The sharpness of the tips (<1µm radius) and the application of Nanopatches to the skin at a defined velocity by a spring-loaded mechanical applicator, prevent a 'bed of nails' effect one might expect from a wider distribution of application force across many thousands of individual tips, against the high elasticity of the skin(104). In contrast to ballistic delivery of vaccine (such as EPI) which are associated with extremely high velocities (>100ms^{-1}), mechanical application (1.96ms^{-1}) does not induce significant trauma-related cell death, potentially inducing excessive inflammation and reduced tolerability, and also a reduction in the number of viable APC remaining available for antigen uptake (327).

Using this custom-designed applicator, Nanopatches have been used to efficiently deliver a range of coated vaccines including coated plasmid DNA, VLP, split influenza virion, recombinant protein and killed virus vaccines, where induced responses were equivalent to those following IM delivery, but with a vastly reduced dose of vaccine (270-274, 328). This demonstrates the potential for dose-sparing by targeting vaccine antigen to the highly stimulatory environment of the skin. Chen *et al* optimised a method of dry-coating vaccine onto microprojections (Figure 5-1B).

Dry-coating offers benefits for easier patch distribution and storage and improved thermostability. An inactivated influenza vaccine coated onto the Nanopatch was shown to retain the ability to induce anti-HA titres in mice after 6 months of storage at 23°C (280).

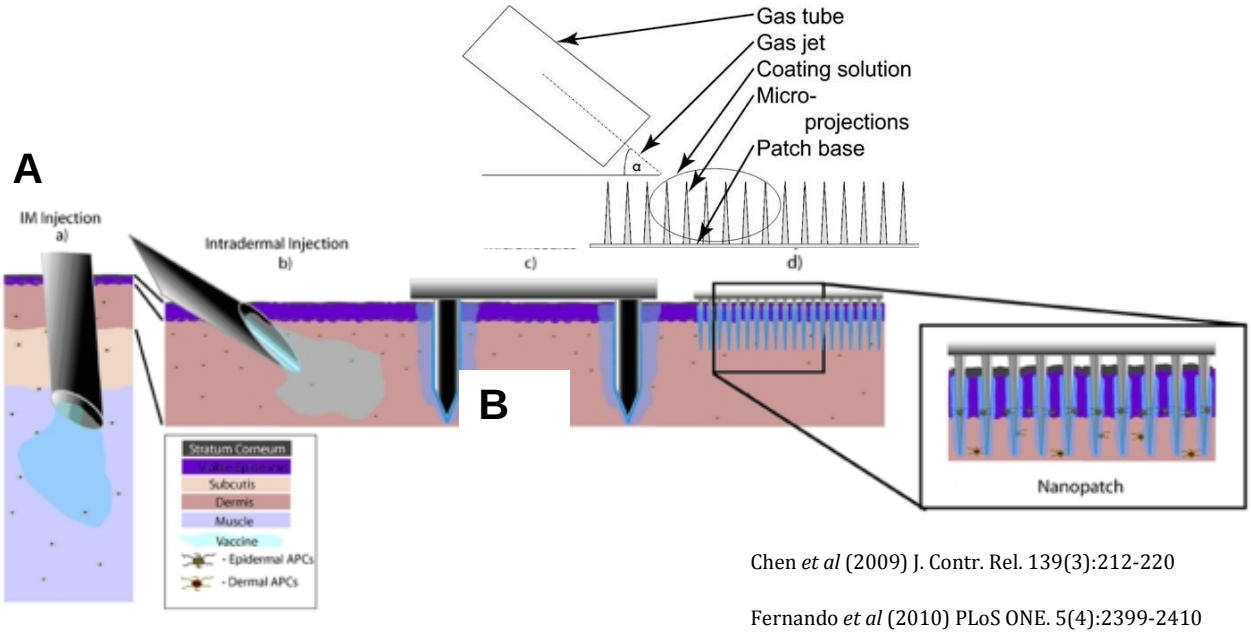

Chen *et al* (2009) J. Contr. Rel. 139(3):212-220

Fernando *et al* (2010) PLoS ONE. 5(4):2399-2410

FIGURE 5-1: The Nanopatch concept.

(A) A schematic from (271) demonstrating the Nanopatch in comparison to other needle-based (a+b) and ~700µm microneedle-based (c) vaccine delivery methods. Drawn to scale (human skin). (B) A demonstration of the Nanopatch dry-coating method. Taken from (270). A volume of coating solution containing vaccine is applied to a Nanopatchby pipette.The solution immediately distributes across its surface by capillary attraction due to the nature of attractive forces on the micro-nanoscale. A stream of nitrogen gas is applied at a 45° angle in a circular motion to rapidly remove all water whilst depositing the vaccine as a solid carbohydrate-based coating, covering each individual microprojection.

Live, recombinant viral vector vaccines based on Adenoviruses and MVA are among the most promising platforms for the development of new T cell inducing vaccines, particularly in 'prime-boost' combinations where different vectors are used to prime, and to boost responses against a common transgene antigen (329). Highly immunogenic vaccines based on live, infective organisms such as human and simian Adenoviral and Poxviral vectors encoding malaria, TB or HIV antigens must retain stable conformation of viral protein structures to ensure infection of host cells for efficient expression of transgene. This is a major consideration in formulation of live vaccines for lyophilisation. However, all lyophilised vaccines currently in use must currently be stored between 4 and 8°C and reconstituted vaccines lose potency rapidly(330). Thus a network of tightly controlled refrigeration facilities from manufacture to immunisation (or 'cold chain') must be guaranteed for the optimal vaccine safety and potency.

Alternatives are desirable; especially within the context of malaria vaccine provision in low resource settings since cold chain storage can be one of the major contributors to overall vaccination campaign costs. Maintenance of an uninterrupted cold chain is estimated to account for 14% of an immunisation campaign's total expenditure (92, 94). A vaccine technology incorporating a thermostable formulation within an easily distributable delivery platform would be ideal for the delivery of live, vectored vaccines in countries of high environmental temperatures and unreliable power supplies, such as those countries affected by malaria.

The successful thermostabilisation of live recombinant viral vector vaccines has been reported by Alcock *et al,* with E1/E3-deleted human Adenovirus type 5 (AdHu5) and modified Vaccinia Ankara (MVA) remaining stable for up to 6 months at temperatures up to 45°C. Virus suspensions were formulated with the vitrifying sugars trehalose and sucrose, commonly used as cryoprotectants for biological products, before desiccation and deposition as a solidified carbohydrate glass on the fibres of a support membrane. Viral titre was completely recovered from membrane fibres and vaccine immunogenicity in mice was retained only when these stabilising sugars were included (331). Whilst the advances demonstrated by this study remove the costly refrigeration requirement in the clinic or the field, needles were still required for delivery.

This chapter describes the development of needle-free dry-coated live viral vector vaccine patches for induction of cellular responses in both homologous and heterologous vectored prime-boost regimes using Ad and MVA. Initially, proof-of-concept was established using a 'quasi-static' method of applying Nanopatches by hand for the delivery of liquid vaccine, placed onto the surface of the ears of mice before application. Secondly, live viral vector vaccines were formulated for dry-coating, with attention to maintaining viral viability after coating and after storage. Thirdly, immunogenicity and protection against parasite challenge following applicator-assisted 'velocity' application of microprojections coated with viral vector vaccines was evaluated using one experimental, and one clinically relevant prime-boost regimen, where both Nanopatch/ID and Nanopatch/Nanopatch combinations of prime and boost were assessed.

The majority of the work described in this chapter constitutes a collaborative project between the Jenner Institute and the Drugs and Genes Delivery Group (D^2G^2) at the University of Queensland, funded by the Bill and Melinda Gates Foundation. The contribution of members of all the D^2G^2 particularly: C. McNeilly, M. Crichton, C. Primiero, S. Yukiko,X. Chen, G. Fernando, H. Corbett and A. Raphael to the collection of data presented is gratefully acknowledged (specific details in figure legends).

5.2 STATEMENT OF HYPOTHESES

Here, I propose that the Nanopatch will enable successful delivery of liquid and stable dry-coated live, viral vector vaccines into the APC-rich epidermis and/or dermis and induce antigen-specific immunogenicity and protective efficacy, of levels at least equivalent to ID immunisation, within prime-boost regimes. The Nanopatch

delivery system will demonstrate inherent practical advantages as compared to liquid, ID immunisation including improved thermostability. Finally, informed by previously published studies with the Nanopatch where as little as 1/30th of the delivered dose of inactivated influenza vaccine was required for equivlent immunogenicityas compared to IM immunisation (271, 280), a lower dose of viral vector vaccine will be required for equivalence to ID immunisation.

5.3 RESULTS

5.3.1 Nanopatch application methods, microprojection morphologies used within this chapter

Nanopatches were fabricated from silicon wafers by DRIE at the Rutherford Appleton Laboratories, Oxford (Figure 5-2, Ai). Individualarrays comprise densely of packed silicon microprojections at a density 21,025cm^{-2}) on a base measuring 4mm$^{2.}$ (Figure 5-2, Aii). Application of Nanopatches to the skin was performed using two methods. The first was a hand-applied method involving manually pushing three Nanopatches (arranged on the end of a hand applicator – Figure 5-2B) on to the dorsal ear skin following deposition of 5μL liquid vaccine onto the ear surface (method 1). The application force was measured to be 36N ± 6.3N[7] (Figure 5-2, Bii). The application velocity was negligible (~0ms^{-1}) as force was applied very slowly by pressing onto the ear, so this method was termed **'quasi-static'** application to differentiate from application at a '**velocity**' of 1.96ms^{-1}using the mechanical applicator.

In velocity application, vaccines were formulated and dry-coated onto microprojections using unique methodology described by Chen *et al* (270, 271, 274). Coated Nanopatches were applied to the skin using a device designed to achieve a reproducible application velocity of 1.96ms^{-1} using a spring and mass for a dynamic application, details of which are described in Figure 5-2, Ci and by Crichton *et al* (189). For applicator-assisted patch delivery, the ventral side of the pinna was chosen for its lower number of hair follicles. The ear pinna of an anaesthetised mouse is placed onto a square linoleum block with similar elastic recoil properties as human subcutaneous tissue (Figure 5-2, Cii). Payload-coated patches (such as methylene blue dye - Figure 5-2, Ciii) are placed onto an adhesive carbon disc onto the end of the outer casing of the applicator and a mass is retracted inside and affixed with a pin (Figure 5-2, Ci). Upon release of the pin, the mass strikes the carbon disc and transfers the patch to the skin. The mass recoils after initial impact, but the patch remains in place for 5 minutes to allow diffusion of dry-coated vaccine from microprojections into the skin before removal (Figure 5-2, Civ).

Following fabrication by DRIE, SEM was used to confirm uniformity of microprojection shape, length, pitch and sharpness. Figure 5-2, D+E show representative SEM images of microprojections from two Nanopatches used throughout the studies in this chapter. Images B+C are SEM images of a prototype Nanopatch with 40μm conical microprojections (**'NP40'**), whilst images D+E are of

[7] The average force in Newtons (± SD) applied during 22 separate hand applications onto a measuring balance, as if applying to the mouse ear pinna.

‘NP110’ microprojections, which comprise a 70µm tapered cylindrical shaft with a 40µm conical tip.

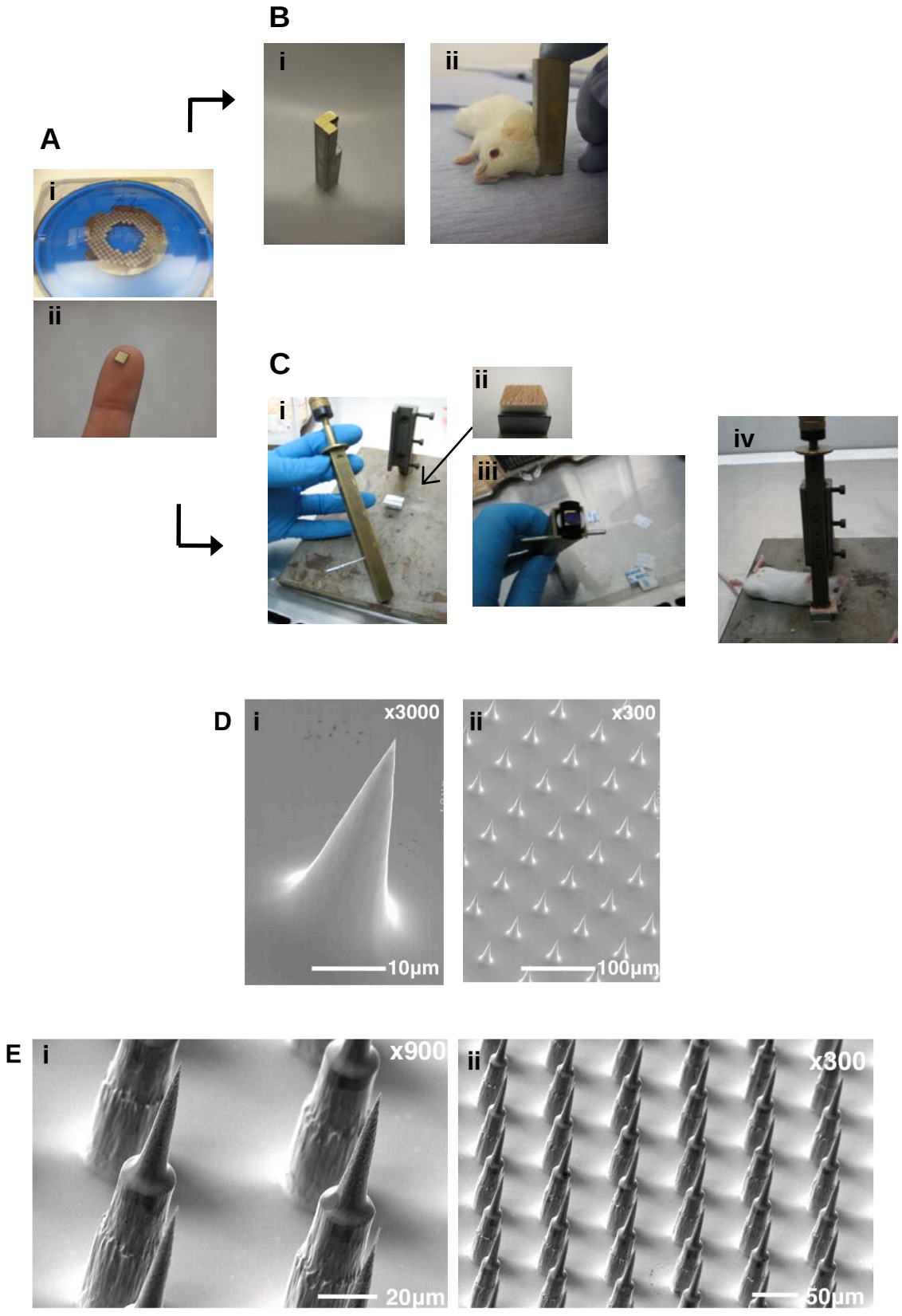
A
i
ii
B
i
ii
C
i
ii
iii
iv
D
i
x3000
10µm
ii
x300
100µm
E
i
x900
20µm
ii
x300
50µm

FIGURE 5-2: Nanopatch application methods and microprojection morphologies used within this chapter.

(A-D) In this chapter vaccines were delivered by one of two Nanopatch methods – either by hand application of liquid vaccine - 'quasi-static' (shown in B) or spring-applicator assisted delivery of vaccine-coated Nanopatches - 'velocity' (shown in C). Wafers of defined microprojection dimensions are produced by DRIE, and are diced to create individual 4mm^2 arrays (microprojection density 21,025 cm^{-2}, 3364 per patch)(A). One single Nanopatch is shown relative to a human forefinger (A ii). For liquid hand delivery, three such 4mm^2 Nanopatches were arranged in shape to best fit the that of the ear pinnae and affixed to a 70mm steel hand applicator (B i), which was applied to the ear following pipette placing of 5uL vaccine onto the dorsal of the pinnae (B ii). Scanning Electron Microscopy (SEM) was used to image microprojection morphology of two different Nanopatches used within these experiments (at 45°tilt, 15kV).(D) NP40 had conical microprojectionsof total length 40µm (used only in liquid hand delivery experiments. (E) NP110 microprojections consisted of a cylindrical shaft plus conical tip of total length 110 µm (70 µm + 40µm). SEM assisted by X.Chen, D^{2}G^2.

5.3.2 Quasi-static application of Nanopatches to the skin for liquid vaccine delivery

5.3.2.1 Penetration characteristics of quasi-static NP40 microprojections in murine skin

The penetration characteristics of NP40 microprojections following quasi-static application to murine skin were assessed. After application, ears were snap frozen with the Nanopatch *in situ*to prevent microchannel closure before removal immediately prior to imaging. Penetration of the SC was found to be inconsistent across the area underneath the Nanopatch, with only approximately 35% of projections penetrating through the SC (Figure 5-3A). In areas where penetration was successful, microchannel openings were observed spaced approximately 70µm amongst corneocytes of the SC, indicating that individual microchannels had been created by Nanopatch microprojections (Figure 5-3Aii). Delivery of a lipophillic dye (Vybrant® DiD) was assessed following quasi-static application of NP40 microprojections. Confocal and transmission micrographs confirm the delivery of the dye to the SC and VE with no dye present in the dermal compartment (D) as histologically determined, within a tightly defined single microchannel (Figure 5-3B). In the same experiment, dye-loaded microchannels were counted and measured from opening to tip (where dye was located at its deepest point). A histogram plotting penetration depth against frequency of penetrations (n=185) revealed penetration and diffusion of DiD was limited to the SC and VE (mean max. depth 8.98±2.48µm), with no penetrations reaching into the dermis (Figure 5-3C). This confirmed the earlier histological observation.

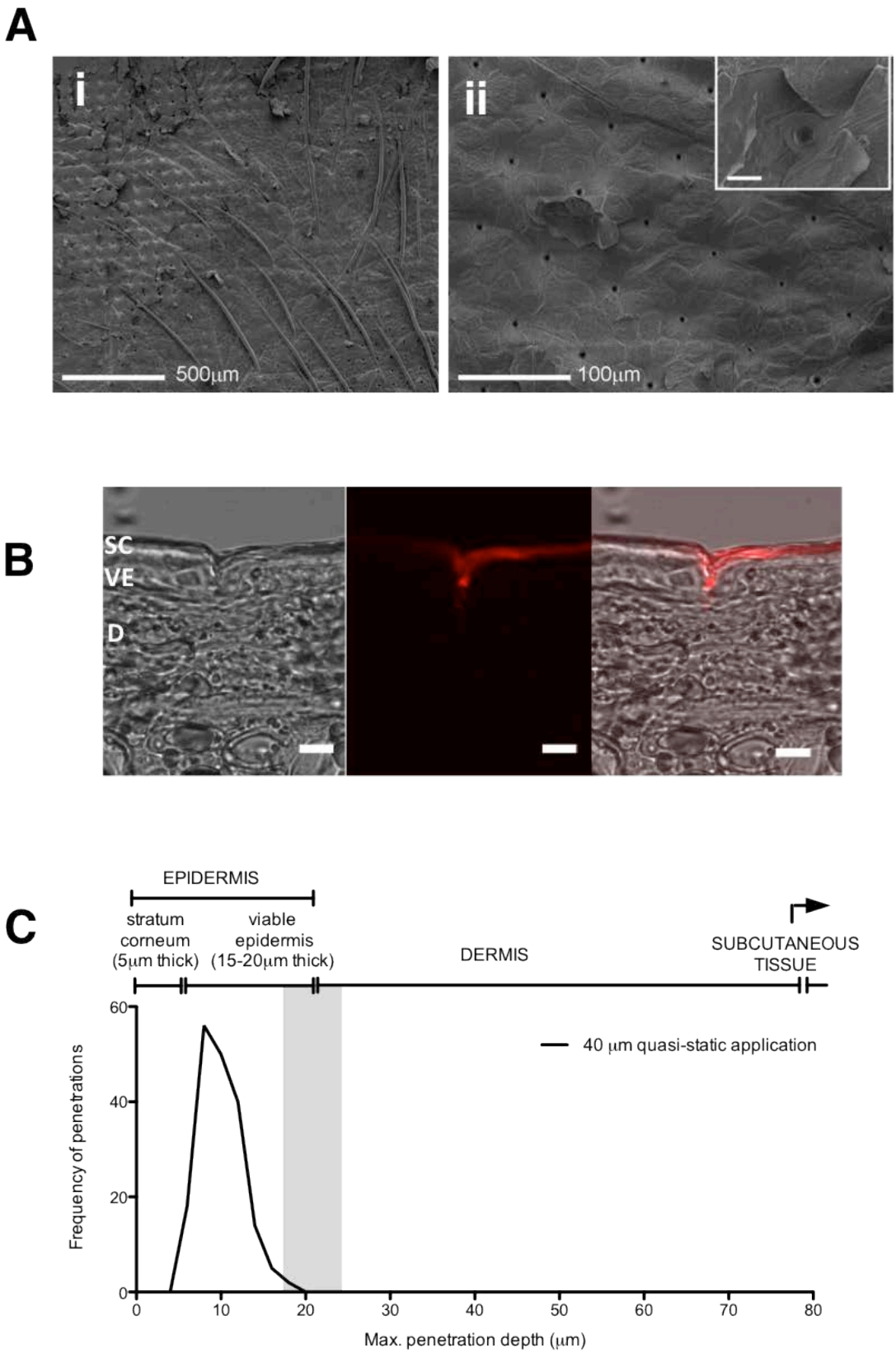

FIGURE 5-3: NP40 microprojections pierce the *stratum corneum*, and create microchannels into underlying tissue to enable delivery of liquid payload into the epidermis.

(A) Surface penetration tracked ('microchannels') following insertion of NP40 microprojections into murine skin using a quasi-static hand-applied method. (Ai) Far field view with variable penetration over the imaged area. (Aii) A selected area of efficient penetration, inset is a single microchannel opening, scale bar = 10µm. (B) Transmission and confocal microscopy images show cryo-sections of murine skin following delivery of liquidVybrant® DiDby NanopatchNP40 by quasi-static application. Panels are from left to right: transmitted light, fluorescence, light and fluorescence combined. SC = *stratum corneum*, VE = viable epidermis, D= dermis. (C) Histogram presentation of the microprojection penetration depths in murine skin. DiD was delivered by quasi-static application of NP40 microprojections *in vivo* before excision and confocal imaging of skin-cryo-sections. Maximum depths (corresponding to microprojection tips) of DiD-loaded microchannels were measured (n=185). Shaded area refers to epidermal-dermal basal layer. Murine skin measurements are taken from (177). Data collected by M. Crichton.

5.3.2.2 Immunogenicity and protective efficacy following homologous prime-boost immunisation with quasi-static application of NP40

A series of experiments were performed to evaluate the immunogenicity of prime-boost immunisation using the quasi-static application method for delivery of liquid vaccine to the skin, compared to the intradermal route. The homologous MVA.PbCSP prime-boost regimen was adopted. Standard prime and boost doses of $1x10^6$ PFU were used as previously performed within our laboratory (276, 332). This regimen when delivered by needle has previously demonstrated limited immunogenicity and protective efficacy against experimental liver-stage infection[8], rendering it a useful model to fully evaluate methods aiming to enhance immunogenicity and protection (such as targeting previously poorly accessible but reportedly highly inductive sites such as the VE/dermis)(253). Immunogenicity was assessed by quantifying CD8+ responses to the H2-K^d-restricted epitope Pb9, within PbCSP (described in 2.3.1.1). Protective efficacy was evaluated using the *P.berghei* sprorozoite challenge model of malaria.

In the first of these experiments, female BALB/c mice were given a prime immunisation of $1x10^6$ PFU MVA.PbCSP either intradermally or by NP40 with quasi-static application (by hand). A boost immunisation of $1x10^6$ PFU MVA.PbCSP was given ID 2 weeks following the prime. Blood was taken for re-stimulation of PBMC with Pb9 in an IFN-γ ELISPOT 12 days following the prime, and 2 weeks following the boost immunisation (Figure 5-4, Ai). Two weeks post-boost mice were sacrificed and spleens were harvested for Pb9 re-stimulation and IFN-γ ELISPOT on splenocytes (Figure 5-4, Aii). ELISPOT responses are expressed as mean IFN-γ secreting SFC (Spot Forming Cells) per million PBMC splenocytes.

Whilst NP40-primed responses were low, values were all above zero following background subtraction with a mean response of 466 SFC/million PBMC as compared to 1113 SFC/million PBMC after ID priming (the difference was not statistically significant, ns). However, all NP40-primed responses were boosted from

[8] Proposed underlying mechanisms for this decreased efficacy are described in 1.6.5

the post-prime level upon secondary immunisation with one particularly high outlier (P=0.002, NP40 vs. NP40/ID, Figure 5-4, Ai). As expected when using this model, ID-primed responses were only marginally boosted from the post-prime level (Figure 5-4, Ai).The splenic response following NP40/ID was similar to that following ID/ID immunisation (Figure 5-4, Aii). Intracellular Cytokine Staining revealed a high variability in the frequencies of splenic CD8+ IFN-γ+ cells across the NP40/ID immunised group, with 2 of 5 mice exhibiting particularly high responses (10.5% and 5.82% CD8+ IFN-γ+), and others exhibiting similar responses to ID/ID immunised mice (Figure 5-4B).

In a separate experiment using the same prime-boost schedule to investigate the ability of NP40 to boost pre-primed responses, mice were primed either by ID or NP40. Each group of 10 was then sub-divided into two groups of 5, one of which was boosted ID, and one by NP40 (by quasi-static application), two weeks after the prime. Blood was taken for IFN-γ ELISPOT 12 days following the prime, and 2 weeks following the boost immunisation. Spleens were taken 2 weeks following the boost. (Figure 5-4C). ID priming was slightly more efficient than NP40 priming (ns) but when NP40-primed responses were boosted ID they were increased to a greater extent. The NP40/ID post-boost response was significantly increased above that following ID/NP40, and NP40/NP40 immunisation (P<0.0001, Figure 5-4, Ci). Although NP40 was able to boost NP40-primed responses marginally, NP40 boosting had no effect on responses primed ID. A similar effect to that observed with PBMC was seen with splenic responses 2 weeks post-boost, where NP40/ID was found to be a significantly more immunogenic combination than either ID/NP40 or NP40/NP40 (P=0.0014, Figure 5-4, Cii).

When the protective efficacy of these prime-boost combinations was examined 2 weeks following the boost immunisation, NP40/ID was the only group to exhibit partial protection (Figure 5-4D). In what is recognised a poorly protective regime, 40% of NP40-primed, ID-boosted mice remained aparasitaemic during the monitoring period, whereas all other route combinations failed to demonstrate inhibition of the release of pre-erythrocytic parasites from the liver and entering the stage of erythrocytic replication. The 2 NP40/ID immunised mice that did succumb were delayed in their acquisition of parasites until day 6 and day 10, perhaps suggesting a partial inhibitory effect. Acquisition of parasites by ID/ID immunised mice was slightly delayed as compared to naïve animals (day 8 as compared to day 5), though these differences were not statistically assessed due to low experimental numbers.

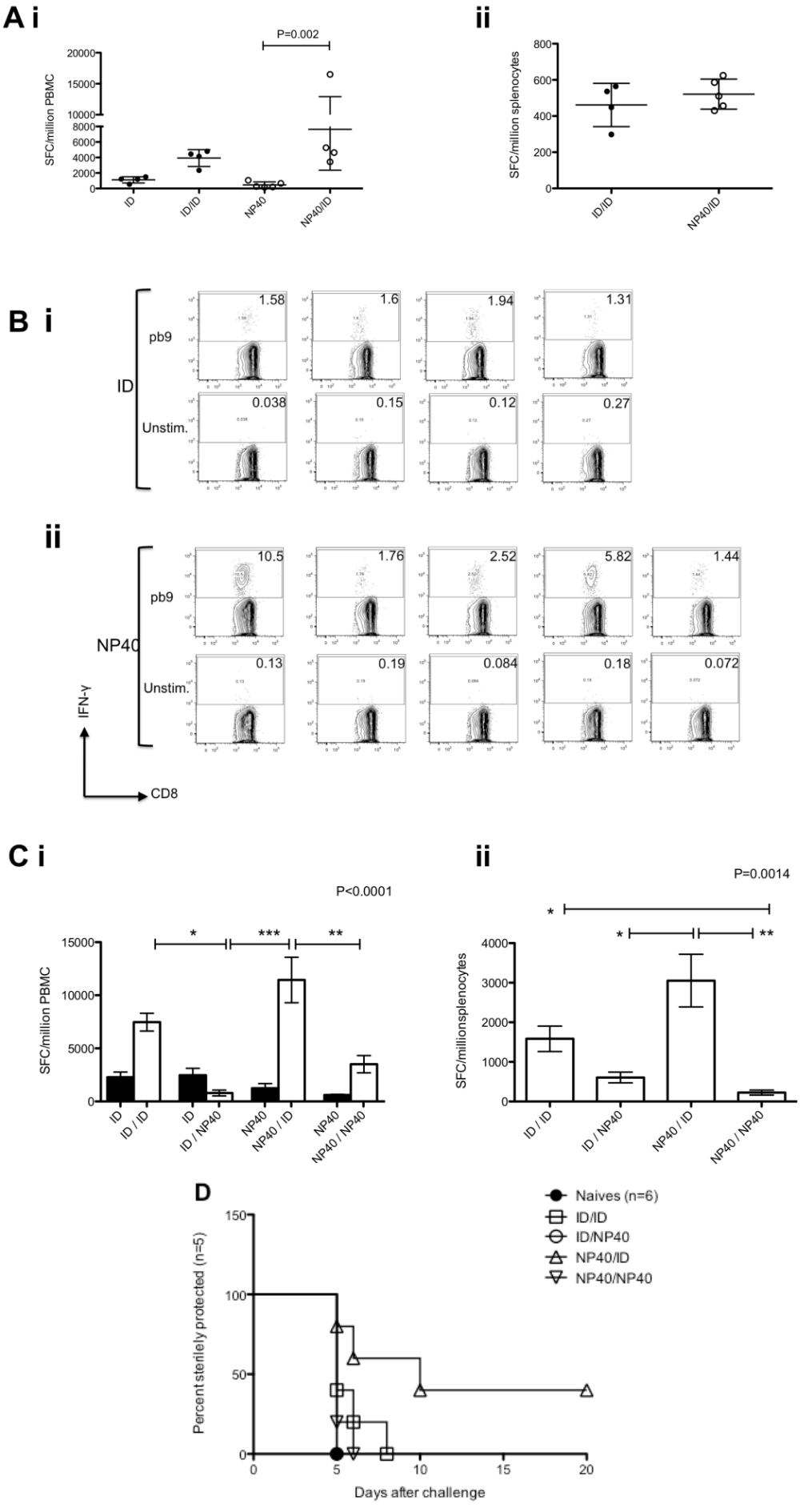
A i
P=0.002
SFC/million PBMC
20000
15000
10000
8000
6000
4000
2000
0
ID
ID/ID
NP40
NP40/ID
ii
SFC/million splenocytes
800
600
400
200
0
ID/ID
NP40/ID
B i
ID
pb9
Unstim.
1.58
1.6
1.94
1.31
0.038
0.15
0.12
0.27
ii
NP40
pb9
Unstim.
10.5
1.76
2.52
5.82
1.44
0.13
0.19
0.084
0.18
0.072
IFN-γ
CD8
C i
P<0.0001
SFC/million PBMC
15000
10000
5000
0
*
***
**
ID
ID / ID
ID
ID / NP40
NP40
NP40 / ID
NP40
NP40 / NP40
ii
P=0.0014
SFC/millionsplenocytes
4000
3000
2000
1000
0
*
*
**
ID / ID
ID / NP40
NP40 / ID
NP40 / NP40
D
Percent sterilely protected (n=5)
150
100
50
0
0
5
10
15
20
Days after challenge
Naives (n=6)
ID/ID
ID/NP40
NP40/ID
NP40/NP40

FIGURE 5-4: NP40 delivery of MVA.PbCSP induces Pb9-specific CD8+ T cells that are expanded upon boost, and can partially protect against parasite challenge.

(A) Female BALB/c (6-8 weeks, n=5) were immunised with $1x10^6$ PFU MVA.PbCSP either ID or by quasi-static application of NP40. Both groups were boosted with $1x10^6$ PFU MVA.PbCSP ID after 2 weeks. Blood was taken for stimulation of PBMC with Pb9 and IFN-γ ELISPOT 12 days following the prime and 2 weeks post-boost. Spleens were taken for IFN-γ ELISPOT (Aii) and ICS following Pb9 re-stimulation (B) 2 weeks post-boost. ICS staining and gating strategy as follows: singlets > size gate (lymphocytes) > CD8 PercPCy5.5+ > IFN-γ APC+. Background (unstimulated samples) was subtracted. One mouse in ID group was lost to unrelated death before the post-prime bleed. P=0.002 by Kruskall Wallis and Dunn's post-comparison (C). Female BALB/c mice were immunised with $1x10^6$ PFU MVA.PbCSP ID or by NP40 (n=10). Two weeks later, n=5 were boosted ID and n=5 were boosted with NP40 per group ($1x10^6$ PFU MVA.PbCSP). Blood was taken for Pb9 re-stimulation and IFN-γ ELISPOT 12 days (filled bars, Ci) following the prime immunisation and 2 weeks following the boost immunisation (open bars, Ci). Two weeks post-boost mice were sacrificed and spleens harvested for Pb9 re-stimulation of splenocytes in an IFN-γ ELISPOT (Cii). Mean Spot Forming Cells (SFC)/million cells ± SD (A) or SEM are presented (C). P<0.0001 by one way ANoVA with Bonferroni's multiple comparison (Ci). P=0.0014 by Kruskall Wallis with Dunn's post-comparison. (Cii) (D) Immunised mice (n=5, the same as presented in Bi) were challenged 2 weeks after the boost with 1000 *P. berghei* sporozoites, IV. Mice were monitored by thin blood smear and scored for presence/absence of blood stage parasites from days 5-20 post-challenge. Percentages of group sterilely protected (mice remaining negative for parasites throughout monitoring period) are presented in a Kaplan-Meier survival plot.

5.3.2.3 Dose- and microprojection design-specific differences in immunogenicity following homologous prime-boost immunisation

The Nanopatch/ID prime-boost combination was taken forward into an analysis of the effect of increasing priming dose upon immunogenicity, using the homologous MVA.PbCSP prime-boost schedule. Due to observation that much of the liquid vaccine dose was either retained by the patch, remained on the surface of the ear or was transferred to the surrounding environment following patch application using the quasi-static method, it was thought that increasing the dose concentration may further improve Nanopatch-induced responses. The higher dose chosen was the maximum dose possible i.e. the number of PFU within 10µL of undiluted stock MVA.PbCSP (divided bilaterally between the ear pinnae).

Priming mice with NP40 delivered quasi-statically with either a standard dose of $1x10^6$ PFU or a higher dose of $5x10^7$ PFU induced post-prime responses that were lower than ID priming as had been observed in the previous experiments, the difference being statistically significant between the NP40-primed groups and $5x10^7$ PFU ID (P=0.001, Figure 5-5A). Following a boost of $1x10^6$ PFU given ID, responses induced by NP40 primingwith $1x10^6$ PFU demonstrated boosting to a similar level as those primed ID using the same dose as had been observed in previous experiments, but responses following $5x10^7$ PFU NP110 priming were not increased by the boost immunisation (P=0.019 vs. ID $5x10^7$ PFU/ID).

In a separate experiment, microprojections of a different morphology were used to deliver liquid vaccine by quasi-static application (NP110), using the same vaccine, priming doses and schedule. A standard boost dose of $1x10^6$ PFU MVA.PbCSP was

given 2 weeks later ID. Though not statistically significant, responses post-prime were higher after $5x10^7$ PFU priming by NP110, compared to $1x10^6$ PFU by the same patch (2220±305 compared to 686±183 SFC). NP110 priming induced similar post-prime responses to both doses delivered ID. In this experiment, both $1x10^6$ PFU and $5x10^7$ PFU NP110-primed responses were improved upon boost, with mean post-boost responses notsignificantly different from their matched ID/ID immunised group, though the mean of the $1x10^6$ PFU NP110-primed response was slightly lower due to a low outlier. However, the post-boost response following NP110 priming with $5x10^7$ PFU was significantly lower than ID priming with $1x10^6$ PFU (P=0.039, Figure 5-5B).

These mice were challenged with 1000 *P. berghei* sporozoites 2 days following the final bleed. All unimmunised animals were parasitaemic by day 5 post-challenge, whilst all immunised animals were partially protected. With a priming dose of $5x10^7$ PFU, NP110/ID immunisation demonstrated 60% efficacy compared to 20% efficacy following ID/ID immunisation, and a priming dose of $1x10^6$ PFUinduced 40% as compared to 60% after ID/ID (Figure 5-5C).

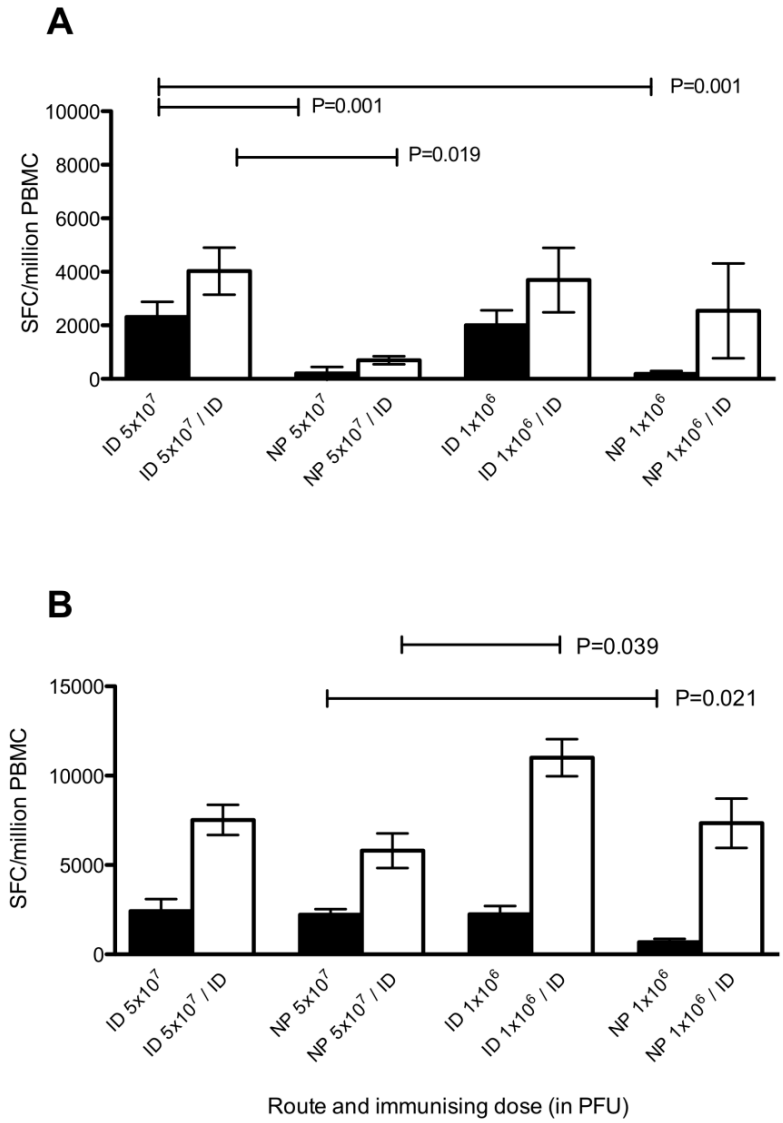
A
P=0.001
P=0.001
P=0.019
SFC/million PBMC
10000
8000
6000
4000
2000
0
ID 5x10^7
ID 5x10^7 / ID
NP 5x10^7
NP 5x10^7 / ID
ID 1x10^6
ID 1x10^6 / ID
NP 1x10^6
NP 1x10^6 / ID
B
P=0.039
P=0.021
SFC/million PBMC
15000
10000
5000
0
ID 5x10^7
ID 5x10^7 / ID
NP 5x10^7
NP 5x10^7 / ID
ID 1x10^6
ID 1x10^6 / ID
NP 1x10^6
NP 1x10^6 / ID
Route and immunising dose (in PFU)
C
Naives
5x10^7 PFU NP110/ 1x10^6 PFU ID
1x10^6 PFU NP110/ 1x10^6 PFU ID
5x10^7 PFU ID/ 1x10^6 PFU ID
1x10^6 PFU ID/ 1x10^6 PFU ID
Percent sterilely protected (n=6)
150
100
50
0
0
5
10
15
20
Days after challenge

FIGURE 5-5: Priming dose and microprojection design specific differences in immunogenicity following quasi-static application.

(A) Female BALB/c mice were immunised with MVA.PbCSP either by NP40 with quasi-static application, or by ID injection at two doses $5x10^7$ PFU (undiluted vaccine) or $1x10^6$ PFU. Two weeks later a boost immunisation was delivered ID (all $1x10^6$ PFU, presented here as 'ID'). Blood was taken for isolation of PBMC 1 week post-prime (black bars) and 2 weeks post-boost (open bars). Cells were re-stimulated with Pb9 prior to IFN-γ ELISPOT. Bars represent mean SFC/million PBMC ± SD (B). In a separate experiment, groups of mice were primed using the same doses either byNP110 delivered quasi-statically or ID. Two weeks later mice were boosted ID with $1x10^6$ PFU MVA.PbCSP. Blood was taken for isolation of PBMC 1 week post-prime (black bars) and 2 weeks post-boost (open bars). Error bars are SEM. X-axis labels refer to immunisation dose and route i.e. PRIME/BOOST dose of MVA.PbCSP in PFU. (C) The mice immunised with NP110/ID or ID/ID (presented in B) were subsequently challenged 2 weeks following the boost immunisation with 1000 *P.berghei* sporozoites given IV. Mice were monitored by thin blood smear and scored for presence/absence of blood stage parasites from days 5-20 post-challenge. Open symbols represent ID primed groups and closed symbols represent NP110 primed groups, Percentage of group sterilely protected (mice remaining negative for parasites throughout monitoring period) is presented in a Kaplan-Meier survival plot.

5.3.2.4 Delivery efficiency of quasi-static Nanopatch immunisation is independent of tested dose and microprojection morphology

Doses delivered into the skin ('delivered doses') were hypothesised to differ from doses applied to the surface of the skin ('immunising doses') due to inefficiencies of vaccine delivery using this method. The delivery efficiency of Nanopatch was quantified across a number of doses and after quasi-static application of both NP40 and NP110, as used in previous experiments. Groups of mice were immunised with doses of MVA.PbCSP, mixed with the β particle emitter ^{14}C-OVA, which served as a tracer. β-emission was detected from excised solubilised ears, and eluates obtained from swabs that were used to remove vaccine remaining on the ear following application and calculated as a percentage of the emission from the same immunising volume of labelled vaccine, as a positive control. Delivery efficiencies varied little between doses and microprojection morphologies – with average efficiencies of 23%, 23% and 29% following NP40 delivery of doses of $1x10^6$ PFU, $1x10^7$ PFU and $5x10^7$ PFU respectively, and of 20% for both doses delivered by NP110 (Figure 5-6). A Nanopatch with no microprojections delivered 8% of topically applied vaccine into the ear with 68% being removed from the ear surface. This demonstrates that untreated skin is semi-permeable to MVA, delivery of which has been attributed to entry via hair follicles elsewhere (119). There were no statistically significant differences in the proportion of vaccine delivered into the ear, or remaining on the swab (ranging from 33-48%) between different doses or morphologies. In summary, the delivery efficiency of quasi-static Nanopatch application is approximately 23% of that applied to the ear (Table 5-1), which has implications for interpretation of immunogenicity data, as delivered doses are considerably reduced from immunising doses (assuming that the amount of ^{14}C-OVA present within a delivered amount correlates with viral infection of cells).

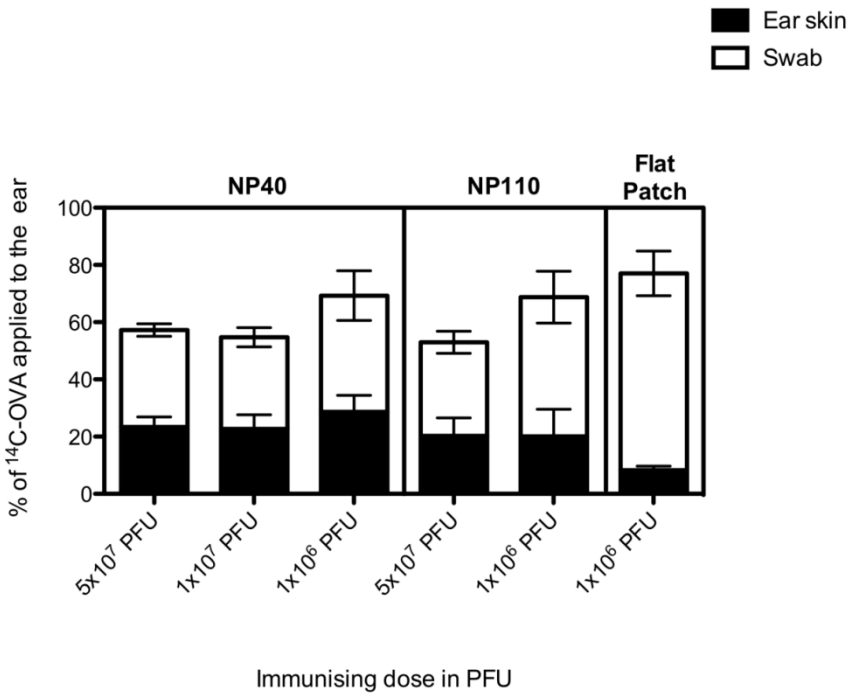

FIGURE 5-6: Delivery efficiency of liquid vaccine delivery by NP40 and NP110 (quasi-static application).

Mice were immunised with MVA.PbCSP at doses of $5x10^7$ PFU, $1x10^7$ PFU or $1x10^6$ PFU by NP40 or of 5x107 PFU or $1x10^7$ PFU by NP110, delivered as 10uL liquid split between the 2 ears. A 'flat patch' control group (i.e. without microprojections) was included (dose of $1x10^6$ PFU). Each vaccine dose also contained 6 nCi of radiolabelled ovalbumin (^{14}C-OVA). Following each immunisation, ears were swabbed once with a cotton bud to remove vaccine not internalised, but remaining on the ear surface. Mice were euthanised and ears were excised before solubilisation using the organic base Solvable® (60°C, 2 hours). (A) The scintillation counts (β emission) from swabs and ears were counted and calculated as a % of that from 10μL labelled vaccine (i.e. prior to application to the skin). Experiment in collaboration with C.McNeilly and S.Yukiko.

Immunising dose (2 ears 5μL/ear)	Nanopatch	Average % delivery	Adjusted 'delivered' dose
$5x10^7$ PFU	NP40	23.35	$1.2x10^7$ PFU
$1x10^7$ PFU	NP40	22.72	$2.3x10^6$ PFU
$1x10^6$PFU	NP40	28.66	$2.9x10^5$ PFU
$5x10^7$ PFU	NP110	20.27	$1.2x10^7$PFU
$1x10^6$PFU	NP110	20.10	$2.0x10^5$ PFU

TABLE 5-1: Table showing the average delivery efficiencies after quasi-static delivery of liquid vaccine by Nanopatch.

Corresponding adjusted 'delivered' doses applicable to experiments in previous figures are given.

5.3.2.5 Liquid, quasi-static Nanopatch delivery of Adenovirus in heterologous Ad/MVA prime-boost regimes

The effect of priming by quasi-static application of NP40 was assessed in AdHu5.PbCSP/MVA.PbCSP immunisation. Female BALB/c mice were immunised

with $1x10^9$ VP AdHu5.PbCSP either ID or by quasi-static application of NP40. Eight weeks later a boost immunisation of $1x10^6$ PFU MVA.PbCSP was given ID. An IFN-γ ELISPOT was performed on PBMC isolated 3 weeks post-prime (peak of the response following Ad immunisation - (252)) or 2 weeks post-boost (Figure 5-7A). Spleens were harvested from mice 2 weeks post-boost and an IFN-γ ELISPOT performed (Figure 5-7B). Similar to MVA.PbCSP immunisation, post-prime responses were lower for NP40 than ID priming (ns). In contrast to MVA.PbCSP/MVA.PbCSP, boosting of NP40-primed responses was ineffective and post-boost responses were not significantly improved from the post-prime level. The magnitude of the post-boost response was significantly lower than that following ID/ID immunisation ($P<0.0001$, Figure 5-7, Ai). Similarly, an IFN-γ ELISPOT performed on splenocytes demonstrated a statistically significantly lower post-boost response following NP40/ID immunisation compared to ID/ID immunisation ($P=0.0017$, Figure 5-7, Aii).

Heterologous Ad/MVA prime-boost regimes are highly immunogenic regimes showing significant promise in clinical trials of malaria vaccines, amongst others (286). Due to the existence of pre-existing immunity to human serotypes, chimpanzee vectors have been developed for human use, and show equivalent immunogenicity and protection against malaria in pre-clinical models (251, 252). NP40-primed human and simian regimes were evaluated in *P.berghei* sporozoite challenge (Figure 5-7B). Groups of mice were immunised with AdCh63.ME-TRAP or AdHu5.PbCSP (both of which contain the Pb9 epitope) either ID or by NP40 ($1x10^9$ VP). A boost immunisation of $1x10^6$ PFU MVA.ME-TRAP/MVA.PbCSP was given eight weeks following the prime, ID. After a further 2 weeks, 1000 *P.berghei* sporozoites were inoculated into the tail vein in a parasite challenge. Percentages of mice that were sterilely protected, i.e. those remaining negative for blood-stage parasite forms to day 20 post-challenge, are presented in Kaplan-Meier survival plots in Figure 5-7, Bi and ii. Mice were bled 2 days before challenge for Pb9 re-stimulation of PBMC and IFN-γ ELISPOT (Figure 5-7, Biii).

Similar to the previous result, the regimes AdCh63.ME-TRAP/MVA.ME-TRAP and AdHu5.PbCSP/MVA.PbCSP where NP40 was used to deliver the priming immunisation demonstrated significantly lower response than ID/ID 2 weeks after the boost ($P=0.0023$ and $P=0.0005$, Figure 5-7). NP40/ID regimes demonstrated no protective efficacy - all immunised mice became parasitaemic on either the fifth or sixth day post-challenge, whereas ID/ID immunised mice demonstrated 100% (AdCh63.ME-TRAP priming) or 40% (AdHu5.PbCSP priming).

Following completion of this experiment, the AdHu5.PbCSP was found to contain a minor contamination with a different Ad vaccine. Since doses of Ad vaccines are calculated based on viral particle number and immunostaining of the common hexon protein, it should be noted that the effective immunogen dose was likely to be reduced due to an overestimation of viral titre (VP/mL) of AdHu5.PbCSP in these experiments. This could explain the level of the AdHu5.PbCSP-primed ID/ID response being lower than that following AdCh63.ME-TRAP when usually it is similar to that of simian vectors (262). Also, the lower level of protective efficacy in sporozoite challenge, which has previously been reported to be within the range of 80-100% following Ad/M immunisation (262). These results indicate that efficacy of quasi-static NP40 immunisation is dependent upon vaccine regimen, since

responses primed by NP40 in MVA/MVA, but not Ad/MVA were capable of secondary expansion, or of conferring protection against challenge. Despite this viral quality issue, the results are comparative so still reflect accurately the relative immunogenicity of the two methods.

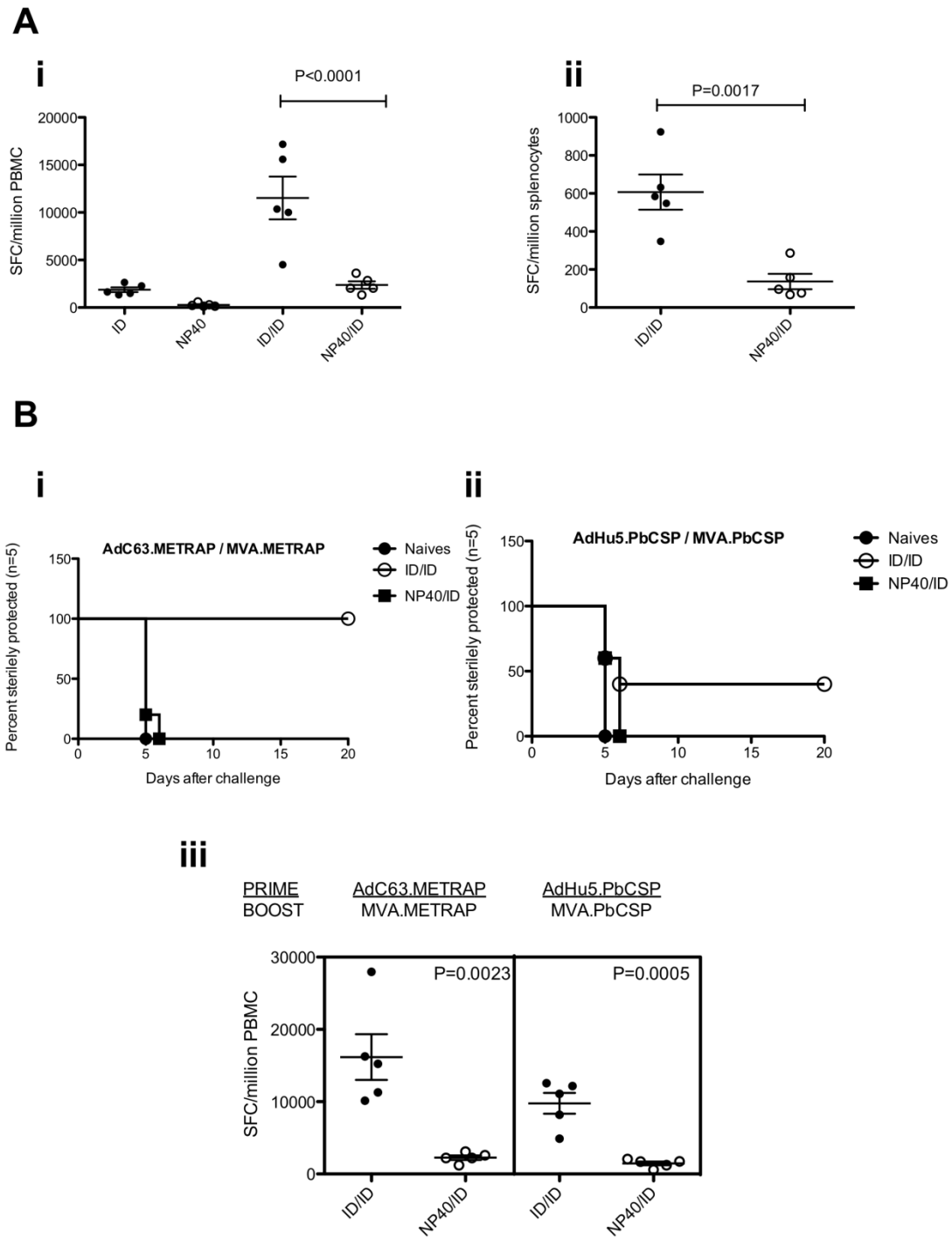

FIGURE 5-7: Nanopatch delivery of human and AdCh63-based vaccines in heterologous prime-boost schedules.

(A) Female BALB/c mice (n=5, aged 6-8 weeks) were immunised with 1x10^9 VP AdHu5.PbCSP either ID or by quasi-static application of NP40. Eight weeks later a boost immunisation of

1x10^6 PFU MVA.PbCSP was delivered ID. Blood was taken 3 weeks following the prime, and 2 weeks following the boost immunisation for isolation of PBMC and re-stimulation with Pb9 in an IFN-γ ELISPOT assay (Ai). Spleens were harvested from euthanised mice 2 weeks post-boost for IFN-γ ELISPOT (Aii). Circles represent mean SFC/million cells and horizontal lines are means ± SEM. P<0.0001 and P=0.0017 by one way ANoVA with Bonferroni's post test (B) Female BALB/c mice were immunised with either AdHu5.PbCSP or AdCh63.ME-TRAP (both transgenes expressing antigens containing the CD8+ Pb9 epitope) at a dose of 1x10^{9}VP. Vaccines were either delivered ID or by NP40 as before. Eight weeks later, a boost vaccine of 1x10^6 PFU MVA.PbCSP, or MVA.ME-TRAP was delivered ID. IFN-γ ELISPOT following Pb9 stimulation of PBMC 2 weeks following the boost is presented in Bii (mean SFC/million PBMC ± SEM) Significance was determined by unpaired t test. Two days later, immunised and naïve mice were challenged with 1000 *P.berghei* sporozoites given into the dilated tail vein. Mice were observed daily and monitored for evidence of blood stage parasiteaemia by thin blood smear and microscopic analysis of stained slides from days 5-20 post-challenge. Percentages of mice sterilely protected (remaining parasite negative to day 20 post-challenge) are presented in the Kaplan Meier survival plots in B i+ii.

5.3.2.6 Summary of section 5.3.2

- Quasi-static application of NP40 to murine skin demonstrated low and variable perforation of the SC (~35% projections). Penetration and delivery of liquid payload into the SC and VE only, with no delivery into the dermis.
- Whilst NP40-primed responses were low post-prime, these responses were equivalent to ID/ID immunisation post-boost in MVA/MVA immunisation (though variable) and were partially protective against challenge (40%).
- Priming with NP40 with a standard dose (1x10^6 PFU) induced higher post-boost responses than a higher priming dose, these responses were improved when NP110 rather than NP40 was used to deliver the prime. Quasi-statically applied NP110-primed responses were partially protective against challenge (60% higher dose prime, 40% standard dose prime).
- Boosting of pre-primed responses by quasi-static application of NP40 was ineffective in MVA/MVA immunisation.
- NP40 delivery of Adenovirus vectored vaccines was ineffective and responses induced were low and were not protective against challenge.
- The proportion of vaccine delivered into the ear following quasi-static immunisation by Nanopatch was not influenced by immunising dose (comparing doses of 1x10^6, 1x10^7 and 5x10^7 PFU) or microprojection morphology (comparing 40μm conical and 110μmcylindrical + conical tip micro-projections). The delivery efficiency was approximately 23%.

5.3.3 Formulation and dry-coating of viral vector vaccines onto NP110microprojections

5.3.3.1 Velocity application of NP110 for delivery of dry-coated payloads

Due to the resource-burdening requirement of conventional vaccines for costly cold storage, stable MVA and Ad dry-coated microprojection patches were developed. The observed variability in penetration of microprojections using quasi-static application, and the increased dose flexibility associated with 110μm microprojections informed our choice of NP110 and the previously described spring-applicator velocity method. The applicator delivers patches to the skin in a more

controlled manner, reducing variability in application method (189). The coating method previously optimised by Chen *et al* i.e. mixing with 1% $^{w}/_{v}$ (10mg/mL) methyl cellulose (MC) was used as was the method of removing excess water by applying a constant jet of nitrogen gas in a circular motion (Figure 5-1B)(270).

To evaluate the penetration and delivery characteristics of this method, cryo-SEM was used to image the surface of mouse ear following velocity application of NP110 microprojections (Figure 5-8A). Images revealed widespread and consistent surface penetration across the area beneath the patch. Figure 5-8Ai shows the bottom right corner of the patched area, and Figure 5-8 Aii shows an area in higher magnification with a single microchannel inset. Dry-coated fluorescent dye delivery into microchannels was demonstrated following velocity application, resulting in direct deposition of dye beyond the epidermal basal layer and into the underlying upper dermis (Figure 5-8B).

The penetration and delivery profile after delivery of NP110 microprojections was broader than that following quasi-static NP40 application, with a mean maximum penetration depth of 42.0±9.86μm SEM and a range of 22-74μm. (Figure 5-8C). Indeed, the deepest points at which dye could be detected were confined to the dermal compartment (40-80μm from the surface), though lateral diffusion into the VE was also observed. Based on previously reported measurements of murine skin, no dye was deposited at depths greater than those corresponding to the dermal compartment (177, 333). Whereas 100% of maximum penetration depths following quasi-static delivery of NP40 were located in the VE, only 3.2% of maximum depths following velocity application of NP110 were within the VE with 96.7% located in the dermis. . In summary, velocity application of NP110 allows penetration and dye delivering into both viable epidermal and dermal layers of the skin, whereas NP40 quasi-static delivery was confined to the VE.

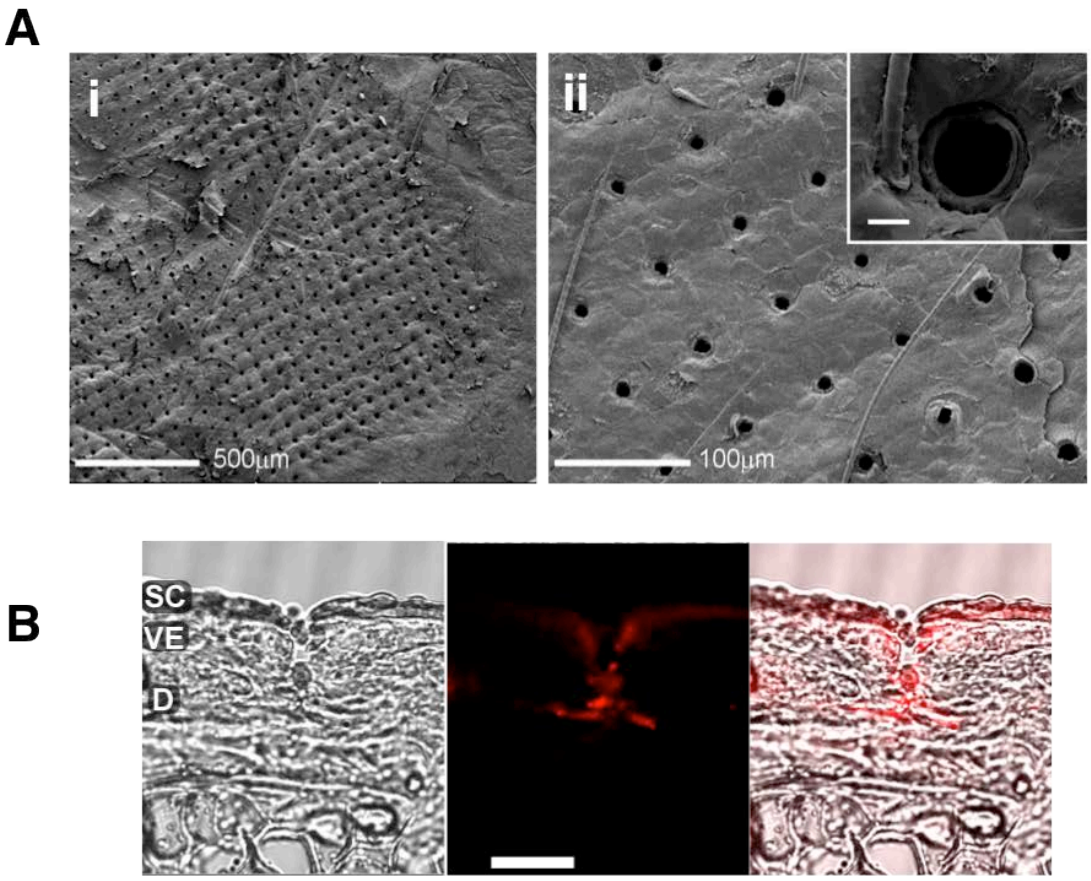

FIGURE 5-8: NP110 microprojections delivered at velocity pierce the *stratum corneum* and deliver dry-coated payloads into the viable epidermis and the dermis.

(A) Cryo-SEM images following velocity application of NP110 microprojections. Surface penetration tracks (microchannel openings) following application of NP110 microprojections at 1.96ms^{-1} by spring-loaded applicator at low magnification of a corner of the patched area (Ai) and higher magnification (Aii). Inset is a single microchannel opening, scale bar = 10μm.

(B) Transmission and confocal microscopy images show representative cryo-sections of murine skin following velocity application of DiD-coated NP110 microprojections (DiD + 1% w/v MC). Panels from left to right: transmitted light, fluorescent, light and fluorescence combined. SC = stratum corneum, VE = viable epidermis, D = dermis. (C) Dry-coated DiD was delivered to murine skin as described above prior to excision and cryo-sectioning of ears pinnae. The maximum depths (corresponding to microchannel tips) of DiD-loaded microchannels were measured and are plotted as a histogram of frequency of penetrations against penetration depth (n=365). Data collected by M.Crichton.

5.3.3.2 Formulation and dry-coating of viral-vectored vaccines onto microprojections

SEM imaging was used to assess microprojection coating morphology following dry-coating of MVA.PbCSP,as compared with an uncoated Nanopatch(Figure 5-9A)using formulations containing $2.5x10^7$ PFU MVA.PbCSP (per patch). Example SEM images (high magnification) are shown in Figure 5-9. Following mixture with the MC, the vaccine formulation was found to be highly viscous, and after drying much of the coating solution was localised to the base of the patch, but with a proportion covering microprojection shafts and tips (Figure 5-9B). This was also reported by Chen *et al*, where the ratio of microprojection coating to base coating was measured to be 2.7:1, when formulating recombinant OVA protein (270).Following application, the coating visualised on microprojection tips was reduced with less coating solution on the base (as observed when comparing images in Figure 5-9 B+C). Breaching of the SC was confirmed by the observation of corneocytes on the tips of projections after removal from the skin (Figure 5-9C, arrows). The dimensions of a single coated microprojection were measured using image analysis software before and after application to the skin (Figure 5-9D). The lateral measurements are reduced following insertion, confirming that coating solution is removed from microprojections during application to skin.

Microprojection coating was variable across the patch, with some material 'bridging' between individual microprojections (Figure 5-9, Ciii), likely due to a high surface tension between coating solution and the silicon microprojections. Upon impact, these 'bridges' may be pushed back towards the base and may or may not diffuse into microchannels. There is a possibility that they may impede initial microprojection penetration of skin by exerting resistance on impact, though this is unproved.

Figure 5-9, E+F demonstrates that coating morphology is both vaccine prep and dose-specific. Using equivalent doses of two MVA vectored vaccines ($2.5x10^7$ PFU) coating is irregular, with some bridging between needles and in the case of MVA.ME-TRAP, vaccine sitting atop the microprojections (Figure 5-9, Ei). However, when lower doses of MVA.PbCSP and MVA.ME-TRAP were coated ($5x10^5$ PFU, Figure 5-9, D+Eii) there was less bridging of material though some material was localised to the base of the patch. In contrast to MVA formulations, when Ad-vectored vaccine was dry-coated onto NP110 patches in formulation with $1\%^w/_v$ MC, a more efficient coating of microprojections was observed at both higher ($1x10^{10}$ VP, Figure 5-10B) and lower ($1x10^9$ VP, Figure 5-10C) coated doses, with minimal bridging between microprojection shafts or coating on the patch base, but better coverage of individual projections.

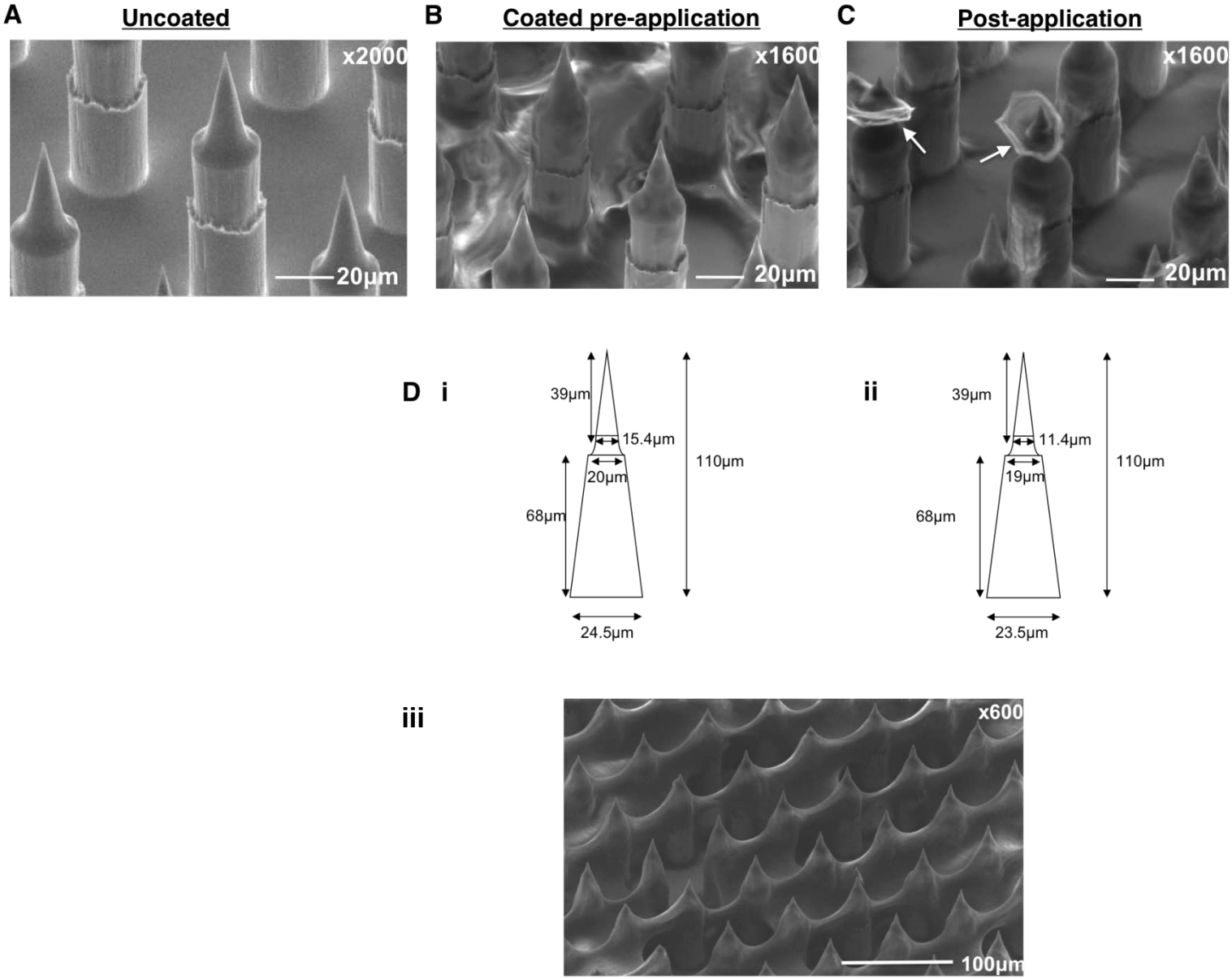
A
Uncoated
x2000
20µm
B
Coated pre-application
x1600
20µm
C
Post-application
x1600
20µm
D i
39µm
15.4µm
20µm
110µm
68µm
24.5µm
ii
39µm
11.4µm
19µm
110µm
68µm
23.5µm
iii
x600
100µm

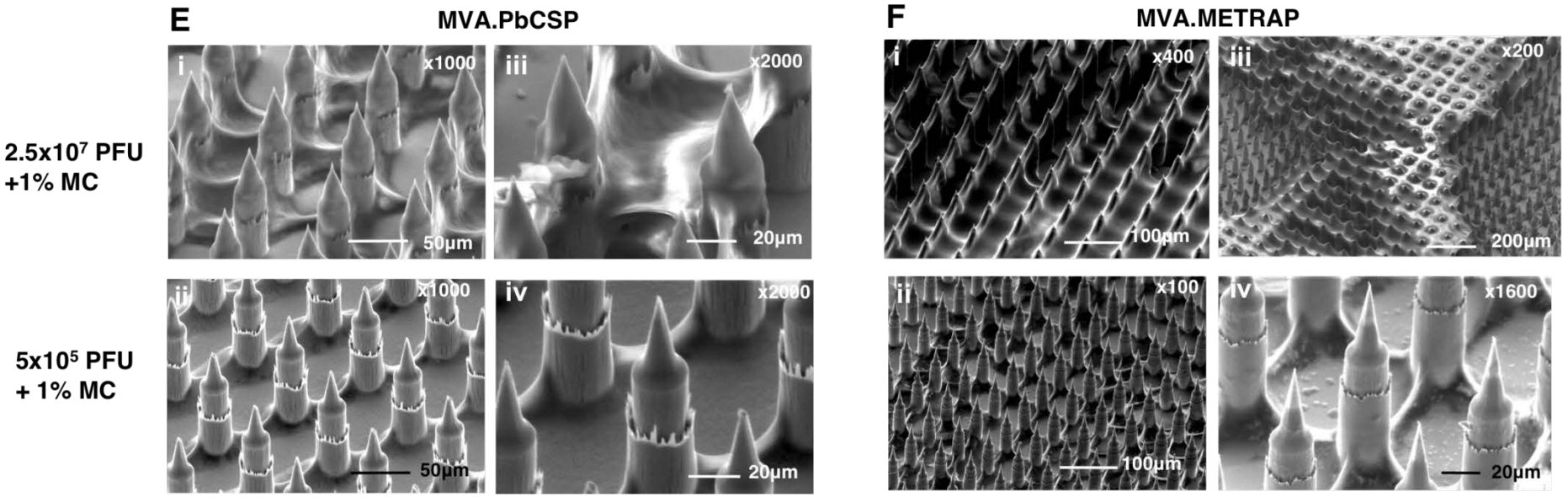

FIGURE 5-9: MVA formulations can be dry-coated onto NP110 microprojections and coated material is reduced following insertion in the skin.

(A) A secondary electron SEM image of uncoated NP110 microprojection at high magnification. (B) SEM (secondary electron) images of an NP110 patch following dry-coating with 2.5x107 PFU MVA.PbCSP + 1% w/v MC(Bi) and after velocity application of an NP110 patch to murine skin (coated with 2.5x107 PFU MVA.PbCSP + 1% w/v MC). Arrows point to extracted corneocytes indicating successful SC penetration (Bii). (C) SEM images were analysed using accompanying software and measurements of microprojection parameters were taken after coating (i), and after insertion (ii) into the skin assisted by spring-loaded applicator and confirmed removal of material following insertion. (iii) Demonstrates 'bridging' of coating material between projections imaged after coating with 2.5x107 PFU MVA.PbCSP + 1% w/v MC. (D-E) Secondary electron SEM images indicating vaccine dose, and vector/prep-specific differences in Poxvirus coating uniformity. SEM was performed at 15kV and at a 45° tilt with the assistance of X. Chen and H. Corbett.

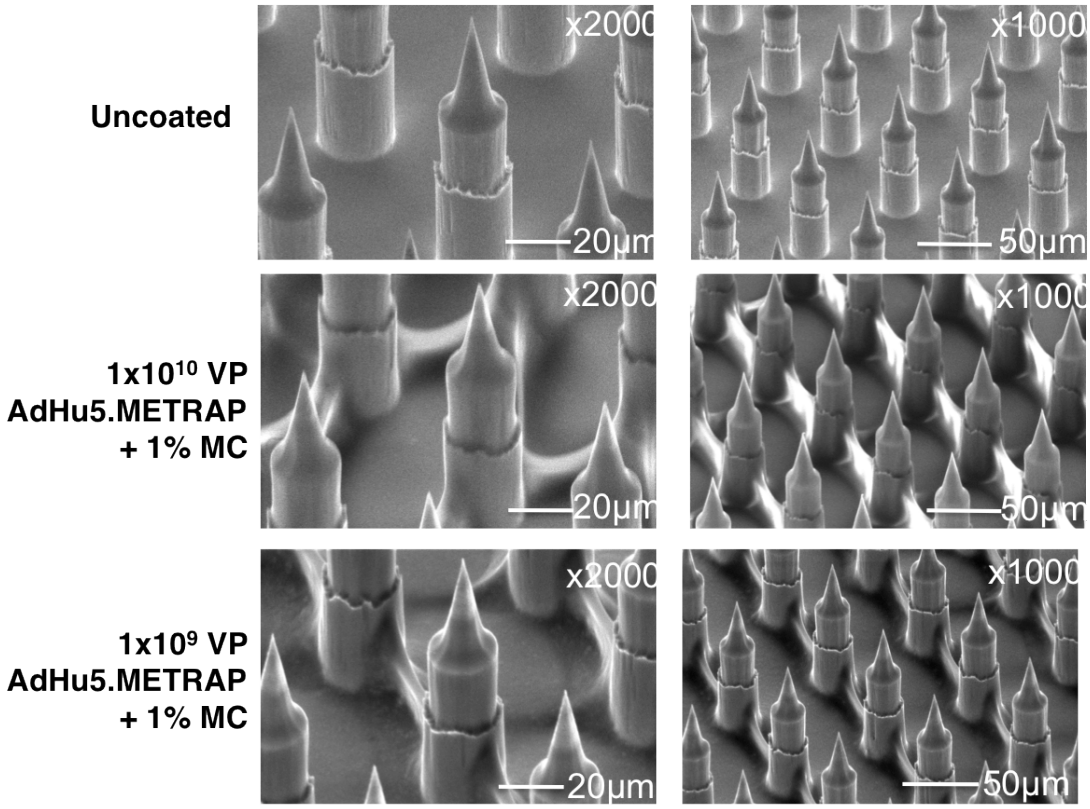

FIGURE 5-10: Ad-vectored vaccine can be dry-coated onto NP110 microprojections in formulation with 1% $^{w}/_{v}$ MC at both higher and lower doses.

(A) Secondary electron SEM image of uncoated NP110 microprojection at two magnifications. (B) SEM (secondary electron) images of an NP110 patch following dry-coating with 1x10^{10}VP (B), or 1x10^{9} VP (C) AdHu5.ME-TRAP. Percentages of MC are $^{w}/_{v}$. SEM was performed at 15kV and at a 45° tilt with the assistance of M.Crichton.

These early observations served to highlight that vector type and formulated dose are factors in the efficiency and consistency of microprojection coating with viral vector vaccines, with MVA formulations considerably more viscous and coating less uniform than Ad formulations. To address this issue, attempts were made to improve the morphology of MVA coating. SEM analysis revealed that decreasing the proportion of the viscosity enhancer MC in the coating solution to decrease overall viscosity did not prevent bridging of coating material between microprojections (not here shown) so the concentration was kept constant at 1% $^{w}/_{v}$. However, addition of the non-ionic surfactant Polysorbate 20 (PS20) was included to improve the surface contact between the coating material and the silicon microprojection during the dry-coating process and therefore to reduce aggregation of the material on top of or between projections, or on the patch base, but rather allow even deposition of material on the shafts. Polysorbates are commonly used in biopharmaceutical preparations to prevent particle aggregation and surface adsorption and conveys an effect at particularly low concentrations (334). A preliminary SEM analysis where PS20 was includedat a range of concentrations revealed optimal microprojection coating and minimal base coating when 0.1% $^{v}/_{v}$. PS20 was used (not shown).

However it is acknowledged that the concentration required for optimal reduction of surface tension between the coating solution and the silicon base may vary with initial viscosity of coating solution e.g. with different formulated doses and so should be determined for each formulation.

To demonstrate this improvement, NP110 patches were coated with $1x10^7$ PFU MVA.PbCSP + 1% $^{w}/_{v}$ MC with and without the addition of 0.1% $^{v}/_{v}$ PS20 (Figure 5-11) and compared with an uncoated patch (Figure 5-11A). Solutions containing MC or PS20 with no vaccine efficiently and uniformly coat microprojections without excess material on the base, confirming that the non-uniform coating previously observed was due to the inclusion of high viscosity vaccines preps rather than the addition of excipients (Figure 5-11, B+C). Vaccine formulations lacking PS20 demonstrated bridging of material between microprojections was observed as before, either between tips (Figure 5-11, Di) or between shafts (Figure 5-11, Dii). However, when PS20 was included, microprojections were efficiently coated with no bridging of material (Figure 5-11E). Though there was some material on the base, a much higher proportion was coated onto microprojection shafts than without surfactant, and importantly, tips remained sharp.

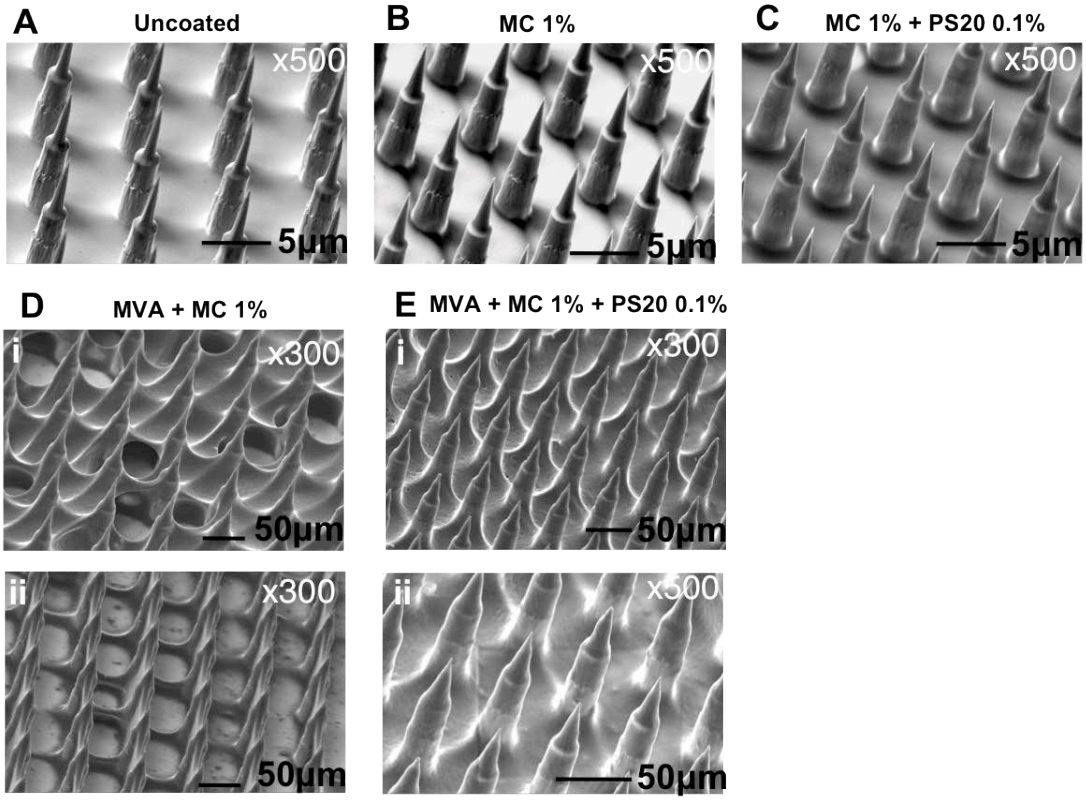

FIGURE 5-11: The surfactant Polysorbate 20 improves microprojection coating when formulated with MVA vaccine.

NP110 patches were dry-coated with $1x10^7$ PFU MVA.PbCSP + 1% $^{w}/_{v}$ MC ± 0.1% $^{v}/_{v}$ PS20 and imaged using a Scanning Electron Microscope (45° tilt, 15kV). Secondary electron images are presented. (A) An uncoated NP110 patch, cleaned with glycerol water (B) NP110 microprojections coated with 1% $^{w}/_{v}$ MC only (C) NP110 microprojections coated with 1% $^{w}/_{v}$ MC + 0.1% $^{v}/_{v}$ PS20 only (D) NP110 microprojections coated with 1% $^{w}/_{v}$ MC + $1x10^7$ PFU MVA.PbCSP without PS20, and (E) NP110 microprojections coated with 1% $^{w}/_{v}$ MC + $1x10^7$ PFU MVA.PbCSP + 0.1% $^{v}/_{v}$ PS20. SEM by X.Chen and S.Yukiko.

5.3.3.3 Confocal microscopy confirmation of coated Ad vaccine delivery in the vicinity of CD207+ cells

Confocal microscopy was used to confirm delivery of dry-coated Ad-vectored vaccine to the skin following velocity application of NP110 (Figure 5-12). NP110 were coated with $2.5x10^9$ VP AdHu5.ME-TRAP in 1% $^{w}/_{v}$ MC + 0.1% $^{v}/_{v}$ PS20 and applied to BALB/c mouse ears using the applicator device. Twenty minutes following immunisation mice were euthanised and ears excised, split along the coronal plane and the cartilage removed, leaving SC, VE and dermis as one whole section. Ear sections were fixed and stained with fluorescent monoclonal antibodies raised against MHC II, CD207 (Langerin) and with rabbit α-hexon IgG. The hexon is one the major Adenovirus capsid surface proteins. A secondary stain was specific for α-rabbit IgG, and allowed fluorescent identification of hexon protein. Sections were counterstained with the nuclear DNA stain Hoechst 33342, before imaging using a Zeiss confocal microscope (D^2G^2) at a tissue depth of approx 30μm. Example images are shown in Figure 5-12.

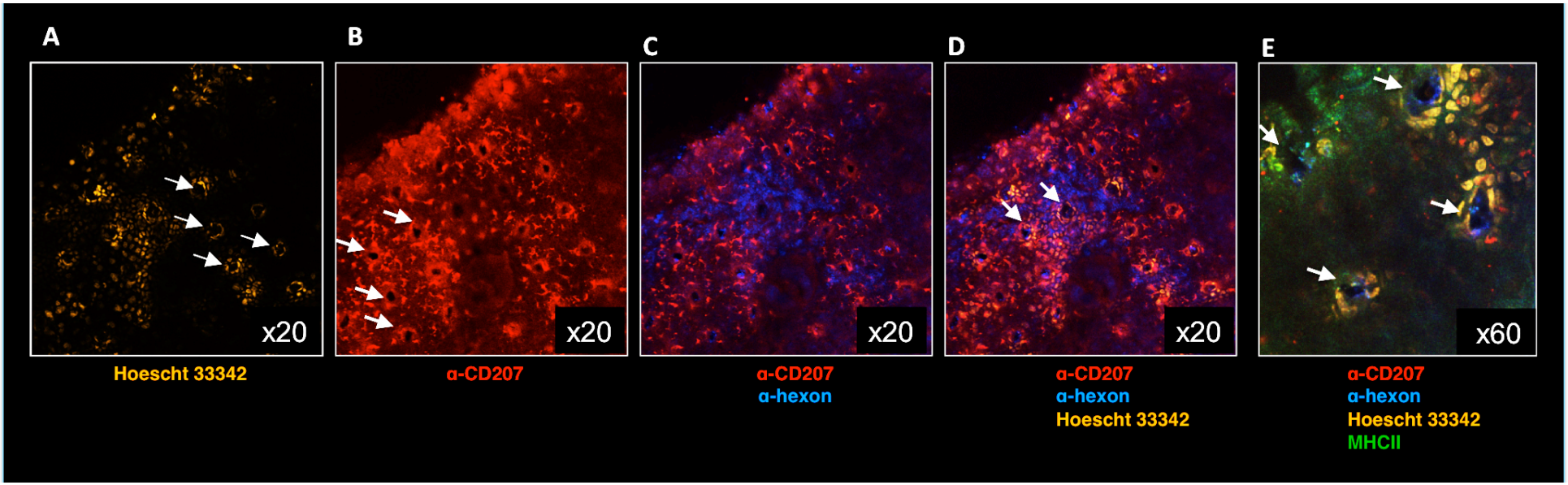

FIGURE 5-12: Confocal imaging of coated Ad-vectored vaccine delivery to murine skin.

NP110 were coated with $2.5x10^9$ VP AdHu5.ME-TRAP in 1% $^{w}/_{v}$ MC and 0.1% $^{v}/_{v}$ PS20 and applied to female BALB/c ears using at $1.96ms^{-1}$. Twenty minutes following immunisation mice were euthanized and ears were excised, before marking the patched side of the ear pinnae (ventral side) and fixing in 2% paraformaldehyde in PBS for 1 hour under agitation. Ear pinnae were split laterally and the cartilage and unpatched side was removed under a dissecting microscope. Patched sections were blocked with 5% BSA/TBS, permeablised using 0.25% Triton X/TBS and stained with MHC II-FITC, CD207-Alexa Fluor 546 and rabbit anti-Hexon IgG. A secondary stain included anti-rabbit Alexa Fluor 633. Ears were counterstained using Hoescht 33342 before imaging using a Carl Zeiss LSM510 confocal microscope, D^2G^2, University of Queensland (at a depth below surface of SC ~30μm). Excitation wavelengths as follows: Hoescht 33342 - Chameleon Ti/sapphire laser, 780nm, FITC - Argon 488nm, Alexa Fluor 546 - HeNe 556nm, Alexa Fluor 633 - HeNe 632nm.

Hoechst staining revealed the creation of microchannels through the tissue characterised by evenly spaced circular gaps in staining as indicated by arrows in Figure 5-12A. These gaps were spaced corresponding to the spacing of microprojections (70μm). Figure 5-12B shows these microchannels are located amongst the highly structured network of CD207+ dendritic cells characteristic of the VE and dermis and also the co-localisation of hexon staining amongst these cells (Figure 5-12C, and with Hoescht 33342 - D)(335). Figure 5-12E shows 4 such microchannels in high magnification, with hexon staining observed on the inside of the microchannel. These images confirm that coated Ad-vectored vaccine is removed from microprojections following insertion into and removal from the skin, and removed material is deposited into tissue rich in CD207+ cells.

5.3.3.4 Dry-coated MVA and Ad release from microprojections into the skinis dependent upon vectortype and coated dose

After demonstrating that dry-coated Ad payload is delivered into the skin, an experiment was performed to quantify the delivery efficiency of both Ad and MVA-vectored microprojection-coated NP110 (Figure 5-13A+B). A second experiment aimed to investigate if the previously observed qualitative dose-specific differences in MVA coating morphology translated to a difference in delivery efficiency by quantifying delivery efficiency following coating of 2 doses of MVA.PbCSP (Figure 5-13, C+D).

In the first experiment, NP110 were coated with 8μL undiluted vaccine (MVA.PbCSP, MVA.ME-TRAP, AdCh63ME-TRAP or AdHu5.ME-TRAP, of differing viral titres) + 1%$^{w}/_{v}$ MC + 0.1% $^{v}/_{v}$PS20, co-formulated with 6nCi ^{14}C-OVA per patch. Following immunisation of BALB/c mouse ears using velocity application of NP110, ears, used patches and swabs (2 swipes of a cotton bud recovered non-internalised, surface-located vaccine) were collected and measured for β-emission using a scintillation counter. Percentage delivery efficiency (the proportion internalised within the ear) was calculated from the sum of the scintillation counts from solubilised ears, swabs and used patches ('100%'). Percentages remaining on the patch, and removed by swab were also calculated and are presented in Figure 5-13A.

Of the four vaccine preps tested, the two Ad-vectored vaccines delivered a greater proportion of^{14}C-OVA into ear skin than the two MVA-vectored preps (17.1% and 14.8% compared to 2.8% and 1.3%) supporting the earlier qualitative SEM observations on coating morphology differences between the two types of vaccine. There was very little difference in delivery efficiency between the two Ad or the two MVA preps. Both MVA vaccine preps had a similar viral titre and so coated doses were similar: 2.3x10^{7} PFU MVA.ME-TRAP, and 3.6x10^{7} PFU. The AdHu5.ME-TRAP immunising dose was significantly lower than AdCh63.ME-TRAP due to differences in stock titre (5x10^{7}VP compared to 1x10^{10} VP), but there was no statistically significant difference in delivery efficiency, though slightly more AdHu5.ME-TRAP was delivered into the ear, whereas slightly more AdCh63.ME-TRAP remained on the surface (Figure 5-13 Bi+ii). However, an equivalent amount was released from microprojections, which was significantly more than for either MVA vaccine (Figure 5-13, Biii).

In a separate experiment, mice were immunised with 5x10^{7} PFU or 1x10^{6} PFU MVA.PbCSP by velocity applied NP110 (coated with 1% $^{w}/_{v}$ MC, 0.1% $^{v}/_{v}$PS20 and

6nCi ^{14}C-OVA per patch). The delivery efficiency was determined by radiometric assay as earlier described. The average percentage of ^{14}C-OVA delivered into the ear was dose-dependent, with 1.2% of $5x10^7$ PFU, and 17.62% of $1x10^6$ PFU, delivered into the ear ($P<0.0001$). Application of NP110 coated with $5x10^7$ PFU also resulted in low deposition of vaccine on the surface of the ear after application (0.6%) and the majority of material remaining on the Nanopatch (>98%). Application of a coated dose of $1x10^6$ PFU resulted in 77% of the material remaining on the patch, and a greater proportion remaining on the ear surface than the higher dose ($P=0.0009$, Figure 5-13D).

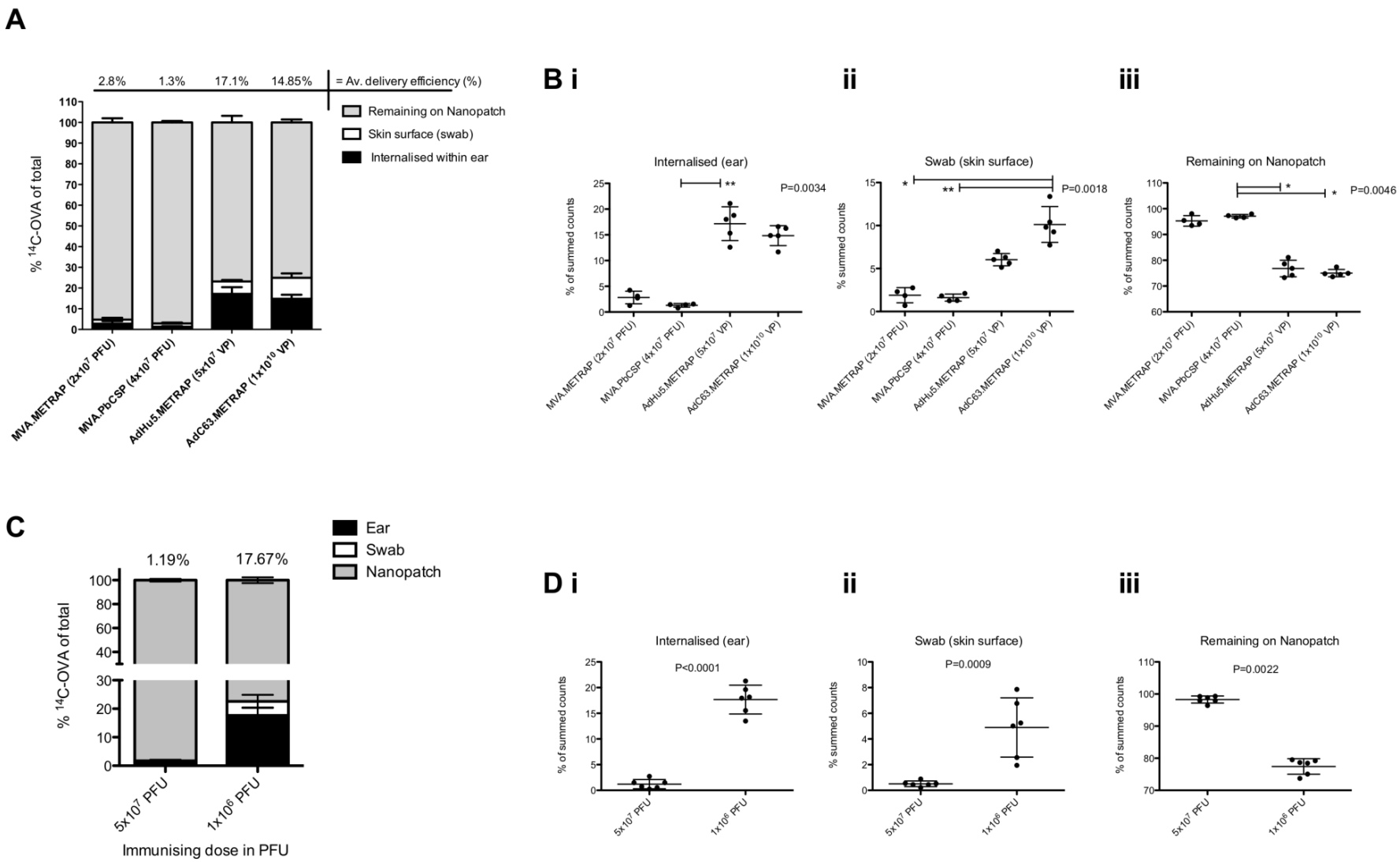
A
2.8%
1.3%
17.1%
14.85%
= Av. delivery efficiency (%)
Remaining on Nanopatch
Skin surface (swab)
Internalised within ear
% 14C-OVA of total
MVA.METRAP (2x10^7 PFU)
MVA.PbCSP (4x10^7 PFU)
AdHu5.METRAP (5x10^7 VP)
AdC63.METRAP (1x10^10 VP)
B i
ii
iii
Internalised (ear)
Swab (skin surface)
Remaining on Nanopatch
% of summed counts
P=0.0034
P=0.0018
P=0.0046
C
Ear
Swab
Nanopatch
1.19%
17.67%
% 14C-OVA of total
5x10^7 PFU
1x10^6 PFU
Immunising dose in PFU
D i
ii
iii
Internalised (ear)
Swab (skin surface)
Remaining on Nanopatch
P<0.0001
P=0.0009
P=0.0022

FIGURE 5-13: Delivery efficiency of vaccine-coated NP110 delivered at velocity by spring-loaded applicator is vaccine and dose-dependent.

(A) NP110 (n=4/5) were coated formulations containing 8µL of undiluted MVA.PbCSP, MVA.ME-TRAP, AdHu5.ME-TRAP or AdCh63.ME-TRAP, 1% $^{w}/_{v}$MC, 0.1% $^{v}/_{v}$ PS20 and 6Ci/µL of the radiolabelled ovalbumin (^{14}C-OVA). Following velocity application, ears were swabbed lightly twice using a cotton bud to remove coating material remaining on the skin surface. Mice were euthanised and ears were excised before solubilisation using the organic base Solvable® (60°C, 2 hours). Elutions from used patches, swabs and ear skin solutions were each measured for scintillation counts. The sum of the radioactive counts from used patches, ears and swabs was calculated and summed and % delivery into the ear/remaining on the swab/remaining on the patch of the sum of the total scintillation count (used patch + swab + solubilised ear) is presented. P<0.05 by Kruskall Wallis + Dunn's comparison. (B) In a second experiment NP110 were coated with MVA.PbCSP (+ ^{14}C-OVA, 1% $^{w}/_{v}$ MC + 0.1% $^{v}/_{v}$ PS20) and delivered to female BALB/c mice ears (n=6) as before. Vaccines were delivered at two immunising doses – 5x10^{7} PFU and 1x10^{6} PFU. Methodology was as above. P<0.05 by unpaired t test (B, i+iii) or Mann Whitney U test (B, ii). Experiments carried out by C. McNeilly and S. Yukiko.

5.3.3.5 Viability of vaccines in formulation and after dry-coating

Poxviruses have a highly complex structure with a robust outer membrane composed primarily of lipids (336). Considering that polysorbates can act as detergents due to their ability to lower surface tension and allowing interaction of water with lipids, it was investigated if PS20, alone or in formulation with methyl cellulose would have an inhibitory effect upon MVA viral viability. Others have reported a loss of inactivated influenza vaccine stability upon formulation with the viscosity enhancer Carboxymethyl Cellulose (CMC), a similar compound to MC (162).

Figure 5-14A shows viral titres following mixing of MVA expressing the fluorescent transgene GFP with 1% $^{w}/_{v}$ MC alone, 0.1% $^{v}/_{v}$PS20 alone, or in a coating formulation containing both MC + PS20. Formulations were added to CEF monolayers in a GFP plaque assay, where plaques were counted by fluorescent microscopy. All formulations exhibited equivalent ability to infect CEF and express the transgene compared to unformulated MVA.GFP, indicating that neither MC nor PS20 have an inhibitory effect upon MVA viability at the concentrations used in Nanopatch coating formulations.

To investigate if dry-coating had a detrimental effect upon MVA viability, vaccine formulations containing MVA.GFPwere coated onto NP110 microprojections (+1% $^{w}/_{v}$ MC with or without 0.1 $^{v}/_{v}$ PS20). Coated material was immediately eluted and to CEF monolayers GFP plaque assay as before. Unformulated virus and coating formulations were also assayed. Titres reclaimed from dried formulations lacking PS20 were statistically significantly lower than that of the coating formulation prior to dry-coating, and than unformulated virus (P=0.001, Figure 5-14B). However, the titre reclaimed from dried formulation containing both MC and PS20 was equivalent to that prior to drying or to unformulated virus. This suggests a role for PS20 in protection during drying, perhaps by decreasing aggregation of viral particles, and hence increasing viability of eluted viruses.

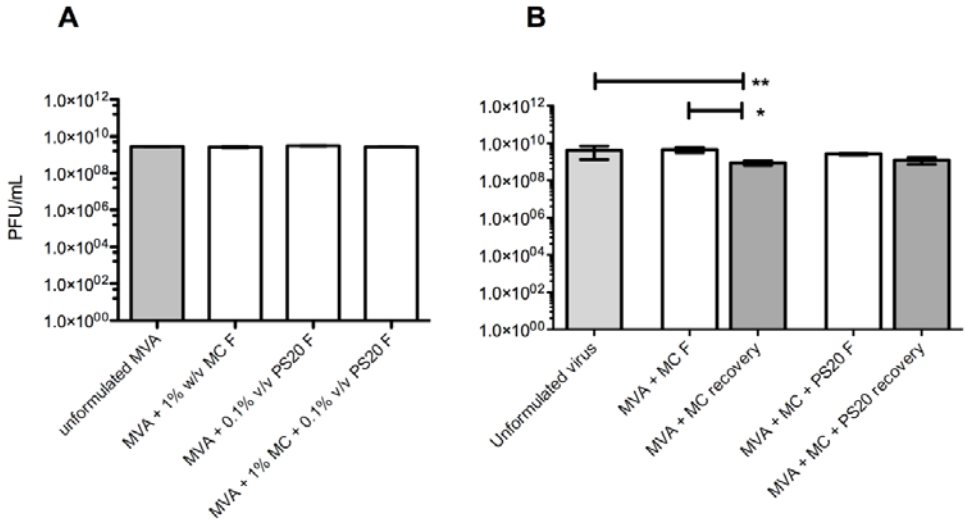

FIGURE 5-14: MVA can be coated onto and recovered from Nanopatch microprojections without loss of viability.

(A) MVA expressing the reporter transgeneGreen Fluorescent Protein (GFP) was mixed with 1% $^{w}/_{v}$ MC , 0.1% $^{v}/_{v}$ PS20 or both and used to infect CEF in a plaque assay. Green plaques were visualised by fluorescence microscopy 2 days following MVA infection and subsequent CMC overlay. Unformulated MVA.GFP (light grey bar) was also assayed. Bars are median titres (PFU/mL) from 2 replicate wells ± range. 'F' = coating formulation. (B) MVA.GFP (1x10^6 PFU) was coated onto NP110 microprojections with 1% $^{w}/_{v}$ MC or with 1% $^{w}/_{v}$ MC + 0.1% $^{v}/_{v}$ PS20. Coated material was immediately eluted from NP110 microprojections into PBS. Unformulated virus (light grey bar, n=4) Coating formulations ('F', open bar, n=2) and post-coating eluates ('recovery', dark grey bar, n=10) were added onto CEF monolayers in a fluorescent plaque assay as described above. Bars represent mean titres (PFU/mL) ± SD. P=0.001 by Kruskall Wallis + Dunn's comparison.

Most Adenoviruses are naturally transmitted between humans within aerosols whereas Poxviruses are extremely large, structurally robust viruses and can undergo complete desiccation within dermal scabs (337). Because of this, it was hypothesised that Adenoviruses would be less resistant to physical stresses during the dry-coating process. In previous studies of liquid Ad stabilisation, the non-reducing disaccharides trehalose and sucrose ($C_{12}H_{22}O_{11}$) were found to improve viral recovery after freeze-thaw, where changes in pH are the cause of destabilisation (338, 339). Dry formulation of Ad vaccine with 10% $^{w}/_{v}$ sucrose + 10% $^{w}/_{v}$ trehalose (0.25M) permitted long-term thermostability (331). Thus, the ability of trehalose and sucrose to mediate a protective effect during formulation and/or dry coating of Ad vaccines was assessed.

Formulations containing AdCh63.ME-TRAP were overlaid on confluent monolayers of 293A cells before fixing and immunostaining with rabbit anti-hexon IgG + goat anti-mouse IgG-HRP conjugated secondary before substrate development. Stained cells indicate infection by a single Ad virus or 'infectious unit', IU. Figure 5-15A demonstrates that mixing Ad with 1% MC with or without 0.1% PS20 had a minimal

effect upon viral titre as compared to unformulated Ad (ns, P=0.081, Figure 5-15A). Additionally, formulation with 10% $^{w}/_{v}$ trehalose, 10% $^{w}/_{v}$ sucrose, or both sugars combined (each 10% $^{w}/_{v}$) had no effect upon viral titre after mixing (P=0.081). In the same experiment, formulations with a range of concentrations of trehalose + sucrose were assessed (20%-2% $^{w}/_{v}$), to assess whether viability could be further improved, since trehalose has also been shown to decrease aggregation of VLP in solution (340). However, all formulations exhibited equivalent viral titres, which were equivalent to unformulated Ad with no statistically significant differences (not shown). These results indicate that mixing of Ad with MC + PS20 does not decrease viability, and that trehalose and sucrose have no effect at the formulation stage.

In a separate experiment, NP110 were coated with $1x10^{7}$ VP AdCh63.ME-TRAP in formulation with 1%$^{w}/_{v}$ MC, + 0.1%$^{v}/_{v}$ PS20, with 10% $^{w}/_{v}$ trehalose, 10% $^{w}/_{v}$ sucrose or both sugars combined (10% $^{w}/_{v}$ each). Coated material (from 4 patches per group) was immediately eluted into PBS from microprojections. Eluates were added to confluent monolayers of 293A cells before hexon immunostaining as before. Without stabilisation, Ad titres were significantly reduced, but formulation with stabilising sugars resulted in an improved recovery of infectious viral titre as compared to the unstabilised formulation. This improved recovery was statistically significant for addition of 10% $^{w}/_{v}$ trehalose, and 10% $^{v}/_{v}$ trehalose + sucrose (P=0.0092, Figure 5-15B), but not for 10% $^{w}/_{v}$ sucrose alone. These data indicate that a combination of trehalose and sucrose is optimal of the formulations tested in providing protection during drying of Ad. The protective effect is conferred at the drying stage, since the sugars demonstrated no effect on Ad titres after mixing with excipients (prior to dry-coating).

Another experiment aimed to investigate the effect of trehalose upon the magnitude of the resulting immune response following immunisation with Ad and MVA-vectored vaccine expressing Pb9. Mice were immunised with NP110 coated with either $4.5x10^{9}$ VP AdCh63.ME-TRAP or $1x10^{7}$ PFU MVA.PbCSP + 1% $^{w}/_{v}$ MC + 0.1% $^{v}/_{v}$ PS20 and with concentrations of trehalose ranging from 0% to 10% $^{w}/_{v}$ NP110 were applied using the velocity application method. Trehalose was also added to liquid vaccine dilutions and PBS, which were delivered ID. Mice were euthanised at the peak of the response (21 days post-Ad, 7 days post-MVA) and spleens were harvested for Pb9 stimulation and IFN-γ ELISPOT. Inclusion of trehalose in the AdCh63.ME-TRAP coating solution markedly improved its immunogenicity. Whilst unstabilised vaccine was not immunogenic, the stabilised response was improved with increasing concentrations of trehalose, and coated NP110 formulations containing 10% $^{w}/_{v}$ trehalose were as immunogenic as ID immunisation (Figure 5-15C, P=0.0425, comparing NP110 0% to NP110 10%). There was no statistically significant relationship between trehalose concentration and magnitude of response (P=0.764).

By contrast, immunogenicity of MVA.PbCSP was not enhanced with the addition of trehalose, as the dry-coated, unstabilised formulation was able to prime a response similar to MVA.PbCSP delivered ID. Responses were not altered significantly with increasing concentrations of trehalose in either group (P= 0.183, Figure 5-15D). Addition of trehalose to PBS did not induce responses, and that ID responses were not significantly altered by trehalose inclusion indicates that the improvement observed with coated Ad was due to protection during dry-coating.

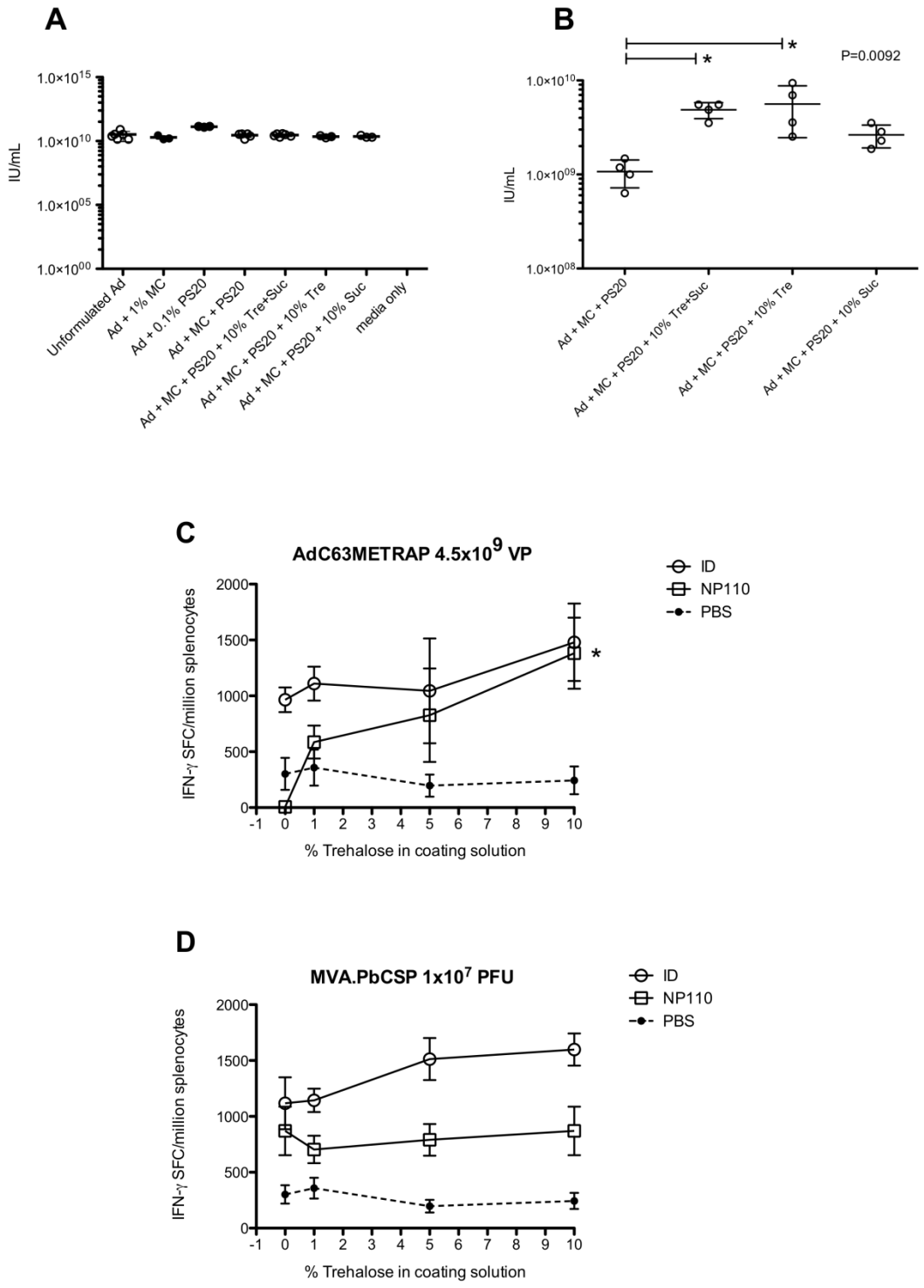

FIGURE 5-15: The disaccharides trehalose and sucrose mediate a protective effect upon dry-coating of Ad-vectored vaccine onto NP110 microprojections.

(A-C) Hexon immunoassays were carried out to assess the effect of formulation of AdCh63.ME-TRAP with MC, PS20 and the disaccharides sucrose and trehalose. (A-B) Hexon immunoassays were performed to ascertain any effect of coating excipients upon virus

viability. AdCh63.ME-TRAP-containing formulations were overlaid on confluent monolayers of 293A cells before fixing and immunostaining with rabbit α-hexon IgG + goat α mouse IgG HRP and DAB substrate development. Viral titres are expressed as infectious units (IU)/mL ± SD. Wells containing media only served as negative controls. (C) Hexon immunoassays carried out after dry-coating of AdCh63.ME-TRAP ($1x10^7$ PFU per patch) in various formulations. Material was immediately eluted from NP110 microprojections following coating. *P=0.0092 by Kruskall Wallis + Dunn's comparison. (C-D) To assess the effect of formulating Ad and MVA-based vaccines with stabilising disaccharide trehalose, female BALB/c mice age 6-8 weeks (n=3) were primed with $4.5x10^9$ VP AdCh63.ME-TRAP (C) or $1x10^7$ PFU MVA.PbCSP (D) by vaccine-coated NP110 (+1% MC + 0.1% PS20) with concentrations of trehalose ranging from 0% to 10% $^w/_v$, applied using the velocity method. Trehalose concentrations were also added to liquid vaccine and to PBS, delivered ID. Mice were euthanised at the peak of the response (AdCh63 – 21 days, MVA – 7 days), and spleens were harvested for Pb9 stimulation and IFN-γ ELISPOT. Symbols represent mean SFC/million splenocytes ± SD. *=P=0.0 425 by Kruskall Wallis with Dunn's comparison, compared to 0% $^w/_v$ trehalose.

5.3.3.6 Long term thermostability of Ad-vectored vaccine by trehalose and sucrose

Trehalose and sucrose have been found to stabilise lyophilised Ad vaccine at 45°C for up to 6 months - highly desirable in the development of an easily distributable vaccine for malaria, which affects countries frequently experiencing ambient temperatures exceeding 35°C (331). Experiments were designed to assess the long-term stability of an Ad-vectored vaccine, with and without disaccharide stabilisation. In the first experiment, NP110 were coated with $1x10^9$ VP AdCh63.ME-TRAP per patch + MC + PS20 (in previously described concentrations) + 10% $^w/_v$ trehalose, 10% $^w/_v$ sucrose or both disaccharides combined. Coating material was either eluted from patches immediately after coating, or stored at room temperature in a sealed container with hygroscopic salt lithium chloride, (maintaining constant humidity of 11%) and coating material eluted 1 week, or 3 weeks after coating. Hexon immunoassays were performed at these timepoints to assess the viability of the recovered Ad in IU/mL (Figure 5-16A). At all timepoints, the viral titre recovered following coating with the stabilised (10% $^w/_v$ trehalose and sucrose) formulation were significantly improved compared to unstabilised vaccine (*P=0.092 at 0 weeks, **P=0.0027 at 1 week, and 3 weeks). After immediate elution only, stabilisation with trehalose alone resulted in asignificantly improved titre as compared to unstabilised Ad (*P=0.092, Figure 5-16).

In longer-term stability studies, formulations containing a combination of trehalose and sucrose (10%$^w/_v$each) were able to stabilise AdCh63.ME-TRAP for up to 10 weeks with minimal loss in viability (less than 2 logs when stored at RT, and less than 0.5 $\log_{10}$ at 37°C). Contrastingly, unformulated Ad was rendered completely inactive by 7 weeks when stored at RT and by 1 week at 37°C (Figure 5-16 B+C). The difference in vaccine viability between stabilised and unstabilised was statistically significant after 4 weeks of storage at RT (**P=0.0061, Figure 5-16B) and completely abrogated by 7 weeks. After 10 weeks of storage at 37°C the unstabilised viral titre was statistically significantly reduced as compared to stabilised vaccine (*P=0.0061, Figure 5-16C), which was not reduced below 1 $\log_{10}$ viral particles throughout the 10 weeks (grey area).The actual reduction from week 0 to week 10 was 0.75 $\log_{10}$. The heat stability requirement for another live viral vaccine in freeze-dried formulation (measles) is viral loss must not exceed 1 $\log_{10}$ viral

particles after 7 days storage at 37°C (341). Our formulation exceeds this requirement by 9 weeks.

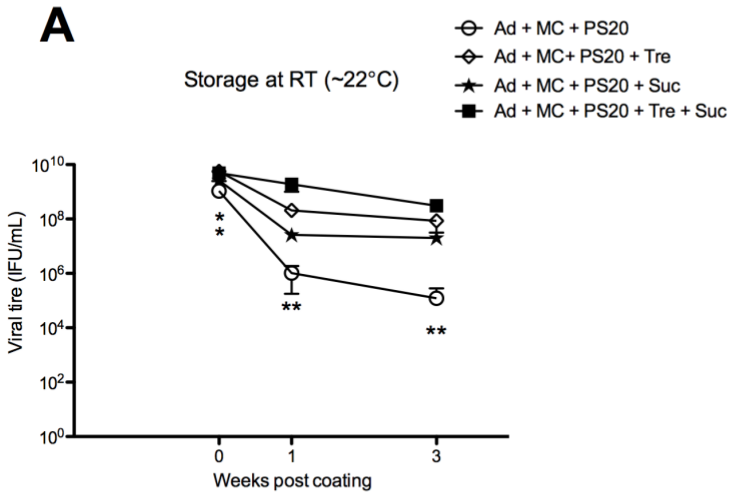
A
Storage at RT (~22°C)
Ad + MC + PS20
Ad + MC+ PS20 + Tre
Ad + MC + PS20 + Suc
Ad + MC + PS20 + Tre + Suc
Viral tire (IFU/mL)
Weeks post coating

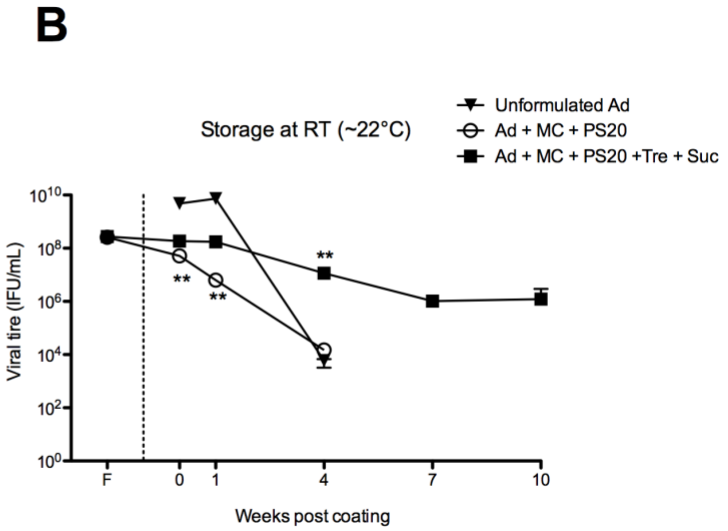
B
Storage at RT (~22°C)
Unformulated Ad
Ad + MC + PS20
Ad + MC + PS20 +Tre + Suc
Viral tire (IFU/mL)
Weeks post coating

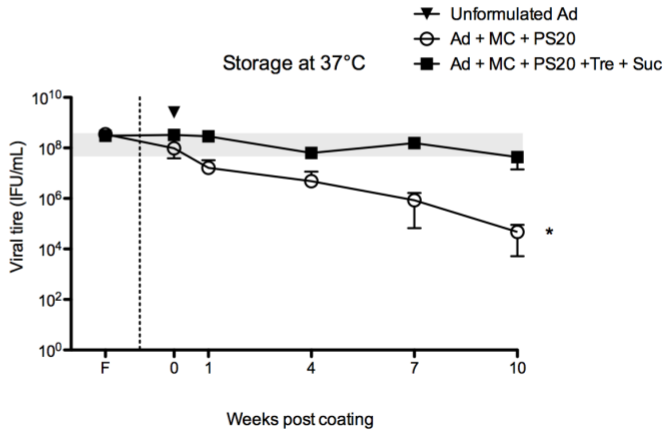
C
Storage at 37°C
Unformulated Ad
Ad + MC + PS20
Ad + MC + PS20 +Tre + Suc
Viral tire (IFU/mL)
Weeks post coating

FIGURE 5-16: Formulation with the disaccharides trehalose and sucrose mediates long-term thermostability of microprojection coated simian Ad-vectored vaccine.

(A) $1x10^9$ VP AdCh63.ME-TRAP were coated onto NP110 (n=4) as formulated with 1% $^{w}/_{v}$ MC, 0.1% $^{v}/_{v}$ PS20, + 10% $^{w}/_{v}$ sucrose + trehalose (0.25M), or 10% $^{w}/_{v}$ each disaccharide separately. Formulations were immediately eluted from 4 patches (timepoint '0') into PBS or were stored at RT (~22°C) in sealed containers containing hygroscopic lithium chloride salts to maintain a constant relative humidity of 11%. Coated formulations of stored patches (n=4 per timepoint) were eluted into PBS at 1 week, or 3 weeks after coating. Eluates were incubated on confluent monolayers of 293A cells in a hexon immunoassay. *=P=0.0092 / **=P=0.0027/ by one way ANoVA + Bonferonni's comparison. (B+C) NP110 Nanopatches (n=4/group/timepoint) were coated with $1x10^9$ VP AdCh63.ME-TRAP + 1% $^{w}/_{v}$ MC ± 10% $^{w}/_{v}$ trehalose + sucrose. Formulations were immediately eluted from 4 patches (timepoint '0') into PBS, or were stored at room temperature (B) or at 37°C (C) in sealed containers at a constant relative humidity of 11%. Coated formulations were eluted into PBS at 1, 4, 7 or 10 weeks after coating. Eluates (or formulations prior to coating – 'F') were added to 293A monolayers in hexon immunoassays as detailed above. **P=0.0054 by one way ANoVA (B), *=P=0.028 by Mann Whitney U test (C). Grey portion in (C) refers to the range of titres fulfilling the heat stability requirement set by the WHO for the storage of another live viral vaccine (freeze-dried measles) i.e. vaccine viability should not decrease more than 1 log_{10} in 7days of storage at 37℃ (341). Assays carried out by C. Primiero.

In summary, dry-coating of Ad-based vaccines reduces viral viability, which can be recovered by addition of trehalose and sucrose, particularly when combined. Disaccharide stabilisation also permits long-term stabilisation of Ad-coated Nanopatches for up to 10 weeks at 37°C.

5.3.3.7 Summary of section 5.3.3

- Velocity application of NP110 demonstrated efficient perforation of the SC consistently across the area beneath the patch, with maximum penetration resticted to the dermis and with and dye delivery into both the VE and dermis.
- Viral vector vaccines were successfully coated onto NP110 microprojections. Coating morphology was vector- and dose-specific (with Ad>MVA and lower dose MVA>higher dose MVA in terms of microprojection coverage). Coating was improved when the surfactant PS20 was included.
- Coated vaccine (MVA) was removed upon insertion into murine skin, and coated Ad was deposited into tissue rich in CD207+ cells after patch application.
- In accordance with the qualitative SEM observations, the delivery efficiency was greater when Ad and lower dose MVA formulations were coated (~15-17%) than higher dose MVA formulations (1.19%), with the majority of coated material remaining on the patch.
- Viral vectors remained viable following formulation with MC and PS20 and retained the ability to infect cells and express recombinant transgene. Recovered MVA titres were improved with the addition of PS20, and the stabilising sugars trehalose and sucrose were a requirement for protection of Ad during dry-coating.
- Trehalose and sucrose inclusion afforded long term thermostability for Ad formulations, with approximately 0.75 log_{10} viral loss after 10 weeks of storage at 37°C (exceeding the WHO requirement for heat stability of another live viral vaccine - (341)).

5.3.4 Immunogenicity and protective efficacy of velocity-applied dry-coated Nanopatch

5.3.4.1 MVA / MVA immunisation

Vaccine-coated Nanopatches were evaluated in immunogenicity and challenge experiments in homologous prime-boost immunisation. Figure 5-17 demonstrates immunogenicity of MVA.PbCSP prime-boost immunisation, where the prime only, or both the prime and boost are delivered by vaccine-coated NP110, delivered at velocity. BALB/c mice (n=10/5) were primed with doses of $1x10^6$ PFU (n=5), or $5x10^7$ PFU (n=10) MVA.PbCSP - either ID, or by dry-coated NP110. These immunising doses correspond to delivered doses of $5.9x10^5$ PFU, and $1.8x10^5$ PFU, respectively –Figure 5-13. An IFN-γ ELISPOT was performed 7 days post-immunisation (Figure 5-17A). NP110 immunisation successfully primed a Pb9-specific response in all mice, and at both doses. However, though $5x10^7$ PFU primed responses similar to ID priming with either dose, but NP110 priming with $1x10^6$ PFU induced significantly lower responses than both ID groups (P=0.0162). Two weeks after the prime, groups of ten were split into 2 groups of 5 and all mice were boosted either ID or by NP110 coated with $1x10^6$ PFU or $5x10^7$ PFU MVA.PbCSP to investigate both NP110/ID and NP110/NP110 prime-boost combinations. An IFN-γ ELISPOT performed 2 weeks following the boost revealed that NP110/ID immunisation induced levels that were slightly lower but not statistically significantly lower than ID immunised groups at both doses (Figure 5-17B). NP110 priming with $5x10^7$ PFU was slightly improved over priming with $1x10^6$ PFU (ns). When NP110-primed responses were boosted with NP110 with boosting doses of $1x10^6$ PFU or $5x10^7$ PFU boosting with either dose was inefficient, and post-boost responses were significantly decreased as compared to all ID immunised groups (P<0.0001, Figure 5-17C).

Immunised mice in this experiment were challenged with 1000 *P. berghei* sporozoites. (Figure 5-17, D+E) Priming with $5x10^7$ PFU (delivered dose $5.9x10^5$ PFU) induced protection in 40% of mice, and priming with $1x10^6$ PFU ($1.8x10^5$ PFU) was 20% protective, when the boost immunisation was given ID. This was compared to 20% ($5x10^7$ PFU) and 60% ($1x10^6$ PFU) after ID/ID immunisation. No NP110/NP110 regimes demonstrated protection against acquisition of blood stage parasites.

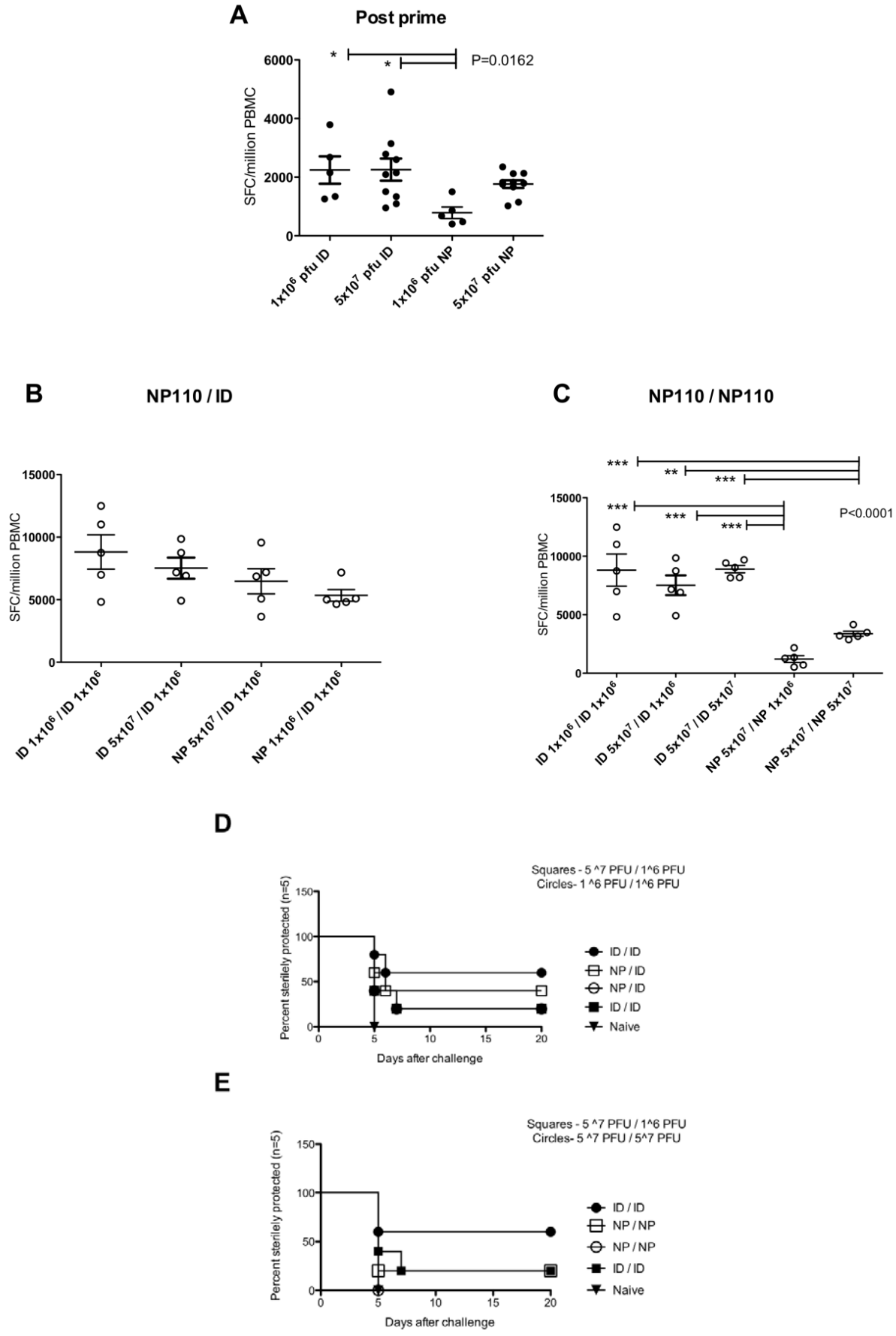

FIGURE 5-17: Nanopatch delivery of dry-coated vaccines in MVA/MVA immunisation, delivered

at velocity.
(A-C) Female BALB/c mice were primed with $5x10^7$ PFU (n=10) or $1x10^6$ PFU MVA.PbCSP (n=5), either by vaccine-coated NP110 or ID. Two weeks later, groups of 10 were split into two groups of 5 and all groups were boosted either with $1x10^6$ PFU ID, $1x10^6$ PFU by NP110 or $5x10^7$ by NP110. Blood was taken for isolation of PBMC and Pb9 stimulation in an IFN-γ ELISPOT was performed 1 week after the prime (B), or 2 weeks after the boost immunisation (C). Statistical comparisons were made using Kruskall Wallis with Dunn's comparison (A) or One way ANoVA with Bonferroni's comparison (B+C). (D+E) Immunised mice were challenged with 1000 *P.berghei* sporozoites 2 days after the post-boost bleed. Naïve animals were also challenged. All animals were monitored for 20 days following challenge for evidence of blood stage parasitaemia (by thin blood smear). Proportions of sterilely protected animals per group are represented as Kaplan Meier plots – (D) – NP110 / ID immunised groups, (E) NP110 /NP110 immunised groups. 'NP' = Nanopatch, NP110.

5.3.4.2 AdCh63 / MVA immunisation

Immunogenicity and protection against challenge following priming, and boosting of CD8+ responses by NP110 was assessed using the AdCh63/MVA heterologous regimen.Mice were immunised with $5x10^9$ VP AdCh63.ME-TRAP either ID or as coated onto NP110 microprojections as formulated with 1% $^w/_v$ MC, 0.1% $^v/_v$ PS20 and 10% $^w/_v$ sucrose+trehalose mixture. Using this exact formulation, an assessment of delivery efficiency was carried out using the radiolabelled carbon assay described in Figure 5-18. In this instance, delivery efficiency was found to be 11% (internalised within the ear, as a proportion of the total coated amount). Hence, in this experiment, ID-primed controls were included at both full dose ($5x10^9$ VP) and at 11% ($5.5x10^8$ VP) and at the boost - full dose ($2x10^7$ PFU) and 2.8% ($5x10^5$ PFU). The value of 2.8% for delivery of the boost vaccine, MVA.ME-TRAP was taken from the assay in Figure 5-13A. Hence, NP110-primed mice were boosted ID or by coated NP110, with $2x10^7$ PFU MVA.ME-TRAP. ID controls were boosted with either $2x10^7$ PFU, or $5x10^5$ PFU, accordingly. Dose adjustment of the ID control at the prime only was included as a control for NP110/ID immunisation, and dose adjustment of both prime and boost, to control for NP110/NP110 immunisation.

Blood was taken for Pb9-specific immunogenicity by IFN-γ ELISPOT 3 weeks post-prime, 2 days before the boost immunisation (8 weeks) and 2 weeks following the boost (Figure 5-18A). Week 3 responses from mice receiving the same treatment at the mice were pooled and are presented in Figure 5-18B. NP110-primed responses were equivalent to those primed with 11% of the dose formulated, supporting the value of 11% for the delivery efficiency of NP110 using this formulation. Full dose ID priming was only slightly higher than these groups, and not statistically significantly so. NP110-primed responses had a low level of variability, reiterating the consistency of the velocity application method. Responses contracted from week 3 to week 8, whereupon a boost immunisation was delivered. All responses were increased upon boosting, but the magnitude of the post-boost response was highly variable between groups (Figure 5-18A). Boosting of full dose ID primed responses with full dose ID was most successful, followed by ID/ID with dose reduction of the prime only, or the prime + boost: post-boost responses were equivalent between these groups. Though the NP/ID response after the boost was lower than ID/ID immunisation, only the full dose ID/ID post-boost response was significantly higher (*=P=0.0005, Figure 5-18B). NP110-primed responses were less efficiently boosted

by NP110 and were significantly lower than ID/ID (***P=0.0005) and ID 11%/ID (*P=0.0005) 2 weeks after the boost.

Mice immunised as above were subsequently challenged with 1000 *P.berghei* sporozoites given into the dilated tail vein, 2 weeks after the boost (2 days after the post-boost bleed). Mice were monitored by thin blood smear for evidence of blood stage parasitaemia. Naïve animals were simultaneously challenged, all of which were parasitaemic by day 6 post-challenge. 67% of ID/ID immunised mice, given full doses, were sterilely protected against blood stage infection, whilst 85% of those receiving an 11% dose at the prime, and a full dose boost (both given ID) remained without parasites throughout the monitoring period (Figure 5-18C). Conversely, neither ID/ID immunisation where the boosting dose was reduced, nor NP110/NP110 immunisation were protective. NP110/ID immunisation was partially protective, with 1/6 (17%) of immunised mice remaining without blood stage parasitaemia.

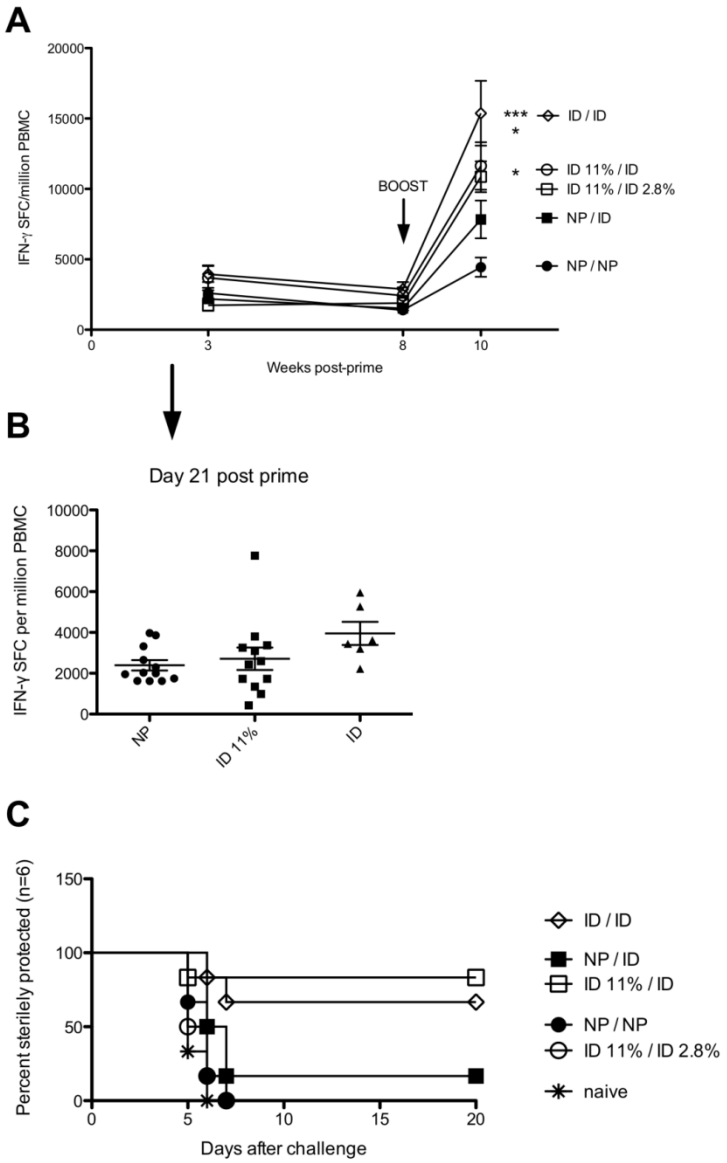

FIGURE 5-18: Nanopatch delivery of stabilised dry-coated AdCh63/MVA heterologous prime-boost immunisation, delivered at velocity.

Female BALB/c mice aged 8 weeks were immunised with $5x10^9$ VP AdCh63.ME-TRAP dry-coated onto NP110 microprojections, formulated with 1% $^{w}/_{v}$ MC, 0.1% $^{v}/_{v}$ PS20 and 10% $^{w}/_{v}$ trehalose/sucrose mixture. Using this exact formulation a delivery efficiency of 11% was previously determined using radiolabelled ^{14}Carbon containing OVA assay (as in Figure 5-13) by X. Chen. Thus, both full dose ($5x10^9$ VP) and adjusted dose (11% = $5.5x10^8$ VP) ID immunised controls were included. All mice were boosted 8 weeks post-prime with either $2x10^7$ PFU MVA.ME-TRAP by coated NP110 (+1% $^{w}/_{v}$ MC + 0.1% $^{v}/_{v}$ PS20), $2x10^7$ PFU ID (acting as a control for NP110 /ID immunisation), or $5x10^5$ PFU ID (acting as a control for NP110 /NP110 immunisation, 2.8% delivery efficiency of MVA.ME-TRAP is taken from the experiment in Figure 5-13). (A+B) Blood was taken for assessment of Pb9-specific immunogenicity 3 weeks (B) and 8 weeks following the priming immunisation, and 2 weeks after the boost immunisation, by IFN-γ ELISPOT. (C) Two days after the final bleed mice were challenged with 1000 *P.berghei* sporozoites IV. Mice were monitored by thin blood smear for signs of blood stage parasitaemia from days 5-20 post-challenge. A group of naïve, unimmunised animals were concurrently challenged and monitored.

5.3.4.3 Summary of 5.3.4

MVA/MVA

- NP110 delivery of dry-coated MVA.PbCSP at a dose of $5x10^7$ PFU induced a similar response 7 days post-prime as compared to the same dose delivered ID (though the actual delivered dose by NP110 was approximately 100 times less, $5x10^5$ PFU). Delivery of a lower dose of MVA.PbCSP - $1x10^6$ PFU induced a signifcantly lower response.
- Despite this, both NP110-primed responses were boosted ID, with post-boost responses similar to ID/ID immunisation.
- NP110 boosting of NP110 primed responses induced low post-boost responses, though the response was increased slightly with a higher coated boosting dose.
- Whilst NP110/NP110 immunisation was not protective in *P. berghei* challenge, 40% of $5x10^7$ PFU-primed (actual dose $5.9x10^5$ PFU), and 20% of $1x10^6$ PFU ($1.8x10^5$ PFU)-primed micewere protected after NP110/ID immunisation.

AdCh63/MVA

- NP110 delivery of AdCh63.ME-TRAP induced an equivalent response post-prime as compared to an equivalent delivered dose given ID, and only slightly lower than a dose ~9 times higher given ID.
- Responses were improved upon an ID delivered MVA.ME-TRAP boost, but less efficiently boosted by MVA-coated NP110.
- The resultant response following NP110/ID immunisation was 17% protective against *P. berghei* challenge.

5.4 DISCUSSION

5.4.1 Overall summary

The development of simple, inexpensive, needle-free alternatives to conventional needle-based immunisation is a global heath priority recognised by the Bill and Melinda Gates Foundation when setting out their 14 Grand Challenges in Global Health in 2002. Another challenge was to develop ‘vaccines that do not require refrigeration’ (91, 342). Importantly, and in addition to high levels of immunogenicity and protective efficacy, the ideal vaccine against malaria should remain thermostable at high ambient temperatures and be easily distributable to be accessible to target populations. Removing the significant costs associated with conventional vaccine administration and refrigeration would allow improved access and greater population coverage. The Nanopatch vaccine delivery system was developed to meet the above needs.

In this chapter, the live, recombinant viral vector vaccines Adenovirus and MVA were formulated and dried onto microprojection patches without loss of viability. Their delivery into the cutaneous microenvironment (known to be rich in APC) was demonstrated using a simple, non-invasive, applicator-assisted method without the use of needles. Furthermore, delivery of dry-coated vaccine by Nanopatch primes

immune responses equivalent to that resulting from the current most immunogenic needle-based route of administration for this vaccine type, with only a fraction of the delivered priming dose. Additionally, dry-coated Adenovirus remained stable after storage at 37°C for at least 10 weeks. This exceeds the requirement set by the WHO for heat stability of another live, viral vector vaccine, (freeze-dried measles) that viral loss must not decrease more than 1 $\log_{10}$ after 7 days of storage at 37°C(341). Recent work by PATH has yielded a heat stable measles vaccine that remains stable for 8 weeks at 37°C in formulation with sucrose and trehalose. Here, using a similar formulation, another live viral vaccine remained stable for a further 2 weeks(343).

5.4.2 Penetration and delivery characteristics of Nanopatch in murine skin

One of the strengths of the Nanopatch is in its ability to target immune inductive sites such as the VE, which is inaccessible by needle-based ID injection. Penetration depth and accurate deposition of vaccine into the dermis by needle can be highly dependent upon vaccinator expertise. Efficient penetration of almost 100% of microprojections and deposition of dry-coated fluorescent payload into both epidermal and dermal compartments was demonstrated using 110μm microprojections (NP110) delivered by spring-loaded mechanical applicator. This applicator was designed to deliver patches in a controlled manner allowing more consistent penetration and vaccine delivery to the skin, with minimal skills training. In contrast, when 40μm microprojections (NP40) were delivered quasi-statically, penetration of the SC was considerably more variable with less than half the total number puncturing the surface of the skin, also confirmed by confocal microscopy following delivery of liquid fluorescent dye. It was observed that delivery of the dye payload following quasi-static delivery of NP40 microprojections was restricted to the epidermal compartment, whereas delivery of dry-coated NP110 microprojections at velocity resulted in a broader delivery profile including significant dermal deposition. The openings of microchannels formed on the surface of the skin were of a smaller diameter after NP40 quasi-static application compared to applicator-applied NP110 microprojections, indicating only partial penetration of the conical 40μm microprojections, since the base widths of the two microprojection morphologies were equivalent.

These observations are in accordance with Crichton *et al* who, using similar conical microprojections, noted that deflection acts to limit the maximum depth of penetration to the VE alone(189). Vybrant® DiD was selected as the fluorescent dye in these experiments, due to its lipophilic nature. DiD should be retained in place following contact with lipid-rich cell membranes, allowing visualisation of microchannels without dye diffusion. However, after dry-coated dye was delivered by NP110 microprojections, some lateral diffusion was observed at the micro-channel tip (Figure 5-8B). It is proposed this is due to the fact that the dermis is less lipid-rich than the epidermis, allowing some diffusion of dye. This suggests that dry-coated payloads delivered in this way are able to diffuse from the microprojection and into the cutaneous environment easily, and further supports the dermal location of payload deposition using this method.

The penetration depths following velocity application demonstrated here are corroborated by Fernando *et al,* who measured the average penetration depth of NP110 in murine skin to be 42µm with 93% of all projections breaching the SC. Additionally, protein-based inactivated influenza vaccine was delivered to sites containing MHC II+ APC by 40% of these projections, as visualised using confocal microscopy. By analysis of cell volume and density, the authors conclude that antigen was directly targeted to approximately 1600 LC and 450 dermal DC per Nanopatch application, translating to over half the total number of pAPC expected to reside within the area of skin beneath the patch, agreeing with theorectical expecations based on a probability model(271).

5.4.3 Quasi-static delivered Nanopatch-induced immunogenicity and protection against *P. berghei* sporozoite challenge

The data suggest that APC interaction after liquid payload delivery using quasi-static application of NP40 microprojections may be limited to LC of the epidermis. Whilst at one time considered the archetypal APC, the role of LC in inducing immunity versus tolerance still remains undefined (299). It is argued that LC may play a part in dampening, rather than orchestrating immune responses and as such form a vital part of the body's tolerance to self or innocuous antigen, and are less efficient at inducing rigorous immune responses to antigen as are other cutaneous DC, since there is evidence from several models to suggest that LC are not involved in the induction of adaptive immune responses (76, 77, 321). In contrastto the NP40 method, the NP110 microprojection velocity application method demonstrated the ability to access both epidermal and dermal environments and hence is able to maximise upon the immune potential of the skin, as epidermal Langerhans cells (LC; CD11b+ CD207+) and dermal Langerin+ ($CD11b^{lo}$ CD207+ CD103+) and dermal interstitial dendritic cells ($CD11b^{hi}$ CD205+) can be accessed.

A proof-of-concept experiment sought to ascertain whether Pb9-specific T-cell responses could be induced following quasi-static delivery of liquid MVA.PbCSP, in a homologous prime-boostimmunisation schedule. Interestingly, a standard dose of $1x10^6$PFU induced responses that were boosted ID, whereas a higher dose of $5x10^7$ PFU did not. However, delivery of both doses by quasi-static delivery of NP110 induced responses that were expanded upon boost. Though the penetration and delivery characteristics of NP110 delivered quasi-statically were not determined here, it is tempting to speculate that the reason for dose-specific differences in induction of a response that undergo secondary expansion may lie in the location of vaccine deposition and the populations of APC residing there. Additionally, MVA is highly cytopathic especially towards DC, a cell type for which it has a tropism, and furthermore retains many of the immune evasion proteins of Vaccinia virus from which it was derived (27). As a consequence the majority of MVA vector and insert antigens are released from apoptotic cells and internalised by bystander cells for cross presentation (344). If NP110 quasi-static delivery accesses both the epidermis and dermis (as NP110 velocity application does) a larger number of invasion targets would be available for the efficient uptake of a higher dose of vaccine antigen. Further work is required to assess the effect of epidermal vs. dermal delivery of vaccine upon the resultant immune response.

Quasi-static delivery of NP40 in MVA/MVA regimes resulted in equivalent levels of immunogenicity and protection after MVA/MVA prime-boost immunisation, when the boost was given ID. NP40 boosting of responses that were primed ID or by NP40 was found to be ineffective. Mice immunised with the NP40/ID regimen were also partially protected against *P.berghei* sporozoite challenge (40% of group did not demonstrate progression to the blood stage of infection). This is impressive since the actual delivered priming dose was only ~23% of that delivered ID. In a second challenge, NP110 quasi-static delivery demonstrated equivalent immunogenicity and protection against challenge as compared to ID/ID immunisation, but with 50 times less the immunising dose (corresponding to 250 times less the *delivered*dose). These data highlight the dose-sparing potential of targeting vaccine delivery to the superficial layers of the skin. In contrast, quasi-static application of NP40 was not able to prime a response that could be efficiently boosted in Ad/MVA immunisation (and responses were not protective against challenge).

5.4.4 Formulation of live viral vector vaccines for dry-coating

Acknowledging the limitations of both the quasi-static application method and the potential benefits of a thermostable, easily distributable vaccine product, a method for dry-coating live viral vectors onto Nanopatchmicroprojections was developed. A successful pre-erythrocytic vaccine against malaria will be required to induce exceptionally high levels of cellular immunity in order to arrest the parasite at the intrahepatocyte stage to prevent symptoms associated with malarial disease (345, 346). Live, recombinant viral vector vaccines are among the most promising platforms for the development of new T cell inducing vaccines with the potential to meet this high threshold (286, 347). Highly immunogenic vaccines based on live, infective organisms must retain stable conformation of viral protein structures to ensure infection of host cells and efficient expression of transgene. Here, no significant loss of viral viability during formulation or following dry-coating of MVA was shown, after immediate elution when formulated with MC and PS20. Adenovirus vaccines were found to require stabilisation by trehalose and sucrose for retention of viability during dry-coating, but these protective disaccharides were found to afford long-term benefits (section 5.4.5). Dry-coating of a live viral vaccine has yet to be published, though delivery of live replicating mycobacterial BCG formulation and dry-coating onto 700μm microneedles was reported, as was the induction of BCG-specific CD4+ T cells following application to HGP(150).Other groups in the microneedle field have demonstrated successful coating and stabilisation of inactivated whole influenza, influenza VLP, live bacterial vaccines using CMC and trehalose, which was found to significantly improve immunogenicity and protection by preservation of HA antigen structure(18, 150, 162, 163).

Coating morphology was distinctly different from that following coating of other vaccine types including plasmid and protein based vaccines, where coating solution was localised to microprojection tips (270-272, 274). Coating was highly dose-dependent, since a higher coated dose resulted in a higher viscosity and bridging of material between projections. Higher coated doses were associated with significantly reduced delivery efficiency as compared to lower coated doses, even after addition of the surfactant to improve microprojection coverage. Dose-dependent delivery efficiency was also observed by Corbett *et al* when coating a VLP-based HPV

vaccine containing alum, where lower delivery efficiencies were observed with higher coated doses, associated with base-localisation and bridging of coating material (274). The majority of coated material remains on the patch following application of higher dose of MVA, suggesting that vaccine resting on the base/bridging between needles cannot be delivered and that precise optimisation of coating formulations and dose is critical for efficient delivery of coated MVA.

In contrast, coating of Adenovirus-based vaccines, at both high and low coated doses resulted in a more even coverage of microprojections, and little difference in delivery efficiency was higher than with high doses of MVA, and varied little between Ad preps of differing viral titre when coated undiluted. One reason for this distinction may lie in their different methods of manufacture and the nature of the resulting prep. Adenovirus vaccines are highly purified by isopycnic CsCl density gradient ultracentrifugation, whilst Poxviruses are purified through a sucrose cushion, resulting in a less purified final prep with some host cell debris remaining. Additionally, whilst positively-charged Adenovirus capsids are protein-based and have a diameter of approximately 40nm, Poxvirus virions are much larger (200nm x 400nm) with a lipid-based outer envelope, which may attract adherent cellular debris, making Poxvirus preps more viscous than Adenovirus preps (284). The addition of the surfactant PS20 enabled improvement in the proportion of the coated vaccine localised to the projection, rather than the base, or bridging between projections by a reduction of surface attraction between the coating material and the silicon base. The surfactant was also thought to reduce aggregation of particles within coating solutions reducing viscosity, hence aiding their dry-coating onto microprojections, and increasing the proportion of viable viruses in the dried formulation.

5.4.5 Adenoviral protection during drying and during storage at elevated temperatures afforded by stabilising disaccharides

Glass-forming sugars such as trehalose and sucrose are widely used as stabilisers due to their natural role in anhydrobiosis– the basis upon which some insects and plants such as*Selaginella lepidophylla* (the “resurrection plant”) survive complete desiccation in dry environments. There are two proposed mechanisms for the protective ability of these disaccharides, reviewed in (348). Firstly, the ‘water displacement hypothesis’ states that the disaccharide molecule replaces water in the hydration shell of proteins, forming hydrogen bonds with αα side chains thus preventing morphological change. Secondly, that the disaccharides form a syrup depositing around proteins and cells and hardening to a solid glass upon dehydration, immobilising and protecting against mechanical degradation.

Addition of trehalose and sucrose had an effect in both mediating protection during dryingbut were not required in MVA formulations. Additionally, the ability to prime an equivalent immune response following AdCh63 immunisation by NP110 as compared to ID immunisation was entirely dependent upon addition of trehalose in the coating formulation. This was a similar finding for Alcock *et al,* in that whilst unstabilised AdHu5 had a significantly lower immediate recoverable titre and lower immunogenicity following lyophilisation, there was no difference between stabilised and unstabilised MVA vaccines. Addition of stabilising sugars sucrose and trehalose afforded protection of AdHu5 titres and immunogenicity during drying, such that they

were equivalent to a liquid control stored at -80°C. Whilst both viruses were subject to decreases in titre and immunogenicity in liquid, and in dried form at elevated temperatures when unstabilised (>27°C for 1 week AdHu5, >45°C for 1 month, MVA), addition of trehalose and sucrose was able to stabilise AdHu5 and MVA for up to 6 months at with no significant loss in viability. MVA remained stable for up to 12 months at lower temperatures (>37°C)(331). Similarly, our results demonstrate that whilst MVA remains stable during drying, unless mixed with the stabilising sugars Ad recovery from microprojections is significantly reduced, particularly in formulations containing trehalose, rather than sucrose alone. The glass transition temperature (T_g), the temperature at which the glass softens and becomes liquid, is higher for trehalose than sucrose, suggesting that for long term thermostability, trehalose is more important. However, the higher solubility of sucrose in water at may promote immediate and complete reconstitution from microprojections. Extensions to this work could investigate this, with the aim of further optimising both vaccine stability on the patch and release from microprojections within the skin.

Elsewhere, when inactivated virus and VLP vaccines for influenza were coated onto 700μm microneedles using a dip-coating method, the HI was found to decrease, but could be completely restored with the addition of trehalose into the coating formulation (161). The loss of viability was attributed to the coating process as loss was observed microneedle-delivered coated and IM-delivered coated then reconstituted vaccine, and trehalose was proposed to prevent aggregation of particles, worsened by mixing with CMC (152, 154, 157, 162). Destabilisation without trehalose was found to occur over two timescales. HI dropped to <10% in the minutes-hours following dip-coating, associated with residual moisture during gradual drying with an increase in particle size with drying time (with and without trehalose). Using the dry-coating method, all moisture is actively removed within 5 minutes of application of a coating solution by nitrogen jet, perhaps explaining the retention of viability following MVA and partial retention of viability following Ad coating. Secondly, during long-term storage, where trehalose stabilised HI activity was independent of temperature over a range of 4-37°C for 28 days(163). Here, trehalose-sucrose affordedstabilisation of Ad over a range of 22-37°C for 10 weeks.

Interestingly, all studies investigating trehalose stabilisation of influenza vaccines have noted a shift in IgG isotypes following immunisation of mice. Unstabilised vaccine induced an IgG response dominated by IgG1 (Th2), whereas IM delivery was primarily composed of the IgG2a (Th1) isotype. After stabilisation, IgG2a titres in microneedle-immunised mice were 1 order of magnitude higher than other groups (152, 158, 161). One hypothesis for this could that an increased bioavailability of virus in stabilised formulations induces a stronger danger signal (due to the reduction in aggregation of viral particles) resulting in an increased level of pro-inflammation influencing a Th1 shift. An analysis of the effect of stabilisation upon immunisation with Adenovirus vectors would be beneficial in the further optimisation of Nanopatch Adenovirus-vectored vaccine delivery, supported by the fact that antigen-specific CD8+ responses were shown to improve with an increasing concentration of trehalose in the mixture.
Other experiments could also extend the monitoring period to 6 months or longer, and investigate a potential cryoprotective effect during inadvertent vaccine freeze-thaw, as may occur in the field (349). The role of stabilising sugars (if any) upon viability of MVA coated vaccine patches remains to be delineated. In their study,

Alcock *et al* noted that despite retaining stability during desiccation and short term storage with or without sugar addition, stabilised MVA viability was not retained beyond 4 months at temperatures above 37°C, perhaps due to a lower recorded T_g of MVA sugar glass compared to AdHu5 glass, and hence a higher residual moisture content, perhaps weakening the protective glasses encapsulating viral proteins (331). Elsewhere, studies of Ad stabilisation by sucrose and mannitol during lyophilisation have linked a low final moisture content of the dried product with maximal recovery of reconstituted viral titre, by minimising hydrolysis reactions (339). Packaging in nitrogen or argon and with hygroscopic salts may improve long-term stability by minimising oxidation, and hydrolysis, respectively. Amino acids such as histidine or arginine may act to quench free radicals generated during storage degradation, conferring further protection to coated viruses(350).

5.4.6 Inherent differences in physical stability between Adenoviral and Poxviral vectors

These studies (and the observations of Alcock *et al*) highlight the differences between Adenoviruses and Poxviruses in terms of their physical stability. Poxviruses such as MVA are of a large size and have a highly condensed core, perhaps affording some natural protection against desiccation and long-term storage even at high temperatures. However, lipid enveloped viruses are generally considered more labile than non-enveloped viruses due to their complex outer structure (290, 337, 351). A more likely explanation may lie in their differential adaptation for infection route and/or survival outside of the body - whilst the only route of natural Adenovirus infection is mucosal and primarily by aerosol inhalation, Poxviruses are also adapted for cutaneous infection. Further to this, Poxviruses may be completely dried out in dermal scabs and remain infectious outside of the body for long periods of time(337)[9]. This may go some way to explain why AdCh63 delivery by quasi-static application of NP40 (epidermal deposition) was not successful, whereas delivery of MVA, was. In dry-coated NP110 application, only when AdCh63 vaccine was formulated with trehalose and sucrose were responses induced. This proposes that stabilisation enabled an increased viable delivery dose to be available; sufficient to overcome a 'dose threshold' necessary for efficient priming of a response by Ad, such as was not available without stabilisation. The link between delivered dose and resulting CD8+ T cell response was also noted by Alcock *et al*. Whilst drops in infective titre observed during thermal inactivation of AdHu5 corresponded to a proportional decrease in immunogenicity, a 4-log drop in MVA infectious titre resulted in only a 100-fold reduction of response (331).

[9] The first commerically available smallpox vaccine was a freeze-dried preparation - Dryvax, which demonstrated thermostability over a range of 0^0C - 25^0C for 96 hours. 352. Lee KN, Hutson CL, Kline R, Curns AT, Dougherty C, Allen C, et al. Smallpox vaccine stability after maintenance at temperatures not recommended for shipping. Vaccine. 2006;24(7):884-6.

5.4.7 Assessment of immunogenicity and protection against challenge following delivery of dry-coated viral vector vaccine regimes

Velocity-delivered dry-coated NP110 was assessed in terms of immunogenicity and protection against experimental parasite challenge in the murine model in both homologous and heterologous prime-boost regimes. Similar immune responses were induced after priming with MVA.PbCSP-coated NP110and boosting ID as when priming and boosting ID with an immunising dose of $5x10^7$ PFU, though post-boost responses were significantly lower following $1x10^6$ PFU Nanopatch priming compared to ID. Though the percentage delivery efficiency was higher for $1x10^6$ PFU than $5x10^7$ PFU, the higher dose still delivered a higher total number of PFU into the skin ($5.9x10^5$ as compared to $1.8x10^5$ PFU) explaining higher immunogenicity and protective efficacy of the higher dose, despite the fact that 98% remains on the patch. Stabilised AdCh63.ME-TRAP priming by Nanopatch was successful and comparable to ID immunisation and could be efficiently boosted ID (though to a lower level than ID-primed groups) and immunised mice were partially protected against malaria. Despite an incomplete understanding of dose response following Nanopatch immunisation, when ID doses were adjusted to equal that delivered by Nanopatch, responses after AdCh63.METRAP were similar, demonstrating a clear dose-sparing benefit.

Nanopatch/Nanopatch immunisation was ineffective, and unable to protect against blood stage infection in any challenge experiment where it was assessed.In MVA/MVA immunisation, it has been shown that the boosting, but not priming of responses is highly sensitive to a reduction in dose when given ID (Section 3.3.1.9 + Figure 3-10). Whilst priming with $1x10^2$ PFU induces a response that is increased to equivalent levels as $1x10^6$ PFU priming (after a standard dose boost), priming of responses with $1x10^6$ PFU and boosting with $1x10^2$ PFU is inefficient, and responses significantly lower. With this in mind, and given that the delivered dose is significantly less by Nanopatch (>18%), the delivered dose by Nanopatch is likely to insufficient for optimal secondary expansion.

Inefficiencies of delivery are to be expected in the implementation of such a non-invasive method of delivery since liquid vaccine is not delivered as a bolus as it is when given ID, but deposited into discrete microchannels. An additional factor to consider with the dry-coated model is the efficiency and rate of release of coated vaccine into the skin and how this may differ with coated dose. In order to access the full potential of Nanopatches in prime-boost immunisation in the clinical situation, a system whereby both immunisations can be given by the same route is preferred, removing the requirement for needles completely. Improvements in coating methods and delivery efficiency will allow further assessment of Nanopatch boosting. A more efficient dry-coating method has been optimised increasing the delivery efficiency of a trivalent inactivated influenza vaccine from 6.5% to 32.5% (280). A second dip-coating method is also under development, and holds promise for much higher delivery efficiency (up to 80% of that coated) and hence more cost-effective Nanopatch immunisation(353).

5.5 CONCLUDING STATEMENT

The data presented here confirm the hypothesis that viral vector vaccines may be successfully and stably dry-coated onto Nanopatch microprojections, delivered into murine skin and induce antigen-specific immunogenicity and protection against parasite challenge. Due to the nature of the vaccines, formulations could be further optimised for improved delivery efficiency, which may allow greater flexibility for efficient delivery of boosting as well as priming immunisations by Nanopatch. Whilst the dose-response relationship is yet to be ascertained, the data here support a dose-sparing aptitude of the Nanopatch, with equivalent responses with as little as 1% of the ID delivered dose of MVA, and 11% of the ID delivered dose of Ad. Importantly, the potential logistical benefits for Nanopatch vaccine delivery are demonstrated, in terms of a simple, reproducible method for penetration and delivery, which may lend itself to self-application, and in thermostability of viral vector vaccines in formulation.

CHAPTER 6 CONCLUDING CHAPTER

6.1 OVERALL SUMMARY

The work presented in this thesis has evaluated the delivery of the live, viral vector malaria vaccines Adenovirus and MVA by two distinct solid silicon microneedle-based patch technologies to mice. Delivery was assessed as compared to needle-based existing immunisation methods by way of enumeration of IFN-γ secreting CD8+ T cells in the circulation or in the spleen, and using the *P. berghei* murine malaria challenge. Until now, the microneedle field has focussed upon delivery of subunit vaccines, with only one study demonstrating the delivery of live mycobacterial vaccine using a similar technology (150). This thesis, along with the published paper by Carey *et al* (265), report upon cellular immunogenicity induced by live, viral vaccines delivered by microneedle patches, for the first time.

Microneedle-coated patches hold promise for reducing resource-dependency and improving cost-effectiveness of such a vaccine patch technology. A significant hurdle to the efficient coating and delivery of live vaccines is their strict requirement for maintenance of an intact protein structure during coating and storage. Here, it was demonstrated that Adenovirus and MVA vectors can be successfully coated onto and delivered by microprojection patches, with no significant loss in viability within 10 weeks of storage at 37^0C when formulated with stabilising disaccharides. This is a significant result for the development of delivery systems for a vaccine urgently needed by millions at risk living in malaria-endemic countries where temperatures are high.

A significant challenge remains in increasing the delivery efficiency of both technologies, which may permit more efficient boosting by patch, in addition to priming, since elimination of the needle is desirable in a clinical context. This would also allow a greater appreciation of the dose-response curve following patch immunisation, in relation to needle-based methods. However, here it is shown that despite delivering less vaccine to the animal, patch responses were similarly immunogenic and protective as compared to ID immunisation, suggesting a potential dose-sparing effect.

The data presented within form a basis for future commercialisation of these microneedle products, and highlight potential factors for consideration in the selection of patch design parameters, vaccine doses and formulation excipients. It is demonstrated that there are differences in the events in the induction of immune responses by patch as compared to ID, enabling a better understanding of mechanisms with which to inform further development, and proving inherent differences between the two methods of vaccine delivery to the skin. This work has produced one paper in publication, one in the late stages of preparation and both technologies are due to enter clinical assessment in the near future.

6.2 SUMMARY OF MAIN CONCLUSIONS

6.2.1 ImmuPatch

In AdCh63/MVA and MVA/MVA schedules, ImmuPatch primes a response that can be optimally expanded upon ID boost, demonstrating similar levels of Pb9-specific CD8+ T cell immunogenicity and levels of partial (MVA/MVA) and high (AdCh63/MVA) levels of protection against malaria challengeas compared to ID/ID immunisation. ImmuPatch design, specifically the parameter of TAV strongly influences post-prime and post-ID responses, with small volume patches priming the lowest post-prime, but the highest post-boost response. These patch/ID regimes also confer higher levels of protection against sporozoite challenge. TAV is significantly positively correlated with vaccine delivery to the dLN, though negatively correlated in the skin. Careful selection of priming patch and dose is necessary, as T280b delivery of $1x10^{10}$VP was ineffective, but delivery of $1x10^{9}$ VP was not.

Patch/patch regimes induce lower immunogenicity, but can be improved by optimal patch selection. Selection of a small TAV patch to prime responses, and a large TAV patch to boost is more effective than either homologous combination. Data from MVA/MVA immunisation delivered ID suggest that a threshold dose is required for boosting, but not primingsuggesting that patch boosting could be improved with improved delivery efficiency (or applying a higher boosting dose). A possible reason for this is the induction of vector-specific, in addition to antigen-specific clones during priming with viral vectors, meaning a higher availability of insert antigen is required to compete with MVA-specific clones for proliferative and anti-apoptotic resources after MVA boost. Recent work has investigated the effect of inflammatory mediators upon the mobilisation of secondary responses. In contrast to the induction of a primary response, the expansion of CD8+ T cells on secondary expansion was strongly dependent upon systemic inflammation, perhaps for the recruitment of innate cells to peripheral sites to assist in re-activation of homed memory cells(354). An increased expression of inflammatory cytokines during skin memory cell re-activation may also be beneficial in inducing MHC II expression in keratinocytes, allowing them to present antigen to skin-resident T cells (59). This indicates that ID immunisation (and possibly immunisation large TAV patches, yet to be confirmed) is more efficient than small TAV patches in boosting responses than small TAV patches due to the induction of inflammatory response. Incorporating an adjuvant within the boost, but not the prime immunisation may be one way to investigate this.

Mechanisms underlying the improved ability of small TAV patches to prime a response that could be optimally boosted were investigated. ImmuPatch preferentially primes a T_{CM}-biased response early in the response compared to ID immunisation (predominantly T_{EM}), enabling more efficient boosting despite demonstrating a lower response (with no demonstrable expansion and contraction) following a single immunisation, as T_{CM} is more readily expanded upon re-activation(31). Small TAV patches were found to prime a response with greater frequencies of T_{CM} than large TAV patches (265), providing an explanation for the heterogeneity in post-ID boost responses observed using patches of varying TAV. It has been shown that inflammatory mediators can influence both contraction kinetics and the acquisition of memory characteristics during a CD8+ T cell response (36).

ImmuPatch F was shown to induce a low level of inflammation following delivery of MVA as compared to ID during the priming stage of the response. It is proposed that this lack of overt inflammation is related to the early accumulation of T_{CM}, which enable F primed responses to be efficiently boosted. This observation also has clinical consequences in potentially reduced adverse local effects, particularly in the delivery of live cytopathic viruses such as MVA. It remains to be determined whether the expression of pro-inflammatory cytokines increases with TAV, but this is likely considering that larger TAV patches are associated with a higher availability of antigen as measured by transgene expression, which may be associated with increased viral infection and activation of intracellular signalling pathways.

The differences in inflammatory state between patch F and ID immunisation are proposed to mediate the observed differences in cellular trafficking from the immunisation site to the dLN (which in turn gives rise to the specific characteristics of the T cell response). Whereas large TAV patch delivery of MVA induced a largely similar magnitude, kinetic and composition of innate cells, as ID, a small TAV patch demonstrated delayed infiltration of lower magnitude, with no influx of circulatory pDC (themselves potent mediators of inflammation) and a greater proportion of LC entering the dLN 120h following immunisation. This suggests minimal involvement of circulating innate cells which rapidly infiltrate inflammatory sites (as after ID), but a slower migration of skin-derived mDC, specifically epidermally resident. The role, if any of dermal DC cell types, such as Langerin+ dermal DC could also be further evaluated, particularly within the context of cross presentation of antigen, as is associated with the cytopathic inhibition of DC demonstrated by MVA infection (27, 82). The significance of this subset in terms of antigen-carrying capacity, and ability to present antigen to T cells remains to be defined but the majority of LC at 120h were found to be MHC II^{hi} CD80+ and thus capable of presentation, in patch F immunised mice. Thus, whilst fewer CD11c+ cells enter the dLN following patch F immunisation, at 120h mDCs there are of a higher activation than after ID. Detection of a luminescent transgene suggested a difference in either biodistribution of antigen between the skin and the dLN or a difference in the rate of its translocation amongst patches (as only one timepoint was studied), perhaps mediated by differences in lymphatic drainage brought about by interstitial pressure within the skin. It remains to be determined if the differences observed in the kinetics and composition of cells migrating to the dLN following patch F are influenced by a sustained persistence of vaccine in the skin following application of small TAV patches.

6.2.2 Nanopatch

The overall aim of this work was to develop a dry-coating, thermostable viral vector vaccine patch, for alleviation of the burdens of liquid vaccine delivery. First, liquid delivery by quasi-static application of NP40 was assessed. Similar to ImmuPatch, Nanopatch primed a lower response than ID, which was boosted as efficiently as ID priming.A higher priming dose was less efficient at inducing a response that could be efficiently boosted (similar to the result following ImmuPatch priming of AdCh63.ME-TRAP responses by T280b). Again, patch priming of responses was more efficient than boosting of responses, andquasi-static NP40 priming with Adenovirus was found to be inefficient, perhaps due to an inadequate dose delivery by Nanopatch. Adenovirus priming is thought to be more dose-sensitive than MVA priming in part

due to the increased propensity of MVA to infect cutaneous cells, whereas Adenovirus is better adapted for mucosal infection (290, 337).

Due to inconsistent perforation of the SC using this method and variability in responses, an applicator was used to deliver patches to the skin at a velocity determined to be optimal for overcoming the skin's elastic resistance (189). Interestingly, delivery characteristics via the two methodologies were significantly different. Whilst the quasi-static NP40 method selectively delivered liquid to the epidermis, the applicator delivered NP110-coated payload into both epidermal and dermal compartments. Confocal microscopy of Ad-coated patches demonstrated delivery to tissue with a high proportion of CD207+ with LC-like morphology (though this was unlikely to be the deepest point of penetration). This observation may have implications for the study of cutaneous dendritic cell subsets, the individual roles of which in the induction of an immune response are under intense debate. The ability to selectively deliver to LC (quasi-static NP40 method) or LC + dermal DC and Langerin+ dermal DC (velocity NP110 method) may prove a useful tool in the delineation of the role of these cells in the induction of responses against foreign antigen, particularly alongside recently described constitutive or conditional ablation mouse models(355). The selective targeting of one particular DC subset over another will be important in the transcutaneous delivery of antigens where a specific cell type has been proposed to be involved in the presentation of antigens, such as the CD103+ cross presentation of HSV-1 antigens, or in the case that a particular subset is undesirable, such as LC in the induction of T_{reg} in cutaneous leishmania infection (78, 82).

At the time of writing this thesis, there was no published demonstration of the stabilisation and coating of live viruses and their delivery by microneedle technology. Adenovirus and MVA were successfully dry-coated with minimal loss to viability, once correctly formulated with glass-forming disaccharides (required for Ad only). When MVA and Ad-coated patches were delivered by spring-loaded applicator, responses were primed that were equivalent to dose-matched controls and, after ID boosting were partially protective (even though delivery efficiency was low). Boosting by Nanopatch was disappointing, but is likely to be improved upon optimisation of vaccine release in the skin (i.e. by dip-coating to localise vaccine to the tips and shafts rather than the base), which would also reduce vaccine wastage and associated costs (353). Coating morphology was affected by vector type (with Ad coating more uniform, and associated with a higher delivery efficiency, than MVA) and vector dose, impacting upon coating solution viscosity, the negative effects improved upon by addition of a surfactant. The addition of stabilising sugars had long term in addition to immediate benefits, with vaccine remaining stable at temperatures of 22°C and 37°C for 10 weeks. This could be extended, as previous reports of stabilisation of Ad and MVA have determined long term stability for up to 6 months (331). Additionally, Prausnitz *et al* observed a shift in IgG isotype patterns from Th2-biased to Th1-biased following stabilisation into microneedle coatings containing inactivated influenza virus and VLP, perhaps due to increased bioavailability and danger signalling (though a mechanism is not put forth by the authors)(152, 155). It would be valuable to further investigate the protective mechanism of trehalose/sucrose stabilisation of live vectors, and if their inclusion similarly alters the functionality of the CD8+ T cell response.

6.3 FUTURE OUTLOOK

A remaining challenge is to reduce costs lost in undelivered vaccine to maximise the full benefits of dose-sparing. For delivery of a malaria vaccine (which preferably would cost less than $1/dose) patch manufacturing costs must be low. DRIE silicon microfabrication with its requirements for clean rooms, resources, high expertise, and high-grade materials currently carry a cost per unit of approximately $1 USD, 50 times that of a standard needle and syringe, though streamlining of processes in scale-up is expected to decrease this cost. Wet-etch manufacture is less expensive due to its simpler, more easily scalable method. Injection-moulded polymer microneedles (356) and dissolving needles (169169) for low cost, flexibility of dosing, high delivery efficiency, complete lack of waste and the potential for composite layers dissolving at different rates hold high promise for prime-boost immunisation for diseases such as malaria. However, silicon is desirable because of its adaptability and its high yield strength (7000mPa) which is considerably higher than most polymers (20-80mPa)(132). The benefits of applicator delivery (i.e. reducing the required microneedle length for accurate penetration through the SC) will have to be set against the increased costs of including such a device. Accurate skin penetration and delivery testing in a diverse population of ages, ethnicities and sexes will be required. Most importantly, in each application, the microneedle delivery method will need to demonstrate at least equivalence as compared to the needle method to warrant change from existing protocols, even though needle-free immunisation offers significant logistical benefits.

The evaluation of protective efficacy of microneedle immunisation for the delivery of vaccines to date has focused upon mucosal pathogens, primarily influenza. The successful induction of protective mucosal immune responses in these studies is likely in part to be due to the communication between skin and mucosal immune systems. It remains to be demonstrated if microneedle delivery of vaccines induces skin-homing T cells that are effective against cutaneous pathogens such as HSV-1 or *Leishmania major*, two pathogens with complex relationships with cutaneous DC subsets. For the first time, the data presented here demonstrate the induction of sufficient systemic immunity to mediate partial protection against challenge with a non-mucosal pathogen, *P. berghei,* at the liver and in doing so extends the applicability of transcutaneous immunisation via microneedle patch to diseases where pathogen inhibition is mediated at non-mucosal sites.

To conclude, this thesis proposes microneedle patch technologies for the needle-free delivery of a future malaria vaccine regimen, offering significant logistical advantages of particular interest in delivering vaccines to countries with poor healthcare and transport infrastructure. ImmuPatch and Nanopatch, if the correct design parameters, methodologies, doses and coating procedures are selected, hold promise to match, or with further optimisation, exceed the efficacy of needle-based immunisation.

REFERENCES

1. Carey JB, Pearson FE, Vrdoljak A, McGrath MG, Crean AM, Walsh PT, et al. Microneedle array design determines the induction of protective memory CD8+ T cell responses induced by a recombinant live malaria vaccine in mice. PLoS ONE. 2011;6(7):e22442. Epub 2011/07/30.
2. Plotkin SA. Vaccines: past, present and future. Nature medicine. 2005;11(4 Suppl):S5-11. Epub 2005/04/07.
3. O'Hagan DT, Rappuoli R. Novel approaches to vaccine delivery. Pharmaceutical research. 2004;21(9):1519-30. Epub 2004/10/23.
4. Stittelaar KJ, Osterhaus AD. MVA: a cuckoo in the vaccine nest? Vaccine. 2001;19(27):V-VI. Epub 2001/06/08.
5. Kaufmann SH. Immunology's foundation: the 100-year anniversary of the Nobel Prize to Paul Ehrlich and Elie Metchnikoff. Nat Immunol. 2008;9(7):705-12. Epub 2008/06/20.
6. Ehreth J. The global value of vaccination. Vaccine. 2003;21(7-8):596-600. Epub 2003/01/18.
7. WHO. Immunization surveillance, assessment and monitoring. [4 March 2011]; Available from: (http://www.who.int/immunisation_monitoring/diseases/en/)
8. Offit PA. The Cutter incident, 50 years later. The New England journal of medicine. 2005;352(14):1411-2. Epub 2005/04/09.
9. Ulmer JB, Donnelly JJ, Parker SE, Rhodes GH, Felgner PL, Dwarki VJ, et al. Heterologous protection against influenza by injection of DNA encoding a viral protein. Science. 1993;259(5102):1745-9. Epub 1993/03/19.
10. Fuller DH, Loudon P, Schmaljohn C. Preclinical and clinical progress of particle-mediated DNA vaccines for infectious diseases. Methods. 2006;40(1):86-97. Epub 2006/09/26.
11. Draper SJ, Heeney JL. Viruses as vaccine vectors for infectious diseases and cancer. Nature reviews Microbiology. 2010;8(1):62-73. Epub 2009/12/08.
12. Spohn G, Bachmann MF. Exploiting viral properties for the rational design of modern vaccines. Expert review of vaccines. 2008;7(1):43-54. Epub 2008/02/07.
13. Fifis T, Mottram P, Bogdanoska V, Hanley J, Plebanski M. Short peptide sequences containing MHC class I and/or class II epitopes linked to nano-beads induce strong immunity and inhibition of growth of antigen-specific tumour challenge in mice. Vaccine. 2004;23(2):258-66. Epub 2004/11/09.
14. Fifis T, Gamvrellis A, Crimeen-Irwin B, Pietersz GA, Li J, Mottram PL, et al. Size-dependent immunogenicity: therapeutic and protective properties of nano-vaccines against tumors. Journal of immunology. 2004;173(5):3148-54. Epub 2004/08/24.
15. Manolova V, Flace A, Bauer M, Schwarz K, Saudan P, Bachmann MF. Nanoparticles target distinct dendritic cell populations according to their size. European journal of immunology. 2008;38(5):1404-13. Epub 2008/04/05.
16. Rollier CS, Reyes-Sandoval A, Cottingham MG, Ewer K, Hill AV. Viral vectors as vaccine platforms: deployment in sight. Current opinion in immunology. 2011;23(3):377-82. Epub 2011/04/26.
17. Appaiahgari MB, Vrati S. IMOJEV((R)): a Yellow fever virus-based novel Japanese encephalitis vaccine. Expert review of vaccines. 2010;9(12):1371-84. Epub 2010/11/26.
18. Anderson RM, May RM. Immunisation and herd immunity. Lancet. 1990;335(8690):641-5. Epub 1990/03/17.

19. Janeway CA, Jr. Approaching the asymptote? Evolution and revolution in immunology. Cold Spring Harb Symp Quant Biol. 1989;54 Pt 1:1-13. Epub 1989/01/01.
20. Matzinger P. Tolerance, danger, and the extended family. Annual review of immunology. 1994;12:991-1045. Epub 1994/01/01.
21. Oppenheim JJ, Yang D. Alarmins: chemotactic activators of immune responses. Current opinion in immunology. 2005;17(4):359-65. Epub 2005/06/16.
22. Haraldsen G, Balogh J, Pollheimer J, Sponheim J, Kuchler AM. Interleukin-33 - cytokine of dual function or novel alarmin? Trends in immunology. 2009;30(5):227-33. Epub 2009/04/11.
23. Bianchi ME. DAMPs, PAMPs and alarmins: all we need to know about danger. Journal of leukocyte biology. 2007;81(1):1-5. Epub 2006/10/13.
24. Bevan MJ. Cross-priming. Nature immunology. 2006;7(4):363-5. Epub 2006/03/22.
25. Liu L, Chavan R, Feinberg MB. Dendritic cells are preferentially targeted among hematolymphocytes by Modified Vaccinia Virus Ankara and play a key role in the induction of virus-specific T cell responses in vivo. BMC immunology. 2008;9:15. Epub 2008/04/17.
26. Yewdell JW, Bennink JR. Mechanisms of viral interference with MHC class I antigen processing and presentation. Annu Rev Cell Dev Biol. 1999;15:579-606. Epub 1999/12/28.
27. Pascutti MF, Rodriguez AM, Falivene J, Giavedoni L, Drexler I, Gherardi MM. Interplay between modified vaccinia virus Ankara and dendritic cells: phenotypic and functional maturation of bystander dendritic cells. Journal of virology. 2011;85(11):5532-45. Epub 2011/03/18.
28. Curtis MM, Way SS. Interleukin-17 in host defence against bacterial, mycobacterial and fungal pathogens. Immunology. 2009;126(2):177-85. Epub 2009/01/08.
29. Badovinac VP, Porter BB, Harty JT. Programmed contraction of CD8(+) T cells after infection. Nature immunology. 2002;3(7):619-26. Epub 2002/06/11.
30. Sallusto F, Lenig D, Forster R, Lipp M, Lanzavecchia A. Two subsets of memory T lymphocytes with distinct homing potentials and effector functions. Nature. 1999;401(6754):708-12. Epub 1999/10/28.
31. Sallusto F, Geginat J, Lanzavecchia A. Central memory and effector memory T cell subsets: function, generation, and maintenance. Annual review of immunology. 2004;22:745-63. Epub 2004/03/23.
32. Bachmann MF, Wolint P, Schwarz K, Jager P, Oxenius A. Functional properties and lineage relationship of CD8+ T cell subsets identified by expression of IL-7 receptor alpha and CD62L. Journal of immunology. 2005;175(7):4686-96. Epub 2005/09/24.
33. Opferman JT, Ober BT, Ashton-Rickardt PG. Linear differentiation of cytotoxic effectors into memory T lymphocytes. Science. 1999;283(5408):1745-8. Epub 1999/03/12.
34. Lanzavecchia A, Sallusto F. Progressive differentiation and selection of the fittest in the immune response. Nature reviews Immunology. 2002;2(12):982-7. Epub 2002/12/04.
35. Moulton VR, Farber DL. Committed to memory: lineage choices for activated T cells. Trends in immunology. 2006;27(6):261-7. Epub 2006/05/11.
36. Badovinac VP, Harty JT. Programming, demarcating, and manipulating CD8+ T-cell memory. Immunological reviews. 2006;211:67-80. Epub 2006/07/11.

37. Badovinac VP, Porter BB, Harty JT. CD8+ T cell contraction is controlled by early inflammation. Nature immunology. 2004;5(8):809-17. Epub 2004/07/13.
38. Harty JT, Badovinac VP. Influence of effector molecules on the CD8(+) T cell response to infection. Current opinion in immunology. 2002;14(3):360-5. Epub 2002/04/26.
39. Kaech SM, Wherry EJ, Ahmed R. Effector and memory T-cell differentiation: implications for vaccine development. Nature reviews Immunology. 2002;2(4):251-62. Epub 2002/05/11.
40. Masopust D, Kaech SM, Wherry EJ, Ahmed R. The role of programming in memory T-cell development. Current opinion in immunology. 2004;16(2):217-25. Epub 2004/03/17.
41. Lambert PH, Laurent PE. Intradermal vaccine delivery: will new delivery systems transform vaccine administration? Vaccine. 2008;26(26):3197-208. Epub 2008/05/20.
42. Kravitz H. A simplified technique for vaccination against smallpox. Pediatrics. 1961;27:219-26. Epub 1961/02/01.
43. Lane JM, Ruben FL, Neff JM, Millar JD. Complications of smallpox vaccination, 1968: results of ten statewide surveys. The Journal of infectious diseases. 1970;122(4):303-9. Epub 1970/10/01.
44. Liu L, Zhong Q, Tian T, Dubin K, Athale SK, Kupper TS. Epidermal injury and infection during poxvirus immunization is crucial for the generation of highly protective T cell-mediated immunity. Nat Med. 2010;16(2):224-7. Epub 2010/01/19.
45. WHO. Smallpox Factsheet. 2001 [Accessed on 16 January 2011]; Available from: http://www.who.int/mediacentre/factsheets/smallpox/en/index.html.
46. McConkey SJ, Reece WH, Moorthy VS, Webster D, Dunachie S, Butcher G, et al. Enhanced T-cell immunogenicity of plasmid DNA vaccines boosted by recombinant modified vaccinia virus Ankara in humans. Nat Med. 2003;9(6):729-35. Epub 2003/05/27.
47. Bejon P, Lusingu J, Olotu A, Leach A, Lievens M, Vekemans J, et al. Efficacy of RTS,S/AS01E vaccine against malaria in children 5 to 17 months of age. The New England journal of medicine. 2008;359(24):2521-32. Epub 2008/12/10.
48. Bejon P, Mwacharo J, Kai OK, Todryk S, Keating S, Lang T, et al. Immunogenicity of the candidate malaria vaccines FP9 and modified vaccinia virus Ankara encoding the pre-erythrocytic antigen ME-TRAP in 1-6 year old children in a malaria endemic area. Vaccine. 2006;24(22):4709-15. Epub 2006/04/20.
49. Dunachie SJ, Walther M, Epstein JE, Keating S, Berthoud T, Andrews L, et al. A DNA prime-modified vaccinia virus ankara boost vaccine encoding thrombospondin-related adhesion protein but not circumsporozoite protein partially protects healthy malaria-naive adults against Plasmodium falciparum sporozoite challenge. Infect Immun. 2006;74(10):5933-42. Epub 2006/09/22.
50. Wilck MB, Seaman MS, Baden LR, Walsh SR, Grandpre LE, Devoy C, et al. Safety and immunogenicity of modified vaccinia Ankara (ACAM3000): effect of dose and route of administration. J Infect Dis. 2010;201(9):1361-70. Epub 2010/03/31.
51. Seaman MS, Wilck MB, Baden LR, Walsh SR, Grandpre LE, Devoy C, et al. Effect of vaccination with modified vaccinia Ankara (ACAM3000) on subsequent challenge with Dryvax. The Journal of infectious diseases. 2010;201(9):1353-60. Epub 2010/03/31.
52. Casares S, Inaba K, Brumeanu TD, Steinman RM, Bona CA. Antigen presentation by dendritic cells after immunization with DNA encoding a major

histocompatibility complex class II-restricted viral epitope. The Journal of experimental medicine. 1997;186(9):1481-6. Epub 1997/11/14.
53. Dupuis M, Murphy TJ, Higgins D, Ugozzoli M, van Nest G, Ott G, et al. Dendritic cells internalize vaccine adjuvant after intramuscular injection. Cellular immunology. 1998;186(1):18-27. Epub 1998/06/25.
54. (PATH) PfATiH. Intradermal delivery of vaccines: a review of the literature and potential for development for use in low- and middle-income countries. Seattle: 2009.
55. Kupper TS, Fuhlbrigge RC. Immune surveillance in the skin: mechanisms and clinical consequences. Nature reviews Immunology. 2004;4(3):211-22. Epub 2004/03/25.
56. Kendall MA. Needle-free vaccine injection. Handb Exp Pharmacol. 2010(197):193-219. Epub 2010/03/11.
57. Miller LS, Modlin RL. Human keratinocyte Toll-like receptors promote distinct immune responses. The Journal of investigative dermatology. 2007;127(2):262-3. Epub 2007/01/18.
58. Sugita K, Kabashima K, Atarashi K, Shimauchi T, Kobayashi M, Tokura Y. Innate immunity mediated by epidermal keratinocytes promotes acquired immunity involving Langerhans cells and T cells in the skin. Clinical and experimental immunology. 2007;147(1):176-83. Epub 2006/12/21.
59. Black AP, Ardern-Jones MR, Kasprowicz V, Bowness P, Jones L, Bailey AS, et al. Human keratinocyte induction of rapid effector function in antigen-specific memory CD4+ and CD8+ T cells. European journal of immunology. 2007;37(6):1485-93. Epub 2007/05/17.
60. Kim BS, Miyagawa F, Cho YH, Bennett CL, Clausen BE, Katz SI. Keratinocytes function as accessory cells for presentation of endogenous antigen expressed in the epidermis. The Journal of investigative dermatology. 2009;129(12):2805-17. Epub 2009/06/26.
61. Etchart N, Hennino A, Friede M, Dahel K, Dupouy M, Goujon-Henry C, et al. Safety and efficacy of transcutaneous vaccination using a patch with the live-attenuated measles vaccine in humans. Vaccine. 2007;25(39-40):6891-9. Epub 2007/09/04.
62. Glenn GM, Scharton-Kersten T, Vassell R, Matyas GR, Alving CR. Transcutaneous immunization with bacterial ADP-ribosylating exotoxins as antigens and adjuvants. Infection and immunity. 1999;67(3):1100-6. Epub 1999/02/20.
63. Glenn GM, Scharton-Kersten T, Vassell R, Mallett CP, Hale TL, Alving CR. Transcutaneous immunization with cholera toxin protects mice against lethal mucosal toxin challenge. Journal of immunology. 1998;161(7):3211-4. Epub 1998/10/06.
64. Berry LJ, Hickey DK, Skelding KA, Bao S, Rendina AM, Hansbro PM, et al. Transcutaneous immunization with combined cholera toxin and CpG adjuvant protects against Chlamydia muridarum genital tract infection. Infect Immun. 2004;72(2):1019-28. Epub 2004/01/27.
65. Belyakov IM, Hammond SA, Ahlers JD, Glenn GM, Berzofsky JA. Transcutaneous immunization induces mucosal CTLs and protective immunity by migration of primed skin dendritic cells. The Journal of clinical investigation. 2004;113(7):998-1007. Epub 2004/04/02.
66. Prausnitz MR, Mikszta JA, Cormier M, Andrianov AK. Microneedle-based vaccines. Current topics in microbiology and immunology. 2009;333:369-93. Epub 2009/09/22.

67. Banchereau J, Steinman RM. Dendritic cells and the control of immunity. Nature. 1998;392(6673):245-52. Epub 1998/04/01.
68. Valladeau J, Saeland S. Cutaneous dendritic cells. Seminars in immunology. 2005;17(4):273-83. Epub 2005/06/15.
69. Schuler G, Steinman RM. Murine epidermal Langerhans cells mature into potent immunostimulatory dendritic cells in vitro. The Journal of experimental medicine. 1985;161(3):526-46. Epub 1985/03/01.
70. Steinman RM, Cohn ZA. Identification of a novel cell type in peripheral lymphoid organs of mice. I. Morphology, quantitation, tissue distribution. The Journal of experimental medicine. 1973;137(5):1142-62. Epub 1973/05/01.
71. Schuler G, Romani N, Steinman RM. A comparison of murine epidermal Langerhans cells with spleen dendritic cells. The Journal of investigative dermatology. 1985;85(1 Suppl):99s-106s. Epub 1985/07/01.
72. Wilson NS, Villadangos JA. Lymphoid organ dendritic cells: beyond the Langerhans cells paradigm. Immunology and cell biology. 2004;82(1):91-8. Epub 2004/02/27.
73. Girolomoni G, Caux C, Lebecque S, Dezutter-Dambuyant C, Ricciardi-Castagnoli P. Langerhans cells: still a fundamental paradigm for studying the immunobiology of dendritic cells. Trends in immunology. 2002;23(1):6-8. Epub 2002/01/22.
74. Merad M, Manz MG, Karsunky H, Wagers A, Peters W, Charo I, et al. Langerhans cells renew in the skin throughout life under steady-state conditions. Nat Immunol. 2002;3(12):1135-41. Epub 2002/11/05.
75. Allan RS, Smith CM, Belz GT, van Lint AL, Wakim LM, Heath WR, et al. Epidermal viral immunity induced by CD8alpha+ dendritic cells but not by Langerhans cells. Science. 2003;301(5641):1925-8. Epub 2003/09/27.
76. Allan RS, Waithman J, Bedoui S, Jones CM, Villadangos JA, Zhan Y, et al. Migratory dendritic cells transfer antigen to a lymph node-resident dendritic cell population for efficient CTL priming. Immunity. 2006;25(1):153-62. Epub 2006/07/25.
77. Furmanov K, Elnekave M, Lehmann D, Clausen BE, Kotton DN, Hovav AH. The role of skin-derived dendritic cells in CD8+ T cell priming following immunization with lentivectors. Journal of immunology. 2010;184(9):4889-97. Epub 2010/04/02.
78. Kautz-Neu K, Noordegraaf M, Dinges S, Bennett CL, John D, Clausen BE, et al. Langerhans cells are negative regulators of the anti-Leishmania response. The Journal of experimental medicine. 2011;208(5):885-91. Epub 2011/05/04.
79. Bursch LS, Wang L, Igyarto B, Kissenpfennig A, Malissen B, Kaplan DH, et al. Identification of a novel population of Langerin+ dendritic cells. J Exp Med. 2007;204(13):3147-56. Epub 2007/12/19.
80. Nagao K, Ginhoux F, Leitner WW, Motegi S, Bennett CL, Clausen BE, et al. Murine epidermal Langerhans cells and langerin-expressing dermal dendritic cells are unrelated and exhibit distinct functions. Proceedings of the National Academy of Sciences of the United States of America. 2009;106(9):3312-7. Epub 2009/02/17.
81. Poulin LF, Henri S, de Bovis B, Devilard E, Kissenpfennig A, Malissen B. The dermis contains langerin+ dendritic cells that develop and function independently of epidermal Langerhans cells. J Exp Med. 2007;204(13):3119-31. Epub 2007/12/19.
82. Bedoui S, Whitney PG, Waithman J, Eidsmo L, Wakim L, Caminschi I, et al. Cross-presentation of viral and self antigens by skin-derived CD103+ dendritic cells. Nature immunology. 2009;10(5):488-95. Epub 2009/04/08.

83. Stoitzner P, Tripp CH, Eberhart A, Price KM, Jung JY, Bursch L, et al. Langerhans cells cross-present antigen derived from skin. Proc Natl Acad Sci U S A. 2006;103(20):7783-8. Epub 2006/05/05.
84. Ueno H, Schmitt N, Palucka AK, Banchereau J. Dendritic cells and humoral immunity in humans. Immunology and cell biology. 2010;88(4):376-80. Epub 2010/03/24.
85. Kane M. Unsafe injections. Bulletin of the World Health Organization. 1998;76(1):99-100. Epub 1998/06/06.
86. Kane A, Lloyd J, Zaffran M, Simonsen L, Kane M. Transmission of hepatitis B, hepatitis C and human immunodeficiency viruses through unsafe injections in the developing world: model-based regional estimates. Bull World Health Organ. 1999;77(10):801-7. Epub 1999/12/11.
87. Kermode M. Unsafe injections in low-income country health settings: need for injection safety promotion to prevent the spread of blood-borne viruses. Health Promot Int. 2004;19(1):95-103. Epub 2004/02/21.
88. Organisation WH. World Health Report. World Health Organization, 2002.
89. Millar MA, Pisani E. The cost of unsafe injections. Bulletin of the World Health Organization. 1999;77(10):808-11.
90. Hauri AM, Armstrong GL, Hutin YJ. The global burden of disease attributable to contaminated injections given in health care settings. International journal of STD & AIDS. 2004;15(1):7-16. Epub 2004/02/11.
91. Varmus H, Klausner R, Zerhouni E, Acharya T, Daar AS, Singer PA. Public health. Grand Challenges in Global Health. Science. 2003;302(5644):398-9. Epub 2003/10/18.
92. Wolfson LJ, Gasse F, Lee-Martin SP, Lydon P, Magan A, Tibouti A, et al. Estimating the costs of achieving the WHO-UNICEF Global Immunization Vision and Strategy, 2006-2015. Bulletin of the World Health Organization. 2008;86(1):27-39. Epub 2008/02/01.
93. Kline RL, Regnery RL, Armstrong GL, Damon IK. Stability of diluted smallpox vaccine under simulated clinical conditions. Vaccine. 2005;23(41):4944-6. Epub 2005/07/12.
94. Lloyd J. Technologies for vaccine delivery in the 21st century. Department of Vaccines and Biologicals, World Health Organization, 2000.
95. Falagas ME, Zarkadoulia E. Factors associated with suboptimal compliance to vaccinations in children in developed countries: a systematic review. Curr Med Res Opin. 2008;24(6):1719-41. Epub 2008/05/14.
96. Jacobson RM, Swan A, Adegbenro A, Ludington SL, Wollan PC, Poland GA. Making vaccines more acceptable--methods to prevent and minimize pain and other common adverse events associated with vaccines. Vaccine. 2001;19(17-19):2418-27. Epub 2001/03/21.
97. Duff AJ. Incorporating psychological approaches into routine paediatric venepuncture. Archives of disease in childhood. 2003;88(10):931-7. Epub 2003/09/23.
98. Nir Y, Paz A, Sabo E, Potasman I. Fear of injections in young adults: prevalence and associations. The American journal of tropical medicine and hygiene. 2003;68(3):341-4. Epub 2003/04/11.
99. Johnson DR, Nichol KL, Lipczynski K. Barriers to adult immunization. The American journal of medicine. 2008;121(7 Suppl 2):S28-35. Epub 2008/07/01.
100. Bos JD, Meinardi MM. The 500 Dalton rule for the skin penetration of chemical compounds and drugs. Exp Derm. 2000;9(3):165-9. Epub 2000/06/06.

101. Mitragotri S. Immunization without needles. Nat Rev Immunol. 2005;5(12):905-16. Epub 2005/10/22.
102. Glenn GM, Rao M, Matyas GR, Alving CR. Skin immunization made possible by cholera toxin. Nature. 1998;391(6670):851. Epub 1998/03/12.
103. Glenn GM, Scharton-Kersten T, Alving CR. Advances in vaccine delivery: transcutaneous immunisation. Expert opinion on investigational drugs. 1999;8(6):797-805. Epub 2005/07/05.
104. Bal SM, Ding Z, van Riet E, Jiskoot W, Bouwstra JA. Advances in transcutaneous vaccine delivery: do all ways lead to Rome? Journal of controlled release : official journal of the Controlled Release Society. 2010;148(3):266-82. Epub 2010/09/28.
105. Kahlon R, Hu Y, Orteu CH, Kifayet A, Trudeau JD, Tan R, et al. Optimization of epicutaneous immunization for the induction of CTL. Vaccine. 2003;21(21-22):2890-9. Epub 2003/06/12.
106. Frech SA, Kenney RT, Spyr CA, Lazar H, Viret JF, Herzog C, et al. Improved immune responses to influenza vaccination in the elderly using an immunostimulant patch. Vaccine. 2005;23(7):946-50. Epub 2004/12/18.
107. Guebre-Xabier M, Hammond SA, Ellingsworth LR, Glenn GM. Immunostimulant patch enhances immune responses to influenza virus vaccine in aged mice. Journal of virology. 2004;78(14):7610-8. Epub 2004/06/29.
108. Nicolas JF, Guy B. Intradermal, epidermal and transcutaneous vaccination: from immunology to clinical practice. Expert Rev Vaccines. 2008;7(8):1201-14. Epub 2008/10/11.
109. Van Kampen KR, Shi Z, Gao P, Zhang J, Foster KW, Chen DT, et al. Safety and immunogenicity of adenovirus-vectored nasal and epicutaneous influenza vaccines in humans. Vaccine. 2005;23(8):1029-36. Epub 2004/12/29.
110. Tan G, Xu P, Lawson LB, He J, Freytag LC, Clements JD, et al. Hydration effects on skin microstructure as probed by high-resolution cryo-scanning electron microscopy and mechanistic implications to enhanced transcutaneous delivery of biomacromolecules. Journal of pharmaceutical sciences. 2010;99(2):730-40. Epub 2009/07/08.
111. Gupta PN, Vyas SP. Colloidal carrier systems for transcutaneous immunization. Curr Drug Targets. 2011;12(4):579-97. Epub 2011/01/14.
112. Bramson J, Dayball K, Evelegh C, Wan YH, Page D, Smith A. Enabling topical immunization via microporation: a novel method for pain-free and needle-free delivery of adenovirus-based vaccines. Gene therapy. 2003;10(3):251-60. Epub 2003/02/07.
113. Hooper JW, Golden JW, Ferro AM, King AD. Smallpox DNA vaccine delivered by novel skin electroporation device protects mice against intranasal poxvirus challenge. Vaccine. 2007;25(10):1814-23. Epub 2007/01/24.
114. Zhao YL, Murthy SN, Manjili MH, Guan LJ, Sen A, Hui SW. Induction of cytotoxic T-lymphocytes by electroporation-enhanced needle-free skin immunization. Vaccine. 2006;24(9):1282-90. Epub 2005/10/18.
115. Tezel A, Paliwal S, Shen Z, Mitragotri S. Low-frequency ultrasound as a transcutaneous immunization adjuvant. Vaccine. 2005;23(29):3800-7. Epub 2005/05/17.
116. Dahlan A, Alpar HO, Stickings P, Sesardic D, Murdan S. Transcutaneous immunisation assisted by low-frequency ultrasound. International journal of pharmaceutics. 2009;368(1-2):123-8. Epub 2008/11/18.

117. Marjukka Suhonen T, Bouwstra JA, Urtti A. Chemical enhancement of percutaneous absorption in relation to stratum corneum structural alterations. Journal of controlled release : official journal of the Controlled Release Society. 1999;59(2):149-61. Epub 1999/05/20.
118. Maheshwari C, Pandey RS, Chaurasiya A, Kumar A, Selvam DT, Prasad GB, et al. Non-ionic surfactant vesicles mediated transcutaneous immunization against hepatitis B. International immunopharmacology. 2011. Epub 2011/05/26.
119. Mahe B, Vogt A, Liard C, Duffy D, Abadie V, Bonduelle O, et al. Nanoparticle-based targeting of vaccine compounds to skin antigen-presenting cells by hair follicles and their transport in mice. The Journal of investigative dermatology. 2009;129(5):1156-64. Epub 2008/12/05.
120. Combadiere B, Vogt A, Mahe B, Costagliola D, Hadam S, Bonduelle O, et al. Preferential amplification of CD8 effector-T cells after transcutaneous application of an inactivated influenza vaccine: a randomized phase I trial. PloS ONE. 2010;5(5):e10818. Epub 2010/06/04.
121. Mitragotri S. Current status and future prospects of needle-free liquid jet injectors. Nat Rev Drug Discov. 2006;5(7):543-8. Epub 2006/07/04.
122. Lin MT, Pulkkinen L, Uitto J, Yoon K. The gene gun: current applications in cutaneous gene therapy. International journal of dermatology. 2000;39(3):161-70. Epub 2000/04/12.
123. Guebre-Xabier M, Hammond SA, Epperson DE, Yu J, Ellingsworth L, Glenn GM. Immunostimulant patch containing heat-labile enterotoxin from Escherichia coli enhances immune responses to injected influenza virus vaccine through activation of skin dendritic cells. Journal of virology. 2003;77(9):5218-25. Epub 2003/04/15.
124. Matyas GR, Friedlander AM, Glenn GM, Little S, Yu J, Alving CR. Needle-free skin patch vaccination method for anthrax. Infection and immunity. 2004;72(2):1181-3. Epub 2004/01/27.
125. Glenn GM, Thomas DN, Poffenberger KL, Flyer DC, Ellingsworth LR, Andersen BH, et al. Safety and immunogenicity of an influenza vaccine A/H5N1 (A/Vietnam/1194/2004) when coadministered with a heat-labile enterotoxin (LT) adjuvant patch. Vaccine. 2009;27 Suppl 6:G60-6. Epub 2009/12/17.
126. Yu J, Cassels F, Scharton-Kersten T, Hammond SA, Hartman A, Angov E, et al. Transcutaneous immunization using colonization factor and heat-labile enterotoxin induces correlates of protective immunity for enterotoxigenic Escherichia coli. Infection and immunity. 2002;70(3):1056-68. Epub 2002/02/21.
127. Alarcon JB, Hartley AW, Harvey NG, Mikszta JA. Preclinical evaluation of microneedle technology for intradermal delivery of influenza vaccines. Clinical and vaccine immunology : CVI. 2007;14(4):375-81. Epub 2007/03/03.
128. Laurent PE, Bourhy H, Fantino M, Alchas P, Mikszta JA. Safety and efficacy of novel dermal and epidermal microneedle delivery systems for rabies vaccination in healthy adults. Vaccine. 2010;28(36):5850-6. Epub 2010/07/06.
129. Mikszta JA, Dekker JP, 3rd, Harvey NG, Dean CH, Brittingham JM, Huang J, et al. Microneedle-based intradermal delivery of the anthrax recombinant protective antigen vaccine. Infection and immunity. 2006;74(12):6806-10. Epub 2006/10/13.
130. Dean CH, Alarcon JB, Waterston AM, Draper K, Early R, Guirakhoo F, et al. Cutaneous delivery of a live, attenuated chimeric flavivirus vaccine against Japanese encephalitis (ChimeriVax)-JE) in non-human primates. Human vaccines. 2005;1(3):106-11. Epub 2006/10/03.
131. Gerstel MS, Place VA, inventors; Drug delivery device patent 3964482. 1976.

132. Donnelly RF, Raj Singh TR, Woolfson AD. Microneedle-based drug delivery systems: microfabrication, drug delivery, and safety. Drug delivery. 2010;17(4):187-207. Epub 2010/03/20.
133. Laurent PE, Bonnet S, Alchas P, Regolini P, Mikszta JA, Pettis R, et al. Evaluation of the clinical performance of a new intradermal vaccine administration technique and associated delivery system. Vaccine. 2007;25(52):8833-42. Epub 2007/11/21.
134. Jiang J, Moore JS, Edelhauser HF, Prausnitz MR. Intrascleral drug delivery to the eye using hollow microneedles. Pharmaceutical research. 2009;26(2):395-403. Epub 2008/11/04.
135. Patel SR, Lin AS, Edelhauser HF, Prausnitz MR. Suprachoroidal drug delivery to the back of the eye using hollow microneedles. Pharmaceutical research. 2011;28(1):166-76. Epub 2010/09/22.
136. Gupta J, Felner EI, Prausnitz MR. Rapid pharmacokinetics of intradermal insulin administered using microneedles in type 1 diabetes subjects. Diabetes technology & therapeutics. 2011;13(4):451-6. Epub 2011/03/02.
137. Arora A, Prausnitz MR, Mitragotri S. Micro-scale devices for transdermal drug delivery. International journal of pharmaceutics. 2008;364(2):227-36. Epub 2008/09/23.
138. Henry S, McAllister DV, Allen MG, Prausnitz MR. Microfabricated microneedles: a novel approach to transdermal drug delivery. Journal of pharmaceutical sciences. 1998;87(8):922-5. Epub 1998/08/04.
139. Mikszta JA, Alarcon JB, Brittingham JM, Sutter DE, Pettis RJ, Harvey NG. Improved genetic immunization via micromechanical disruption of skin-barrier function and targeted epidermal delivery. Nature medicine. 2002;8(4):415-9. Epub 2002/04/03.
140. McAllister DV, Wang PM, Davis SP, Park JH, Canatella PJ, Allen MG, et al. Microfabricated needles for transdermal delivery of macromolecules and nanoparticles: fabrication methods and transport studies. Proceedings of the National Academy of Sciences of the United States of America. 2003;100(24):13755-60. Epub 2003/11/19.
141. Birchall J, Coulman S, Pearton M, Allender C, Brain K, Anstey A, et al. Cutaneous DNA delivery and gene expression in ex vivo human skin explants via wet-etch micro-fabricated micro-needles. Journal of drug targeting. 2005;13(7):415-21. Epub 2005/11/26.
142. Coulman SA, Barrow D, Anstey A, Gateley C, Morrissey A, Wilke N, et al. Minimally invasive cutaneous delivery of macromolecules and plasmid DNA via microneedles. Current drug delivery. 2006;3(1):65-75. Epub 2006/02/14.
143. Widera G, Johnson J, Kim L, Libiran L, Nyam K, Daddona PE, et al. Effect of delivery parameters on immunization to ovalbumin following intracutaneous administration by a coated microneedle array patch system. Vaccine. 2006;24(10):1653-64. Epub 2005/10/26.
144. Matriano JA, Cormier M, Johnson J, Young WA, Buttery M, Nyam K, et al. Macroflux microprojection array patch technology: a new and efficient approach for intracutaneous immunization. Pharmaceutical research. 2002;19(1):63-70. Epub 2002/02/12.
145. Gill HS, Prausnitz MR. Coated microneedles for transdermal delivery. Journal of controlled release : official journal of the Controlled Release Society. 2007;117(2):227-37. Epub 2006/12/16.

146. Gill HS, Prausnitz MR. Coating formulations for microneedles. Pharmaceutical research. 2007;24(7):1369-80. Epub 2007/03/27.
147. Zhu Q, Zarnitsyn VG, Ye L, Wen Z, Gao Y, Pan L, et al. Immunization by vaccine-coated microneedle arrays protects against lethal influenza virus challenge. Proceedings of the National Academy of Sciences of the United States of America. 2009;106(19):7968-73. Epub 2009/05/07.
148. Pearton M, Kang SM, Song JM, Kim YC, Quan FS, Anstey A, et al. Influenza virus-like particles coated onto microneedles can elicit stimulatory effects on Langerhans cells in human skin. Vaccine. 2010;28(37):6104-13. Epub 2010/08/06.
149. Gill HS, Soderholm J, Prausnitz MR, Sallberg M. Cutaneous vaccination using microneedles coated with hepatitis C DNA vaccine. Gene therapy. 2010;17(6):811-4. Epub 2010/03/05.
150. Hiraishi Y, Nandakumar S, Choi SO, Lee JW, Kim YC, Posey JE, et al. Bacillus Calmette-Guerin vaccination using a microneedle patch. Vaccine. 2011;29(14):2626-36. Epub 2011/02/01.
151. Koutsonanos DG, del Pilar Martin M, Zarnitsyn VG, Sullivan SP, Compans RW, Prausnitz MR, et al. Transdermal influenza immunization with vaccine-coated microneedle arrays. PloS ONE. 2009;4(3):e4773. Epub 2009/03/11.
152. Kim YC, Quan FS, Yoo DG, Compans RW, Kang SM, Prausnitz MR. Improved influenza vaccination in the skin using vaccine coated microneedles. Vaccine. 2009;27(49):6932-8. Epub 2009/09/19.
153. Koutsonanos DG, Del Pilar Martin M, Zarnitsyn VG, Jacob J, Prausnitz MR, Compans RW, et al. Serological Memory and Long-term Protection to Novel H1N1 Influenza Virus After Skin Vaccination. The Journal of infectious diseases. 2011. Epub 2011/06/21.
154. Kim YC, Quan FS, Compans RW, Kang SM, Prausnitz MR. Formulation of microneedles coated with influenza virus-like particle vaccine. AAPS PharmSciTech. 2010;11(3):1193-201. Epub 2010/08/03.
155. Quan FS, Kim YC, Vunnava A, Yoo DG, Song JM, Prausnitz MR, et al. Intradermal vaccination with influenza virus-like particles by using microneedles induces protection superior to that with intramuscular immunization. Journal of virology. 2010;84(15):7760-9. Epub 2010/05/21.
156. Song JM, Kim YC, Lipatov AS, Pearton M, Davis CT, Yoo DG, et al. Microneedle delivery of H5N1 influenza virus-like particles to the skin induces long-lasting B- and T-cell responses in mice. Clin Vaccine Immunol. 2010;17(9):1381-9. Epub 2010/07/16.
157. Weldon WC, Martin MP, Zarnitsyn V, Wang B, Koutsonanos D, Skountzou I, et al. Microneedle vaccination with stabilized recombinant influenza hemagglutinin induces improved protective immunity. Clin Vaccine Immunol. 2011;18(4):647-54. Epub 2011/02/04.
158. Quan FS, Kim YC, Compans RW, Prausnitz MR, Kang SM. Dose sparing enabled by skin immunization with influenza virus-like particle vaccine using microneedles. Journal of controlled release : official journal of the Controlled Release Society. 2010;147(3):326-32. Epub 2010/08/10.
159. Kim YC, Quan FS, Yoo DG, Compans RW, Kang SM, Prausnitz MR. Enhanced memory responses to seasonal H1N1 influenza vaccination of the skin with the use of vaccine-coated microneedles. The Journal of infectious diseases. 2010;201(2):190-8. Epub 2009/12/19.
160. Pearton M, Allender C, Brain K, Anstey A, Gateley C, Wilke N, et al. Gene delivery to the epidermal cells of human skin explants using microfabricated

microneedles and hydrogel formulations. Pharmaceutical research. 2008;25(2):407-16. Epub 2007/08/03.
161. Quan FS, Kim YC, Yoo DG, Compans RW, Prausnitz MR, Kang SM. Stabilization of influenza vaccine enhances protection by microneedle delivery in the mouse skin. PloS ONE. 2009;4(9):e7152. Epub 2009/09/26.
162. Kim YC, Quan FS, Compans RW, Kang SM, Prausnitz MR. Formulation and coating of microneedles with inactivated influenza virus to improve vaccine stability and immunogenicity. Journal of controlled release : official journal of the Controlled Release Society. 2010;142(2):187-95. Epub 2009/10/21.
163. Kim YC, Quan FS, Compans RW, Kang SM, Prausnitz MR. Stability kinetics of influenza vaccine coated onto microneedles during drying and storage. Pharmaceutical research. 2011;28(1):135-44. Epub 2010/04/14.
164. Ito Y, Kashiwara S, Fukushima K, Takada K. Two-layered dissolving microneedles for percutaneous delivery of sumatriptan in rats. Drug development and industrial pharmacy. 2011. Epub 2011/05/07.
165. Ito Y, Yoshimitsu J, Shiroyama K, Sugioka N, Takada K. Self-dissolving microneedles for the percutaneous absorption of EPO in mice. Journal of drug targeting. 2006;14(5):255-61. Epub 2006/08/03.
166. Ito Y, Hagiwara E, Saeki A, Sugioka N, Takada K. Feasibility of microneedles for percutaneous absorption of insulin. European journal of pharmaceutical sciences : official journal of the European Federation for Pharmaceutical Sciences. 2006;29(1):82-8. Epub 2006/07/11.
167. Lee JW, Choi SO, Felner EI, Prausnitz MR. Dissolving Microneedle Patch for Transdermal Delivery of Human Growth Hormone. Small. 2011. Epub 2011/01/06.
168. Raphael AP, Prow TW, Crichton ML, Chen X, Fernando GJ, Kendall MA. Targeted, needle-free vaccinations in skin using multilayered, densely-packed dissolving microprojection arrays. Small. 2010;6(16):1785-93. Epub 2010/07/29.
169. Sullivan SP, Koutsonanos DG, Del Pilar Martin M, Lee JW, Zarnitsyn V, Choi SO, et al. Dissolving polymer microneedle patches for influenza vaccination. Nature medicine. 2010;16(8):915-20. Epub 2010/07/20.
170. Miyano T, Tobinaga Y, Kanno T, Matsuzaki Y, Takeda H, Wakui M, et al. Sugar micro needles as transdermic drug delivery system. Biomedical microdevices. 2005;7(3):185-8. Epub 2005/09/01.
171. Donnelly RF, Morrow DI, Singh TR, Migalska K, McCarron PA, O'Mahony C, et al. Processing difficulties and instability of carbohydrate microneedle arrays. Drug development and industrial pharmacy. 2009;35(10):1242-54. Epub 2009/06/27.
172. Burton SA, Ng CY, Simmers R, Moeckly C, Brandwein D, Gilbert T, et al. Rapid intradermal delivery of liquid formulations using a hollow microstructured array. Pharmaceutical research. 2011;28(1):31-40. Epub 2010/06/29.
173. Martanto W, Moore JS, Couse T, Prausnitz MR. Mechanism of fluid infusion during microneedle insertion and retraction. Journal of controlled release : official journal of the Controlled Release Society. 2006;112(3):357-61. Epub 2006/04/22.
174. Martanto W, Moore JS, Kashlan O, Kamath R, Wang PM, O'Neal JM, et al. Microinfusion using hollow microneedles. Pharmaceutical research. 2006;23(1):104-13. Epub 2005/11/26.
175. Gupta J, Park SS, Bondy B, Felner EI, Prausnitz MR. Infusion pressure and pain during microneedle injection into skin of human subjects. Biomaterials. 2011. Epub 2011/06/21.
176. Harvey AJ, Kaestner SA, Sutter DE, Harvey NG, Mikszta JA, Pettis RJ. Microneedle-based intradermal delivery enables rapid lymphatic uptake and

distribution of protein drugs. Pharmaceutical research. 2011;28(1):107-16. Epub 2010/04/01.
177. Mulholland WJ, Arbuthnott EA, Bellhouse BJ, Cornhill JF, Austyn JM, Kendall MA, et al. Multiphoton high-resolution 3D imaging of Langerhans cells and keratinocytes in the mouse skin model adopted for epidermal powdered immunization. J Invest Dermatol. 2006;126(7):1541-8. Epub 2006/04/29.
178. Kendall M. Engineering of needle-free physical methods to target epidermal cells for DNA vaccination. Vaccine. 2006;24(21):4651-6. Epub 2005/09/16.
179. Wesley NO, Maibach HI. Racial (ethnic) differences in skin properties: the objective data. Am J Clin Dermatol. 2003;4(12):843-60. Epub 2003/12/04.
180. Calleja-Agius J, Muscat-Baron Y, Brincat MP. Skin ageing. Menopause Int. 2007;13(2):60-4. Epub 2007/06/02.
181. Kendall M, Rishworth S, Carter F, Mitchell T. Effects of relative humidity and ambient temperature on the ballistic delivery of micro-particles to excised porcine skin. J Invest Dermatol. 2004;122(3):739-46. Epub 2004/04/17.
182. Diridollou S, de Rigal J, Querleux B, Leroy F, Holloway Barbosa V. Comparative study of the hydration of the stratum corneum between four ethnic groups: influence of age. Int J Dermatol. 2007;46 Suppl 1:11-4. Epub 2007/10/09.
183. Ghoreishi M, Dutz JP. Tolerance induction by transcutaneous immunization through ultraviolet-irradiated skin is transferable through CD4+CD25+ T regulatory cells and is dependent on host-derived IL-10. Journal of immunology. 2006;176(4):2635-44. Epub 2006/02/04.
184. Stein P, Rechtsteiner G, Warger T, Bopp T, Fuhr T, Prufer S, et al. UV exposure boosts transcutaneous immunization and improves tumor immunity: cytotoxic T-cell priming through the skin. The Journal of investigative dermatology. 2011;131(1):211-9. Epub 2010/08/27.
185. Loser K, Beissert S. Regulation of cutaneous immunity by the environment: an important role for UV irradiation and vitamin D. International immunopharmacology. 2009;9(5):587-9. Epub 2009/06/23.
186. Bal SM, Caussin J, Pavel S, Bouwstra JA. In vivo assessment of safety of microneedle arrays in human skin. European journal of pharmaceutical sciences : official journal of the European Federation for Pharmaceutical Sciences. 2008;35(3):193-202. Epub 2008/07/29.
187. Haq MI, Smith E, John DN, Kalavala M, Edwards C, Anstey A, et al. Clinical administration of microneedles: skin puncture, pain and sensation. Biomedical microdevices. 2009;11(1):35-47. Epub 2008/07/30.
188. Kaushik S, Hord AH, Denson DD, McAllister DV, Smitra S, Allen MG, et al. Lack of pain associated with microfabricated microneedles. Anesthesia and analgesia. 2001;92(2):502-4. Epub 2001/02/13.
189. Crichton ML, Ansaldo A, Chen X, Prow TW, Fernando GJ, Kendall MA. The effect of strain rate on the precision of penetration of short densely-packed microprojection array patches coated with vaccine. Biomaterials. 2010;31(16):4562-72. Epub 2010/03/17.
190. Verbaan FJ, Bal SM, van den Berg DJ, Dijksman JA, van Hecke M, Verpoorten H, et al. Improved piercing of microneedle arrays in dermatomed human skin by an impact insertion method. Journal of controlled release : official journal of the Controlled Release Society. 2008;128(1):80-8. Epub 2008/04/09.
191. Roth RR, James WD. Microbial ecology of the skin. Annu Rev Microbiol. 1988;42:441-64. Epub 1988/01/01.

192. Donnelly RF, Singh TR, Tunney MM, Morrow DI, McCarron PA, O'Mahony C, et al. Microneedle arrays allow lower microbial penetration than hypodermic needles in vitro. Pharmaceutical research. 2009;26(11):2513-22. Epub 2009/09/17.
193. Gittard SD, Narayan RJ, Jin C, Ovsianikov A, Chichkov BN, Monteiro-Riviere NA, et al. Pulsed laser deposition of antimicrobial silver coating on Ormocer microneedles. Biofabrication. 2009;1(4):041001. Epub 2010/07/28.
194. Wang PM, Cornwell M, Prausnitz MR. Minimally invasive extraction of dermal interstitial fluid for glucose monitoring using microneedles. Diabetes technology & therapeutics. 2005;7(1):131-41. Epub 2005/03/02.
195. Gupta J, Gill HS, Andrews SN, Prausnitz MR. Kinetics of skin resealing after insertion of microneedles in human subjects. Journal of controlled release : official journal of the Controlled Release Society. 2011. Epub 2011/06/07.
196. Birchall JC, Clemo R, Anstey A, John DN. Microneedles in clinical practice--an exploratory study into the opinions of healthcare professionals and the public. Pharmaceutical research. 2011;28(1):95-106. Epub 2010/03/20.
197. Simonsen L, Kane A, Lloyd J, Zaffran M, Kane M. Unsafe injections in the developing world and transmission of bloodborne pathogens: a review. Bull World Health Organ. 1999;77(10):789-800. Epub 1999/12/11.
198. Organisation WH. World Malaria Report. World Health Organization, 2008.
199. [17 June 2011]; The World Bank - Malaria.]. Available from: http://go.worldbank.org/QP5C2FX810.
200. Holding PA, Snow RW. Impact of Plasmodium falciparum malaria on performance and learning: review of the evidence. The American journal of tropical medicine and hygiene. 2001;64(1-2 Suppl):68-75. Epub 2001/06/27.
201. Brooke BD, Kloke G, Hunt RH, Koekemoer LL, Temu EA, Taylor ME, et al. Bioassay and biochemical analyses of insecticide resistance in southern African Anopheles funestus (Diptera: Culicidae). Bull Entomol Res. 2001;91(4):265-72. Epub 2001/10/06.
202. Hastings IM, Watkins WM, White NJ. The evolution of drug-resistant malaria: the role of drug elimination half-life. Philosophical transactions of the Royal Society of London Series B, Biological sciences. 2002;357(1420):505-19. Epub 2002/05/25.
203. Laveran CL. Classics in infectious diseases: A newly discovered parasite in the blood of patients suffering from malaria. Parasitic etiology of attacks of malaria: Charles Louis Alphonse Laveran (1845-1922). Rev Infect Dis. 1982;4(4):908-11. Epub 1982/07/01.
204. Ross R. The role of the mosquito in the evolution of the malarial parasite: the recent researches of Surgeon-Major Ronald Ross, I.M.S. 1898. Yale J Biol Med. 2002;75(2):103-5. Epub 2002/09/17.
205. Newbold C, Craig A, Kyes S, Rowe A, Fernandez-Reyes D, Fagan T. Cytoadherence, pathogenesis and the infected red cell surface in Plasmodium falciparum. International journal for parasitology. 1999;29(6):927-37. Epub 1999/09/10.
206. Control CfD. [11-05-11]; Available from: http://www.dpd.cdc.gov/DPDX/HTML/ImageLibrary/M-R/Malaria/body_Malaria_il1.htm.
207. Doolan DL, Dobano C, Baird JK. Acquired immunity to malaria. Clinical microbiology reviews. 2009;22(1):13-36, Table of Contents. Epub 2009/01/13.
208. Nussenzweig RS, Vanderberg J, Most H, Orton C. Protective immunity produced by the injection of x-irradiated sporozoites of plasmodium berghei. Nature. 1967;216(5111):160-2. Epub 1967/10/14.

209. Hoffman SL, Goh LM, Luke TC, Schneider I, Le TP, Doolan DL, et al. Protection of humans against malaria by immunization with radiation-attenuated Plasmodium falciparum sporozoites. The Journal of infectious diseases. 2002;185(8):1155-64. Epub 2002/04/04.
210. Clyde DF, Most H, McCarthy VC, Vanderberg JP. Immunization of man against sporozite-induced falciparum malaria. Am J Med Sci. 1973;266(3):169-77. Epub 1973/09/01.
211. Rieckmann KH, Carson PE, Beaudoin RL, Cassells JS, Sell KW. Letter: Sporozoite induced immunity in man against an Ethiopian strain of Plasmodium falciparum. Transactions of the Royal Society of Tropical Medicine and Hygiene. 1974;68(3):258-9. Epub 1974/01/01.
212. Rieckmann KH. Human immunization with attenuated sporozoites. Bulletin of the World Health Organization. 1990;68 Suppl:13-6. Epub 1990/01/01.
213. Rieckmann KH, Beaudoin RL, Cassells JS, Sell KW. Use of attenuated sporozoites in the immunization of human volunteers against falciparum malaria. Bulletin of the World Health Organization. 1979;57 Suppl 1:261-5. Epub 1979/01/01.
214. Luke TC, Hoffman SL. Rationale and plans for developing a non-replicating, metabolically active, radiation-attenuated Plasmodium falciparum sporozoite vaccine. The Journal of experimental biology. 2003;206(Pt 21):3803-8. Epub 2003/09/25.
215. Casares S, Brumeanu TD, Richie TL. The RTS,S malaria vaccine. Vaccine. 2010;28(31):4880-94. Epub 2010/06/18.
216. Olotu A, Lusingu J, Leach A, Lievens M, Vekemans J, Msham S, et al. Efficacy of RTS,S/AS01E malaria vaccine and exploratory analysis on anti-circumsporozoite antibody titres and protection in children aged 5-17 months in Kenya and Tanzania: a randomised controlled trial. Lancet Infect Dis. 2011;11(2):102-9. Epub 2011/01/18.
217. Lusingu J, Olotu A, Leach A, Lievens M, Vekemans J, Olivier A, et al. Safety of the malaria vaccine candidate, RTS,S/AS01E in 5 to 17 month old Kenyan and Tanzanian Children. PloS ONE. 2010;5(11):e14090. Epub 2010/12/03.
218. Crompton PD, Pierce SK, Miller LH. Advances and challenges in malaria vaccine development. J Clin Inv. 2010;120(12):4168-78. Epub 2010/12/03.
219. Walther M, Dunachie S, Keating S, Vuola JM, Berthoud T, Schmidt A, et al. Safety, immunogenicity and efficacy of a pre-erythrocytic malaria candidate vaccine, ICC-1132 formulated in Seppic ISA 720. Vaccine. 2005;23(7):857-64. Epub 2004/12/18.
220. Webster DP, Dunachie S, McConkey S, Poulton I, Moore AC, Walther M, et al. Safety of recombinant fowlpox strain FP9 and modified vaccinia virus Ankara vaccines against liver-stage P. falciparum malaria in non-immune volunteers. Vaccine. 2006;24(15):3026-34. Epub 2006/02/21.
221. Hermsen CC, Verhage DF, Telgt DS, Teelen K, Bousema JT, Roestenberg M, et al. Glutamate-rich protein (GLURP) induces antibodies that inhibit in vitro growth of Plasmodium falciparum in a phase 1 malaria vaccine trial. Vaccine. 2007;25(15):2930-40. Epub 2006/08/18.
222. Biswas S, Dicks MD, Long CA, Remarque EJ, Siani L, Colloca S, et al. Transgene Optimization, Immunogenicity and In Vitro Efficacy of Viral Vectored Vaccines Expressing Two Alleles of Plasmodium falciparum AMA1. PLoS One. 2011;6(6):e20977. Epub 2011/06/24.
223. Draper SJ, Goodman AL, Biswas S, Forbes EK, Moore AC, Gilbert SC, et al. Recombinant viral vaccines expressing merozoite surface protein-1 induce antibody-

and T cell-mediated multistage protection against malaria. Cell Host Microbe. 2009;5(1):95-105. Epub 2009/01/22.
224. Draper SJ, Biswas S, Spencer AJ, Remarque EJ, Capone S, Naddeo M, et al. Enhancing blood-stage malaria subunit vaccine immunogenicity in rhesus macaques by combining adenovirus, poxvirus, and protein-in-adjuvant vaccines. Journal of immunology. 2010;185(12):7583-95. Epub 2010/11/26.
225. Douglas AD, de Cassan SC, Dicks MD, Gilbert SC, Hill AV, Draper SJ. Tailoring subunit vaccine immunogenicity: maximizing antibody and T cell responses by using combinations of adenovirus, poxvirus and protein-adjuvant vaccines against Plasmodium falciparum MSP1. Vaccine. 2010;28(44):7167-78. Epub 2010/10/13.
226. Wu Y, Ellis RD, Shaffer D, Fontes E, Malkin EM, Mahanty S, et al. Phase 1 trial of malaria transmission blocking vaccine candidates Pfs25 and Pvs25 formulated with montanide ISA 51. PloS ONE. 2008;3(7):e2636. Epub 2008/07/10.
227. Outchkourov NS, Roeffen W, Kaan A, Jansen J, Luty A, Schuiffel D, et al. Correctly folded Pfs48/45 protein of Plasmodium falciparum elicits malaria transmission-blocking immunity in mice. Proceedings of the National Academy of Sciences of the United States of America. 2008;105(11):4301-5. Epub 2008/03/12.
228. Schwenk RJ, Richie TL. Protective immunity to pre-erythrocytic stage malaria. Trends in parasitology. 2011. Epub 2011/03/26.
229. Doolan DL, Hoffman SL. The complexity of protective immunity against liver-stage malaria. Journal of immunology. 2000;165(3):1453-62. Epub 2000/07/21.
230. John CC, Moormann AM, Sumba PO, Ofulla AV, Pregibon DC, Kazura JW. Gamma interferon responses to Plasmodium falciparum liver-stage antigen 1 and thrombospondin-related adhesive protein and their relationship to age, transmission intensity, and protection against malaria. Infect Immun. 2004;72(9):5135-42. Epub 2004/08/24.
231. Reece WH, Pinder M, Gothard PK, Milligan P, Bojang K, Doherty T, et al. A CD4(+) T-cell immune response to a conserved epitope in the circumsporozoite protein correlates with protection from natural Plasmodium falciparum infection and disease. Nat Med. 2004;10(4):406-10. Epub 2004/03/23.
232. Ferreira A, Schofield L, Enea V, Schellekens H, van der Meide P, Collins WE, et al. Inhibition of development of exoerythrocytic forms of malaria parasites by gamma-interferon. Science. 1986;232(4752):881-4. Epub 1986/05/16.
233. Schofield L, Ferreira A, Altszuler R, Nussenzweig V, Nussenzweig RS. Interferon-gamma inhibits the intrahepatocytic development of malaria parasites in vitro. J Immunol. 1987;139(6):2020-5. Epub 1987/09/15.
234. Mellouk S, Maheshwari RK, Rhodes-Feuillette A, Beaudoin RL, Berbiguier N, Matile H, et al. Inhibitory activity of interferons and interleukin 1 on the development of Plasmodium falciparum in human hepatocyte cultures. Journal of immunology. 1987;139(12):4192-5. Epub 1987/12/15.
235. Tsuji M, Miyahira Y, Nussenzweig RS, Aguet M, Reichel M, Zavala F. Development of antimalaria immunity in mice lacking IFN-gamma receptor. Journal of immunology. 1995;154(10):5338-44. Epub 1995/05/15.
236. Yang Y, Xiang Z, Ertl HC, Wilson JM. Upregulation of class I major histocompatibility complex antigens by interferon gamma is necessary for T-cell-mediated elimination of recombinant adenovirus-infected hepatocytes in vivo. Proceedings of the National Academy of Sciences of the United States of America. 1995;92(16):7257-61. Epub 1995/08/01.
237. Sedegah M, Finkelman F, Hoffman SL. Interleukin 12 induction of interferon gamma-dependent protection against malaria. Proceedings of the National Academy

of Sciences of the United States of America. 1994;91(22):10700-2. Epub 1994/10/25.
238. Mellouk S, Hoffman SL, Liu ZZ, de la Vega P, Billiar TR, Nussler AK. Nitric oxide-mediated antiplasmodial activity in human and murine hepatocytes induced by gamma interferon and the parasite itself: enhancement by exogenous tetrahydrobiopterin. Infection and immunity. 1994;62(9):4043-6. Epub 1994/09/01.
239. Nussler AK, Renia L, Pasquetto V, Miltgen F, Matile H, Mazier D. In vivo induction of the nitric oxide pathway in hepatocytes after injection with irradiated malaria sporozoites, malaria blood parasites or adjuvants. European journal of immunology. 1993;23(4):882-7. Epub 1993/04/01.
240. Seguin MC, Klotz FW, Schneider I, Weir JP, Goodbary M, Slayter M, et al. Induction of nitric oxide synthase protects against malaria in mice exposed to irradiated Plasmodium berghei infected mosquitoes: involvement of interferon gamma and CD8+ T cells. The Journal of experimental medicine. 1994;180(1):353-8. Epub 1994/07/01.
241. Berenzon D, Schwenk RJ, Letellier L, Guebre-Xabier M, Williams J, Krzych U. Protracted protection to Plasmodium berghei malaria is linked to functionally and phenotypically heterogeneous liver memory CD8+ T cells. Journal of immunology. 2003;171(4):2024-34. Epub 2003/08/07.
242. Reyes-Sandoval A, Harty JT, Todryk SM. Viral vector vaccines make memory T cells against malaria. Immunology. 2007;121(2):158-65. Epub 2007/04/28.
243. Reyes-Sandoval A, Wyllie DH, Bauza K, Milicic A, Forbes EK, Rollier CS, et al. CD8+ T Effector Memory Cells Protect against Liver-Stage Malaria. J Immunol. 2011;187(3):1347-57. Epub 2011/07/01.
244. Stewart MJ, Vanderberg JP. Malaria sporozoites leave behind trails of circumsporozoite protein during gliding motility. J Protozool. 1988;35(3):389-93. Epub 1988/08/01.
245. Singh AP, Buscaglia CA, Wang Q, Levay A, Nussenzweig DR, Walker JR, et al. Plasmodium circumsporozoite protein promotes the development of the liver stages of the parasite. Cell. 2007;131(3):492-504. Epub 2007/11/06.
246. Romero P, Maryanski JL, Corradin G, Nussenzweig RS, Nussenzweig V, Zavala F. Cloned cytotoxic T cells recognize an epitope in the circumsporozoite protein and protect against malaria. Nature. 1989;341(6240):323-6. Epub 1989/09/28.
247. Plebanski M, Gilbert SC, Schneider J, Hannan CM, Layton G, Blanchard T, et al. Protection from Plasmodium berghei infection by priming and boosting T cells to a single class I-restricted epitope with recombinant carriers suitable for human use. Eur J Immunol. 1998;28(12):4345-55. Epub 1998/12/23.
248. Reyes-Sandoval A, Pearson FE, Todryk S, Ewer K. Potency assays for novel T-cell-inducing vaccines against malaria. Current opinion in molecular therapeutics. 2009;11(1):72-80. Epub 2009/01/27.
249. Aidoo M, Lalvani A, Allsopp CE, Plebanski M, Meisner SJ, Krausa P, et al. Identification of conserved antigenic components for a cytotoxic T lymphocyte-inducing vaccine against malaria. Lancet. 1995;345(8956):1003-7. Epub 1995/04/22.
250. Gilbert SC, Plebanski M, Harris SJ, Allsopp CE, Thomas R, Layton GT, et al. A protein particle vaccine containing multiple malaria epitopes. Nature biotechnology. 1997;15(12):1280-4. Epub 1997/11/14.
251. Reyes-Sandoval A, Sridhar S, Berthoud T, Moore AC, Harty JT, Gilbert SC, et al. Single-dose immunogenicity and protective efficacy of simian adenoviral vectors against Plasmodium berghei. Eur J Immunol. 2008;38(3):732-41. Epub 2008/02/13.

252. Sridhar S, Reyes-Sandoval A, Draper SJ, Moore AC, Gilbert SC, Gao GP, et al. Single-dose protection against Plasmodium berghei by a simian adenovirus vector using a human cytomegalovirus promoter containing intron A. Journal of virology. 2008;82(8):3822-33. Epub 2008/02/08.
253. Moore AC, Hill AV. Progress in DNA-based heterologous prime-boost immunization strategies for malaria. Immunol Rev. 2004;199:126-43. Epub 2004/07/06.
254. Geiben-Lynn R, Greenland JR, Frimpong-Boateng K, Letvin NL. Kinetics of recombinant adenovirus type 5, vaccinia virus, modified vaccinia ankara virus, and DNA antigen expression in vivo and the induction of memory T-lymphocyte responses. Clinical and vaccine immunology : CVI. 2008;15(4):691-6. Epub 2008/02/15.
255. Carroll MW, Moss B. Poxviruses as expression vectors. Current opinion in biotechnology. 1997;8(5):573-7. Epub 1997/11/14.
256. Carroll MW, Moss B. Host range and cytopathogenicity of the highly attenuated MVA strain of vaccinia virus: propagation and generation of recombinant viruses in a nonhuman mammalian cell line. Virology. 1997;238(2):198-211. Epub 1997/12/24.
257. Brookes RH, Hill PC, Owiafe PK, Ibanga HB, Jeffries DJ, Donkor SA, et al. Safety and immunogenicity of the candidate tuberculosis vaccine MVA85A in West Africa. PloS ONE. 2008;3(8):e2921. Epub 2008/08/14.
258. Berthoud TK, Hamill M, Lillie PJ, Hwenda L, Collins KA, Ewer KJ, et al. Potent CD8+ T-cell immunogenicity in humans of a novel heterosubtypic influenza A vaccine, MVA-NP+M1. Clinical infectious diseases : an official publication of the Infectious Diseases Society of America. 2011;52(1):1-7. Epub 2010/12/15.
259. Mwau M, Cebere I, Sutton J, Chikoti P, Winstone N, Wee EG, et al. A human immunodeficiency virus 1 (HIV-1) clade A vaccine in clinical trials: stimulation of HIV-specific T-cell responses by DNA and recombinant modified vaccinia virus Ankara (MVA) vaccines in humans. The Journal of general virology. 2004;85(Pt 4):911-9. Epub 2004/03/25.
260. Tatsis N, Ertl HC. Adenoviruses as vaccine vectors. Molecular therapy : the journal of the American Society of Gene Therapy. 2004;10(4):616-29. Epub 2004/09/29.
261. Mizuguchi H, Kay MA, Hayakawa T. Approaches for generating recombinant adenovirus vectors. Advanced drug delivery reviews. 2001;52(3):165-76. Epub 2001/11/24.
262. Reyes-Sandoval A, Berthoud T, Alder N, Siani L, Gilbert SC, Nicosia A, et al. Prime-boost immunization with adenoviral and modified vaccinia virus Ankara vectors enhances the durability and polyfunctionality of protective malaria CD8+ T-cell responses. Infect Immun. 2010;78(1):145-53. Epub 2009/10/28.
263. Dudareva M, Andrews L, Gilbert SC, Bejon P, Marsh K, Mwacharo J, et al. Prevalence of serum neutralizing antibodies against chimpanzee adenovirus 63 and human adenovirus 5 in Kenyan children, in the context of vaccine vector efficacy. Vaccine. 2009;27(27):3501-4. Epub 2009/05/26.
264. McCoy K, Tatsis N, Korioth-Schmitz B, Lasaro MO, Hensley SE, Lin SW, et al. Effect of preexisting immunity to adenovirus human serotype 5 antigens on the immune responses of nonhuman primates to vaccine regimens based on human- or chimpanzee-derived adenovirus vectors. Journal of virology. 2007;81(12):6594-604. Epub 2007/04/13.

265. Carey JB, Pearson FE, Vrdoljak A, Crean AM, Walsh PT, O'Mahony C, et al. Microneedle array design determines the induction of protective memory CD8+ T cell responses induced by a recombinant live malaria vaccine in mice. PLoS One. 2011;6(7).
266. McGrath MG, Vrdoljak A, O'Mahony C, Oliveira JC, Moore AC, Crean AM. Determination of parameters for successful spray coating of silicon microneedle arrays. Int J Pharm. 2011;415(1-2):140-9. Epub 2011/06/15.
267. Barriers I-IStVD. [12 May 2011]; Available from: http://www.immupatch.com.
268. Wilke N, Mulcahy A, Ye S-R, Morissey A. Process optimization and characterization of silicon microneedles fabricated by wet etch technology. Microelectronics Journal. 2005;36:650-6.
269. Enfield J, O'Connell ML, Lawlor K, Jonathan E, O'Mahony C, Leahy M. In-vivo dynamic characterization of microneedle skin penetration using optical coherence tomography. J Biomed Opt. 2010;15(4):046001. Epub 2010/08/31.
270. Chen X, Prow TW, Crichton ML, Jenkins DW, Roberts MS, Frazer IH, et al. Dry-coated microprojection array patches for targeted delivery of immunotherapeutics to the skin. J Control Release. 2009;139(3):212-20. Epub 2009/07/07.
271. Fernando GJ, Chen X, Prow TW, Crichton ML, Fairmaid EJ, Roberts MS, et al. Potent immunity to low doses of influenza vaccine by probabilistic guided micro-targeted skin delivery in a mouse model. PloS ONE. 2010;5(4):e10266. Epub 2010/04/28.
272. Prow TW, Chen X, Prow NA, Fernando GJ, Tan CS, Raphael AP, et al. Nanopatch-targeted skin vaccination against West Nile Virus and Chikungunya virus in mice. Small. 2010;6(16):1776-84. Epub 2010/07/29.
273. Chen X, Kask AS, Crichton ML, McNeilly C, Yukiko S, Dong L, et al. Improved DNA vaccination by skin-targeted delivery using dry-coated densely-packed microprojection arrays. J Control Release. 2010;148(3):327-33. Epub 2010/09/21.
274. Corbett HJ, Fernando GJ, Chen X, Frazer IH, Kendall MA. Skin vaccination against cervical cancer associated human papillomavirus with a novel micro-projection array in a mouse model. PloS ONE. 2010;5(10):e13460. Epub 2010/10/27.
275. Kendall MAF, inventor; Device for Delivery of Bioactive Materials and Other Stimuli patent WO 2005/072630. 2005.
276. Schneider J, Gilbert SC, Blanchard TJ, Hanke T, Robson KJ, Hannan CM, et al. Enhanced immunogenicity for CD8+ T cell induction and complete protective efficacy of malaria DNA vaccination by boosting with modified vaccinia virus Ankara. Nat Med. 1998;4(4):397-402. Epub 1998/04/18.
277. McShane H, Behboudi S, Goonetilleke N, Brookes R, Hill AV. Protective immunity against Mycobacterium tuberculosis induced by dendritic cells pulsed with both CD8(+)- and CD4(+)-T-cell epitopes from antigen 85A. Infection and immunity. 2002;70(3):1623-6. Epub 2002/02/21.
278. Falkner FG, Moss B. Transient dominant selection of recombinant vaccinia viruses. Journal of virology. 1990;64(6):3108-11. Epub 1990/06/01.
279. Saito I, Oya Y, Yamamoto K, Yuasa T, Shimojo H. Construction of nondefective adenovirus type 5 bearing a 2.8-kilobase hepatitis B virus DNA near the right end of its genome. Journal of virology. 1985;54(3):711-9. Epub 1985/06/01.
280. Chen X, Fernando GJ, Crichton ML, Flaim C, Yukiko SR, Fairmaid EJ, et al. Improving the reach of vaccines to low-resource regions, with a needle-free vaccine

delivery device and long-term thermostabilization. J Control Release. 2011;152(3):349-55. Epub 2011/03/05.
281. Qiagen. DNeasy Animal Blood & Tissue Kit Handbook. [Accessed on 11 November 2010]; Available from: http://www.qiagen.com/products/genomicdnastabilizationpurification/dneasytissuesystem/dneasybloodtissuekit.aspx#Tabs=t2.
282. Bruna-Romero O, Hafalla JC, Gonzalez-Aseguinolaza G, Sano G, Tsuji M, Zavala F. Detection of malaria liver-stages in mice infected through the bite of a single Anopheles mosquito using a highly sensitive real-time PCR. International journal for parasitology. 2001;31(13):1499-502. Epub 2001/10/12.
283. Simen BB, Duman CH, Simen AA, Duman RS. TNFalpha signaling in depression and anxiety: behavioral consequences of individual receptor targeting. Biological psychiatry. 2006;59(9):775-85. Epub 2006/02/07.
284. Roederer M, Nozzi JL, Nason MX. SPICE: Exploration and analysis of post-cytometric complex multivariate datasets. Cytometry Part A : the journal of the International Society for Analytical Cytology. 2011. Epub 2011/01/11.
285. Lutty GA, Merges C, Threlkeld AB, Crone S, McLeod DS. Heterogeneity in localization of isoforms of TGF-beta in human retina, vitreous, and choroid. Investigative ophthalmology & visual science. 1993;34(3):477-87. Epub 1993/03/01.
286. Hill AV, Reyes-Sandoval A, O'Hara G, Ewer K, Lawrie A, Goodman A, et al. Prime-boost vectored malaria vaccines: progress and prospects. Hum Vaccines. 2010;6(1):78-83. Epub 2010/01/12.
287. Vordermeier HM, Villarreal-Ramos B, Cockle PJ, McAulay M, Rhodes SG, Thacker T, et al. Viral booster vaccines improve Mycobacterium bovis BCG-induced protection against bovine tuberculosis. Infection and immunity. 2009;77(8):3364-73. Epub 2009/06/03.
288. Capone S, Reyes-Sandoval A, Naddeo M, Siani L, Ammendola V, Rollier CS, et al. Immune responses against a liver-stage malaria antigen induced by simian adenoviral vector AdCh63 and MVA prime-boost immunisation in non-human primates. Vaccine. 2010;29(2):256-65. Epub 2010/10/30.
289. Gilbert SC, Schneider J, Hannan CM, Hu JT, Plebanski M, Sinden R, et al. Enhanced CD8 T cell immunogenicity and protective efficacy in a mouse malaria model using a recombinant adenoviral vaccine in heterologous prime-boost immunisation regimes. Vaccine. 2002;20(7-8):1039-45. Epub 2002/01/23.
290. Berk A. Adenoviridae. Knipe DM, Howley PM, editors: Lippincott Williams & Wilkins; 2006.
291. Vogt A, Mahe B, Costagliola D, Bonduelle O, Hadam S, Schaefer G, et al. Transcutaneous anti-influenza vaccination promotes both CD4 and CD8 T cell immune responses in humans. Journal of immunology. 2008;180(3):1482-9. Epub 2008/01/23.
292. Bal SM, Kruithof AC, Zwier R, Dietz E, Bouwstra JA, Lademann J, et al. Influence of microneedle shape on the transport of a fluorescent dye into human skin in vivo. Journal of controlled release : official journal of the Controlled Release Society. 2010;147(2):218-24. Epub 2010/07/24.
293. Minassian AM, Ronan EO, Poyntz H, Hill AV, McShane H. Preclinical Development of an In Vivo BCG Challenge Model for Testing Candidate TB Vaccine Efficacy. PloS ONE. 2011;6(5):e19840. Epub 2011/06/02.
294. Landau I, Boulard Y. Life cycles and Morphology, In: Rodent Malarias. Killick-Kendrick R, Peters W, editors: Adcademic Press, London.; 1978.

295. Puri N, Weyand EH, Abdel-Rahman SM, Sinko PJ. An investigation of the intradermal route as an effective means of immunization for microparticulate vaccine delivery systems. Vaccine. 2000;18(23):2600-12. Epub 2000/04/25.
296. Limberis MP, Bell CL, Wilson JM. Identification of the murine firefly luciferase-specific CD8 T-cell epitopes. Gene therapy. 2009;16(3):441-7. Epub 2009/01/09.
297. Ophorst OJ, Radosevic K, Havenga MJ, Pau MG, Holterman L, Berkhout B, et al. Immunogenicity and protection of a recombinant human adenovirus serotype 35-based malaria vaccine against Plasmodium yoelii in mice. Infection and immunity. 2006;74(1):313-20. Epub 2005/12/22.
298. Stoitzner P. The Langerhans cell controversy: are they immunostimulatory or immunoregulatory cells of the skin immune system? Immunology and cell biology. 2010;88(4):348-50. Epub 2010/05/07.
299. Romani N, Ebner S, Tripp CH, Flacher V, Koch F, Stoitzner P. Epidermal Langerhans cells--changing views on their function in vivo. Immunology letters. 2006;106(2):119-25. Epub 2006/07/11.
300. Asahina A, Tamaki K. Role of Langerhans cells in cutaneous protective immunity: is the reappraisal necessary? Journal of dermatological science. 2006;44(1):1-9. Epub 2006/09/05.
301. Abadie V, Bonduelle O, Duffy D, Parizot C, Verrier B, Combadiere B. Original encounter with antigen determines antigen-presenting cell imprinting of the quality of the immune response in mice. PloS ONE. 2009;4(12):e8159. Epub 2009/12/10.
302. Kersh EN, Kaech SM, Onami TM, Moran M, Wherry EJ, Miceli MC, et al. TCR signal transduction in antigen-specific memory CD8 T cells. J Immunol. 2003;170(11):5455-63. Epub 2003/05/22.
303. Shklovskaya E, Roediger B, Fazekas de St Groth B. Epidermal and dermal dendritic cells display differential activation and migratory behavior while sharing the ability to stimulate CD4+ T cell proliferation in vivo. Journal of immunology. 2008;181(1):418-30. Epub 2008/06/21.
304. Le Borgne M, Etchart N, Goubier A, Lira SA, Sirard JC, van Rooijen N, et al. Dendritic cells rapidly recruited into epithelial tissues via CCR6/CCL20 are responsible for CD8+ T cell crosspriming in vivo. Immunity. 2006;24(2):191-201. Epub 2006/02/14.
305. Eidsmo L, Allan R, Caminschi I, van Rooijen N, Heath WR, Carbone FR. Differential migration of epidermal and dermal dendritic cells during skin infection. Journal of immunology. 2009;182(5):3165-72. Epub 2009/02/24.
306. Calabro S, Tortoli M, Baudner BC, Pacitto A, Cortese M, O'Hagan DT, et al. Vaccine adjuvants alum and MF59 induce rapid recruitment of neutrophils and monocytes that participate in antigen transport to draining lymph nodes. Vaccine. 2011;29(9):1812-23. Epub 2011/01/11.
307. Grassi F, Dezutter-Dambuyant C, McIlroy D, Jacquet C, Yoneda K, Imamura S, et al. Monocyte-derived dendritic cells have a phenotype comparable to that of dermal dendritic cells and display ultrastructural granules distinct from Birbeck granules. Journal of leukocyte biology. 1998;64(4):484-93. Epub 1998/10/10.
308. Heath WR, Carbone FR. Dendritic cell subsets in primary and secondary T cell responses at body surfaces. Nat Immunol. 2009;10(12):1237-44. Epub 2009/11/17.
309. Wollenberg A, Wagner M, Gunther S, Towarowski A, Tuma E, Moderer M, et al. Plasmacytoid dendritic cells: a new cutaneous dendritic cell subset with distinct role in inflammatory skin diseases. The Journal of investigative dermatology. 2002;119(5):1096-102. Epub 2002/11/26.

310. Bachmann MF, Beerli RR, Agnellini P, Wolint P, Schwarz K, Oxenius A. Long-lived memory CD8+ T cells are programmed by prolonged antigen exposure and low levels of cellular activation. European journal of immunology. 2006;36(4):842-54. Epub 2006/03/23.
311. Gopee NV, Roberts DW, Webb P, Cozart CR, Siitonen PH, Warbritton AR, et al. Migration of intradermally injected quantum dots to sentinel organs in mice. Toxicol Sci. 2007;98(1):249-57. Epub 2007/04/04.
312. Reddy ST, van der Vlies AJ, Simeoni E, Angeli V, Randolph GJ, O'Neil CP, et al. Exploiting lymphatic transport and complement activation in nanoparticle vaccines. Nature biotechnology. 2007;25(10):1159-64. Epub 2007/09/18.
313. Badovinac VP, Tvinnereim AR, Harty JT. Regulation of antigen-specific CD8+ T cell homeostasis by perforin and interferon-gamma. Science. 2000;290(5495):1354-8. Epub 2000/11/18.
314. Haring JS, Harty JT. Aberrant contraction of antigen-specific CD4 T cells after infection in the absence of gamma interferon or its receptor. Infection and immunity. 2006;74(11):6252-63. Epub 2006/09/13.
315. Haring JS, Badovinac VP, Harty JT. Inflaming the CD8+ T cell response. Immunity. 2006;25(1):19-29. Epub 2006/07/25.
316. Kupper TS. Immune and inflammatory processes in cutaneous tissues. Mechanisms and speculations. The Journal of clinical investigation. 1990;86(6):1783-9. Epub 1990/12/01.
317. Sallusto F, Palermo B, Lenig D, Miettinen M, Matikainen S, Julkunen I, et al. Distinct patterns and kinetics of chemokine production regulate dendritic cell function. European journal of immunology. 1999;29(5):1617-25. Epub 1999/06/08.
318. Bos JA. Skin Immune System: Cutaneous Immunology and Clinical Immunodermatology. Third ed: CRC Press; 2005.
319. Krug A, Veeraswamy R, Pekosz A, Kanagawa O, Unanue ER, Colonna M, et al. Interferon-producing cells fail to induce proliferation of naive T cells but can promote expansion and T helper 1 differentiation of antigen-experienced unpolarized T cells. The Journal of experimental medicine. 2003;197(7):899-906. Epub 2003/04/02.
320. Brewig N, Kissenpfennig A, Malissen B, Veit A, Bickert T, Fleischer B, et al. Priming of CD8+ and CD4+ T cells in experimental leishmaniasis is initiated by different dendritic cell subtypes. Journal of immunology. 2009;182(2):774-83. Epub 2009/01/07.
321. Ritter U, Meissner A, Scheidig C, Korner H. CD8 alpha- and Langerin-negative dendritic cells, but not Langerhans cells, act as principal antigen-presenting cells in leishmaniasis. European journal of immunology. 2004;34(6):1542-50. Epub 2004/05/27.
322. Flacher V, Bouschbacher M, Verronese E, Massacrier C, Sisirak V, Berthier-Vergnes O, et al. Human Langerhans cells express a specific TLR profile and differentially respond to viruses and Gram-positive bacteria. Journal of immunology. 2006;177(11):7959-67. Epub 2006/11/23.
323. Klechevsky E, Morita R, Liu M, Cao Y, Coquery S, Thompson-Snipes L, et al. Functional specializations of human epidermal Langerhans cells and CD14+ dermal dendritic cells. Immunity. 2008;29(3):497-510. Epub 2008/09/16.
324. Kaplan DH. In vivo function of Langerhans cells and dermal dendritic cells. Trends in immunology. 2010;31(12):446-51. Epub 2010/11/03.

325. Villablanca EJ, Mora JR. A two-step model for Langerhans cell migration to skin-draining LN. European journal of immunology. 2008;38(11):2975-80. Epub 2008/11/11.
326. Cumberbatch M, Dearman RJ, Griffiths CE, Kimber I. Langerhans cell migration. Clinical and experimental dermatology. 2000;25(5):413-8. Epub 2000/09/30.
327. Raju PA, McSloy N, Truong NK, Kendall MA. Assessment of epidermal cell viability by near infrared multi-photon microscopy following ballistic delivery of gold micro-particles. Vaccine. 2006;24(21):4644-7. Epub 2005/09/20.
328. Kask AS, Chen X, Marshak JO, Dong L, Saracino M, Chen D, et al. DNA vaccine delivery by densely-packed and short microprojection arrays to skin protects against vaginal HSV-2 challenge. Vaccine. 2010;28(47):7483-91. Epub 2010/09/21.
329. Bruna-Romero O, Gonzalez-Aseguinolaza G, Hafalla JC, Tsuji M, Nussenzweig RS. Complete, long-lasting protection against malaria of mice primed and boosted with two distinct viral vectors expressing the same plasmodial antigen. Proceedings of the National Academy of Sciences of the United States of America. 2001;98(20):11491-6. Epub 2001/09/13.
330. Chen D, Kristensen D. Opportunities and challenges of developing thermostable vaccines. Expert Rev Vaccines. 2009;8(5):547-57. Epub 2009/04/29.
331. Alcock R, Cottingham MG, Rollier CS, Furze J, De Costa SD, Hanlon M, et al. Long-term thermostabilization of live poxviral and adenoviral vaccine vectors at supraphysiological temperatures in carbohydrate glass. Sci Transl Med. 2010;2(19):19ra2. Epub 2010/04/08.
332. Schneider J, Gilbert SC, Hannan CM, Degano P, Prieur E, Sheu EG, et al. Induction of CD8+ T cells using heterologous prime-boost immunisation strategies. Immunol Rev. 1999;170:29-38. Epub 1999/11/24.
333. Eriksson E, Boykin JV, Pittman RN. Method for in vivo microscopy of the cutaneous micromicrculation of the hairless mouse ear. Microvasc Res. 1980;19:374-9.
334. Kerwin BA. Polysorbates 20 and 80 used in the formulation of protein biotherapeutics: structure and degradation pathways. J Pharm Sci. 2008;97(8):2924-35. Epub 2007/11/02.
335. Romani N, Clausen BE, Stoitzner P. Langerhans cells and more: langerin-expressing dendritic cell subsets in the skin. Immunological reviews. 2010;234(1):120-41. Epub 2010/03/03.
336. Roberts KL, Smith GL. Vaccinia virus morphogenesis and dissemination. Trends Microbiol. 2008;16(10):472-9. Epub 2008/09/16.
337. Moss B, Damon IK. Poxviridae. Knipe PM, Howley PM, editors: Lippincott Williams & Wilkins; 2006.
338. Croyle MA, Roessler BJ, Davidson BL, Hilfinger JM, Amidon GL. Factors that influence stability of recombinant adenoviral preparations for human gene therapy. Pharmaceutical development and technology. 1998;3(3):373-83. Epub 1998/09/22.
339. Croyle MA, Cheng X, Wilson JM. Development of formulations that enhance physical stability of viral vectors for gene therapy. Gene therapy. 2001;8(17):1281-90. Epub 2001/09/26.
340. Lang R, Winter G, Vogt L, Zurcher A, Dorigo B, Schimmele B. Rational design of a stable, freeze-dried virus-like particle-based vaccine formulation. Drug development and industrial pharmacy. 2009;35(1):83-97. Epub 2008/11/19.
341. WHO. Temperature sensitivity of vaccines. World Health Organization, Immunization VaB; 2006 WHO/IVB/06.10.

342. Walgate R. Gates Foundation picks 14 grand challenges for global disease research. Bulletin of the World Health Organization. 2003;81(12):915-6. Epub 2004/03/05.
343. Ohtake S, Martin RA, Yee L, Chen D, Kristensen DD, Lechuga-Ballesteros D, et al. Heat-stable measles vaccine produced by spray drying. Vaccine. 2010;28(5):1275-84. Epub 2009/12/01.
344. Flechsig C, Suezer Y, Kapp M, Tan SM, Loffler J, Sutter G, et al. Uptake of antigens from modified vaccinia Ankara virus-infected leukocytes enhances the immunostimulatory capacity of dendritic cells. Cytotherapy. 2011;13(6):739-52. Epub 2011/01/22.
345. Schmidt NW, Butler NS, Badovinac VP, Harty JT. Extreme CD8 T cell requirements for anti-malarial liver-stage immunity following immunization with radiation attenuated sporozoites. PLoS Path. 2010;6(7):e1000998. Epub 2010/07/27.
346. Schmidt NW, Podyminogin RL, Butler NS, Badovinac VP, Tucker BJ, Bahjat KS, et al. Memory CD8 T cell responses exceeding a large but definable threshold provide long-term immunity to malaria. Proceedings of the National Academy of Sciences of the United States of America. 2008;105(37):14017-22. Epub 2008/09/11.
347. Limbach KJ, Richie TL. Viral vectors in malaria vaccine development. Parasite immunology. 2009;31(9):501-19. Epub 2009/08/21.
348. Chang LL, Shepherd D, Sun J, Ouellette D, Grant KL, Tang XC, et al. Mechanism of protein stabilization by sugars during freeze-drying and storage: native structure preservation, specific interaction, and/or immobilization in a glassy matrix? Journal of pharmaceutical sciences. 2005;94(7):1427-44. Epub 2005/05/28.
349. Matthias DM, Robertson J, Garrison MM, Newland S, Nelson C. Freezing temperatures in the vaccine cold chain: a systematic literature review. Vaccine. 2007;25(20):3980-6. Epub 2007/03/27.
350. Chang LL, Pikal MJ. Mechanisms of protein stabilization in the solid state. Journal of pharmaceutical sciences. 2009;98(9):2886-908. Epub 2009/07/02.
351. Burke CJ, Hsu TA, Volkin DB. Formulation, stability, and delivery of live attenuated vaccines for human use. Crit Rev Ther Drug Carrier Syst. 1999;16(1):1-83. Epub 1999/04/01.
352. Lee KN, Hutson CL, Kline R, Curns AT, Dougherty C, Allen C, et al. Smallpox vaccine stability after maintenance at temperatures not recommended for shipping. Vaccine. 2006;24(7):884-6. Epub 2005/09/27.
353. Chen X, Corbett HJ, Yukiko SR, Raphael AP, Fairmaid EJ, Prow TW, et al. Site-selectively coated, densely-packed microprojection array patches for targeted delivery of vaccines to skin. Advances Functional Materials. 2011;21:464-73.
354. Wirth TC, Martin MD, Starbeck-Miller G, Harty JT, Badovinac VP. Secondary CD8+ T-cell responses are controlled by systemic inflammation. European journal of immunology. 2011;41(5):1321-33. Epub 2011/03/23.
355. Kaplan DH, Kissenpfennig A, Clausen BE. Insights into Langerhans cell function from Langerhans cell ablation models. European journal of immunology. 2008;38(9):2369-76. Epub 2008/09/16.
356. Duan D, Moeckly C, Gysbers J, Novak C, Prochnow G, Siebenaler K, et al. Proposed Title: Enhanced Delivery of Topically-Applied Formulations following Skin Pre-Treatment with a Hand-applied, Plastic Microneedle Array. Curr Drug Deliv. 2011. Epub 2011/06/24.